RV SONNE
CRUISE REPORT SO110
SO - RO
SONNE - ROPOS

SO110-1a: Victoria - Victoria
July 9 - July 15, 1996

SO110-1b: Victoria - Kodiak
July 16 - August 4, 1996

SO110-2: Kodiak - Victoria
August 5 - August 19, 1996

Edited by
Erwin Suess and Gerhard Bohrmann
with contributions by the cruise participants

GEOMAR
Forschungszentrum
für marine Geowissenschaften
der Christian-Albrechts-Universität
zu Kiel

Kiel 1997

GEOMAR REPORT 59

GEOMAR
Research Center
for Marine Geosciences
Christian Albrechts University
in Kiel

Redaktion der Serie: Gerhard Haass
Umschlag: Kerstin Kreis, Harald Gross, GEOMAR Technologie GmbH

Managing Editor: Gerhard Haass
Cover: Kerstin Kreis, Harald Gross, GEOMAR Technologie GmbH

GEOMAR REPORT
ISSN 0936 - 5788

GEOMAR REPORT
ISSN 0936 - 5788

GEOMAR
Forschungszentrum
für marine Geowissenschaften
D-24148 Kiel
Wischhofstr. 1-3
Telefon (0431) 600-2555, 600-2505

GEOMAR
Research Center
for Marine Geosciences
D-24148 Kiel / Germany
Wischhofstr. 1-3
Telephone (49) 431 / 600-2555, 600-2505

Table of Contents

Preface
E. Suess, G. Bohrmann, R. Lutz

The focus of the project SO110 SO-RO was the deployment of the remotely operated deep-diving vehicle ROPOS from board the R.V. SONNE. The targets of this joint German-Canadian-U.S. project were the cold seep sites along the Aleutian convergence zone, which were first discoverd in 1994. For technical reasons however, during the preceeding Leg SO109 which also utilized ROPOS, the cold seep targets of the Cascadia convergence zone could not be visited. Therefore, the initial six days of SO110 were used to deploy the ROV-system at the Second Accretionary Ridge off central Oregon (SO110-1a; Fig. 1). This was followed by ROPOS-deployment at the EDGE-site off Kodiak Island (SO110-1b).

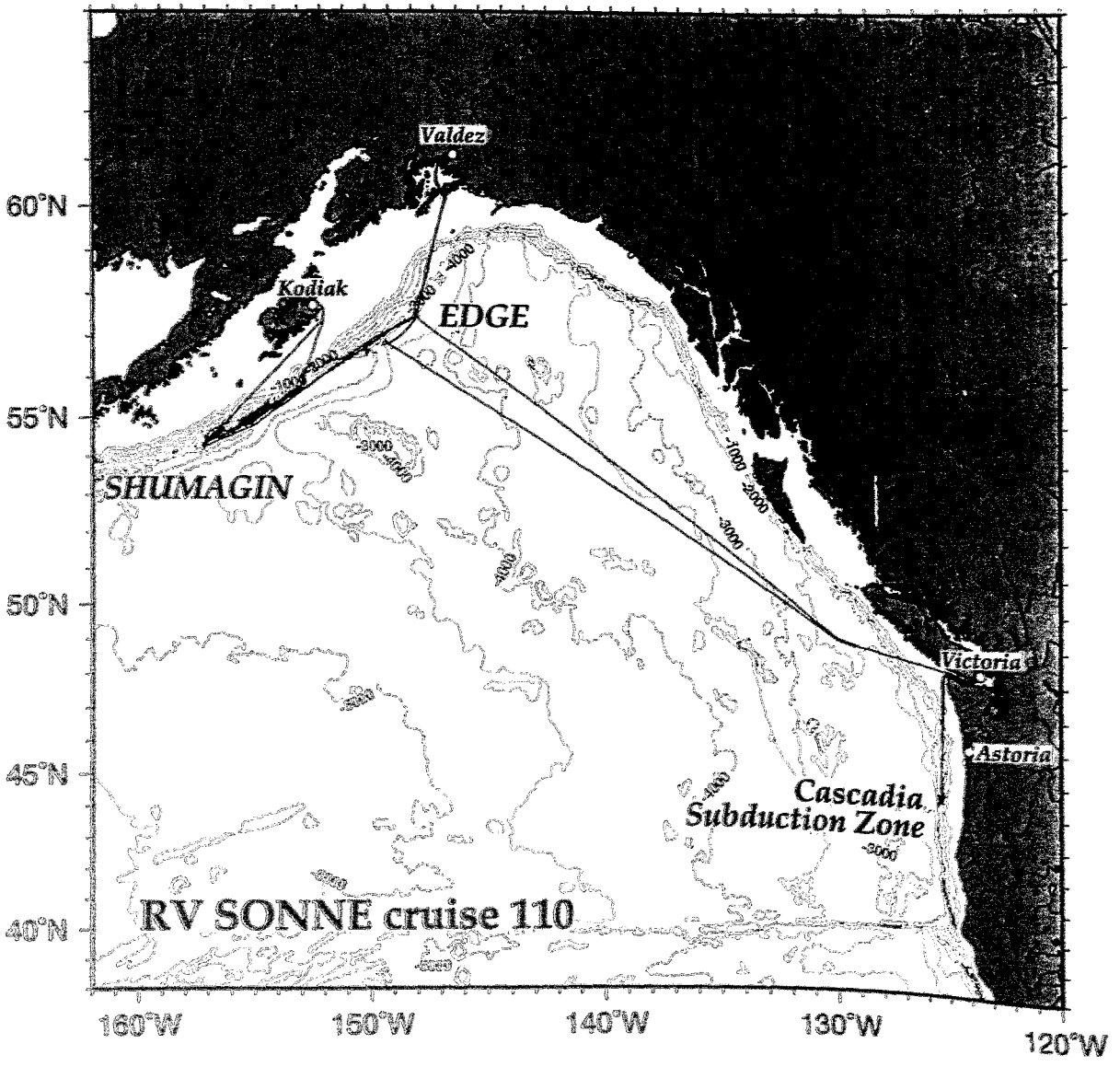

Fig. 1: Cruise track and major working areas of SO110 (SO-RO) cruise.

Finally, the 3rd leg SO110-2, was devoted to work at the Aleutian subduction zone off Kodiak and Shumagin Islands, without the ROV-system (Fig. 1).

This cruise report details the activity of SO110 and is subdivided into the segments SO110-1a, SO110-1b, and SO110-2. The first segment is represented by a short self-contained report, whereas the two other segments are combined because of their regional focus off Alaska. The objectives and the general tectonic framework of the targeted areas the Cascadia and Aleutian margins are detailed in the respective introductory chapters.

This cruise report should also be seen in conjunction with that of SO109. Both projects represent a landmark in German marine geoscience research. For the first time the unmanned deep-sea diving system ROPOS was deployed in a joint effort with Canadian and U.S. groups and as part of a research program exclusively driven by scientific objectives. During both cruises technical problems with the new fiber optic deep-sea cable developed which had to be overcome at the expense of a considerable loss of deployment time of the ROV-system. Nevertheless, significiant scientific and technical success was achieved.

The highlights of this success are the quality of documentation of vent processes not previously achieved, the direct collection of vent fluids from the gas hydrate vents off central Oregon, the documentation of phase separation observed by boiling fluids at the Axial Seamount and the mapping of cold vents off Alaska as well as new insights into the specialized ecosystems of cold seep communities. This could not have been achieved by conventionally towed systems. Accurate sampling, especially of vent fluids and sulfide chimneys, in the area of the phase separation, provided unique sample material which when fully analyzed and evaluated will provide new and basic knowledge about vent processes.

The technological success of the ROPOS system is two-fold: firstly reaching a record diving depth of 4,960 m with all systems operating and secondly accomplishing the longest continuous deployment of the system of almost 30 hours. This demonstrates the greater economic viability and superiority of an unmanned diving system compared to manned submersibles. For the German marine research community it can thus be convincingly shown that the R.V. SONNE with her superior equipment and experienced crew can proficiently handle such ROV deployments. The unanimous opinion of all participating national and international groups was that a leading role in marine research has been achieved through the ROPOS deployments during projects SO109 and SO110. This success was only possible through the cooperation of numerous scientific and administrative departments of reviewing, funding and scheduling agencies, and their determination and good will to see this project throught in spite of setbacks.

The project SO-RO was planned, coordinated and carried out by GEOMAR Research Center and Rutgers University, and the project HYDROTRACE by the Technische Universität Freiberg. Both projects were financed by the Bundesministerium für Bildung, Wissenschaft, Forschung und Technologie, Bonn (Project Nos. 03G0110A/B and 03G0109A/B) as part of their deep-sea

research initiative. Project review and administration was proficiently handled by BEO Warnemünde. On behalf of all participants we wish to thank these departments and their staff for their support and flexibility in overcoming problems and in eventually succeeding in "getting the ROPOS system on the bottom".

Additional financial support was provided by the Canadian side through the National Science and Engineering Council (NSERC) and on the US side through the National Science Foundation (NSF). The Reedereigemeinschaft Forschungsschiffahrt (RF) also provided extra funds for technical requirements to accomodate the ROPOS system on board R.V. SONNE. We would especially like to acknowledge the vessel's master Henning Papenhagen and his crew for their highly professional conduct, their continual flexibility and patience and their contribution in providing an extraordinarily pleasant working atmosphere during both cruises. The ROPOS system was originally developed through funds from the Canadian government and is currently available for research through charter by the Canadian Scientific Submersible Facility (CSSF) in Ottawa. Finally, this success would not have been achieved without the enormous commitment and expertise of the ROPOS team and their enthusiasm and cooperation with the crew of the R.V. SONNE and the science groups.

Scientific crew

Leg SO110-1a: Victoria - Victoria (9 July - 15 July 1996)

Appel, Frank	GEOMAR GTG, Kiel
Banfield, Bob	Institute of Ocean Sciences, Sidney
Barker, Dan	Institute of Ocean Sciences, Sidney
Bohrmann, Gerhard	GEOMAR Forschungszentrum, Kiel
Collier, Bob	Oregon State University, Corvallis
Dählmann, Anke	GEOMAR Forschungszentrum, Kiel
Domeyer, Bettina	GEOMAR Forschungszentrum, Kiel
Greinert, Jens	GEOMAR Forschungszentrum, Kiel
Heeren, Frank	GEOMAR Forschungszentrum, Kiel
Holland, Bob	Institute of Ocean Sciences, Sidney
Illman, Jim	Institute of Ocean Sciences, Sidney
Jungnickel, Ralf	GEOMAR Forschungszentrum, Kiel
Linke, Peter	GEOMAR Forschungszentrum, Kiel
Kulescha, Friedhelm	GEOMAR GTG, Kiel
Jones, Nicola	University, Victoria
von Mirbach, Nico	GEOMAR Forschungszentrum, Kiel
Nakamura, Ko-ichi	Geological Survey of Japan, Ibaraki
Sahling, Heiko	GEOMAR Forschungszentrum, Kiel
Schumann, Marcus	GEOMAR Forschungszentrum, Kiel
Shepherd, Keith	Institute of Ocean Sciences, Sidney
Southward, Eve	University, Victoria
Suess, Erwin, **chief scientist**	GEOMAR Forschungszentrum, Kiel
Tamurri, Keith	Institute of Ocean Sciences, Sidney
Torres, Marta	Oregon State University, Corvallis

Winkler, Gisela	Umweltphysik, Universität Heidelberg
Zuleger, Evelyn	GEOMAR Forschungszentrum, Kiel

Leg SO110-1b: Victoria - Kodiak (16 July - 4 August 1996)

Appel, Frank	GEOMAR GTG, Kiel
Banfield, Bob	Institute of Ocean Sciences, Sidney
Barker, Dan	Institute of Ocean Sciences, Sidney
Bohrmann, Gerhard	GEOMAR Forschungszentrum, Kiel
Dählmann, Anke	GEOMAR Forschungszentrum, Kiel
Driscoe, Rick	Institute of Ocean Sciences, Sidney
Domeyer, Bettina	GEOMAR Forschungszentrum, Kiel
Greinert, Jens	GEOMAR Forschungszentrum, Kiel
Heeren, Frank	GEOMAR Forschungszentrum, Kiel
Holland, Bob	Institute of Ocean Sciences, Sidney
Jungnickel, Ralf	GEOMAR Forschungszentrum, Kiel
Large, Michelle	Humboldt State University, Arca
Linke, Peter	GEOMAR Forschungszentrum, Kiel
Levai, Gyongyver	Rutgers State University of New Jersey
Lutz, Rich	Rutgers State University of New Jersey
Kulescha, Friedhelm	GEOMAR GTG, Kiel
Maher, Norm	MBARI, Moss Landing
von Mirbach, Niko	GEOMAR Forschungszentrum, Kiel
Moyer, Craig	Rutgers State University of New Jersey
Orange, Daniel	MBARI, Moss Landing
Sahling, Heiko	GEOMAR Forschungszentrum, Kiel
Shepherd, Keith	Institute of Ocean Sciences, Sidney
Suess, Erwin, **chief scientist**	GEOMAR Forschungszentrum, Kiel
Winkler, Gisela	Umweltphysik, Universität Heidelberg
Zuleger, Evelyn	GEOMAR Forschungszentrum, Kiel

Leg SO110-2: Kodiak - Victoria (5 August - 19 August 1996)

Beck, Denise	GEOMAR Forschungszentrum, Kiel
Biebow, Nicole	GEOMAR Forschungszentrum, Kiel
Bohrmann, G. **chief scientist**	GEOMAR Forschungszentrum, Kiel
Dählmann, Anke	GEOMAR Forschungszentrum, Kiel
Didié, Claudia	GEOMAR Forschungszentrum, Kiel
Domeyer, Bettina	GEOMAR Forschungszentrum, Kiel
Greinert, Jens	GEOMAR Forschungszentrum, Kiel
Heinze, Jutta	GEOMAR GTG, Kiel
Jung, Carmen	GEOMAR Forschungszentrum, Kiel
Käding, Arne	GEOMAR Forschungszentrum, Kiel
Kulescha, Friedhelm	GEOMAR GTG, Kiel
Levai, Perl	Rutgers State University of New Jersey
Petersen, Asmus	GEOMAR GTG, Kiel
Saffer, Demian	MBARI, Moss Landing

Sahling, Heiko	GEOMAR Forschungszentrum, Kiel
Schäfer-Pinto, Angela	GEOMAR Forschungszentrum, Kiel
Schiller, Johannes	Umweltphysik, Universität Heidelberg
Schumann, Marcus	GEOMAR Forschungszentrum, Kiel
von Mirbach, Niko	GEOMAR Forschungszentrum, Kiel
Wallmann, Klaus	GEOMAR Forschungszentrum, Kiel
Weinrebe, Willi	GEOMAR Forschungszentrum, Kiel
Yun, Janet	MBARI, Moss Landing
Zuleger, Evelyn	GEOMAR Forschungszentrum, Kiel

Reedereigemeinschaft Forschungsschiffahrt GmbH, Bremen
Personnel aboard RV SONNE

Leg SO110-1:	**Leg SO-110-2:**
Angermann, Rudolf	Angermann, Rudolf
Behnisch, Holm	Behnisch, Holm
Bekaan, Steffen	Bekaan, Steffen
Bethkegen Becher, Hans	Bethke gen Becher, Hans
Drakopoulos, Evgenios	Drakopoulos, Evgenios
Grund, Fritz, H.	Grund, Fritz, H.
Hentschel, Rainer	Hadamek, Peter
Hoffmann, Wolf-Hilmar	Hentschel, Rainer
Korte, Detlef	Hoffmann, Wolf-Hilmar
Krause, Niels	Korte, Detlef
Liebe, Thomas	Krause, Niels
Lindemann, Erhard	Klein, Andreas
Lohmueller, Karl-Heinz	Lindemann, Erhard
Martin, Andreas	Lohmueller, Karl-Heinz
Melsbach, Herbert	Melsbach, Herbert
Mueller, Werner	Mueller, Werner
Naeve, Ingo	Naeve, Ingo
Papenhagen, Henning	Papenhagen,Henning
Rossa, Georg	Rossa, Georg
Sandersfeld, Uwe	Sandersfeld, Uwe
Schlosser, Thomas	Schlosser, Thomas
Schramme, Heinrich	Schramme, Heinrich
Schrapel, Andreas	Slotta, Werner
Slotta, Werner	Sturm, Wolfgang
Staengl, Guenter	Szymanski, Leszek
Sturm, Wolfgang	Thaysen, Uwe
Szymanski, Leszek	Tiemann, Frank
Teiohert, Klaus	Teichert, Klaus
Teske, Roland	Unterberger, Anton
Tiemann, Frank	Vor, Hans-Jürgen

Addresses of participating research institutes

GEOMAR Forschungszentrum für marine Geowissenschaften
der Christian-Albrechts-Universität zu Kiel
Wischhofstraße 1-3
24148 Kiel, Germany

GEOMAR Technologie GmbH
Wischhofstraße 1-3
24148 Kiel, Germany

Department of Oceanography
Humboldt State University
Arcata, CA 95521, USA

Institute of Marine and Coastal Sciences
Rutgers - The State University of New Jersey
New Brunswick, New Jersey 08903, USA

Monterey Bay Aquarium
Research Institute
7642 Sandholdt,
Moss Landing, California 95039, USA

College of Oceanic & Atmospheric Sciences
Oregon State University
Corvallis, OR 97331-5503, USA

School of Earth and Ocean Research
University of Victoria
3800 Finnerty Road
P.O. Box 1700
Victoria, BC; V8W 3P6, Canada

University of Washington
College of Oceanography
Box 357940
Seattle, WA 98195, USA

Institut für Umweltphysik
Universität Heidelberg
Im Neuenheimer Feld 366
69120 Heidelberg, Germany

Marine Geology Department
Geological Survey of Japan
1-1-3 Higashi
Tsukuba, Ibaraki 305, Japan

Part I
Cruise Report
SONNE 110 Leg 1a

9 July - 15 July, 1996 (Victoria - Victoria)

Table of contents **Page**

1 Introduction

E. Suess, G. Bohrmann

The segment of the Cascadia convergent margin off Oregon is the first at which tectonic dewatering has been observed and documented (Kulm et al., 1986; Suess et al., 1985). Since this discovery it has become one of the classic sites for our understanding of fluid venting processes at active margins and the formation of accretionary complexes (Moore et al., 1990; Westbrook et al., 1994; 1995).

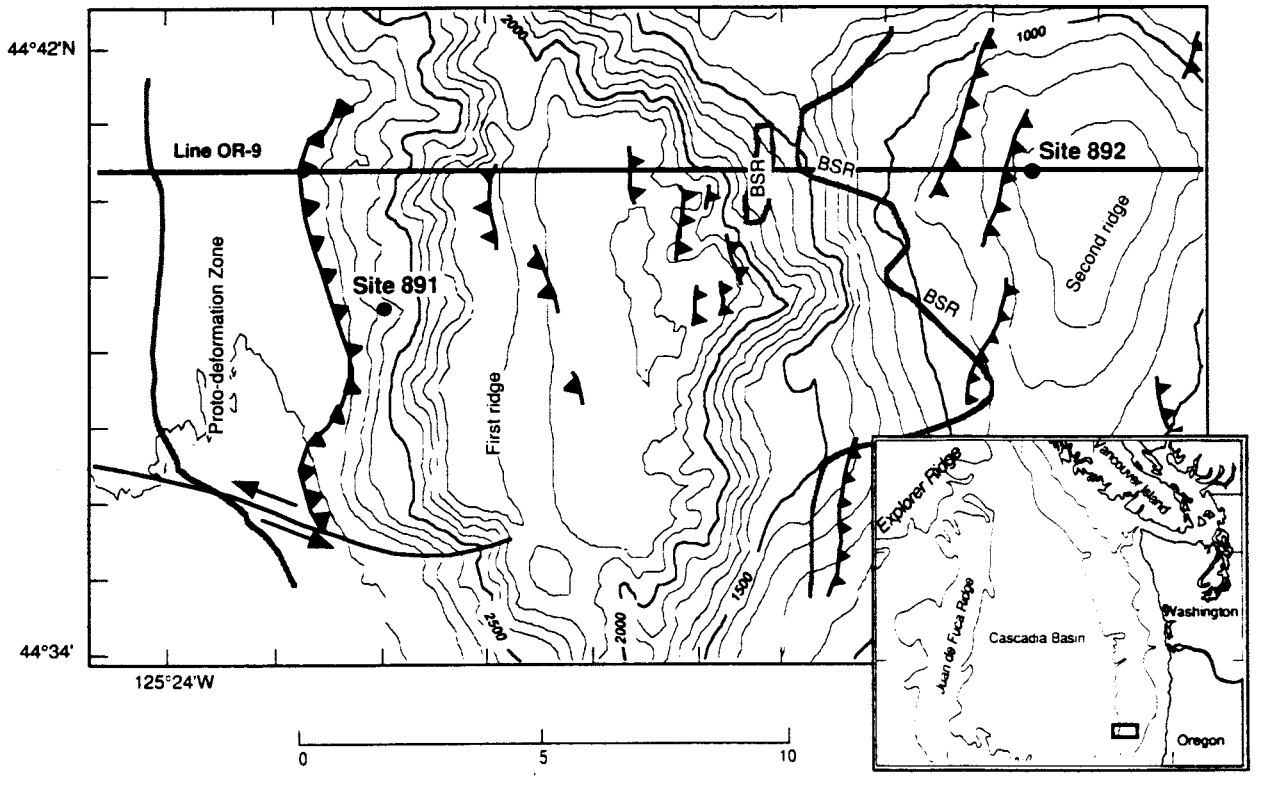

Fig. 2: Bathymetry of the the first and second ridge of the accretionary prism off Oregon in the area of ODP Sites 891 and 892. Seismic line OR-9 is indicated as well as the position of the thrust fault traces (heavy toothed lines). The seaward limits of the proto-deformation zone and of the BSR are shown by heavy gray lines (from Westbrook et al., 1994).

The style of accretion alternates along this margin between thrust faults dipping towards the continent and those dipping towards the oceanic plate (Figs. 2 and 3). The surface expressions of accretion are N-S trending ridges of progressively older age towards the continental plate. Ponded sediment basins develop between the ridges. The detailed structure of the seaward-verging (dipping towards the oceanic plate) accretionary complex was established in previous seismic and bathymetric surveys. During ODP-drilling Leg 146 and the work by R.V. SONNE during SO109, gas hydrates and active fluid venting were shown to occur near the summit of this ridge. These provided the basis for targeting the Second Accretionary Ridge for detailed investigations by ROPOS.

A well-developed BSR underlies the crest of the Second Accretionary Ridge (Carson et al., 1994, Figs. 3 and 4). It extends down the seaward flank of the ridge and continues landward. Two major faults cut through the BSR causing a slight upward bulging of the reflector. The fault nearest the ridge crest (water depth = 720 m) was intersected at 105 mbsf by drilling at ODP-Site 892. The drill hole also intersected the BSR at 73 mbsf. Active flow was indicated by geochemical anomalies in the pore water, by overpressure from a packer test, and by local temperature excursions (1.6°C and 2.5°C) above the linear geothermal gradient. Aggregates of gas hydrates were found in the upper 19 mbsf at Site 892 and are inferred to be distributed throughout the 73 m thick section above the BSR.

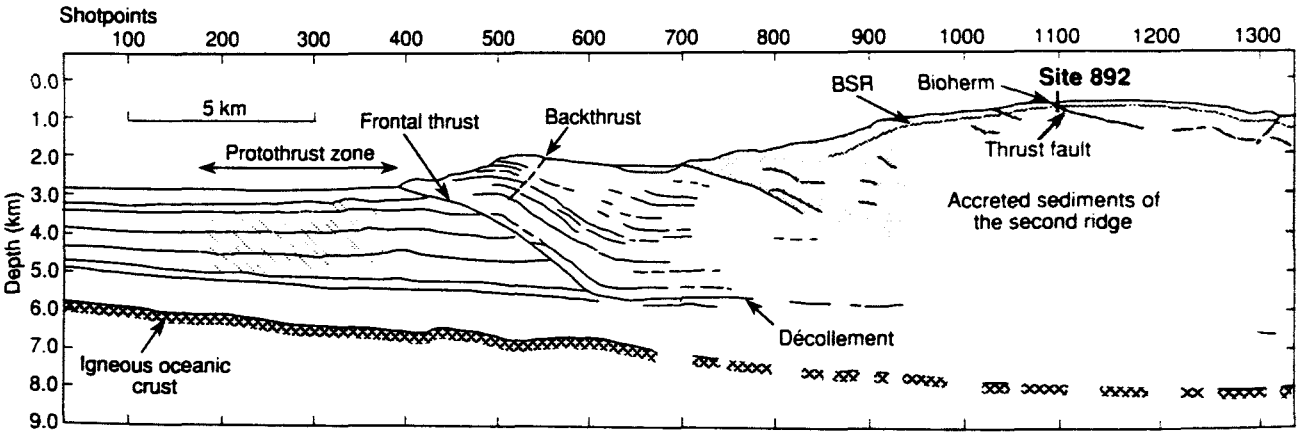

Fig. 3: Depth-converted migrated seismic-reflection section OR-9, showing from west to east the flat-lying Cascadia Basin deposits, the proto-deformation zone characterized by blind thrusts, the First Ridge of the lower slope underlain by a seaward-verging thrust fault and the Second Ridge lines (from Westbrook et al. 1994).

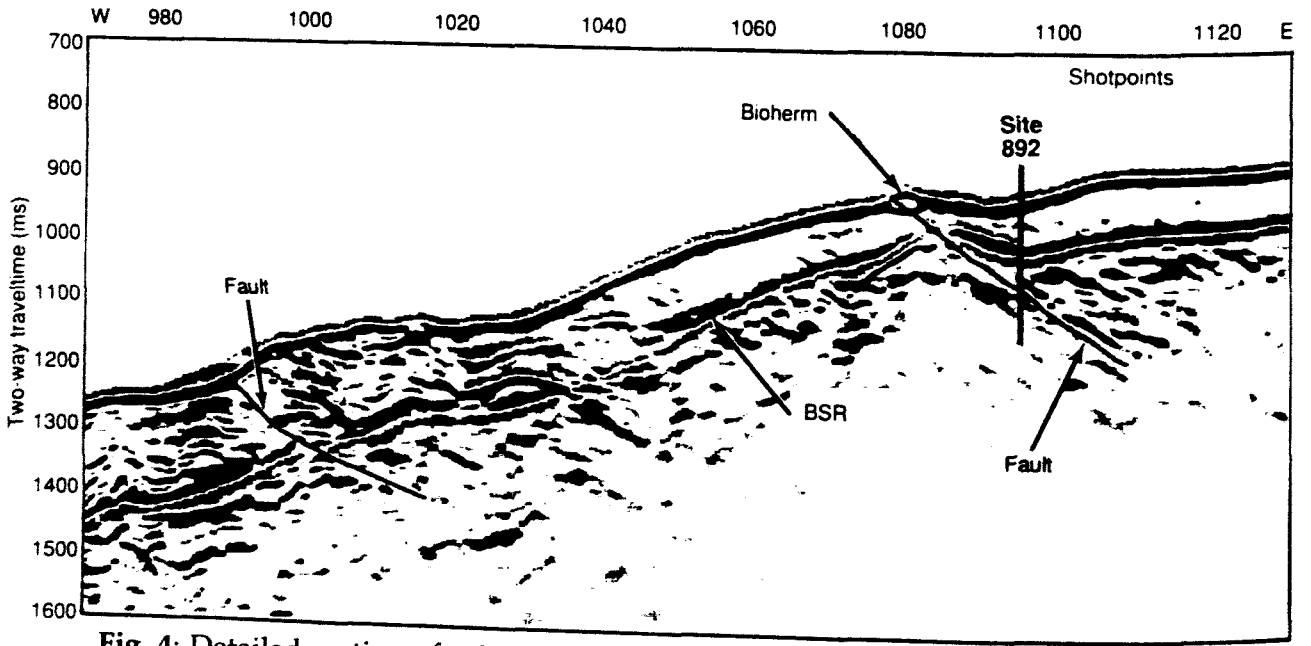

Fig. 4: Detailed section of seismic line OR-9 near ODP Site 892. The distribution of the BSR, major faults and a large carbonate outcrop („bioherm") are indicated (from Westbrook et al., 1994).

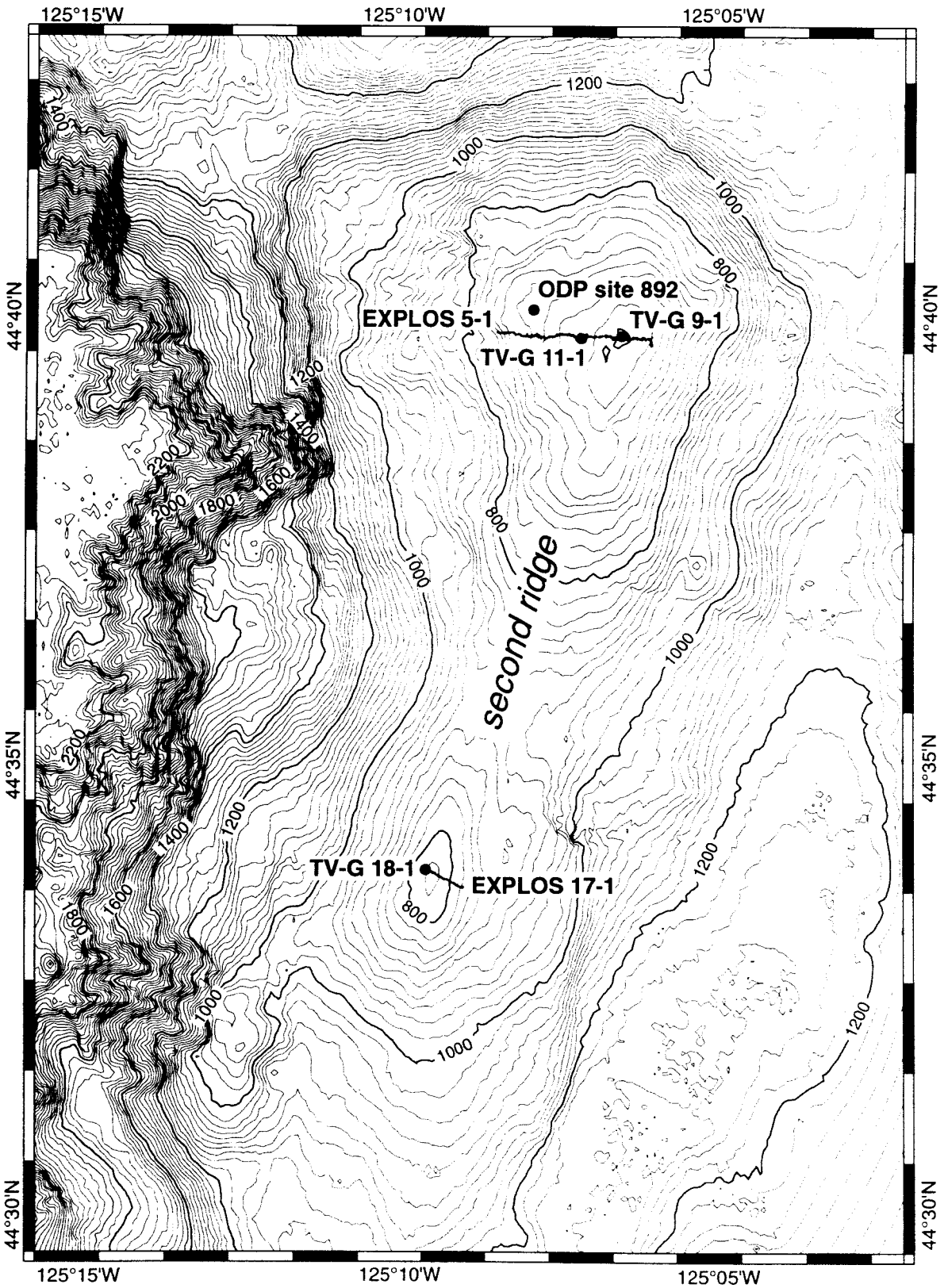

Fig. 5: Bathymetry of the second accretionary ridge off Oregon. Locations of SO110-1a EXPLOS tracks and TV-grab sample sites are indicated.

The ridge crest, where Gloria backscatter intensity (Carson et al., 1994) has the greatest magnitude, in a roughly north-south trending linear region some 2 - 3 km wide and more than 20 km long, was the site for ROPOS deployment. The ridge is cut by faults striking parallel to the topography. Surface off-sets and the association of faults with growing folds indicate that some of the faults are active. Surface off-sets are thrusts which along with compressional folds suggest the Second Accretionary Ridge is currently undergoing shortening and uplift. The northern summit of the ridge correlates with a hydrogeologically active out-of-sequence thrust zone, with extensive carbonate build up and vigorous seep activity.

These massive carbonate deposits (= bioherm) are scattered over the summit area and seaward flank of the ridge. They are the surface trace of outcropping faults and their carbon originates exclusively from methane (Linke et al., 1994; Moore et al., 1994; Ritger et al., 1987). The volume of carbonate deposited suggests a long-term discharge of methane-rich fluids along fault zones which cut across the BSR. The ridge to the south continuous to show high back-scatter intensities but the topography becomes distinctly smoother than in the north. This is probably related to the absence or at least significant reduction of the rugged bioherm carbonates. The depth of the ridge crest deepens from 585 m in the north to 785 m in the south 20 km away (Fig. 5).

With such detailed information available the targets for ROPOS-deployment, EXPLOS-survey, CTD-cast, and coring by TV-grab were readily available during the initial few days of work during SO110.

2 Cruise narrative and preliminary results

E. Suess

Week of 8 - 16 July 1996

After completing repair work on the glass-fibre cable of ROPOS and changing scientific crew, R.V. SONNE departed Ogden Pier in Victoria on July 8 at 08:30 p.m. local time and steamed for the Cascadia accretionary margin off central Oregon. Upon arrival during the night of 9 July, a current meter was deployed at the western flank of the Second Accretionary Ridge. The objective was to monitor the near-bottom field of flow that controls the distribution of a large methane plume which was mapped during Leg SO109.

Prior to deployment of ROPOS, gaps in the HYDROSWEEP data of the area were filled in and a CTD cast taken from the immediate vicinity of the current meter mooring. During the few days of the cruise this station was repeatedly sampled at 6-10 hour intervals in order to correlate changes of the methane plume with changes in the current field. On 10 July at 07:00 local time ROPOS was deployed without any problems despite gusty northerly winds (maximum 9 m/sec) and high northwesterly seas. The western flank of the Second Accretionary Ridge was surveyed and sampled by ROPOS for nearly 9 hours. The highly flexible camera system was used extensively and provided high quality documentation of active sites. Sampling included vent communities and carbonate precipitates.

Towards the end of 10 July an EXPLOS-survey was carried out across ridge. On the summit (565 m water depth) gas bubbles were clearly seen rising from a vent field covered with carbonate boulders. Several gas bubbles escaped simultaneously from a single spot. The activity lasted for several seconds and was interrupted by a pause before activity resumed. The carbonate boulders showed bizarre dissolution features and appeared to be wrapped in white-blue bacterial mats. Macrofauna was rather rare, both living and dead specimens being smaller than those observed in the bioherm area of the western flank. The bubble field was several 10 m^2 in area. Other large active vent fields were observed that were marked by thriving faunal communities surrounded by carbonate edifices, however no free gas was seen to escape. A CTD-cast right at the bubble field confirmed that the escaping gas was methane and that vertical transport by rising bubbles and simultaneous dissolution is probably responsible for the mushroom-shaped methane plume. The plume maximum, verified by several samples, contained up to 73,000 nL methane/L of seawater.

At night HYDROSWEEP surveys were extended to the southern crest of the ridge, about 10 km farther south and were completed the following night. On the morning of 11 July at 06:00 deployment of ROPOS began in the area of the newly found bubble field on the northern summit. Deployment went smoothly despite increasing winds, however, re-locating the bubble field was difficult. Numerous small vent fields in the vicinity were sampled and documented. Small vent organisms and large amounts of carbonate precipitates were also sampled. The ROPOS suction sampler was also deployed to sample fluids a few cm above the sea bottom or directly from

the vents. One of the samples contained more than 350,000 nL of methane/L, though significant degassing and loss of sample took place upon recovery.

Two deployments of the TV-grab in the bubble field recovered numerous living and non-living vent organisms as well as carbonates and sediments with tremendously high contents of methane and hydrogen sulphide in the porewater. On the morning of 12 July the current meter was recovered. At that time the wind and seas had further increased so that the depoyment of ROPOS was delayed until early afternoon. Instead VESP was deployed successfully and a time series of water samples was taken. However, the VESP data storage probe was irreparably damaged by a water leak which also affected the recording of flow rates and other parameters. The ROPOS survey during the afternoon had to be cut short because of increasing winds, but not before fluid samples were taken by a special titanium sampler which was directly introduced into the vents. An extraordinarily varied vent community as well as their feeding and motion habits were documented. ROPOS recovery during strong swells was complicated and the cage was severely damaged requiring a return to Victoria.

Before departing the working area, the transponders were recovered and an EXPLOS-survey run across the southern part of the ridge. No bioherm structures and only a few dead mollusc specimens were observed. The summit of the southern ridge was largely covered with dense, bacterial mats of whitish and bluish hues. Thin crusts were visible below the bacterial cover in an otherwise rather uniform sediment. At one of the spots with bacterial mats, the deployment of the TV-grab yielded a large piece of interbedded sediment-gas hydrate-carbonates. The hydrate was white and clean and intercalated with thin layers of hydrogen sulfide rich sediment and carbonates. We ended up with so much hydrate that there were not enough sample containers for liquid nitrogen to recover it all. Some pieces were set on fire which was a very impressive spectacle.

On 13 July at around 03:00 R.V. SONNE headed for Victoria, where she tied up at Esquimalt Docks on 14 July at 08:00. On the same day replacment of the winch and repair of the ROPOS cage were started. On 15 July the installation of the new winch drum and the handling gear was completed and the new cable could be mounted, this took up the whole of the 16 July.

3 HYDROSWEEP swathmapping

F. Heeren, R. Kunze

HYDROSWEEP swathmapping carried out during the cruise SO110-1a along the Cascadia Margin filled in gaps left by the mapping of SO109 and extended the mapped area to the south. The objective of the S 110-1a swathmapping survey was to obtain a bathymetric overview of the southern part of the Gas Hydrate Ridge, a feature on the central Cascadia Margin.

HYDROSWEEP (HYDROgraphic multi-beam SWEEPing survey echosounder) is a swathmapping system from the Krupp Atlas Elektronik GmbH, Bremen, Germany. The system uses a field of 59 acoustic beams at a frequency of 15.5 kHz and an angle of 90 degrees, allowing a swathwidth that is twice the water depth. The accuracy of the system is approximately 1 percent of the water depth.

The raw data were preprocessed with the *mbsystem*, a free software program by Caress and Chayes, Lamont-Doherty Earth Observatory, and cleaned with a filtering program compiled by F. Heeren. The velocity function used to convert acoustic travel time into depth (Table 1) was obtained from CTD-site 29-1 during cruise SO109 (44°40.76'N 125°18'W). The processed data are displayed using the GMT system, a free graphic software program by Wessels and Smith (1991).

During SO109, the bathymetry of the Cascadia Continental Margin was mapped between 44°47'N 125°22'W and 44°35'N 124°48'W. SO110-1 filled in data gaps left from So 109, and extended the mapping of the Gas Hydrate Ridge to 44°30'N. The swathmapping tracks are shown in Figure 6.
In the survey area, the Juan de Fuca plate is subducting beneath the North American plate at a rate of approx. 40 mm/yr (De Mets et al., 1990). The oceanic crust in this region is overlain by a thick (approx. 3.5 km) sediment package (MacKay et al., 1992), which prevents the formation of a deep trench west of the first accretionary ridge. The first ridge ranges from a depth of 2900 m to 2000 m, whereas the remarkably broad second ridge ranges from 2200 m to 600 m (Fig. 7). On the top of the second ridge two summits are well defined. The rough morphology of the seaward slope of the ridges includes some well developed channel systems, indicating that no recent mass wasting events have occurred (Figs. 7, 8 and 9).

Table 1: Depth (m) and sound velocity (m/s).

0, 1499	75, 1490	300, 1478	900, 1480	1.500, 1485
10, 1497	100, 1488	400, 1478	1.000, 1481	1.750, 1488
20, 1497	125, 1485	500, 1478	1.100, 1482	2.000, 1491
30, 1495	150, 1482	600, 1478	1.200, 1482	2.500, 1498
50, 1492	200,1479	700, 1479	1.300, 1483	
50, 1492	250, 1479	800, 1479	1.400, 1484	

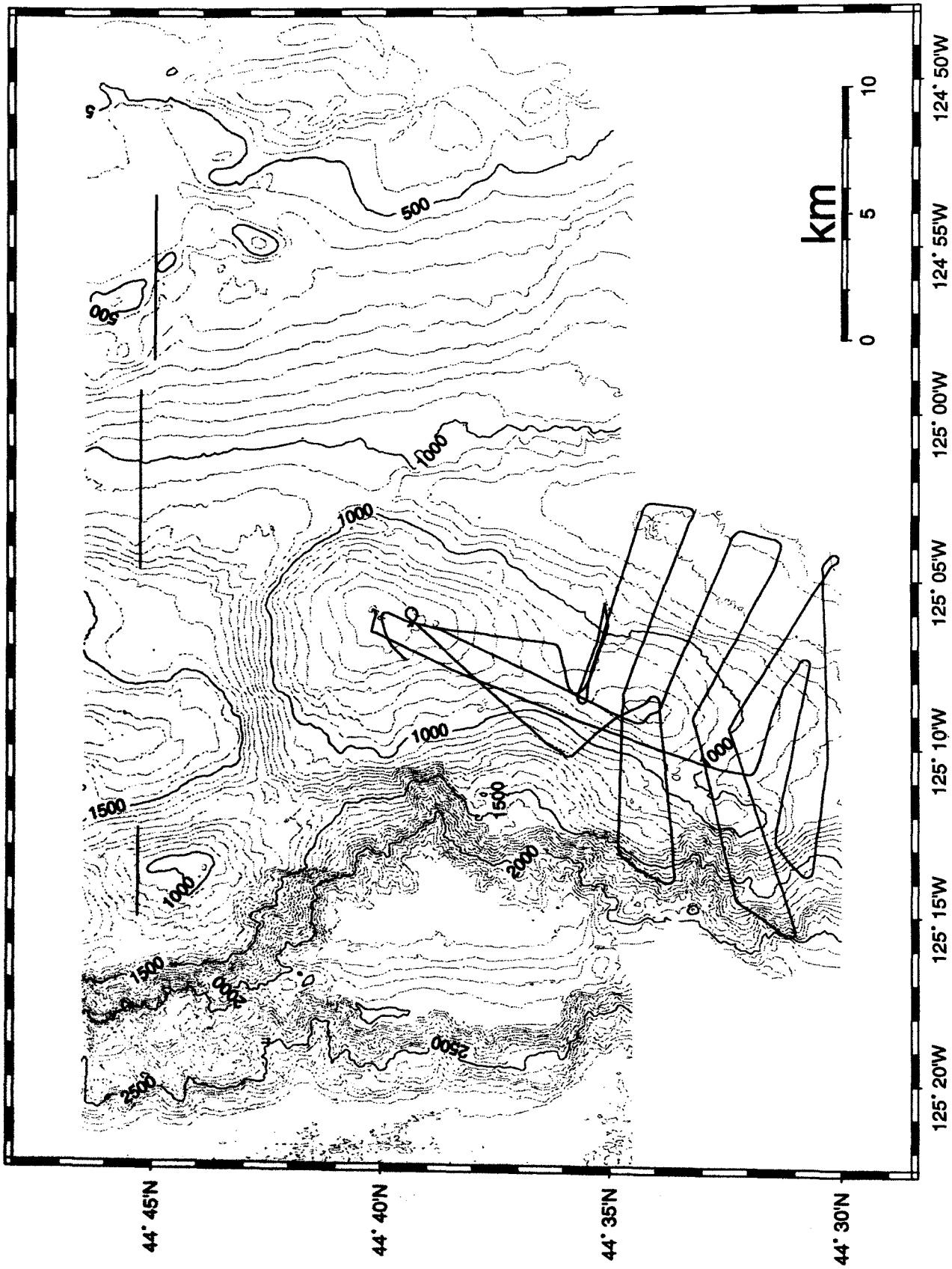

Fig. 6: Shiptracks used to collect HYDROSWEEP data.

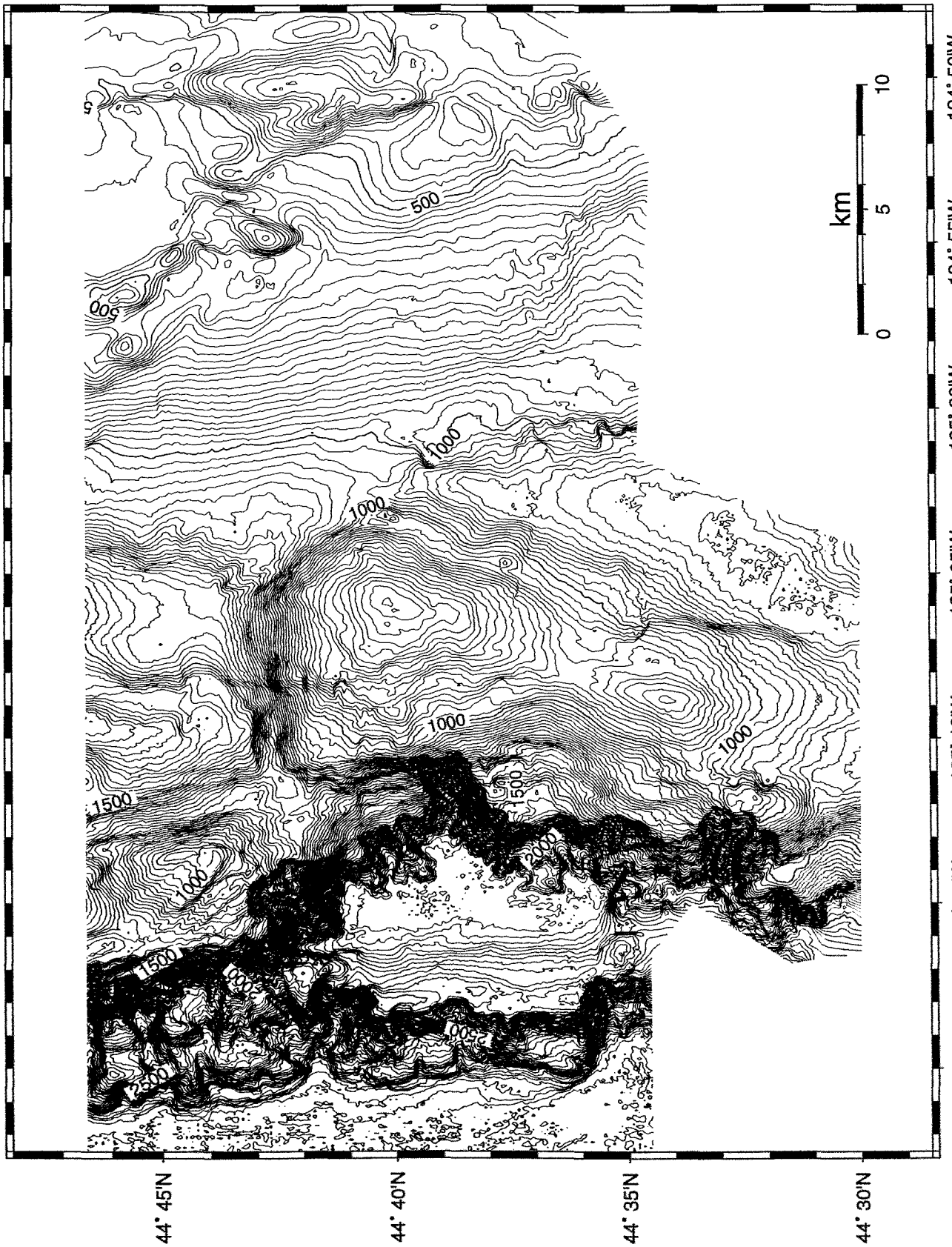

Fig. 7: Bathymetric map of the working area looking northwest. Contour interval is 20 m.

Fig. 8: Perspective view of the working area. Azimuth is 150 degrees, tilt angle is 25 degrees.

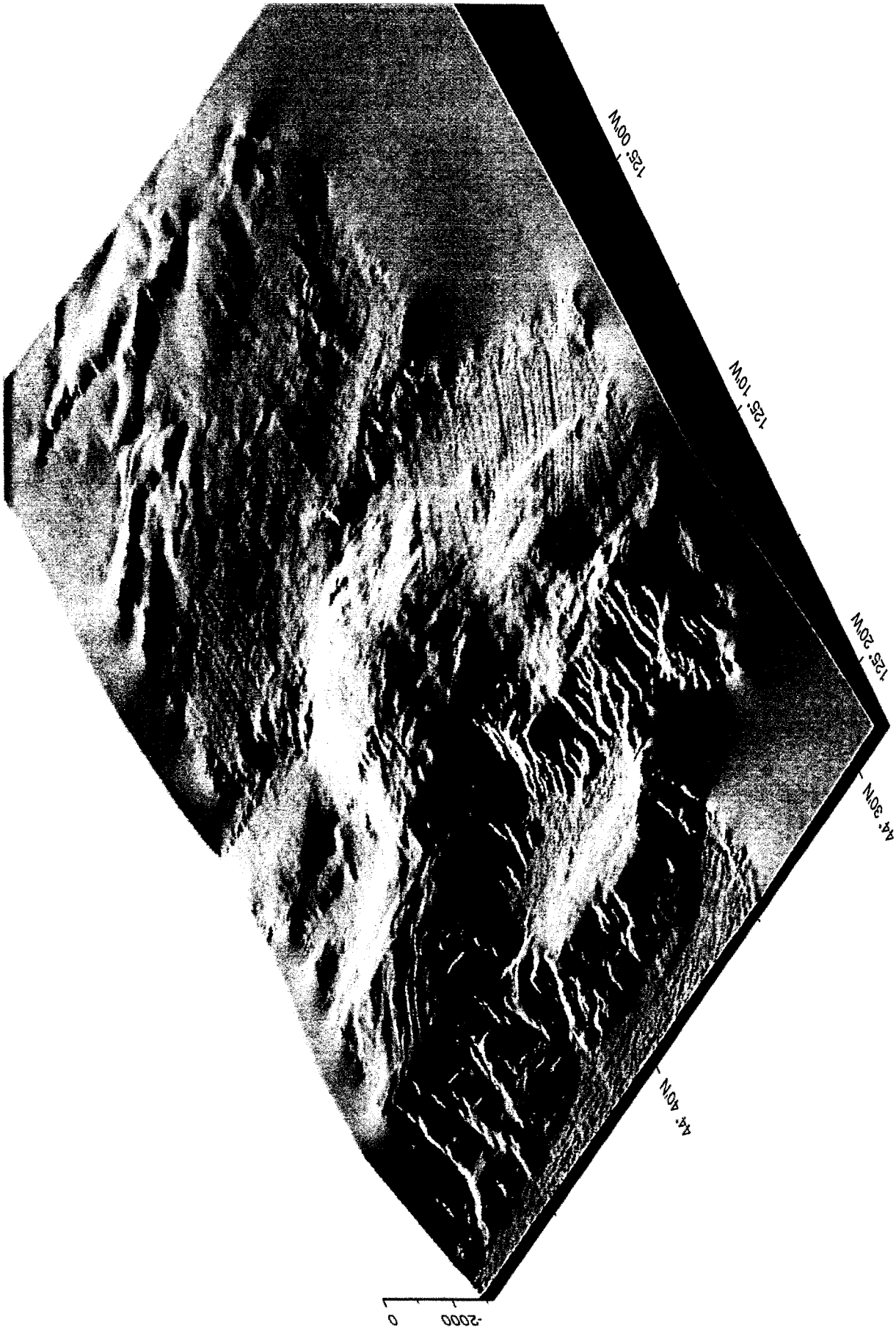

Fig. 9: Perspective view of the working area looking northeast. Azimuth is 220 degrees, tilt angle is 35 degree.

4 Water column sampling program

4.1 Introduction

In this portion of the report, we summarize studies of the water column carried out using the CTD-Rosette sampling system. Other water samples were collected from near-bottom vehicles including VESP and ROPOS, these programs are discussed elsewhere. The five CTD and related water sample locations are shown in Fig. 10 and are tabulated in Tab. 2. Note that since many CTD stations were collected during SO109, we have included the location of those stations on the map for the purpose of discussions to follow.

Table 2: Locations of CTD stations.

Station	Latitude	Longitude	Water depth (m)	Description
03-1	44°39.30'N	125°06.29'W	699	current meter site
06-1	44°39.27'N	125°06.38'W	644	current meter site
10-1	44°39.31'N	125°06.24'W	631	current meter site
12-1	44°40.15'N	125°05:86'W	596	bubble site
16-1	44°40.11'N	125°05.81'W	597	bubble site

Water samples were collected for helium isotopes and tritium (Winckler), methane and methane isotopes (Zuleger and Jones), nutrients (Dählmann and Domeyer) and trace elements (Collier). Methane and nutrients analyses were performed onboard and are discussed below. The other chemical species will be analysed after the cruise.

4.2 CTD program

G. Winckler, R. Collier

The CTD (Conductivity-Temperature-Depth) and associated rosette water sampling system was the new GEOMAR system (the same as used on SO109). The instrumentation package included a Sea-Bird 911plus CTD (S/N 09P10108-0410) with temperature, conductivity, and pressure sensors. The instrument also logged data from a SeaTech 25cm transmissometer and a Datasonics altimeter. The rosette system was a Sea-Bird model 32 twelve-position rosette pylon (software controlled) with 10-L Niskin-type water samplers. The calibration coefficients in the seasoft.con file are the same as used in SO109 and will need correction to the transmissometer coefficients post-cruise. Downcasts proceeded continuously at 50 meters/minute until the bottom-trigger alarm sounded and the altimeter was generally brought to within 3-5 meters above bottom. The first water sample was generally collected at this point; the balance collected on the upcast. Separate data files were collected and processed for each down and up cast and are stored and processed with the file naming format: STN#-1.* and STN#-1UP.*.

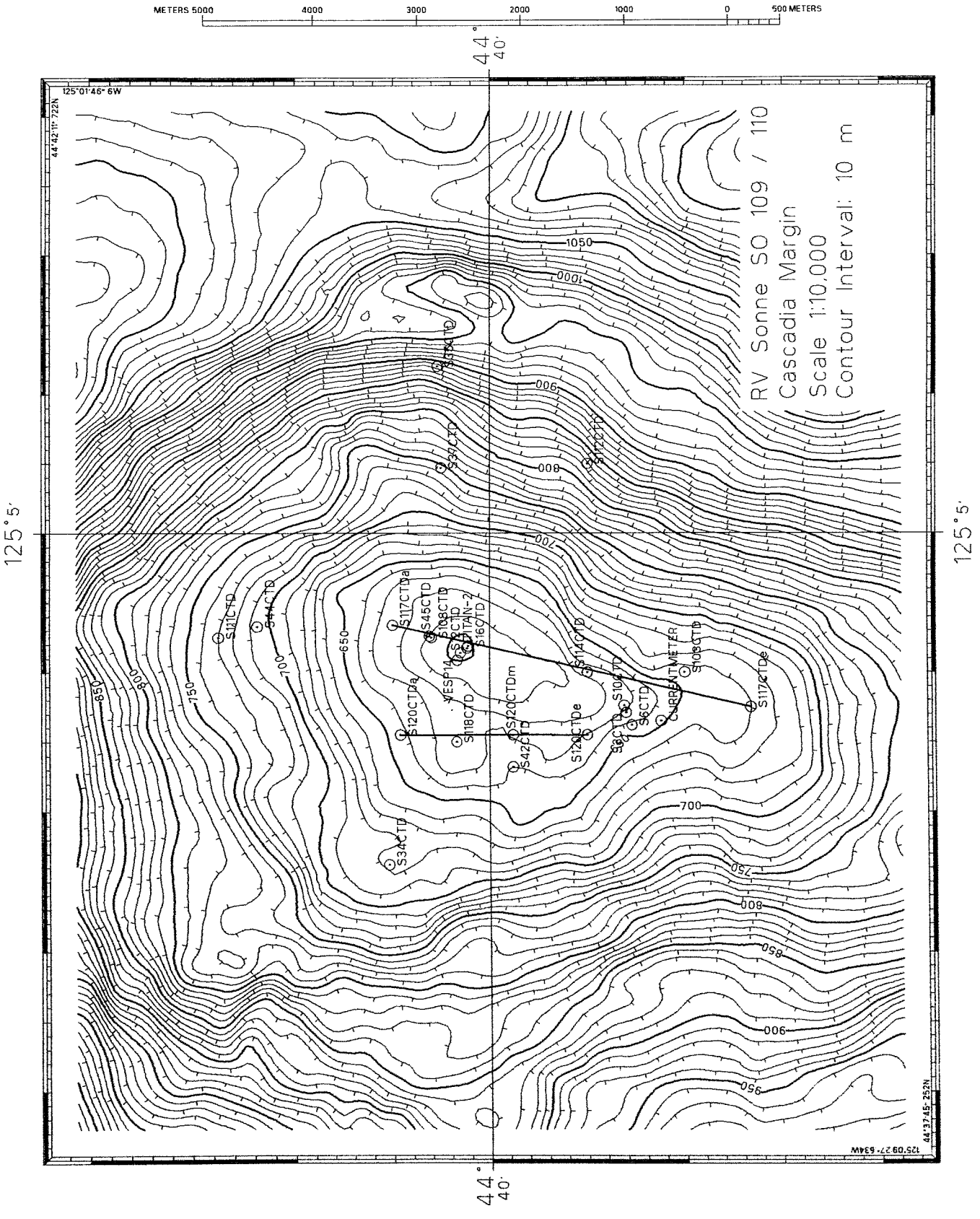

Fig. 10: Map showing CTD locations from SO110-1a and other related sites, including CTDs from cruise SO109.

Table 3: Samples collected from CTD 3-1.

Sample ID bottle	depth (m)	CH4 conc. GEOMAR	CH4 conc. VBC	CH4 isotope analysis VBC	3He/4He Uni HD	metals OSU GEOMAR	nutrients GEOMAR
1	625	x	x	x	-	x	x
2	609	x	x	x	-	-	x
3	595	x	x	x	x	x	x
4	582	x	x	-	-	-	x
5	564	x	x	x	x	x	x
6	550	x	x	-	x	-	x
7	535	x	x	x	x	x	x
8	516	x	x	-	x	x	x
9	499	x	x	x	-	-	x
10	485	x	x	-	-	-	x
11	468	x	x	x	x	x	x
12	449	x	x	-	-	x	x

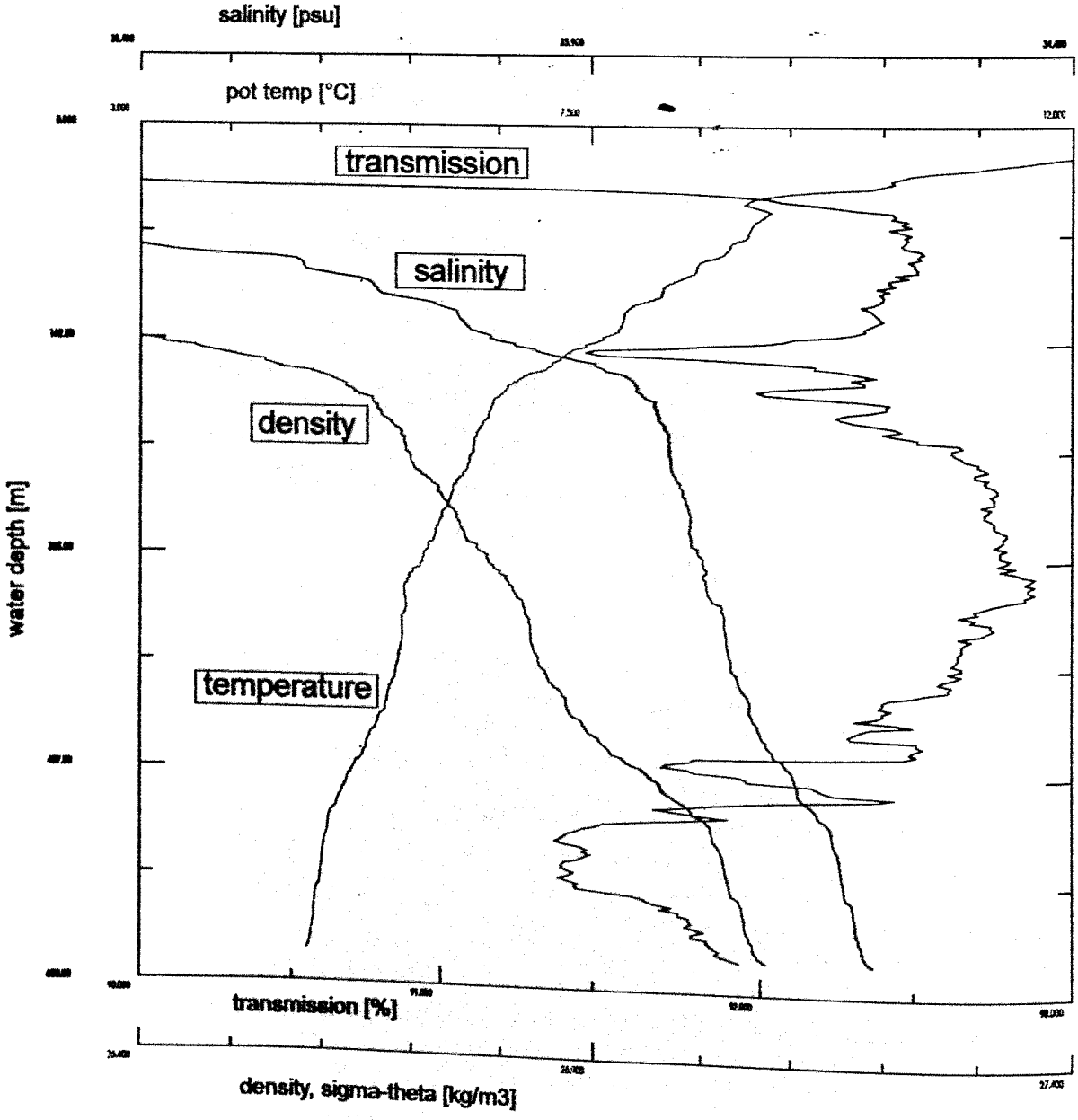

Fig. 11: Hydrographic data from CTD 3-1.

Table 4: Samples collected from CTD 6-1.

Sample ID bottle	depth (m)	CH4 conc. GEOMAR	CH4 conc. VBC	CH4 isotope analysis VBC	3He/4He Uni HD	metals OSU GEOMAR	nutrients GEOMAR
1	634	x	x	x	-	x	x
2	599	x	x	x	-	x	x
3	575	x	x	x	-	-	x
4	556	x	x	x	-	x	x
5	534	x	x	x	-	x	x
6	517	x	x	x	-	-	x
7	506	x	x	x	-	x	x
8	489	x	x	x	-	x	x
9	475	x	x	x	-	-	x
10	475	x	x	x	-	-	x
11	460	x	x	x	-	x	x
12	445	x	x	x	-	x	x

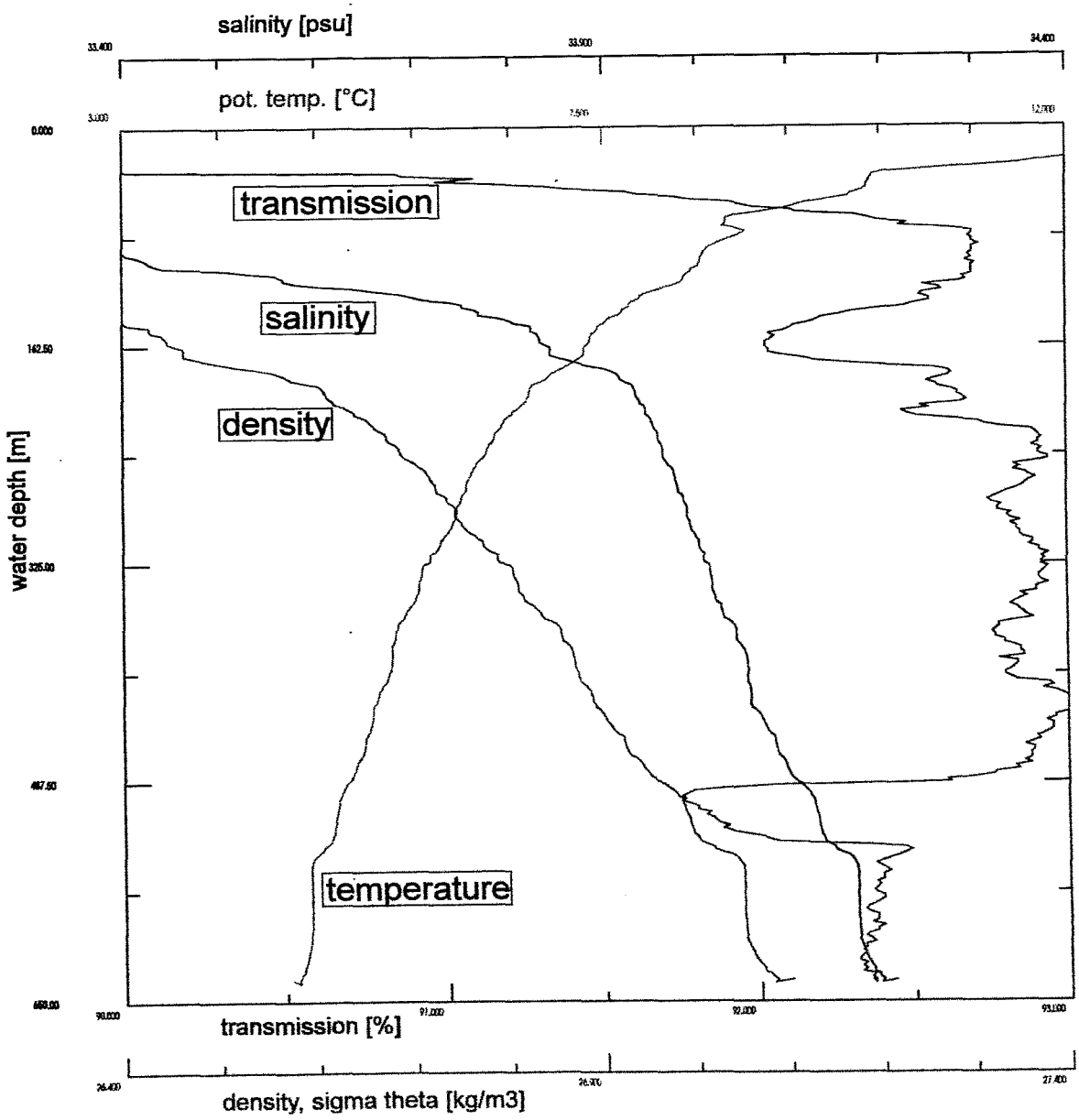

Fig. 12: Hydrographic data from CTD 6-1.

Table 5: Samples collected from CTD 10-1.

Sample ID bottle	depth (m)	CH4 conc. GEOMAR	CH4 conc. VBC	CH4 isotope analysis VBC	3He/4He Uni HD	metals OSU GEOMAR	nutrients GEOMAR
1	619	x	-	-	-	x	-
2	600	x	-	x	-	x	-
3	576	x	-	-	-	x	-
4	555	x	-	x	-	x	-
5	535	x	-	-	-	x	-
6	518	x	-	x	-	x	-
7	505	x	-	-	-	x	-
8	490	x	-	x	-	x	-
9	475	x	-	-	-	x	-
10	460	x	-	x	-	x	-
11	445	x	-	-	-	x	-
12	399	x	-	x	-	x	-

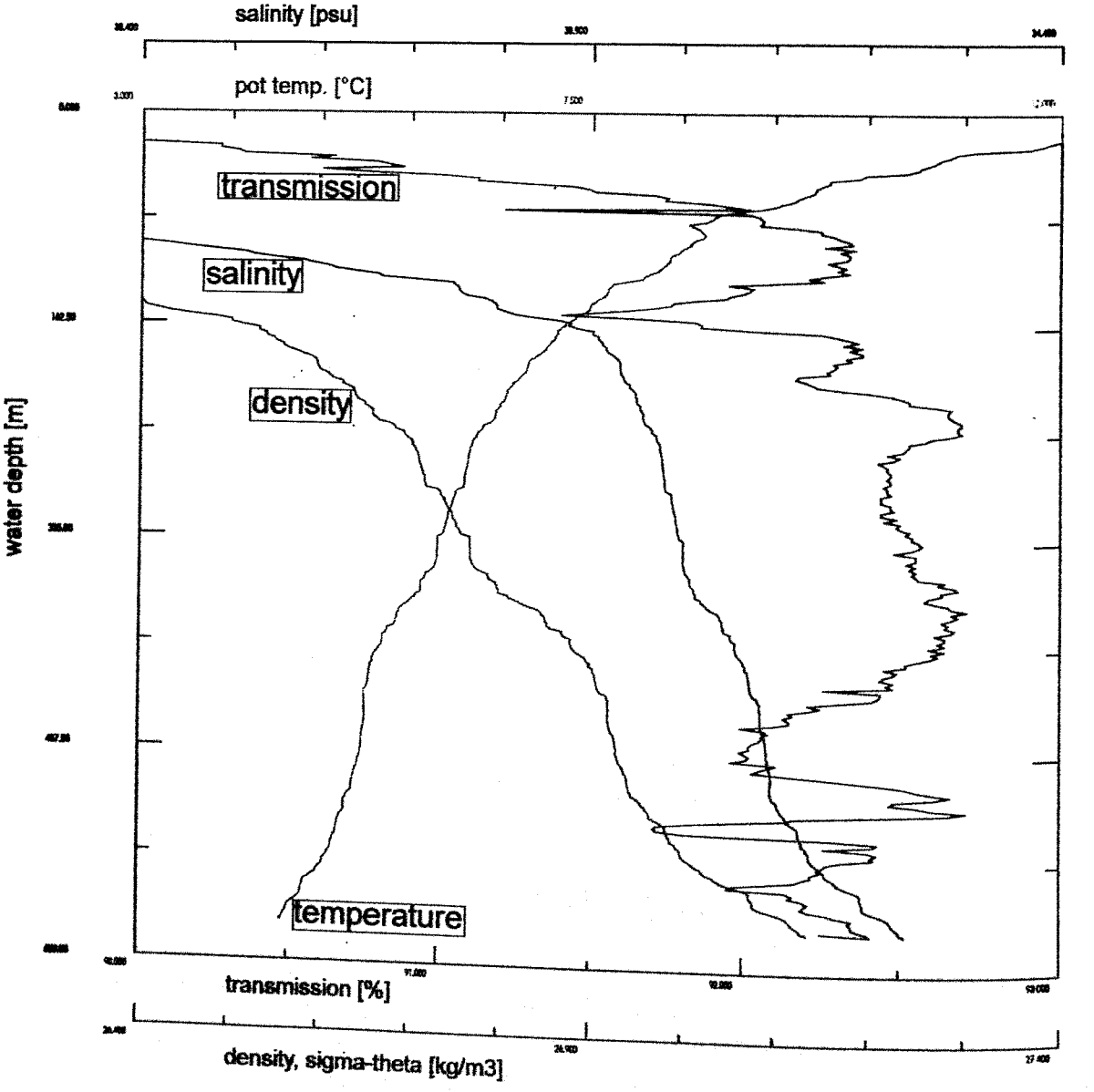

Fig. 13: Hydrographic data from CTD 10-1.

Table 6: Samples collected from CTD 12-1.

Sample ID bottle	depth (m)	CH4 conc. GEOMAR	CH4 conc. VBC	CH4 isotope analysis VBC	3He/4He Uni HD	metals OSU GEOMAR	nutrients GEOMAR
1	584	x	x	x	x	x	x
2	575	x	x	x	x	x	x
3	565	x	x	x	x	x	x
4	550	x	x	x	x	x	x
5	535	x	x	x	x	x	x
6	520	x	x	x	x	x	x
7	504	x	x	-	x	x	x
8	490	x	x	x	x	x	x
9	475	x	x	x	-	x	x
10	450	x	x	x	-	x	x
11	418	x	x	x	-	x	x
12	355	x	x	x	x	x	x

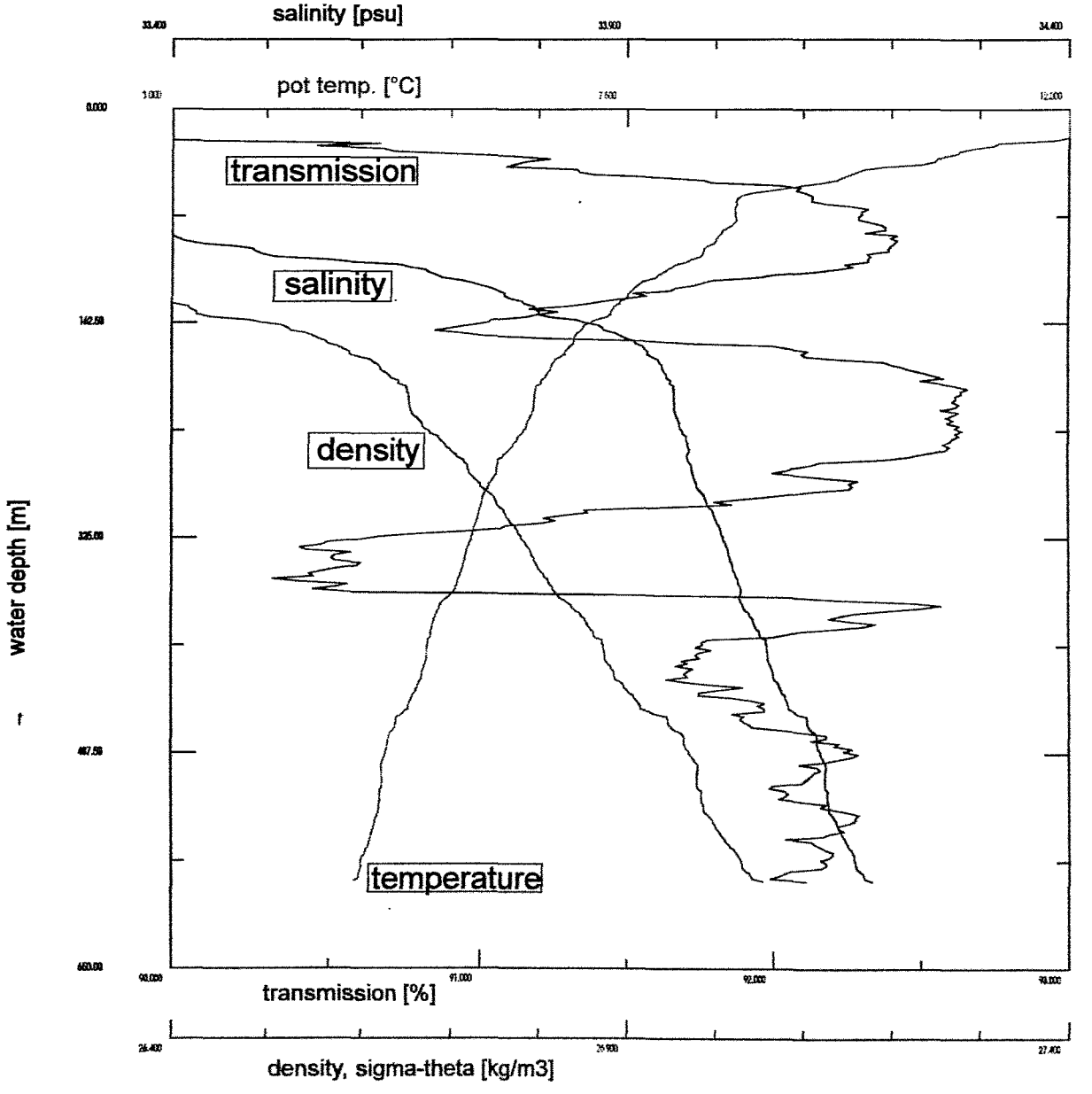

Fig. 14: Hydrographic data from CTD 12-1.

Table 7: Samples collected from CTD 16-1.

Sample ID bottle	depth (m)	CH4 conc. GEOMAR	CH4 conc. VBC	CH4 isotope analysis VBC	3He/4He Uni HD	metals OSU GEOMAR	nutrients GEOMAR
1	590	x	x	x	x	x	x
2	565	x	x	x	x	x	x
3	545	x	x	x	x	x	x
4	524	x	x	-	x	x	x
5	510	x	x	x	x	x	x
6	495	x	x	x	x	x	x
7	480	x	x	x	x	x	x
8	468	x	x	x	x	x	x
9	457	x	x	x	x	x	x
10	444	x	x	x	x	x	x
11	430	x	x	x	x	x	x
12	409	x	x	x	x	x	x

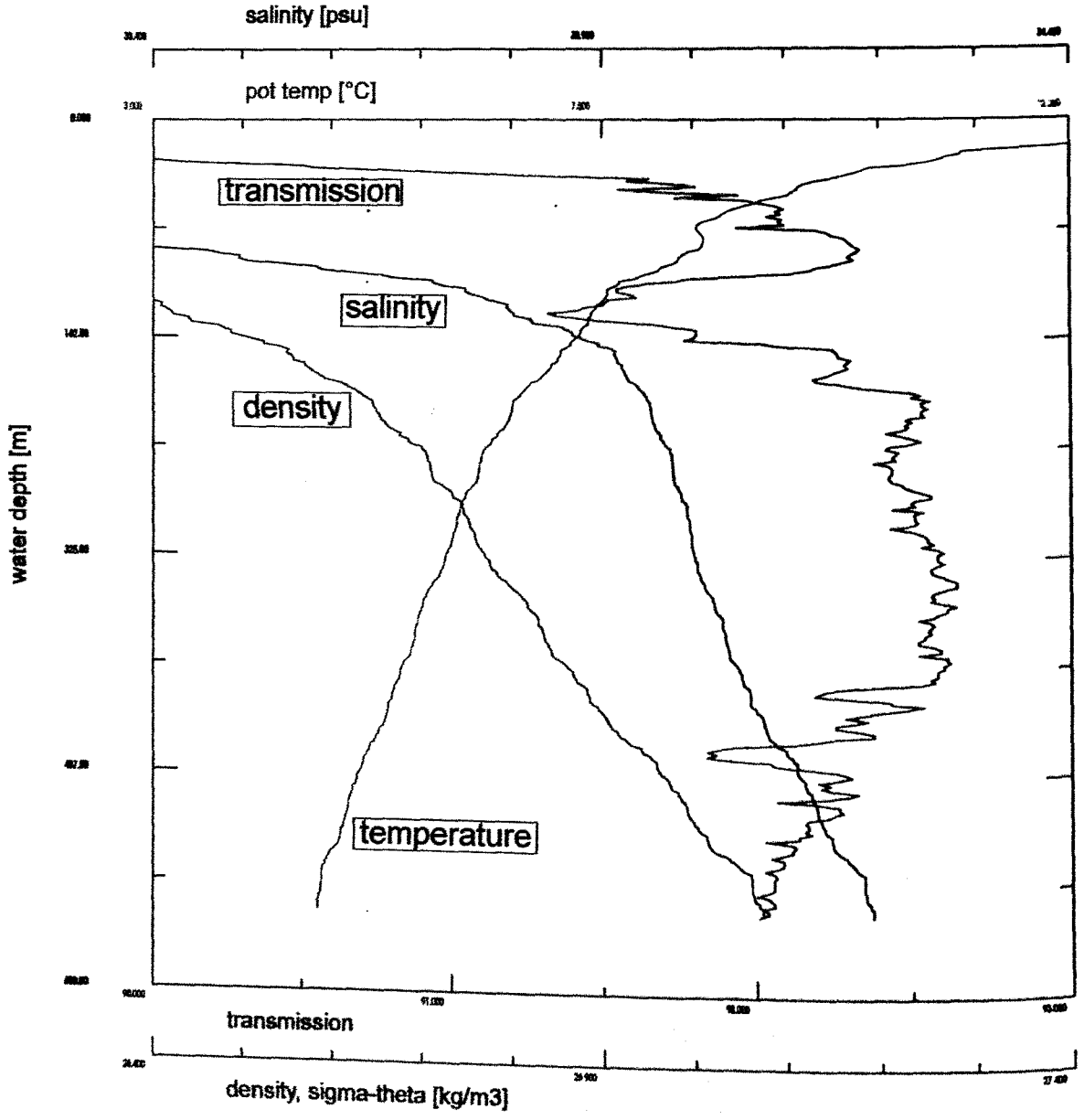

Fig. 15: Hydrographic data from CTD 16-1.

Five CTD stations were occupied - three near the current meter site and two at the summit of the northern portion of the ridge, near the observed vents. In general, there was significantly more particulate matter in the deep water column compared with the previous SO109 cruises, as demonstrated by the transmissometer results (Figs. 11-15). These nepheloid layers in this region are commonly related to near-bottom contact with the shelf/slope and transport off-shore. There was frequently a secondary subsurface maximum near 160m which is probably associated with the shelf break. A very strong particle maximum was observed at station 12-1 at 340 meters depth which was not repeated at any of the other stations. A remarkably well-mixed layer (in T, S, transmission) was observed in the bottom 100m at station 6-1. Again, this was not repeated at any of the other stations. In general, there was little structure in the deep pycnocline that could be created by significant fluid venting nor which would act as a particular trap for chemical anomalies.

Methane anomalies (see below) were generally observed near the bottom or, most commonly, between 480-530m depth. The bottom anomalies are easily understood by their proximity to the source, be it through gas or fluid phase transfer. The shallower anomalies have puzzled earlier investigators including those of SO109, because they are located well above the shallowest local bathymetry (~590m). The rise of nearly 100m depth requires significant buoyancy which was definitely not observed in the density profiles. Therefore, this system does not appear to behave as a buoyant hydrothermal plume. Rather, we hypothesize that the methane is transported to shallower depths as a gas (observed at one of the EXPLOS surveys through this site). The methane distribution in the water column is then a complex function of the physics of bubble injection, rise, dissolution, and horizontal transport by currents. We did not see any "major" bubble plumes -- either accoustically or visually -- yet these are inferred by the huge methane concentrations observed. The variability of depths (density) where the methane maxima have been observed is consistent with this mechanism of transport/equilibration of the signal from the bottom. We note that huge concentrations of methane were observed in some bottom waters collected by ROPOS in the absence of direct bubble injection. Some of the venting fluids are also nearly saturated in methane. At this point, it is premature to estimate the relative flux of methane via gas or fluid transfer, however both are large!

Trace element analyses and noble gas isotope analyses could help separate fluid transfer (which would carry pore fluid trace element anomalies as well) from gas-phase tranfer, which is presumeably pure methane gas and would leave no other major or minor element anomaly in the water column.

4. 3 Methane analyses

E. Zuleger, N. Jones

On-board analysis of methane in water samples serves as a quick and simple means of acquiring information about both the methane distribution in the water column and the flow rates of methane from cold seeps into the ocean. Dissolved methane in the water column is a known indicator of both hydrothermal and

cold vent activity, allowing methane analysis to serve as a useful means of determining further site locations. In the main target area of the SONNE 110-1a expedition, the Oregon subduction margin, water samples were taken mainly near the bottom up to about 350 m depth using a hydrocast rosette. In addition, water samples were taken from areas of vent activity, indicated by the presence of clam fields, by VESP and ROPOS. Immediately after sampling, water was degassed by a headspace vacuum-ultrasonication method and analysed by GC. Additionally, samples were taken for high precision shore determination of CH_4 and $\partial^{13}CH_4$ by helium stripping and GC/GC-C-IRMS analysis.

On-board analyses of dissolved methane were performed using a vacuum-ultrasonication degassing method (Schmitt et al., 1991, Lammers & Suess, 1994) and subsequent determination with a Shimadzu GC 14A gas-chromatograph. This technique yields 70% with 5% standard deviation of measurements (subject to modification after the intercalibration with the He-stripping). This simple and easy-to-handle method has the advantage of a higher sensitivity compared to normal head-space techniques and allows for the results from one hydrocast (max. 12 samples) within 4 hours after recovery. In addition, on shore high precision analyses of CH_4 and $\partial^{13}CH_4$ are planned for selected samples at the School of Earth and Ocean Sciences at the University of Victoria using a total yield helium stripping technique and GC/GC-C-IRMS determination. This method yields aproximately 100% of the dissolved methane with standard deviations of less than 2%. The results of the He-stripping will be used for an improved calibration of the vacuum/ultrasonic method. However, the vacuum/ultrasonic method is a quick tool for the detection of fluid expulsions which avoids interference with He isotope measurements on board.

During Leg 110-1a the data set of dissolved methane in the water column for the Cascadia Margin was very successfully expanded by a total of 60 samples from five hydrocasts (Tab. 2). Three hydrocasts (at stations 3-1, 6-1, 10-1), equipped with 12 Niskin water bottles, were taken in the vicinity of the current meter location (125°06.3′ W; 44°39.4′ N), south of the summit of the northern part of the second ridge of the Cascadia margin, to investigate tidal influences on the methane data. Two hydrocasts were taken at the summit of the northern part of the second ridge, at the so called bubble-field, yielding the highest methane concentrations found thus far at the Cascadia margin, or perhaps anywhere in the world.

The sample locations are plotted in Fig. 10 and the methane concentration data from these five CTD casts are listed in the appendix.

All five hydrocast profiles (Figs. 16a and 16b) show a methane anomaly at approximately 450 to 550 m depth. While the profiles at the current meter location have maxima of 270, 160, and 160 nL/L respectively, the samples from the bubble-field show much higher values of nearly 0.1 mL/L. Profiles from stations 3-1 and 10-1 also appear to have a second anomaly near 580m depth, with values of approximately 120 nL/L. The background value for these samples is aproximately 60 nL/L.

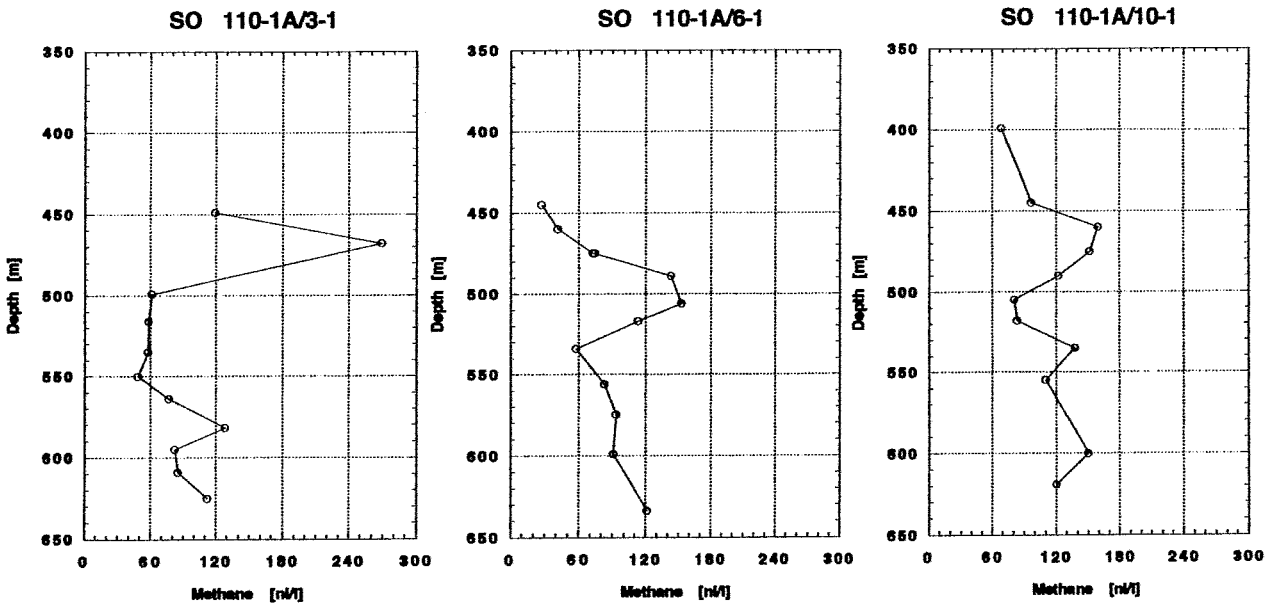

Fig. 16a: Methane distribution at the current meter site (44°39.3′ N; 125°06.3′ W).

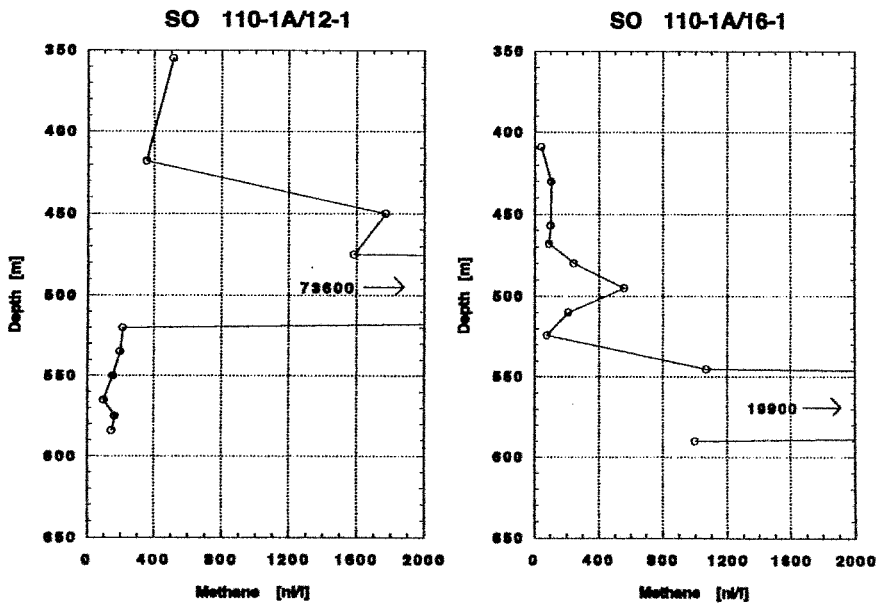

Fig. 16b: Methane distribution in the water column at the bubble field (44°40.1′ N, 125°05.8′ W).

Of the samples taken near the bubble-field, station 16-1 shows an anomaly at 500 m of 557 nL/L and a second even higher anomaly at a depth of 565 m of 19,259 nL/L. Station 12-1 has only one anomaly between 450 and 550 m with methane values up to 73,000 nL/L. In both cases the background is slightly higher at 100 nL/L and 200 nL/L, respectively. In comparison, stations SO109-45-1 and SO109-108-1, which are in close vicinity to stations SO110-12-1 and 16-1, show much lower background levels of 40 nL/L, and much smaller anomalies. Station SO109-

45-1 has a maxima similar to that of all stations in SO110-1a, with 1159 nL/L at aproximately 500 m depth, while the maximum at station SO109-108-1 is located near the seafloor at 596 m with 429 nL/L.

Additionally, several water samples were taken by VESP in the bubble-field region, and by ROPOS during dives 340 and 341. Further detail and the results from these samples can be found in the apropriate sections of this report.

4. 4 Nutrients

A. Dählmann, B. Domeyer

Water samples from CTD were filtered through 0,2 µm cellulose acetate membrane filters and analysed for silicate, nitrate and ammonia, partly by using an autoanalyser system. For further details concerning the analytical methods see chapter 9.

The distribution of nutrients throughout the water column (Fig. 17) shows no evidence for any anomaly, even for those CTD's where methane plumes were observed (CTD 12 and 16; Fig. 16). A relatively high concentration of phosphate at 480 m in CTD 16 is probably not due to the increased methane concentration at 495 m, as much higher contents of methane at greater depths are not accompanied by higher phosphate values.

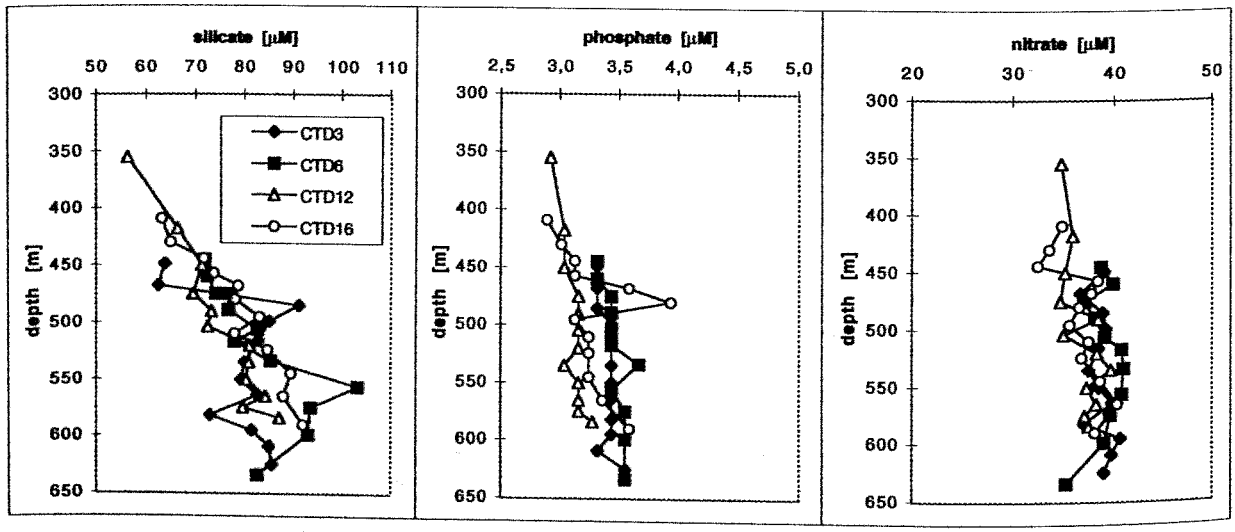

Fig. 17: Nutrients in CTD-rosette water samples.

4. 5 Current meter

R. Collier

The first activity upon arriving at the Bioherm Site (SO110-01-1) was the deployment of a current meter to monitor local bottom currents. The goal of this experiment was to provide the CTD sampling program with the background currents within which we could better locate the origin and dispersion of water

column anomalies generated by gas and/or fluid flow from the site. The deployment was set for ~2.5 days in order to capture several tidal cycles which we suspected might play a significant role in the currents at this site (several reoccupations of the same CTD sites had resulted in significantly different profiles during SO109-1 and 2).

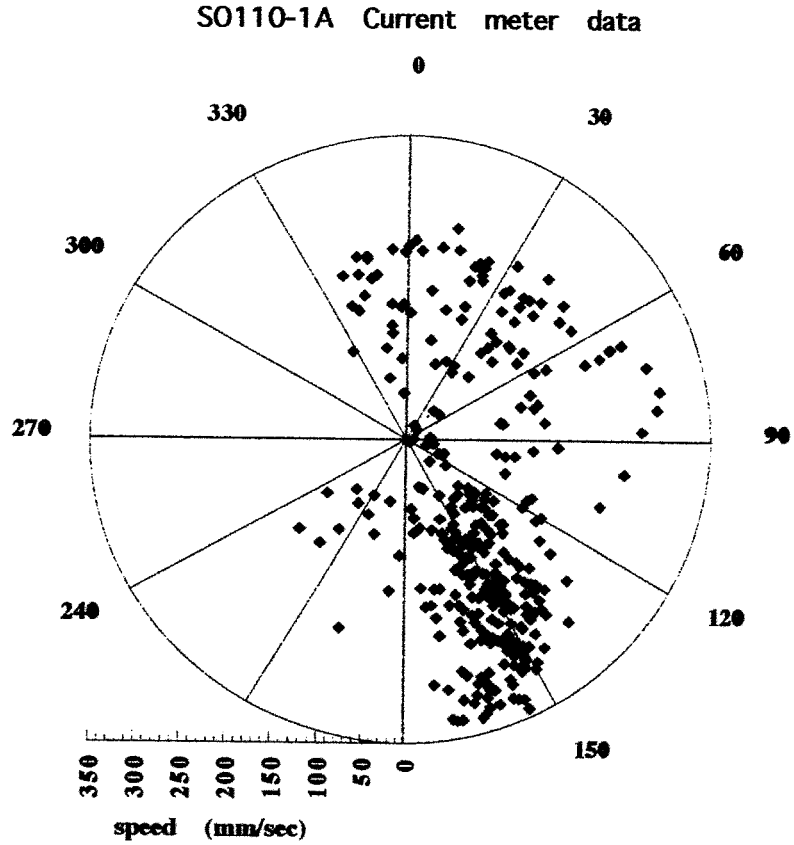

Fig. 18: Polar plot of current direction (q) and speed (r), each point represents one 9-minute period.

We used a microprocessor-controlled vector-averaging current meter (VACM, Alpha Omega model 9407) with sensors to measure water temperature, pressure (depth), rotor speed and vane direction (relative to the meter) and a compass to record the meter orientation relative to the Earth. We set the processor to record the average scalars and current vectors over a 9 minute window, repeated every 10 minutes (6 values per hour).

The small mooring was composed of one 17" benthos glass float (55 lbs floatation) in the center of a weighted spar system with a pressure-actuated strobe flasher and radio transmitter (27.045kHz) for recovery.Seven meters below, the current meter was mounted on the mooring line. Two meters below the current meter was a microprocessor release (Alpha Omega model 9311), set to melt a 200-lb monofilament weak-link at a user-programmed time. The 100-lb anchor was located three meters below the release.

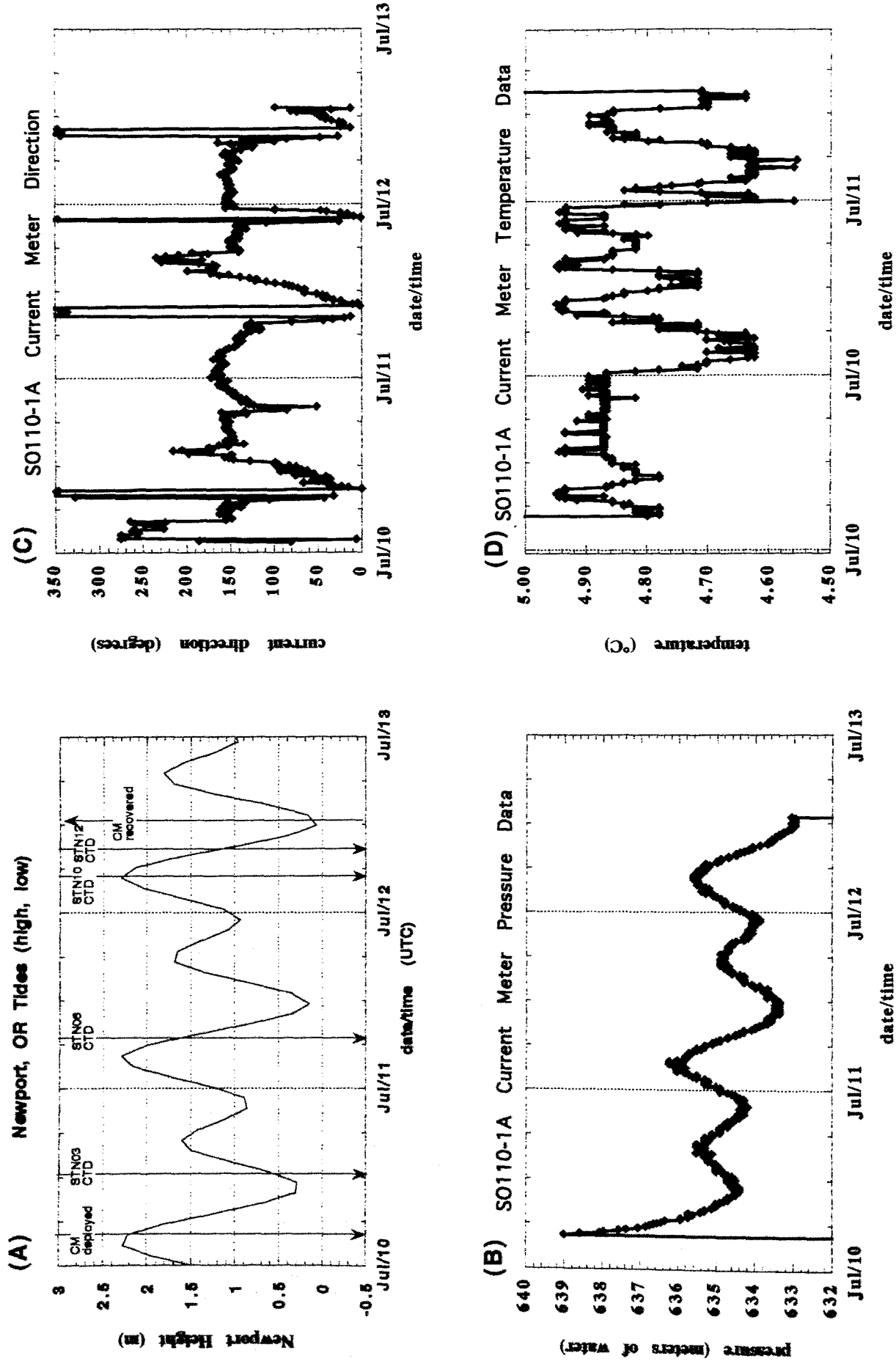

Fig. 19: a) Tide cycle at Newport, Oregon; b) current meter pressure (sea level above meter); c) current meter flow direction; d) current meter temperature data (preliminary calibr.).

The mooring was deployed on July 10, 1996 at 04:26 (UTC), dropped at 44°39.12' N, 125°06.35' W. This was located on the 640m isobath at the southern end of the northern ridge. This is approximately 2000 meters south and 50m below the peak of the ridge (Fig. 10). We placed the meter slightly outside of the primary work area so as not to interfere with ROPOS and other near-bottom operations. The mooring released at 13:00 on July 12, was spotted at the surface 15 minutes later, and was in the lab for data recovery by 13:30. At this point, the data logger contained approximately 350 data records.

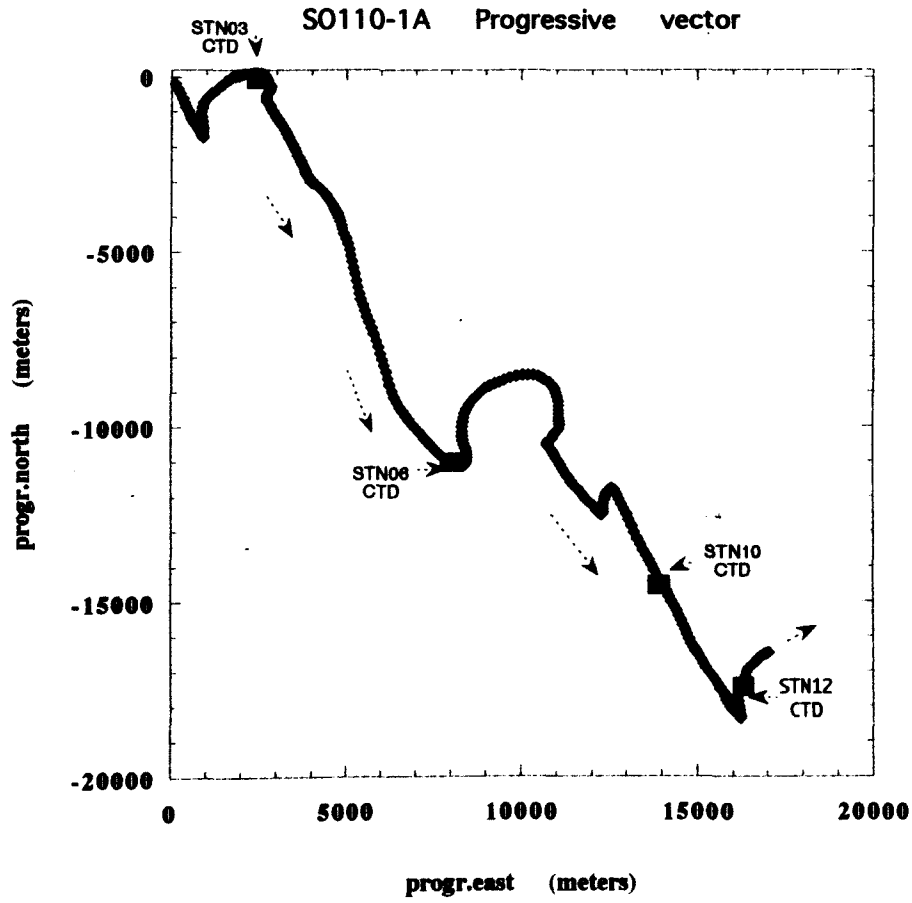

Fig. 20: Progressive vector diagram indicating flow path of an idealized parcel of water following the current meter results.

This brief experiment demonstrated relatively consistent SSE flow (150°) with an average current of ~2 cm/sec. There was clear tidal influence on both the water elevation and the current direction, but the average currents were still to the south (Fig. 18). The tidal phase was almost identical to the tides at Newport, OR (Fig. 19) with a vertical excursion of ~2 meters. There was one period in each tidal cycle that resulted in a circular deviation of the current direction, however the strength of the current during this period was weak. Shortly after the diurnal high tide, the current rotated briefly towards the NNE but rapidly recovered to the SSE before the diurnal low. Significant temperature excursions were also

observed ranging between 4.65-4.85°C (Fig. 19). Within the ambient thermocline, this variation represents nearly 80m of vertical displacement. At this point it is unclear if these changes are related to internal waves or other short term changes in the thermocline structure. Generally, the currents move water along a NW to SE path (Fig. 20). Further discussion of the hydrography is presented in the CTD data section above.

5 ROPOS and VESP operations

5.1 Introduction
P. Linke

ROPOS (**R**emotedly **O**perated **P**latform for **O**cean **S**ciences) was designed and developed in Canada as a cost-effective, fully-equipped, remotely-operated deep-submergence vehicle with complete sampling capabilities. GSC, NOAA, and U. Victoria have worked together to develop ROPOS for the ongoing study of active volcanic and hydrothermal sites on the Juan de Fuca Ridge, including the Axial Volcano, since 1990. Researchers at GSC and at partner institutions in Canada and in the U.S. have employed ROPOS extensively on the Juan de Fuca Ridge.

The ROPOS system consists of 3 major parts (deck unit, cage and ROV). The deck unit includes the winch, winch hydraulics, power supply and the consoles for the remote operation of the vehicle by the 2 pilots and the chief scientist. The ROV is placed in a cage during launch and recovery. Approximately 30 m above the ocean floor the vehicle is released and leaves the cage with it's five 30 horsepower thrusters. With this 2 piece separation the up and down movement of the ship is transmitted only to the cage, whereas ROPOS manoevers unaffected by these movements, connected to the cage with a 200m positively buoyant tether. The vehicle itself is neutrally buoyant and carries 2 manipulators and 2 video cameras (SIT and colour) for on-line video transmission.

An important engineering objective of the previous SO109-3 cruise was to demonstrate the full range of technical abilities of ROPOS operating from the German RV Sonne. Until then, ROPOS had been operated from only two research vessels with a demonstrated compatibility with the system (a DFO vessel in Canada and a NOAA vessel in the U.S.). The HYDROTRACE expedition was the first deployment of ROPOS from a non-Canadian/non-U.S. vessel and the first real test of its portability. The testing of ROPOS during SO109-3 has provided the German research community with the opportunity to observe the capabilities of the vehicle and will stimulate further collaborative research between German, Canadian and U.S. partners. Germany has made a substantial investment in ROPOS operations for 1996-97, and testing of the ROV during SO109-3 was a critical step in the development of ROPOS as an international scientific facility.

Major modifications to the ROPOS system had been made to undertake operations during HYDROTRACE, including the preparations for installation of a new 5,000 m fiber optic cable. Engineering tests and method development also included the implementation of long-baseline navigation (SeaScape) for ROPOS, establishing links between shipboard navigation and the NOAA SeaScape bottom transponder system and operation of the new U. Victoria high-resolution BETACAM video system.

In order to obtain water samples and in situ flow rates from cold seeps we developed a TV-controlled device for the deployment of a Benthic Barrel from a conventional surface research vessel (Linke et al., 1994). The barrel is attached to the central piston of a modified multicorer frame, which operates on a water

hydraulic basis and assures gentle deployment of the barrel once the frame settles on the sea floor. The **VEnt SamPler (VESP)** is equipped with five 5L water bottles and a storage CTD probe which is used to activate the water-sampling cycle and to continuously record conductivity, temperature, pressure and flow data.

The Benthic Barrel is a commercially available 55-gallon polyethylene barrel with a large opening at the bottom and a small exhaust port at the top. The chamber is deployed over a suspected vent site with the purpose of channelling the effluent from the sea floor into a semi-enclosed environment. The internal volume of the chamber is initially flooded with ambient seawater and is then slowly replaced by vented fluids. In this way a water mixture develops within the chamber with increasing amounts of vent fluid. Sequentially timed water samples are collected during deployment by bottles mounted inside the chamber. Changes in the concentration of dissolved components among these bottles are then used to calculate their flux rates (Carson et al., 1990). The exhaust port at the top of the chamber carries a thermistor flowmeter which directly records the flow rate from the chamber.

5.2 ROPOS operations, background and summary

5.2.1 Navigation

P. Linke, J. Illmann

The long-baseline transponder net at the second ridge of the Cascadia margin was established during cruise SO109-2 using the ship's SONARTRACK transponder and NOAA's EG&G deckset. The net had to be recalibrated due to the loss of DGPS and the use of GEOMAR's MORS RM301 deckset (Fig. 21). During the calibration it appeared that one of 4 transponder frequencies could not be interrogated by this new hardware configuration, which caused a reduction in navigation accuracy. For accurate navigation in the net the ROPOS system is equipped with an EDGETECH PS8000 deep-sea rangemeter linked through the fiber optic cable with the on-board navigation PC and a DATASONICS transponder on the vehicle. During VESP-operation the DATASONICS transponder was mounted with brackets on the cable and used as a relay transponder in the net.

5.2.2. ROPOS dive summary

P. Linke

ROPOS Dive 339 (Site 4) July 10, 1996

Target: Second Ridge at Cascadia Margin

Objectives: To sample cold seeps fluids, precipitates and biota.

Summary: Some operational problems were detected: communication with the DATASONICS transponder on the ROV was only possible at the beginning of the dive, ground problems in the science can meant control problems for the TV camera. Shift in the transponder net (Fig. 22).

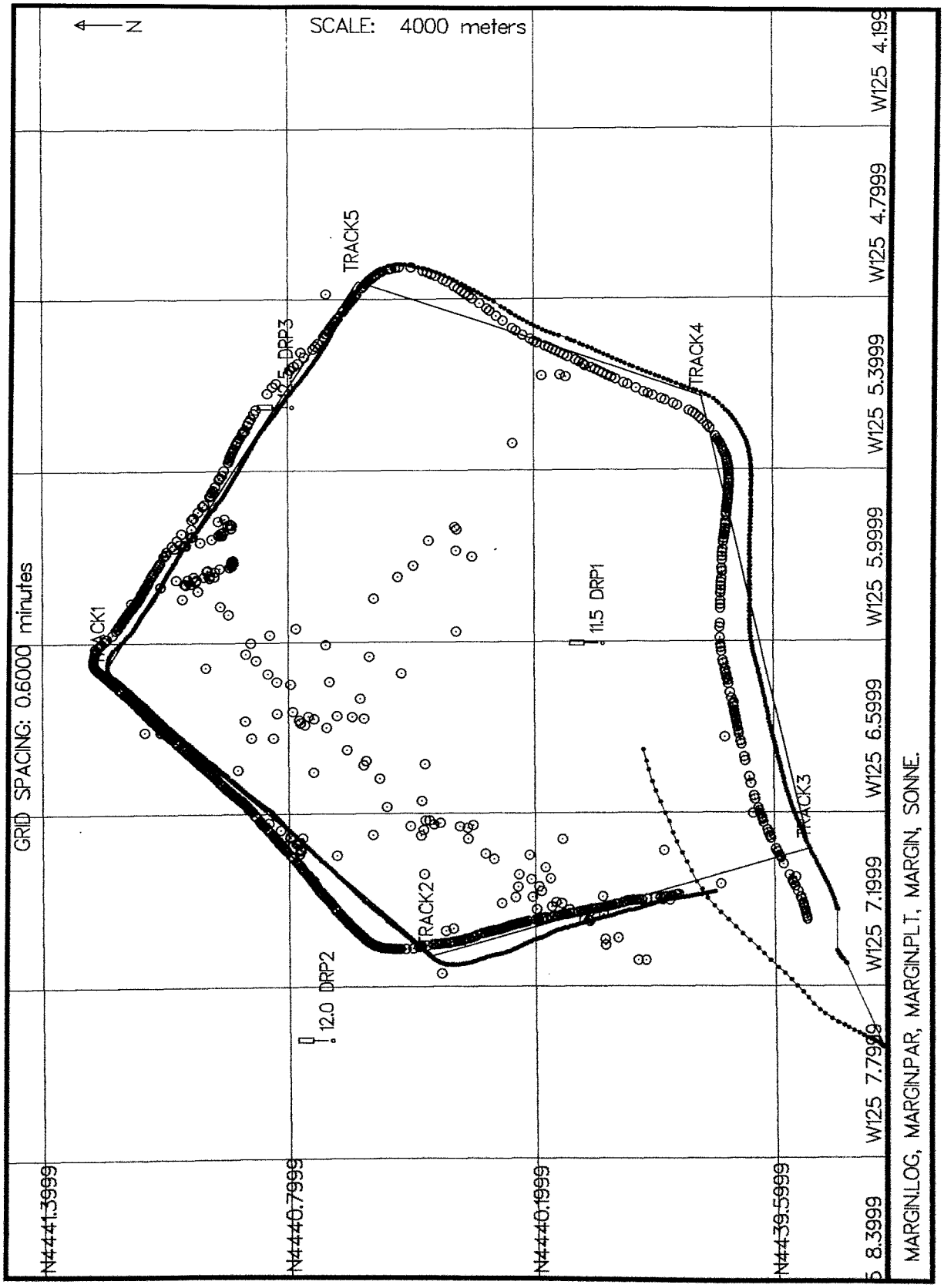

Fig. 21: Calibration of the transponder net at the second ridge at the Cascadia margin; transponder dropping position are indicated by icons.

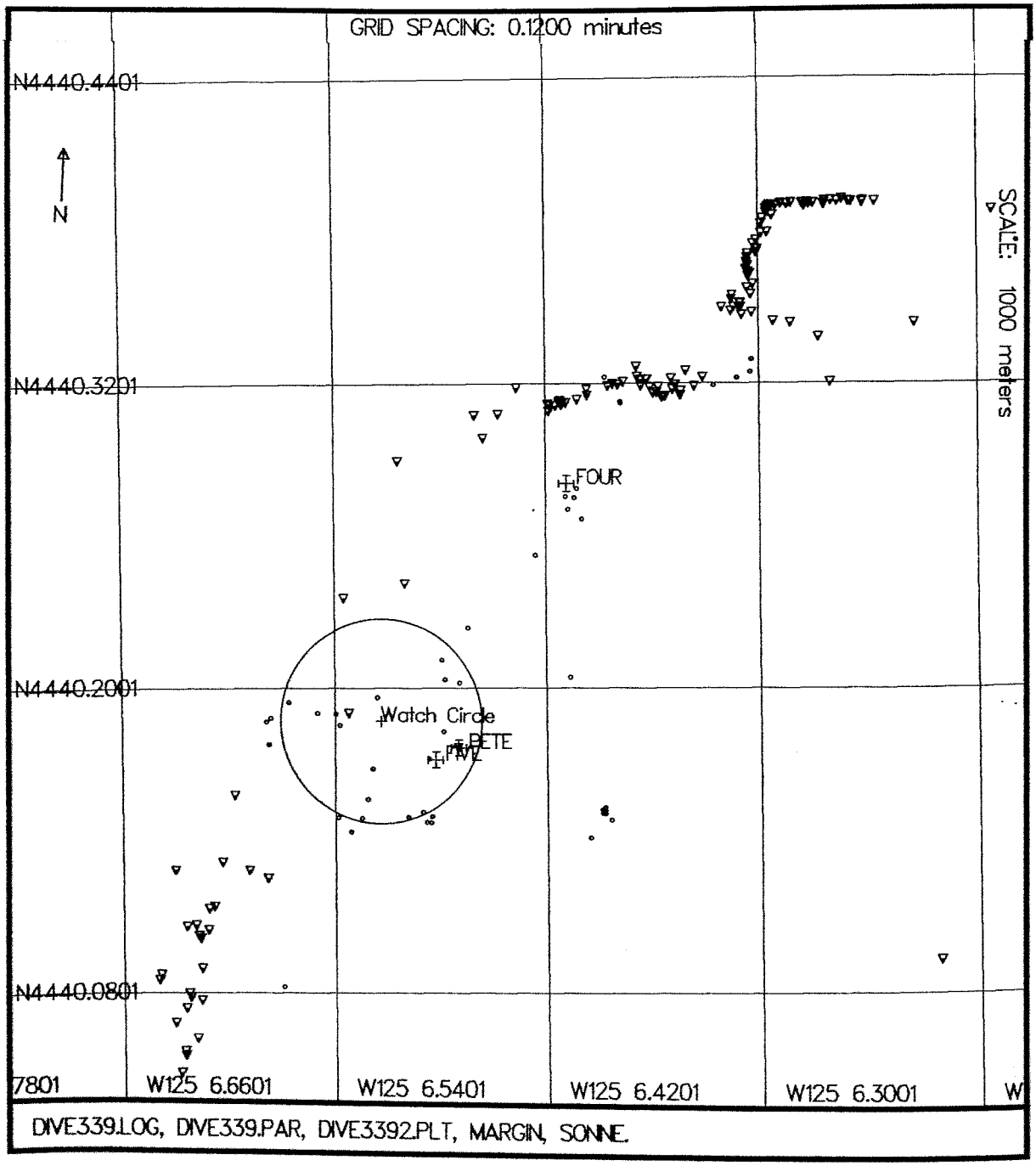

Fig. 22: Navigation plot during ROPOS Dive 339. The watch circle of the ship was shifted several times towards the south to survey the whole extent of the summit. Triangular icons represent ROPOS fixes, small circles indicate cage fixes. For better orientation ROPOS was twice taken back to the cage to get the ship's position (markers four & five), the marker 'Pete' indicates the position of a clam field where most of the sample were taken.

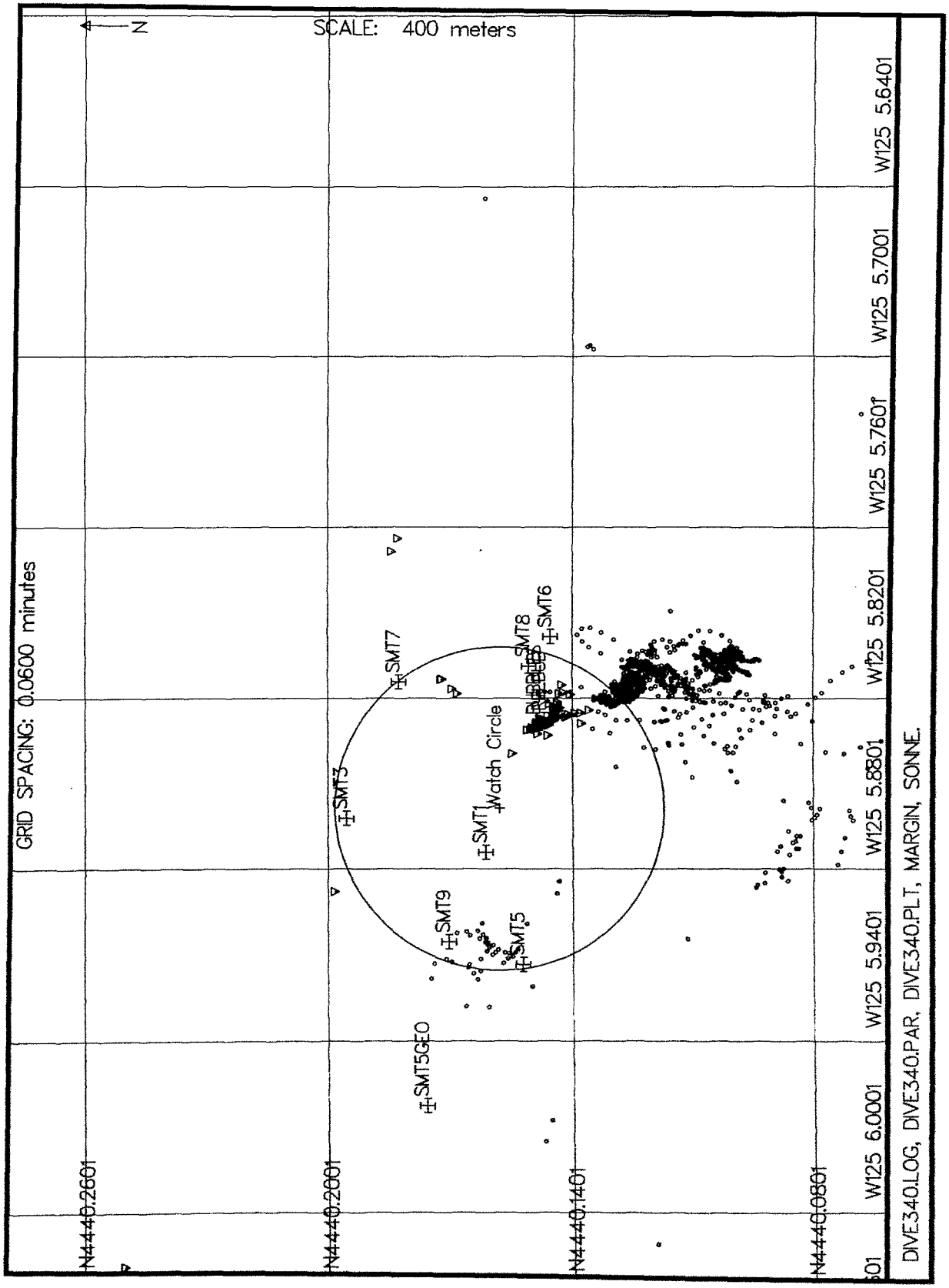

Fig. 23: Navigation plot during ROPOS dive 340. Triangular icons represent ROPOS fixes, small circles indicate cage fixes. Targets for sampling are indicated by markers (Summit = SMT 1 to 8).

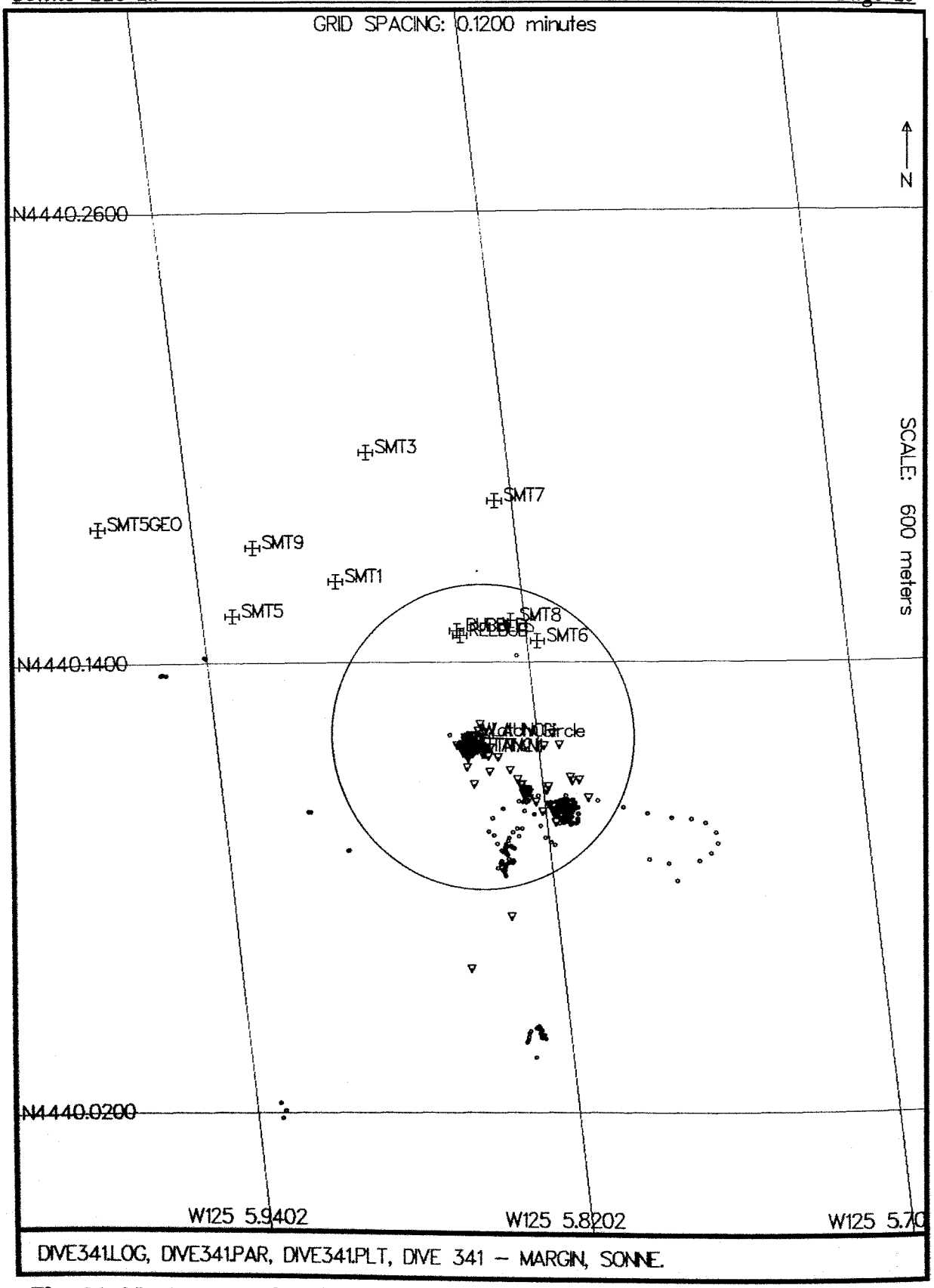

Fig. 24: Navigation plot during ROPOS dive 341. Triangular icons represent ROPOS fixes, small circles indicate cage fixes. The target for the water sampling is indicated by the marker 'TITAN'. Targets of the previous dive are indicated by markers (Summit = SMT 1 to 8).

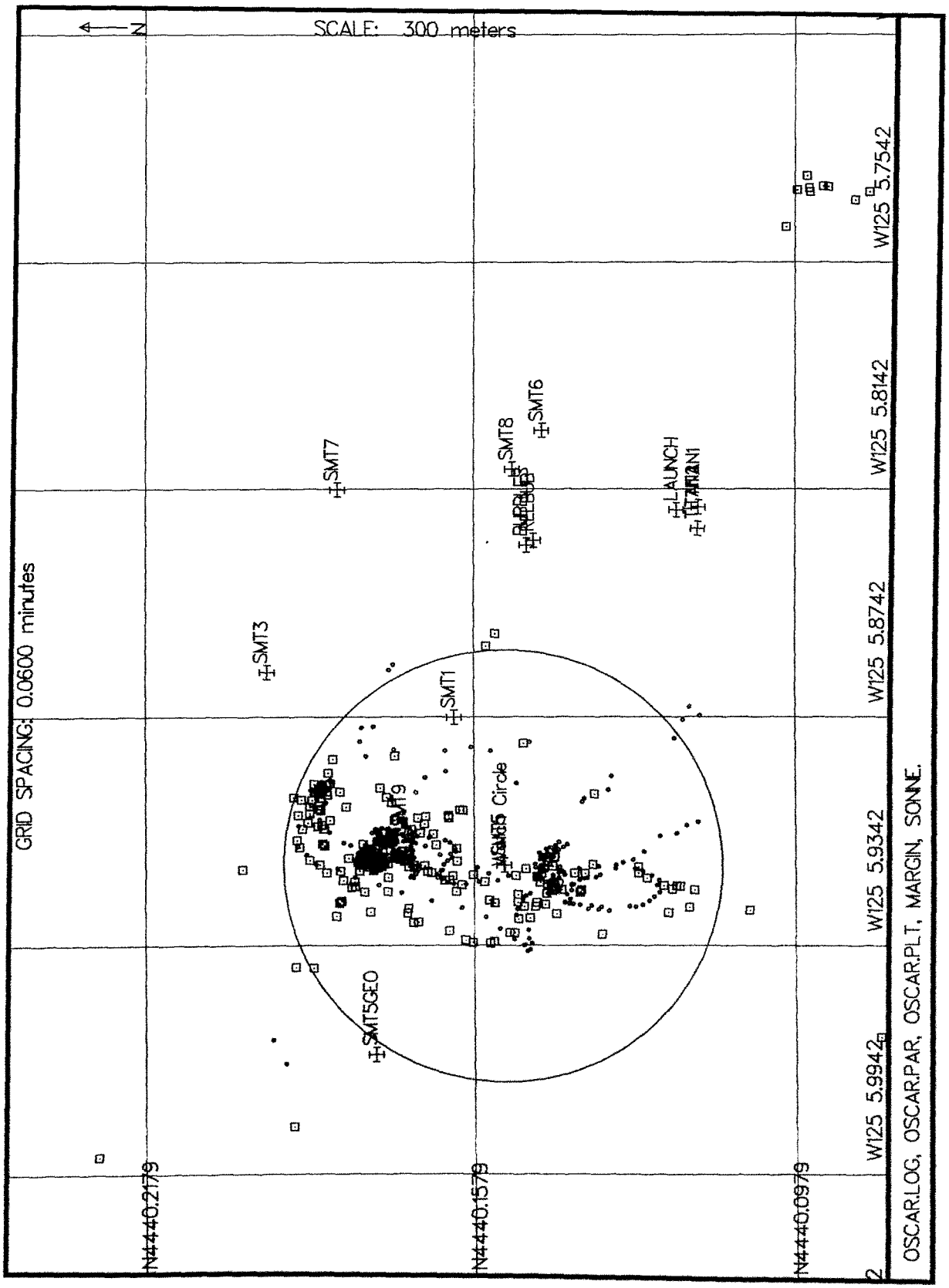

Fig. 25: Navigation plot during VESP deployment; VESP fixes are indicated by the small circles.

The lack of navigation hampered orientation on the ridge. ROPOS was eventually brought back to the cage and the ship was repositioned to enhance navigation and coverage in surveying the ridge. Nevertheless, a new clam field ("pete") was discovered; clams and a carbonate slab with epifauna were recovered. The identification of the water samples with the suction sampler proved to be difficult due to the loss of the colour video camera, which is usually used for the identification of the bottles filled with the suction sampler.

Sample log:

Time	Storage	Sample NO.	Comments
11:05	Sample tray	#4/5	muddy clam colony picked with PacMan
11:10	Sample tray	#4/5	sediment sample with PacMan
10:10	Suction sampler	2 bottles	2 water samples 5 cm above clam colony
14:56	Suction sampler	2 bottles	2 water samples above clam colony ('Pete')
15:08	Sample tray	#2/3	Clam sample with PacMan at 'Pete' field
15:12	Sample tray	#4/5	PacMan sample of single carbonate rock

ROPOS Dive 340 (Site 8) July 11, 1996

Target: Second Ridge at Cascadia Margin, Summit (SMT)

Objectives: To sample cold seeps fluids, precipitates and biota.

Summary: Navigation still poor (Fig. 23). During this dive several cold seep sites with active clam populations and bacterial mats were discovered. At these sites the capability of the ROV-system for detailed surveys and close-up documentation was proved by the use of the high-quality colour video camera. Sediment and carbonate rock samples were taken with PacMan, water samples were taken right above bacterial mats by using the suction sampler.

Sample log:

Time	Storage	Sample NO.	Comments
09:25	Suction sampler #1	SMT-1-1	Sampling ca. 10 cm above yellow bacterial mat; some pieces in the bottle
09:41	Suction sampler #2	SMT-2-1	sampling above different mat
10:10	Suction sampler #3	SMT-3-1	water sample above clam field
10:30	Sample tray #1/2	SMT-3-2	PacMan sample of clams and sediment
12:06	Suction sampler #4	SMT-5-1	water sample above clam field with bacteria
12:12	Sample tray #2/3	SMT-5-2	PacMan sample of clams and sediment
12:40	Sample tray #4/5	SMT-6-1	PacMan sample
13:06	Sample tray #6/7	SMT-7-1	Carbonate sample with claw
15:50	Suction sampler #5	SMT-9-1	Water sample at site where bubbles were observed after bumping into the sediment

ROPOS Dive 341 (Site 15) July 12, 1996

Target: Second Ridge at Cascadia Margin

Objectives: To sample cold seeps fluids.

Summary: Navigation still poor (Fig. 24). Right at the bottom close-ups of an octopus and a sea spider carcass scavenged by bucciniid snails were recorded. Heading NW, an area with carbonate rocks covered with bacterial mats was discovered. Water samples 2 inches above the mats were taken by using the two

titanium samplers mounted on the ROPOS 7-function manipulator. Two additional water samples were taken with the suction sampler. The dive had to be terminated due to bad weather combined with strong winds and an increase in sea swell. Recovery of ROPOS caused damage to the base bars in the cage.

Sample log:

Time	Storage	Sample NO.	Comments
14:12:51	TITAN major sampler	#1 + 2	Samples taken at the marker TITAN
14:23:36	Suction sampler	#1	right above a clam site
14:54:56	Suction sampler	#2	30 cm off bottom; 1 min pumping

5.2.3 Chemical analyses on water sampled by ROPOS

E. Zuleger, A. Dählmann, N. Jones, B. Domeyer

On-board analyses of dissolved methane from ROPOS water samples were performed using a vacuum-ultrasonication degassing method (Schmitt et al., 1991, Lammers and Suess, 1994) and subsequent determination with a Shimadzu GC 14A gas-chromatograph. For further details see the chapter hydrocast samples. During Leg 110-1a the data set of dissolved methane in cold seeps of the Cascadia Margin were successfully completed by samples taken by VESP and ROPOS.

Table 8: Geochemical data of vent water taken during SO110-1a ROPOS dives.

Bottle	CH_4 (nL/L)	SiO_4 (µM)	PO_4 (µM)	NO_3 (µM)	Cl (mM)	Ca (mM)	Mg (mM)
04-1	-	103	0.47	35.8	539	10.2	50.6
04-2	-	106	2.96	35.8	535	10.2	50.4
04-3	-	94	3.31	35.4			
04-4	-	95	3.31	35.5			
04-6	-	92	3.55	34.7			
04-7	-	96	3.20	38.6			
04-8	-	97	3.67	37.9			
08-1	331 666	82	2.88	32.2	536	10.2	51.6
08-2	89 917	77	2.65	30.5	533	10.2	51.7
08-3	47 478	72	2.53	27.1	531	10.0	51.5
08-4	-	79	2.94	32.3	540	10.2	51.9
08-5	59 040	70	2.65	28.6	541	10.1	51.6
08-6	-	73	2.88	32.9	543	10.3	52.3
15-1a	-	96	2.74	38.9	543	10.2	53.4
15-1b	-	98	2.86	40.8	544	10.3	51.7
15-1	43 767	97	2.80	54.6	543	10.3	52.5
15-2	-	88	2.27	34.8	542	10.2	52.4

All chemical data of water samples taken by ROPOS are given in Tab. 8 and are plotted in Fig. 26. Sampling during **ROPOS** dive 340 (station 8-1) and 341 (station 15-1) took place by sucking water into five 2L PE-buckets. All five samples were taken at the bubble-field. Sample 8-1 #1 and 8-1 #2 were sucked from above a bacterial mat, the others were taken right above clam colonies. The methane

concentrations range between 300 µL/L and 47 µL/L and show the probably highest values ever detected in cold vent samples.

For nutrient analyses of ROPOS water samples the vent water (suction sampler, titanium bottles) was filtered through 0,2 µm cellulose acetate membrane filters. Silicate, nitrate, ammonia, chloride, Ca and Mg were measured. A comparison between silicate data of vent fluids gathered with ROPOS and CTD data shows no significant deviation (Fig. 26) although phosphate and nitrate have lower concentrations in some samples. Chloride values are also within the range of normal sea water values, whereas vent fluids are depleted in Ca and Mg, indicating the precipitation of Ca and Mg containing minerals.

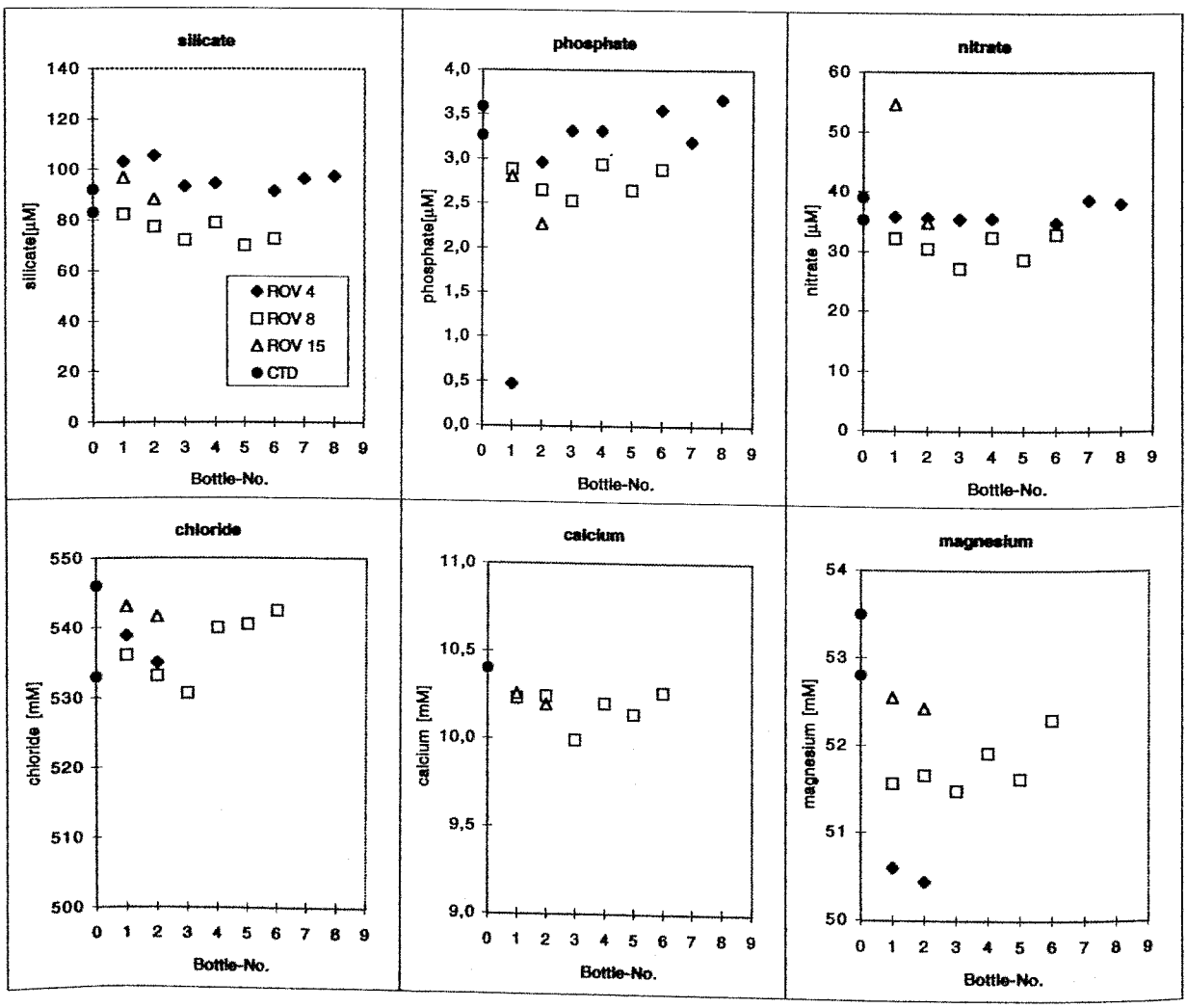

Fig. 26: Nutrients, Cl, Ca and Mg in ROV vent fluid samples (bottle number 0 = minimum and maximum values from deepest water sample of CTD-rosette water.

5.3 VESP deployment and measurements

P. Linke, M. Torres, F. Appel, F. Kulescha, E. Zuleger, N. Jones, A. Dählmann

VESP is a TV-controlled device for the deployment of water samplers with a CTD-probe mounted inside a barrel. The CTD-probe is designed to allow for monitoring of the temperature inside the chamber during deployment. The bottom of the barrel is open and can be pushed into the sediments to assure a seal over the vent sites. The barrel encloses 0.238 m^2 of the sediment surface and has an internal displacement volume of 284 L. Five Niskin water bottles (1.7 L) are mounted vertically around a cylindrical frame, and they are tripped sequentially by a motor located in the center of the frame. The sampling cycle is activated by the telemetry unit on board the ship. A complete description of this instrument and its operation can be found in Linke et al. (1994) and Suess (1992).

During cruise SO110-14, VESP was deployed on the Second Accretionary Ridge over an active vent site. The location of the site was chosen using the video images, and was selected to be in an area of venting which did not contain carbonate blocks which would hamper the sealing of the barrel at the seafloor. During this deployment we collected five fluid samples by sequentially tripping the Niskin bottles every 5 minutes. Upon recovery the fluid samples were analyzed for their dissolved oxygen, methane and nutrient concentration. Unfortunately, the CTD-pressure case was flooded during the deployment. Therefore no temperature, salinity or flow data were recorded.

Table 9: Geochemical data at VESP Site 14-1.

Bottle	CH_4 (nL/L)	O_2 (µM)	SiO_4 (µM)	PO_4 (µM)	NO_3 (µM)
1	109	146.3	35	1.93	25.8
2	168	54.9	72	2.86	36.6
3	132	44.3	82	3.10	38.1
4	869	38.5	95	3.10	41.4
5	627	36.3	95	3.21	40.3

Concentration changes of various tracers in the sequentially triggered water samples can be used to calculate their flux rate into the bottom water as well as enable estimates of total vent fluid flow, as previously shown by Carson et al., (1990), Linke et al., (1994) and Suess et al, (1996). The data obtained during the sequential sampling of vent fluids on station SO110-14 are given in Tab. 9. The data for bottle 1 indicates that this bottle pre-tripped during deployment, and thus the samples record contamination with surface seawater. We have used the data from bottles 2 to 5, which are shown in Fig. 27. The increase in methane levels in the fluids is accompanied by a decrease in oxygen. The data obtained during this cruise are consistent with those obtained during prior deployments in this area, which have been used to estimate a rate of flow on the gas hydrate ridge of 1,700 $Lm^{-2}day^{-1}$ (Suess et al., 1996).

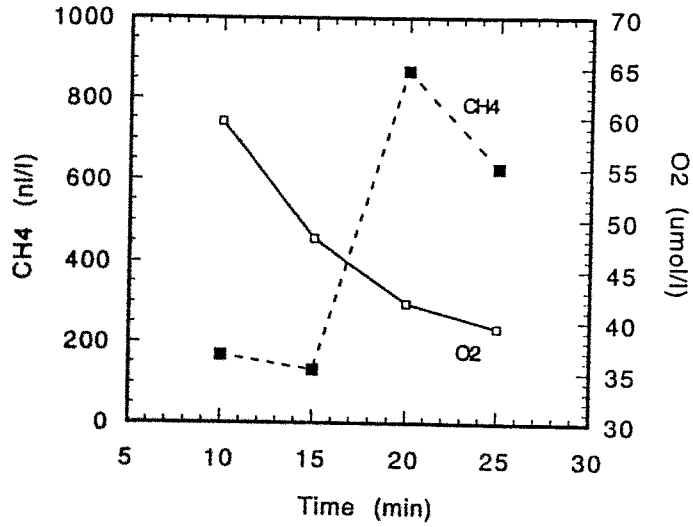

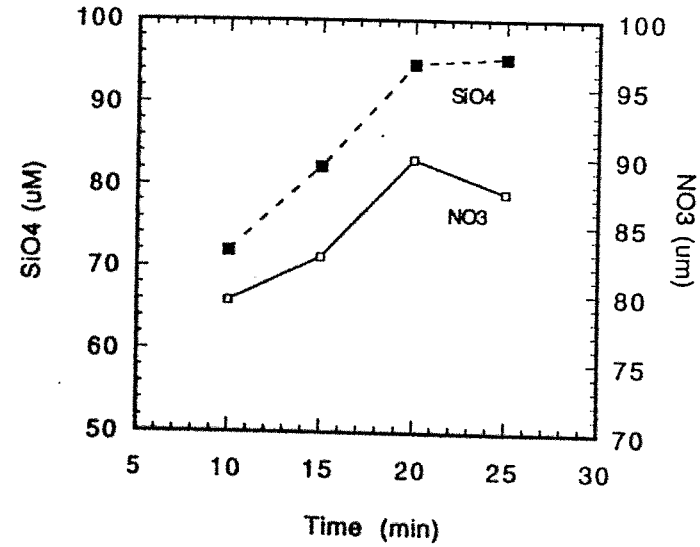

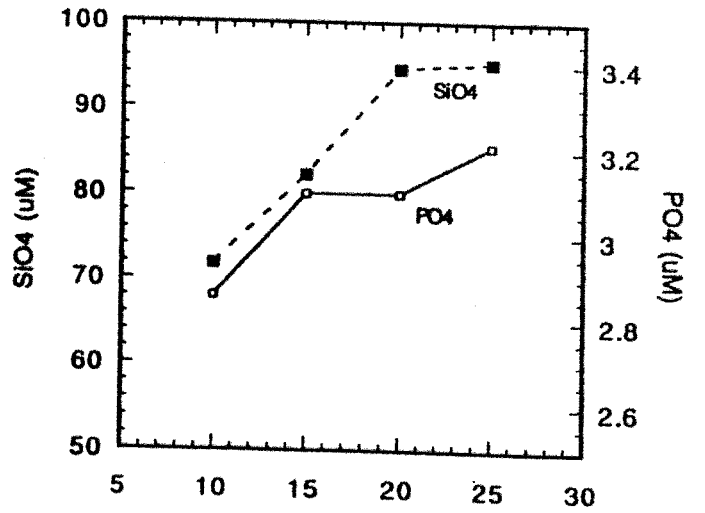

Fig. 27: Chemical data of VESP-samples, taken at the bubble site (44°40.1'N, 125°05.8'W).

6 Biological investigations of cold-seep communities

P. Linke, E. Southward, N. v. Mirbach, H. Sahling

6.1 Introduction

The occurrence of vent biota is among other evidence, one of the most pronounced indicators of fluid expulsion at active continental margins. Due to their visualy bright appearance clam clusters are the first manifestation which can be detected during TV equipped camera tows. Since these are only 'the tip of the iceberg', detailed camera surveys in areas where clam beds have been discovered, are necessary to observe the full scale of the biological phenomena which are associated with the occurrence of pore water escape enriched in hydrogen sulphide and methane. Whereas towed TV-systems barely give the time and opportunity, remotely operated vehicles like ROPOS offer than unique possibility of conducting detailed camera work with high-quality (3 chip) colour video cameras. The neutraley buoyant vehicle is pushed down with the power of its thrusters and gives the observers in the laboratory all the time needed for detailed studies and close-ups of their points of scientific focus. Two manipulators among other sampling tools on ROPOS enabled us to conduct detailed sampling of the biota in respect to fluid expulsion and its geochemical finger print.

6.2 Biological observations with ROPOS

During the ROPOS dives an abrupt transition from dense populations of sea urchins, sea stars and flatfish close to the summit to mostly uncolonized hardgrounds was noted. Given the local topography in this area, which tends to concentrate currents and augment suspension feeder populations, it is obvious that the effluent from this ridge is a major deterrent to colonisation by the indigenous fauna. Two different species of Calyptogena were distinguished and sampled. Whereas the smaller species seems to grow on the summit of the second ridge, the larger species was found to dominate the deeper parts of the ridge and the area described as the 'bioherm'. This consists of large slabs of carbonate rocks with deep erosion channels which are the apparent habitat of the larger species. It is in this area where the shells of dead clams and snails are embedded in the lithifying matrix; a stiff mud overlayer was inhabited by live animals but the zone of accretion must slowly move outward enveloping some of these. On the summit of the ridge the surface of the carbonate rocks was irregular and pitted. The undersides represent a reducing environment. These chunks of carbonate housed a specialised epifauna: some animals appear to be normal deep-sea creatures but capable of coping with the ambient H_2S while others - many on the undersides of the chunks - are most likely seep-indigenous. In areas of apparent enhanced fluid flow i.e. between rocks, dense carpets of blueish-white bacterial mats were discovered and recorded in great detail with the colour camera. These areas lacked colonisation by other macrofaunal organisms suggesting a zonation in respect to fluid flow and substrate. In some areas, where gas bubbles were detected once the vehicle bumped into the sediment, a 'golden slime' could be seen coating rock and sediment on the underside of the blocks. This 'slime' was recovered from this area on TV-G 115 during cruise SO109-2. It is surely prokaryotic (maybe a slime mould) and apparently able to cope with this highly reducing habitat, since gas bubbles were escaping while removing it from the clay layer.
Apart from animals directly associated with active seepage a lot of scavengers and predators were found and documented during the dives, such as hagfish, octopus,

spider crabs and big buccinid snails feeding on a crab carcass.

6.3 Samples from TV-G and ROPOS

Biological samples from cold-seep communities are a challenge in many regards. The main objectives of the investigation undertaken on this cruise were the experiments with living clams, physiological inventory of symbiont-harbouring organisms and defining the taxonomy of the cold-seep associated macrofauna.

With the use of the ROPOS system and its tools we were able to collect distinct samples from the cold-seep community. Compared to the samples taken with the TV-G the samples were small in size but in very good condition. Samples taken out of the sample-tray were transferred immediately to the cold room (+4 °C).

To gain a larger amount of sample material the TV-guided grab (TV-G) was the most successful tool. The sampling area is about 1.82 m^2 (1.06 x 1.72 m), for detailed description see chapter 8. However, no quantitative estimations of biomass, abundance of species or even recovery of different species can be made with this tool, therefore the samples from the TV-G permit only rough estimates of e.g. biomass to be made. Once on deck and after subsampling with cores for sedimentology, porewater chemistry and bacterial counts, all visible organisms were picked from the fairly disturbed surface. The upper layers of the surface were taken and suspended in sea water before sieving them through a sieve with a mesh size of 0.5 mm. Some sediment was taken as a whole. Everything was transferred immediately to the cold room.

All procedures were carried out under in situ temperature to protect the organisms from additional stress. Sediment was washed through a 63 µm sieve and all organisms are roughly separated into taxonomic groups. For observations on living animals and their documentation the organisms were cultivated until fixation in polystyrole aquariums. Whole or dissected organisms were frozen in liquid nitrogen and stored at -20 °C for determination of stable isotopes, enzyme analyses and genetic investigations. For taxonomy the macrofauna was fixed in ethanol or formalin. Soft tissues and hard surfaces were fixed in glutaraldehyde for scanning electron microscopy (SEM).

At the second ridge of the Cascadia margin at least two species of Calyptogena and very large and tiny Solemya were recovered. The clams are known to harbour chemoautotrophic bacteria symbionts in their gills. Besides these known species we also found small limpets attached to hard surfaces and snails on soft and hard sediment. There is strong evidence that both gastropods live in association with bacteria. Filamentous bacteria were attached to the outer shell and the hemolymphe contained a red-coloured pigment. Further investigations and taxonomic work will be carried out at GEOMAR. Another common taxonomic group was the polychaetes. Most remarkable was a very long nereid polychaete up to 20 cm in length. Even after a long time in the aquarium it was still very active. Members of this family are known to live within the sediment. The worm may protect itself against the toxic hydrogen sulphide concentration by pumping oxygenated water through its burrow. Only a few members of the echinoderms were found in the community, some ophiurans and two sea urchins, which is somewhat surprising because of the wide

distribution of this taxonomic group in this depth-range, however a lack in sulphide tolerance has been previously described. Some carbonate crusts were recovered by the TV-G and ROPOS and as known from other environments the diversity of organisms was very high on the hard substrates. Here we found sponges, hydroids, limpets, cnidaria, polyplacophora, nemerteans and a white mat, probably bacteria.

The remarkable gas hydrate-bearing TV-G 18 recovered only a few Calyptogena clams. Some capitellid polychaetes were found in carbonate crusts and in the gas hydrates, but no other organisms could be detected in the gas hydrates. A couple of small living bivalves, not seen alive at the other stations, belong to the yoldia-group of protobranchia.
From the TV-G 09-1 and 11-1 subsamples from the squeeze cake were stored at -20 °C for analysis of chlorophyll a. The samples were taken at a 2 cm intervals to a sediment depth of 10 cm. The chlorophyll determination will be carried out at GEOMAR.

Table 11: Overview of the TV-G and ROPOS samples during cruise SO110-1a.

Station	Location Latitude N Longitude W	Instrument	Water depth (m)	Observation
04 -1	44° 40.20' 125° 06.50'	ROPOS dive #339	608	5 *Calyptogena* sp., shell length about 6 cm
08 -1	44° 40.45' 125° 05.90'	ROPOS dive #340	583	some small *Calyptogena* sp., shell length 2-3 cm
09 -1	44° 39.26' 125° 06.00'	TV-G	596	Lots of small *Calyptogena* sp., shell length around 3 cm
11 -1	44° 40.14' 125° 06.51'	TV-G	524	About 50 *Calyptogena* sp. shell length around 7 cm. 7 specimens of *Solemya* sp.
18 -1	44° 34.52' 125° 08.77'	TV-G	785	Only 6 *Calyptogena sp.* clams. 4 small clams shell length less than 2 cm. not yet identified.

Most of the samples with with Peter Linke at GEOMAR, Kiel.
Sixteen Calyptogena shells are going to be geochemically investigated by Marta Torres. Rich Lutz will carry out the genetic investigation of the Calyptogena species. Eve Southward will determine down to the species level in taxonomy, therefore she has a set of the common fauna and some exotic organisms.

6.4 Cultivation and experiments with living clams

6.4.1 Clam treatment

The cultivation of the clams was conducted in the cold-room at in situ temperature (+4 °C) in original sediment. No air bubbling and no feeding with inorganic or organic compounds was carried out. The water was exchanged by deoxygenated water every 48 h. Dead organisms were picked out of the aquariums and were either

fixed in Formaldehyde or were frozen at -20 °C. Some clams were dissected immediately after collection. Their different tissues were partly deep frozen in liquid nitrogen at - 190 °C or frozen at -20 °C.
During the following legs of the cruise (SO110-1b and SO110-2) all Clayptogena and Solemya clams died in the cold room. The dead clams were frozen at -20 °C or fixed in Formaldehyde. Hence the goal to transport live clams back to GEOMAR wasn't successful.

6.4.2 Video time lapse observation

In order to get an idea of the bioturbation activity of the clams and the rhythm of their pumping activity the clams were observed by a computer controlled time lapse SVHS-BW-video-camera. The camera was mounted on a tripod to observe the sediment in two ways: first verticaly and afterwards horizontaly. The system was adjusted to record for one second each minute. The program ran for 12 hours. The observations were conducted in the cold room, the room light was on during the whole experiment.

6.4.3 Calyptogena clams

The Calyptogena clams were recorded twice. In the first set the camera was mounted almost parallel to the sediment surface and in the second set the camera was mounted above the sediment looking vertically down on the clams.
The animals live half buried in the sediment. Their foot is outstretched downward in the sediment and their inhalant and exhalant siphon protrudes into the water column. The playback of the recorded tape revealed that the Calyptogena clams were quite stationary. Only some of them made a rotationary movement during observation and no clam crawled on the sediment surface. Most of the examined clams opened and closed their valves periodically.

6.4.4 Solemya clams

The Solemya clams were observed in the same way as the Calyptogena clams. The Solemya clams burrowed very actively in the sediment. Within 12 h after placing them in the aquarium they had burrowed entirely into the sediment. This behaviour is consistent with the observation of the TV-grab. In spite of the unsatisfactory video quality Solemya clams were never observed on the sediment surface during the track survey.
The movement of some clams during the video time lapse observation was very intense, their foot kept on burrowing in the sediment and in course of 12 h one clam burrowed diagonaly through an aquarium with a width of 40 cm. Other clams stayed more or less stationary in one position, the siphon directed to the sediment water interface.

6.4.5 Bioirrigation experiments

In order to understand the impact of seep-associated organisms on the fluid flow and geochemistry of cold seep sediments, measurements of their pumping activity were conducted. Seven specimens of *Solemya sp.* were recovered from TV-G 11 and cultivated at ambient temperature in an aquarium filled with ambient sediment in the cold room. A thermistor flowmeter with a micromanipulator was placed directly (ca. 5mm) in front of their exhalant opening. Active pumping was made visible by dropping ink in the vicinity of their siphons. Flowmeter readings were amplified

through a portable unit and recorded on a laptop computer in the cold room. Baseline readings right above the barren sediment surface were recorded to distinguish between flow created by the animal and by the ship's movements (Fig. 28).

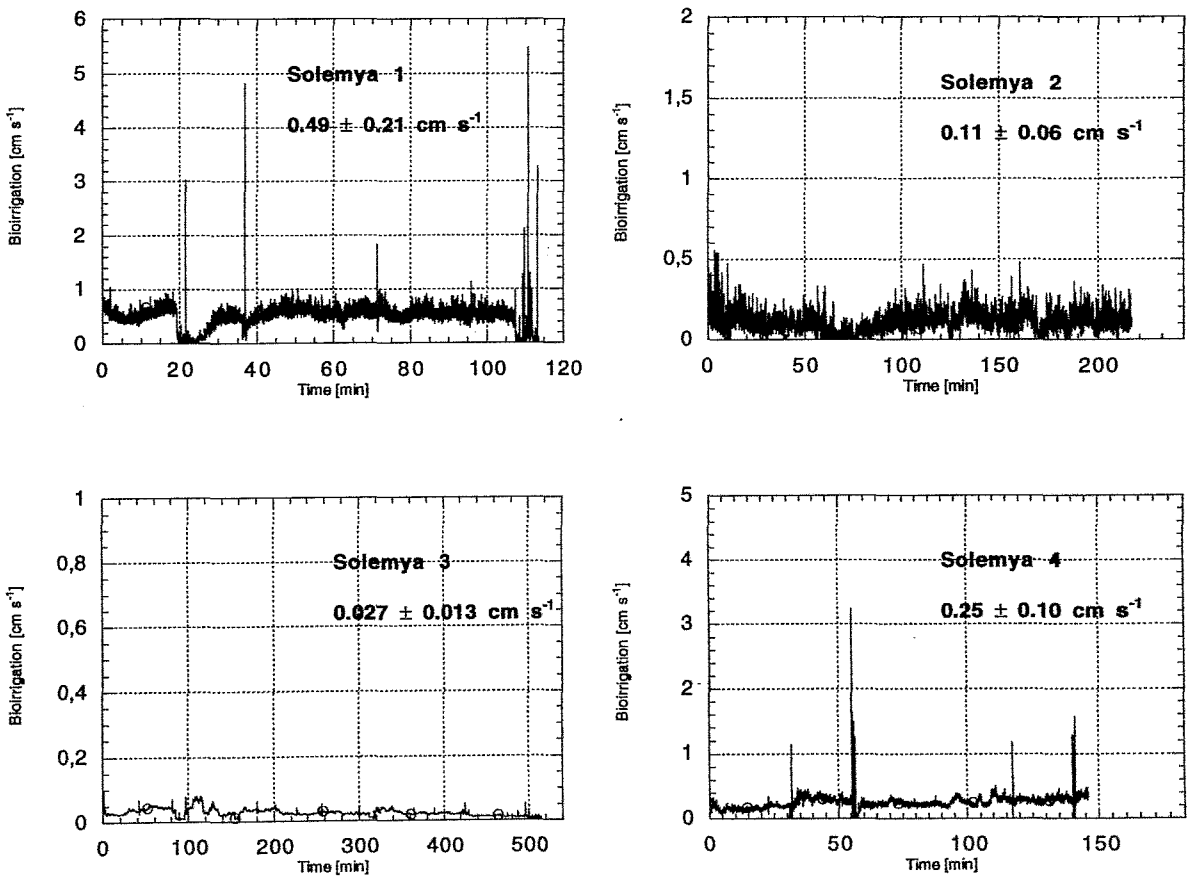

Fig. 28: Flowmeter readings of 4 different Solemya specimens cultivated in an aquarium in the cold room.

7 Vent site survey by TV-sled EXPLOS

G. Bohrmann, J. Greinert

During SO110-1a the TV-sled EXPLOS (Ocean Floor EXPLOration System) was used to find active fluid expulsion sites and to map their occurrences as well as their geological surroundings on the Oregon accretionary complex.
The EXPLOS is equipped with a black-and-white video camera (OSPREY 0111-6006), two still cameras (PHOTOSEA 5000) in stereo mode and 4 halogen lamps (ROS QL 3000; 2 each of 150 and 250 W). Due to the amount of time required for the strobe to cycle, a photo image can be made after every 8 seconds with the total number of images restricted to the amount of the film. We used 33m of 400 ASA KODAK Ektachrome film yielding approximately 800 images. The new fiber optic cable available on R.V. *Sonne* allowed for the addition of a colour camera (MSC 2000-D) to the EXPLOS-sled, which substantially improved the image control on the ship. Unfortunately, we found that the projector lamps were not powerful enough for the colour video signal, and should be replaced in the future by a new lamp system.

In addition, a CTD-System (SIS 6000) was mounted on the sled recording depth, salinity and temperature. All data and images were continously displayed in real time aboard RV SONNE. The system is navigated with a Super-Short-Basline system developed by SIMRAD (SSBL HPR 1507) with a responder mounted on the sled. The instrument was towed at approximately 0.3 to 0.6 knots. Optimal viewing conditions at 2-5 m altitude were maintained by continually adjusting the length of cable through manual winch operation.

Table 12: EXPLOS-tracks taken during SO110-1a on the second accretionary ridge of the Cascadia subduction zone.

Station No	Date	Start (UTC) End (UTC)	Latitude °N	Longitude °W	Water depth
5-1	July 11	01:12	44°40.072	125°05.423	617 m
		06:04	44°40.214	125°07.872	745 m
17-1	July 13	05:11	44°34.047	125°08.328	810 m
		06:18	44°34.236	125°08.920	763 m

The two EXPLOS surveys crossed the ridge crest of the second anticlinal ridge, which was called "gas hydrate ridge" by the scientific party (Fig. 5; Tab. 12). EXPLOS profile 5-1 was performed over the northern summit of the ridge. Because of its 9 km broad dome-like structure, this summit is a remarkable area in the Cascadia accretionary complex where usually elongated more narrow ridges are formed (Carson et al., 1991). Bottom observation started east of the summit at 620 m water depth where the seafloor is covered by a soft sediment interupted by scattered debris of lithified rock samples that seems to be mostly carbonates. Heading upwards the amount of seafloor covered with carbonate rock fragments increased, with a consequent decrease of the soft sediment. Carbonate morphologies included dense slabs, bioturbation casts, irregular edifices, single doughnuts or even chimney structures. A pavement of carbonate blocks occured

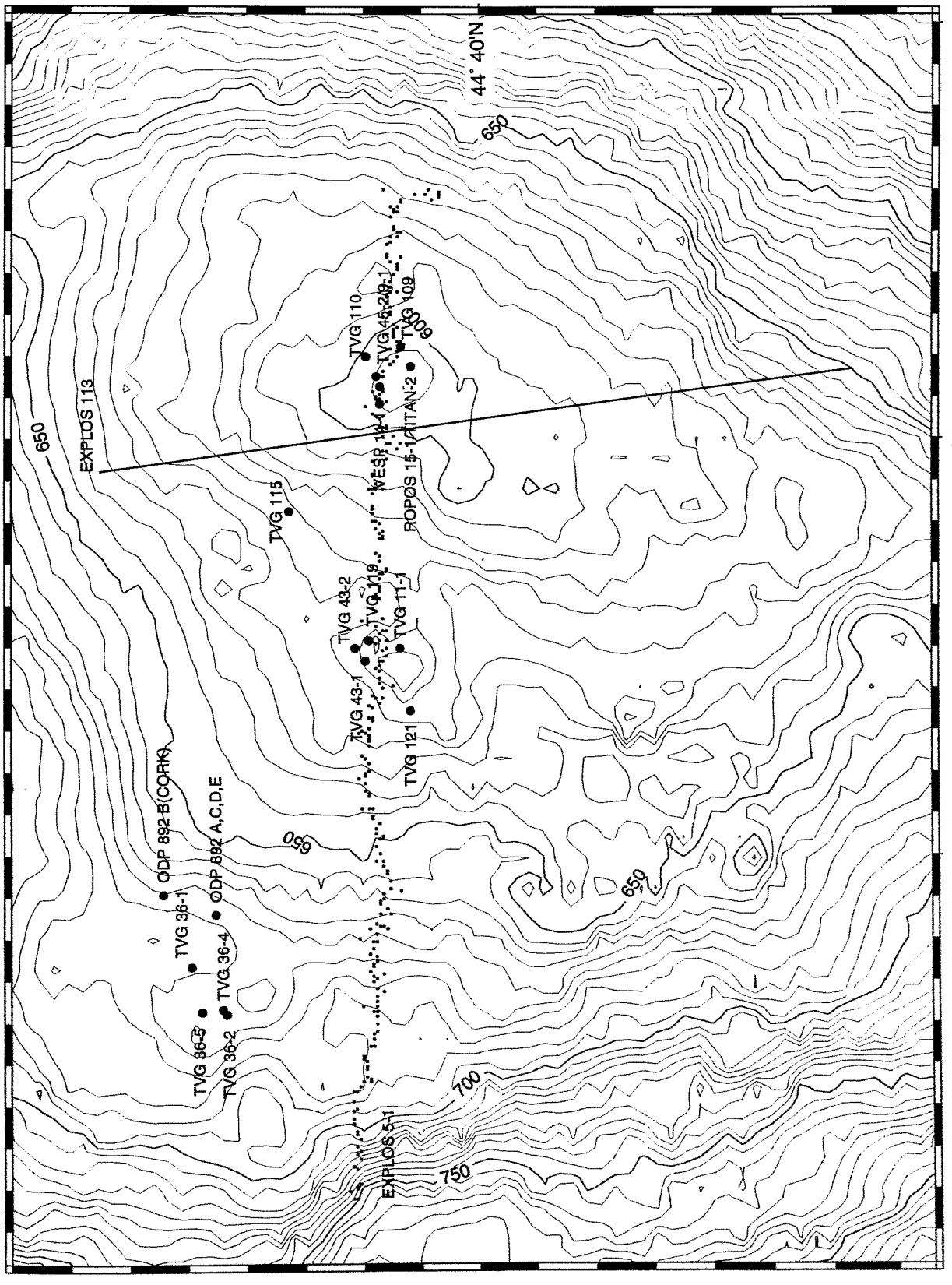

Fig. 29: Northern part of the gas hydrate ridge showing all TV-grab stations (SO109 and SO110) as well as EXPLOS profiles, ODP and VESP sites. The SSBL navigation data of EXPLOS track 05 is shown by small dots.

on top of the ridge between 585 - 595 m. Fractures within the pavement expose outcrops of older cemented rocks between the boulders. It appears as if the ridge has been uplifted, fractured, and eroded, with the oldest strata exposed on the crest of the ridge. Numerous white clam shells were found on this summit area, these are chemosynthetically supported bivalves. Several patches of active fluid venting were found which were densly covered by white and blue bacterial mat of bacteria and other organisms (see chapter 6). The continuous video clearly shows that the rock surfaces around the seeps are mostly coated by these mats. In one case we identified gas bubbles escaping from a fracture between rock boulders. Crossing the summit to the western flank, we again observed soft sediment surfaces with scattered or densly paved carbonate rocks.

After crossing a morphological depression down to 630 m the EXPLOS reached an isolated rocky hill 10-1 m high and approximatly 250-300 m in diameter. This area was characterized by the occurrence of clam shell-cemented rocks that form extensive outcrops. The massive rocks were characterized by cracks and open fractures. Chemosynthetic clams that are related to fluid expulsions from the seafloor occur on the sediment covered bottom of the open cracks. This may indicate that fractures are preferential sites of fluid discharge in this area. The massive appearence of rocks which are dominantly composed of biogenic carbonate shells gave rise to the term "bioherm" (Moore et al., 1992). This „bioherm" was targeted during SO109-1, SO109-2 and this leg (Fig. 29). A second area which was also a "bioherm" (at 675 m water depth) west of the ODP 892 drill site was sampled during SO109-1 (Fig. 29). Following the EXPLOS-5 track to the west a soft sediment covered surface appeared below 650 m water depth. Below 700 m the frequency of carbonate slab deposits increased, coincident with an increase in slope angle.

The second EXPLOS track, 17-1, transversed the southern summit of the same ridge, HYDROSWEEP data indicated it was more narrower than the northern summit (Fig. 5). The EXPLOS observation started on the eastern flank at a depth of 820 m. After reaching the summit area (770 m) we observed numerous fluid venting sites of several meters in diameter which were imaged by the video and still camera systems. Large patches of bacterial mats occurred in a soft sediment environment that contained chemosynthetic clams on ist margins. Close-up images of the blue and white bacterial mat sites showed thin light irregular crusts beneath them which may be carbonates or gas hydrates. After these findings the EXPLOS track was stopped in order to save time for a TV-grab station.

8 Vent sampling by TV-grab

J. Greinert, G. Bohrmann

The TV-guided grab sampler (TV-G) aboard R.V. *Sonne* is capable of sampling an area of 1,82 m^2 (1.06 x 1.72 m) up to 40 cm deep. We used the TV-G to sample vent sites for fauna, bacteria, and geological samples. The TV-G is equipped with a video camera (OSPREY 0111-6006) and two lamps, allowing the surface operator to guide the instrument to a specific sample location along the track and for the sample to be examined within the jaw. Thus, it is possible to decide immediately whether or not sampling was successful. If unsuccessful the TV-G can be opened, discarding the contents of the jaw, and be repositioned for another attempt. The tool is lowered from the ship and deployed on the ocean bottom using continuous visual observation by continually adjusting the winch. The grab is closed by hydraulic pressure with power coming from batteries. The energy supply allows the grab to be closed and opened up to 4 times.

Table 13: Details of TV-grab stations during SO110-1a.

Station	Date	Time (UTC)	Latitude °N	Longitude °W	Water depth
09-1	July 12	01:48	44°40.17'	125°05.87'	595 m
11-1	July 12	06:44	44°40.13'	125°06.50'	615 m
18-1	July 13	08:22	44°34.23'	125°08.89'	771 m

The TV-grab was used after a detailed survey of EXPLOS. We deployed two TV-grabs on the northern gas hydrate ridge, (Tab. 13). TV-G 9 sampled the summit of the ridge whereas TV-G 11 sampled the „bioherm" (at 620 m depth) 800 m to the west (Fig. 29). The TV-G retrieved a large quantity of chemosynthetic fauna at both vent sites as well as numerous carbonate samples of various morphologies. Most of the latter are carbonate slabs and bioturbation casts that possibly formed diagenetically during past fluid events. Other carbonate blocks of irregular surfaces may be precipitated by more recent fluid venting processes. In addition to carbonate, TV-G 11 from the "bioherm" site (at 620 m depth) recovered a carbonate-cemented breccia which may have been formed by hydrofracturing and precipitation by fluid venting.

TV-G 18 was deployed on the southern summit of the gas hydrate ridge where several irregular circular patches of bacterial mats were identified on EXPLOS survey 17-1. During hieving the sediment began to bubble dramatically and frothed; this increased through the water column. We observed bubbles bursting through the sea surface just before the TV-G reached it. Active degassing was still observed on the sediment surface after the grab was on deck. We detected a strong odor of H_2S, which required gas-mask protection during sampling. Large amounts of pure, whitish gas hydrates were found. The pure gas hydrate occurs in layers mm to 10 cm thick that are intercalated dominantly with soft muddy sediment. Although layering of the gas hydrates was generally in parallel stratification, we observed hydrates lining hydrofractures. Based on the

relationship of the thickness of the gas hydrates to the sediment layers in freshly broken blocks we estimate that gas hydrates occupies 40-60% of the total volume.

Decomposition of the hydrates continued on the deck of the vessel. Because the gas hydrates were only found in the center of the TV-G we believe that the decomposition of the hydrates from the margin areas of the grab was the cause of the degassing observed during the ascent through the water column. Angular, mm- to cm-sized fragments of cemented mud were scattered within the sediments and also occured in well defined layers. In some parts such fragments were cemented by authigenic carbonate forming breccias. Because the location of the southern gas hydrate ridge is a area without outcrops or erosion of indurated mudstones, we think the brecciation preserved in the carbonate-cemented mudstones ocurred as a result of hydrofracturing during natural strong degassing events. Such events could be accelerated by the lowering of sea level which would lead to the decomposition of gas hydrates.

Additionally various types of authigenic carbonates were present and seem to have been precipitated *in situ* in the gas hydrate environment. Preliminary XRD measurements made aboard RV SONNE indicate aragonite and to a lesser extent Mg-calcite as the dominat carbonate phase. Most of the authigenic carbonates show an irregular morphology whereas others seem to develop as casts of gas hydrate layers.

The TV-G provided a wealth of samples (pore water, fauna, sediment and authigenic carbonates) that will be used to investigate the gas hydrate environment.

9 Pore water chemistry

9.1 Methane

N. Jones, E. Zuleger

In an effort to further understand the distribution of methane throughout both the water column and the sediment, and the processes which relate the two, several sediment samples from both TV-grabs and ROPOS were degassed and analyzed for methane concentrations. The results, while only rough estimates due to a lack of controlled conditions in the sampling and storing procedures, may further the understanding of the carbon cycle in accretionary systems.

Aproximately 200g of sediment was taken at random from the material brought up at stations ROPOS 4-1, TV-G 9-1, TV-G 11-1, and TV-G 18-1. The sediment was stored in zip-lock bags for analysis on board, and/or in 5ml open syringes with their needle-ends removed for on-shore analysis and immediately frozen. However, since neither of these instruments collect sediment under gas-tight conditions, the amount of gas left in the samples at the time of analysis is unknown.

The analysis consists of a vacuum de-gassing aparatus, through which the addition of phosphoric acid and potassium hydroxide removes both the sorbed and free hydrocarbons from the sediment. The collected gas is then analysed by gas chromatography in order to determine the amount of methane present. Samples of the extracted gas were also collected in evacuated 10mL wheaton bottles for possible carbon isotope analysis using a gas chromatography-Combustion-Isotope Ratio Mass Spectrometry (GC-IR-MS).

The sample from the ROPOS dive had a methane concentration of 100 ppb, the sample from TV-G 11-1 yielded only 45 ppb, and two independent samples from TV-G 9-1 gave concentrations of 7,699 ppb and 2,948 ppb. No higher hydrocarbons were observed in the FID signal. Methane concentrations in aerobic marine sediments of low organic carbon/non-petroliferous areas rarely rise above 50ppbw, and all values below this are generally considered to be background. The only clear conclusion that can be made from these results is that station SO110-9-1 was significantly higher in methane concentration than the other sites.

9.2 Nutrients

A. Dählmann, B. Domeyer, E. Suess

9.2.1 Pore water extraction

Reproducibility and lateral variability of pore water composition has become an important issue in looking at small-scale features such as vents. Hence, we subsampled the relatively large sediment packet recovered by the TV-grab. Subcores were pushed into the sediment where the surface appeared to be least disturbed. These were then segmented in the cold room (4°C) and pore water was collected with a polypropylene squeezer pressurized by argon and fitted with 0,45 µm cellulose acetate membrane filters. Up to a depth of 10 cm slices of 2 cm were

cut, below this to the bottom of the core, slices of 3 cm were cut and squeezed for pore water. Further details are in the cruise report SO110-1b and 110-2.

The pH of the sediment and the alkalinity and the sulfide concentration of the pore water were measured immediately after collecting the pore waters. Subsequently, the pore water were analyzed for silicate, phosphate and ammonia. Because of high sulfide contents, nitrate was not measured on these particular cores. Some samples were analyzed for chloride, calcium and magnesium. A certain volume (1-5 mL) was acidified with 65% HCl suprapur (10 µL/mL sample) for trace element analysis.

9.2.2 Analytical methods

- Photometric methods

Analytical procedures were based on „Methods of Seawater Analysis" (Grasshoff et al. 1983). Modifications were necessary for samples with a high sulfide content. Silicate and phosphate were measured after the elimination of sulfide by bubbling nitrogen through an acidified aliquot of the sample. Ammonia could be measured in diluted samples (1:10). Nitrate data are the sum of nitrate plus nitrite concentration. The method for sulfide determination described in Grasshoff et al. (1983) was adapted to pore waters with a high sulfide content by elevating the amount of zinc acetate gelatin solution to fix the sulfide (1 ml instead of 50µl per 1 ml sample volume). The resulting suspension had to be diluted (up to 1:10,00) prior to analysis. The adaptation was made during analysis of cores TV-G 9 and 11. Therefore the data of these cores are less reliable than the data subsequently analyzed.

- Titration

Ca, Mg and Cl titrations were carried out following the procedure developed by the ODP (Gieskes, Garno and Brumsack, 1991).

- pH / Total Alkalinity

The pH electrodes were calibrated with buffers prepared in artificial seawater (Dickson, 1993). The temperature and voltage of a BIS and Aminopyridine buffer were measured with a temperature probe and a pH meter respectively. For the calibration curves the temperature dependent pH values were calculated. The total alkalinity (TA) was calculated from a single point titration of 0,5 or 1 mL pore water, depending on the sulfide content of the sample. Buffers for calibration were prepared from 0,01 N HCl in 70% (v/v) artificial seawater. To obtain an exact pH of 3,00 and 3,52 an additional amount of acid had to be added to compensate for the alkalinity of salt impurities. This amount is calculated from a Gran titration of 100 ml artificial seawater (Stumm and Morgan, 1996). The TA is calculated from the excess of acid after the addition of from 0,3 up to several mL of 0,01 N HCl, resulting in a voltage corresponding to a pH of between 3,00 and 3,52. This method is established for small amounts of pore water with an alkalinity of about 2 to 3 mM. Data that exceed this value by a factor of 10 may not be quite reliable, because the ionic strength is reduced significantly by the addition of greater amounts of acid. Nevertheless, the advantage of using a very rapid

method by making do with a 1 mL sample volume, justifies its application despite the potential inaccuracy.

- Laboratory studies

Subsamples were taken for trace element analyses and boron and lithium isotope measurements. Chloride, calcium and magnesium were mostly done on board but will be completed and/or repeated in the shore-based laboratory as will sulfate and DIC and $\partial^{13}C$ of ΣCO_2 on selected samples.

9.2.3 Results and discussion

Three TV grabs were recovered and analyzed for their pore water constituents. A summary of cores, numbers and distribution of samples, and geochemical analysis performed on board is given in Tab. 14.

Table 14: Summary of cores, samples and geochemical analyses.

Station	No. of subcores	Core depth [cm]	No. of pore water samples	Analyses
TV-G 9	2	34 / 22	7 / 5 [1]	pH, TA, H_2S, SiO_2, PO_4, NH_4 PW ac.
TV-G 11	2	28 / 22	6 / 5 [1]	pH, TA, H_2S, SiO_2, PO_4, NH_4, PW ac.
TV-G 18	3	22 / 16 / 19	9 / 7 / 8	pH, TA, H_2S, SiO_2, PO_4, NH_4, PW ac., Cl, Ca, Mg

Keywords:
pH: determination of sediment pH
TA: total alkalinity of pore water
H_2S: sulfide concentration in pore water
SiO_2, PO_4, NH_4: nutrient analysis in pore water
Cl, Ca, Mg: titration
PW ac.: acidified pore water sample
[1]: every other sample to Oregon State University (M. Torres)

The outstanding feature in the pore waters of cores TV-G 9 and TV-G 11 is the enormous concentration of free sulfide (Fig 30). The shape of the concentration-vs-depth profiles is very similar in all subcores, exhibiting rather low values within the first 10 cm below the seafloor and then increasing sharply to about 50 mM. Such high sulfide contents have, to our knowledge, never been reported before. They are also remarkable in that they are almost twice as high as seawater sulfate, from which sulfide is generated. This suggests an enormously dynamic system, very likely related to fluid advection, discharge, and pumping activity by vent organisms. It is imaginable that fluid advection carrying methane and/or sulfide from below encounters either anaerobic or aerobic processes of oxidation at about the burrowing depth of vent organisms, 10 cm below the seafloor.

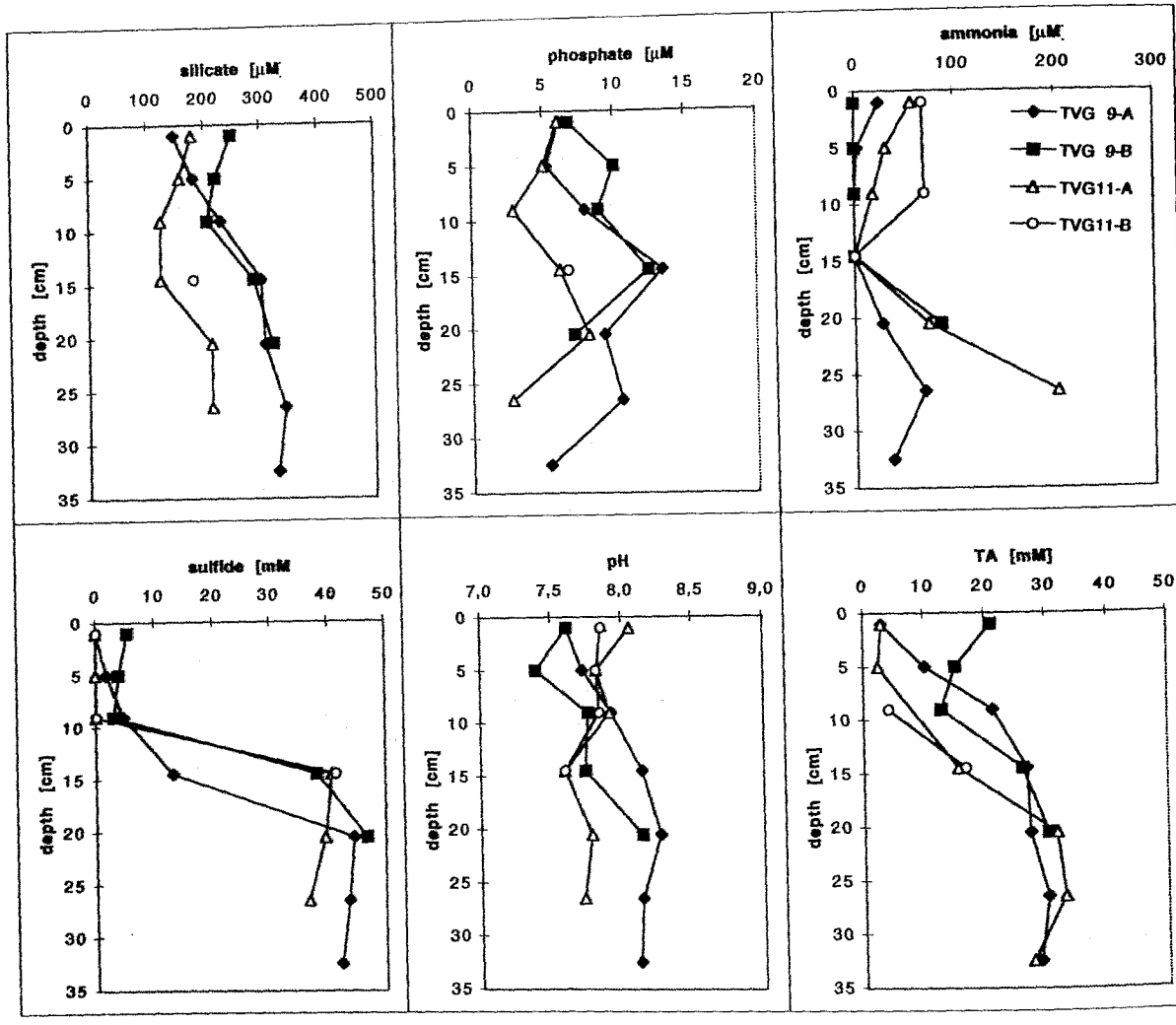

Fig. 30: Geochemical data of pore water at Sites TV-G 9 and 11.

None of the other parameters showed anomalies anywhere near that of sulfide, although SiO_2 exhibits subsurface minima (TV-G 11A and TV-G 9B) which is in agreement with pumping activity of benthic organisms. It should be quite interesting to calculate the carbonate alkalinity after correcting for the sulfide contribution, determine the $\partial^{13}C$ of DIC and measure the Ca- and Mg-contents, because it is suspected that the near-surface sediment at sites TV-G 9 and TV-G 11 is currently undergoing carbonate formation either as cements, crusts, chimneys or other authigenic modes of precipitation.

The core TV-G18 contained a considerable number of large pieces of gas hydrate. The sediment fabric and stratification were disturbed by the decomposition of the hydrate and the escape of methane (Fig. 31). Almost all parameters (TA, SiO_2, pH, H_2S, Ca, Mg) attest to a rather homogenous vertical distribution pattern. This could be an artifact caused by mixing from gas escape or it could indicate strong vertical advection of fluids, if the profiles are interpreted to exhibit very strong upward -convex shapes. This is the classic shape developed in response to vertical advection.

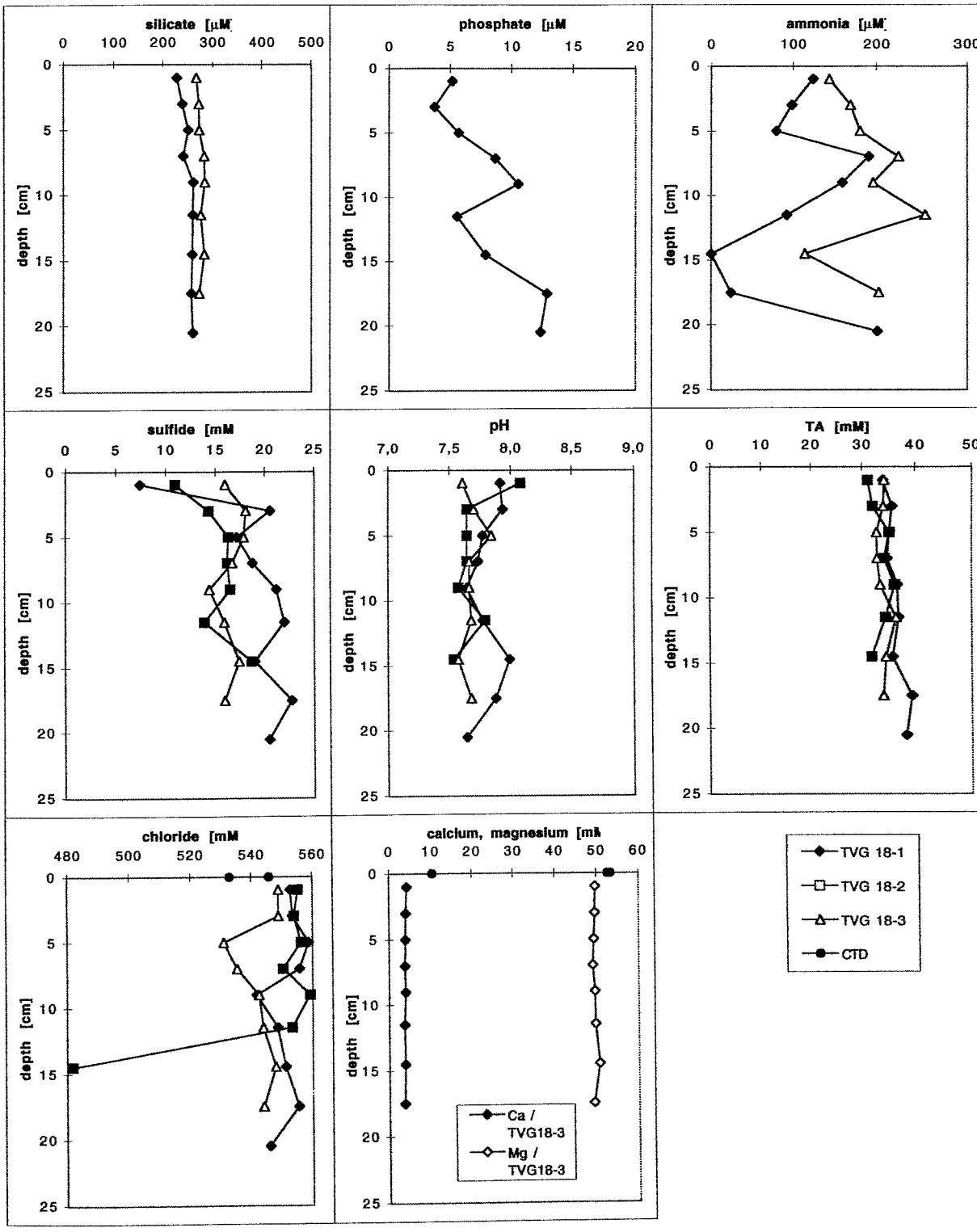

Fig. 31: Geochemical data in TV-G 18 pore water.

The sulfide concentration is about 15 to 20 mM throughout the core, except in the uppermost layer. Consequently, TA values are high (30-40 mM), whereas the pH varies between 7.5 and 8.0.

In most of the upper centimeters of the sediment (TV-G 18-1, -2, -3) pore waters are enriched with Cl relative to the CTD-chlorosity: i.e. 555 mM vs. 546 mM. However, several negative Cl-anomalies (TV-G 18-3 and the deepest sample at subcore -2) are also present. Both of these effects could be explained by the presence of gas hydrates. During hydrate formation salts are excluded and hence enriched in the surrounding pore water. During recovery of the core this effect could be overcompensated for the decomposition of hydrates, as observed and described elsewhere in this report. Injection of hydrate water dilutes the pore water, especially at the immediate contact of hydrate and sediment. Both effects can perhaps be seen in the collected data. The elevated chloride values in the surface sediment implies that the gas hydrates are currently forming at the location of station TV-G 18.

Calcium and magnesium concentrations are below those of ambient seawater and constant throughout the cores, about 4 and 50 mM respectively. The low values may be explained by the precipitation of Ca- and Mg- bearing minerals, mostly carbonates, but also aragonite. At the gas hydrate ridge, sulfide is produced from the oxidation of methane:

$$CH_4 + SO_4^{2-} \rightarrow HCO_3^- + HS^- + H_2O$$

High amounts of methane at this location promote this process. Additionally, the alternative reaction, degradation of organic carbon, decreases the pH, so that carbonate precipitation is prevented (see cruise report SO110-1b and 110-2).
Again, it should be interesting to calculate the carbonate alkalinity and determine the $\partial^{13}C$ of DIC to complement the Ca- and Mg-data in order to verify syngenetic carbonate mineral formation, here at the unique association with gas hydrates.

10 In-situ Eh measurements during the SO110-1a cruise

Ko-ichi Nakamura

10.1 Introduction

Off-line based in-situ Eh measurement systems were attached to the CTD rosette, the EXPLOS sled frame, the VESP, the ROPOS vehicle and the ROPOS cage during cruise SO110-1a at the Cascadia margin, to evaluate the possibilities of in-situ Eh measurement at the cold seep sites.

The in-situ Eh measurement system has been used in surveys of seafloor hydrothermal systems since 1993 by the author. The system has recorded significant electric potential drops of up to several hundreds of mV when it has encountered hydrothermal fluid (plume) during tow-yo CTD surveys, deep-towed side-scan sonar surveys and near-bottom TV-sled surveys at several sites e.g. South-East Pacific Rise (Nakamura et al., 1994; cf. Urabe et al., 1995), TAG hydrothermal field in the North Atlantic (Nakamura, 1994, unpublished cruise report of R.V. Knorr), TAG cruise (Kleinrock et al., 1995), Okinawa Trough hydrothermal sites (Nakamura et al., 1996) and a hydrothermal site near the Rodriguez Triple Junction in the Indian Ocean (K. Tamaki, 1996, unpublished cruise report of R.V. Meteor, M 33/2).

The system also recorded some hydrothermal indications at two EXPLOS survey sites during the SO109-3 cruise at the Juan de Fuca Ridge (Nakamura, 1996, SO109-3 cruise report). In the course of discussion with Prof. Erwin Suess in March 1995, we noticed that the cold seep water in the subduction zones might produce similar Eh anomalies, because the water from cold seep colonies usually contains hydrogen sulfide. A first attempt was made during Leg 1 of the Kaiko-Tokai cruise in the Nankai Trough, south of the main Japanese island, by R.V. L'Atalante in March, 1996. We tried to measure and to collect water samples from cold seeps by the VESP with the in-situ Eh measuring system. But problems with the electric link between the VESP and the armored cable of R.V. L'Atalante frustrated our plans and efforts.

10.2 Equipment and operation

The Eh measurement system is composed of two electrodes and a data logger. The electrodes were a Pt electrode and a reference electrode, which has a Ag-AgCl electrode contained in a pressure balanced zircaroi tube filled with saturated KCl solution. The data logger recorded the electric potential of seawater between the two electrodes at an interval of two seconds.

At the CTD stations 3-1 and 6-1, the system was located near the temperature sensor in the rosette (at the same height from the bottom of the rosette with the temperature sensor). At the EXPLOS stations 5-1 and 17-1, it was fixed to the EXPLOS frame near the CTD sensor, 80 cm from the bottom of the sled. At the VESP station 14-1, two systems were attached, one in the barrel and the other in the frame (outside of the barrel). At the ROPOS station 8-1 (Dive 340), it was located just behind the left manipulator of the vehicle and 95 cm above the

bottom of the vehicle. At ROPOS station 15-1 (Dive 341), it was attached to the rear flame of the cage, which is 140 cm above the bottom of the cage.

Because of the trouble with the data logger, the data at stations 6-1 (CTD), 5-1 (EXPLOS), 8-1 (ROPOS, Dive 340) and 14-1 (VESP, inside the barrel) were incomplete. The trouble in the latter three stations may be related to the reduction of the reference electrode, which is described below.

10.3 Results and discussion

At stations 5-1 (EXPLOS), 8-1 (ROPOS, Dive 340) and 14-1 (VESP, inside the barrel) AgCl coating of the reference electrode was reduced to Ag. It is well known that the Ag-AgCl reference electrode is not so resistant to hydrogen sulfide (H_2S). The reduction of AgCl on the reference electrode was due to the high content of H_2S in seawater at these stations. Such reduction has never occurred in previous surveys of hydrothermal sites even when the Eh electrodes passed or stayed very close to hydrothermal sources (e.g. black smokers). The environment near the seafloor must therefore be more reducing in these cold-seep areas than in hydrothermal areas.

The 14-1 station work by the VESP gave us some additional information on the environment near the seafloor. At this station, although the reference electrode situated inside the barrel was reduced during the 40 minutes deployment of the VESP on the seafloor, the other electrode situated outside the barrel and located 134 cm above the bottom was not reduced. Such phenomena also occurred during Leg 1 of the Kaiko-Tokai cruise in the Nankai Trough.

At the Geotechnical Module station, no. 2, three Eh measurement systems were attached to the frame, at 8 cm, 37 cm and 128 cm above the bottom of the module. The lower two reference electrodes were reduced, but nothing happened to the upper reference electrode. Moreover, the magnitude of the reduction of the lower two sensors were different. The surface of the Ag-AgCl electrode on the lowermost reference electrode was completely reduced, whereas that of the middle one was not completely reduced. About 50% of the original AgCl surface remained on the middle reference electrode. These facts suggest that there are steep gradients in H_2S content just above the seafloor at the cold-seep sites, although the position of the threshold content of H_2S for the reduction of electrodes might change from place to place and through time.

In the hydrothermal area, fluids emitted from the vents have buoyancy due to having higher temperatures than the ambient seawater temperature. The surrounding water mass just above the seafloor can maintain oxygenated conditions by the downward flow of the ambient seawater in hydrothermally driven convection cells. In cold-seep areas, there is no energy to cause convection, this may create somewhat stagnant conditions just above the seafloor compared to hydrothermal areas.

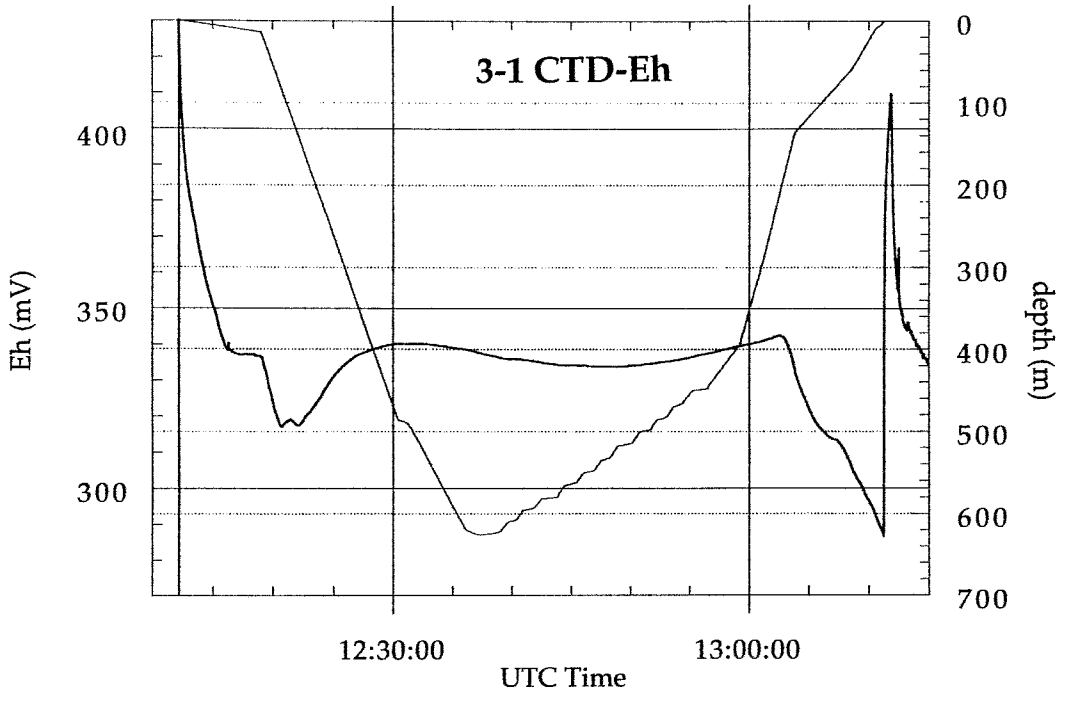

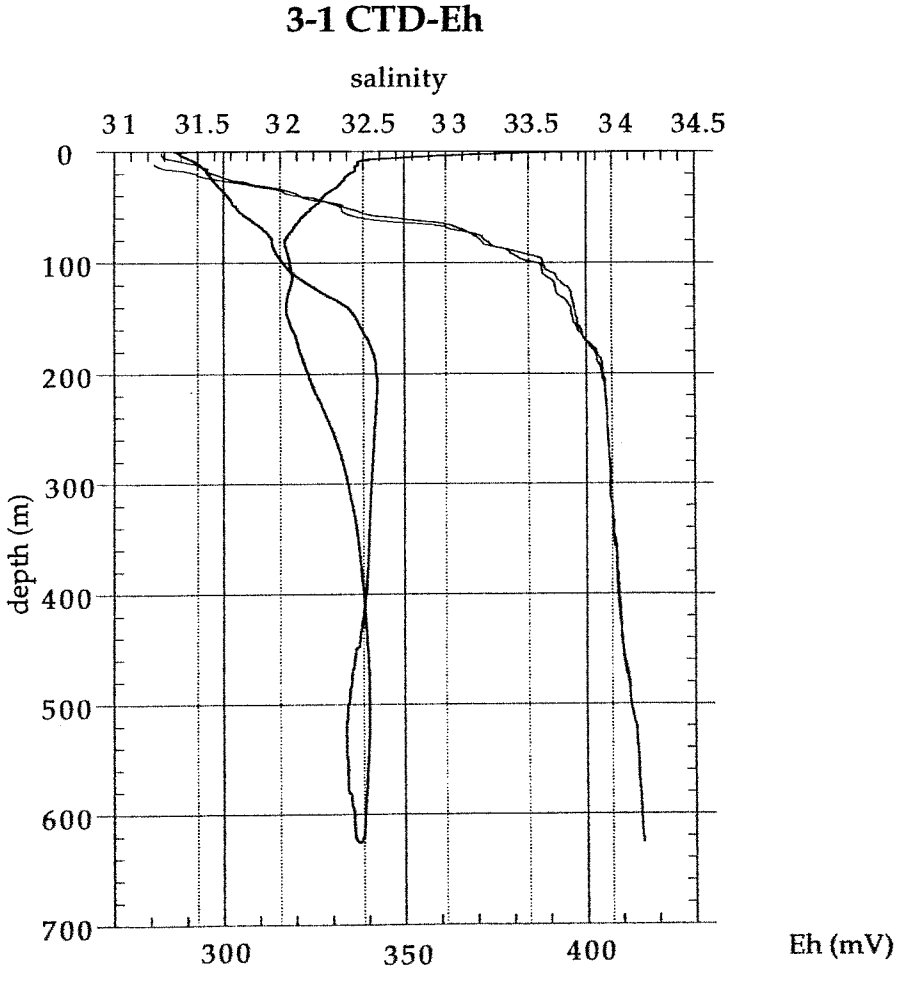

Fig. 32: a) Eh and depth versus time plots and b) Eh and salinity versus depth plots at the CTD station 3-1.

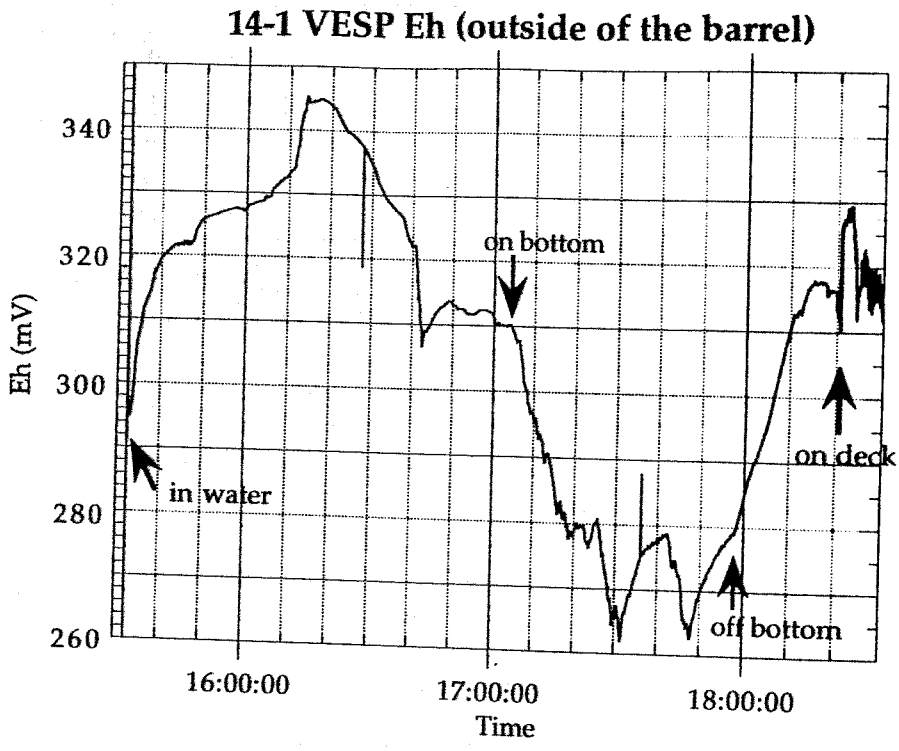

Fig. 33: Eh versus time plot, measured outside of the barrel, at the VESP station 14-1.

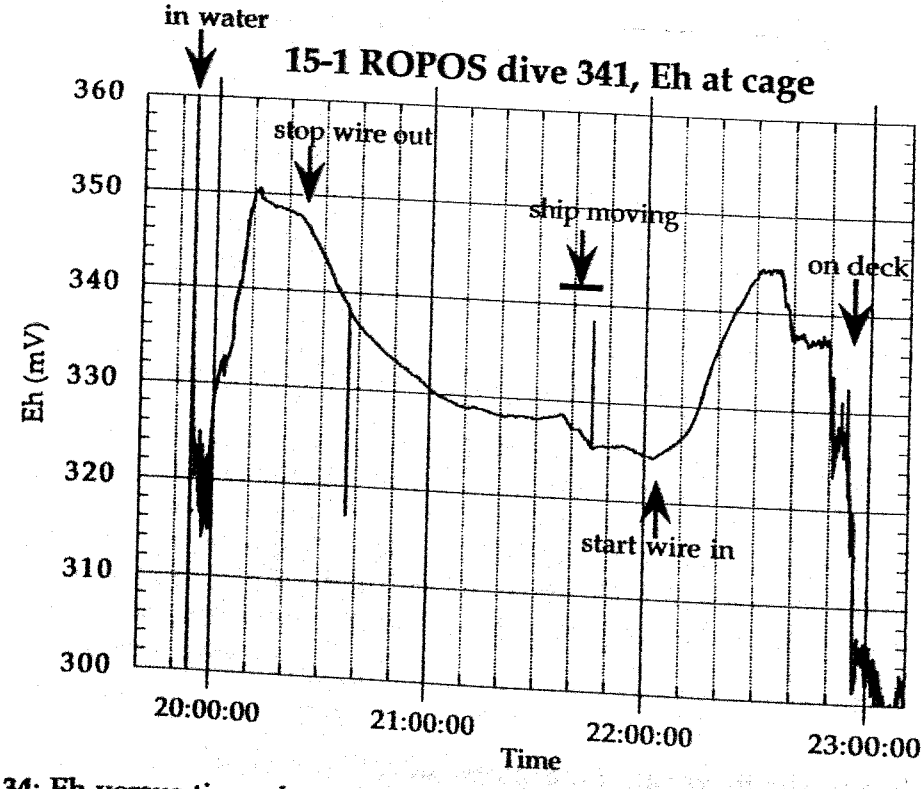

Fig. 34: Eh versus time plot at the ROPOS station 15-1(Dive 341).

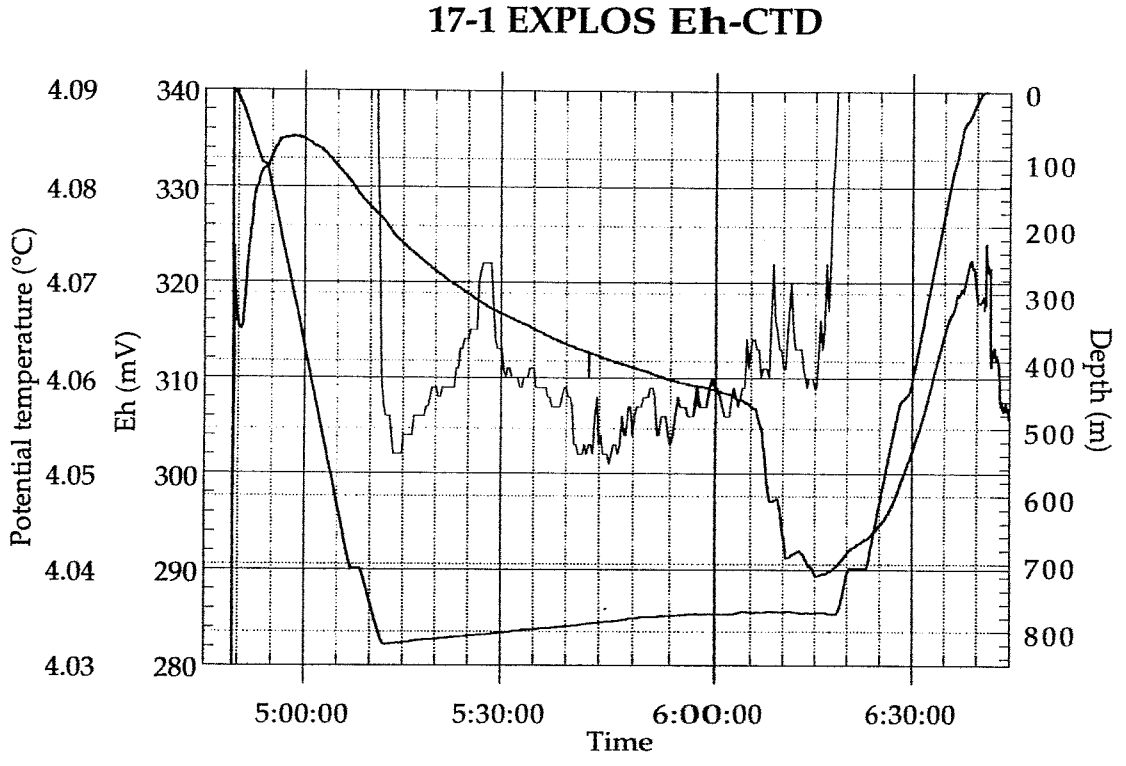

Fig. 35: Eh, potential temperature and depth versus time plots at the EXPLOS station 17-1. There is some uncertainty of up to several minutes on the time correlation between the Eh and CTD records.

Figure 32 shows the results of Eh measurements during the 3-1 CTD cast. The lowering and heaving, speed up to 50 m per minute made it difficult for the electrodes to be equilibrated to the surrounding water at the measured depth. However, there were no apparent Eh anomalies as recorded in the hydrothermal plumes at similar and/or faster speeds. Figure 33 shows the Eh measurement from outside the barrel at the 14-1 VESP station. The fluctuations of the Eh values between 17:25 and 17:58 cannot be explained, because there is no other data available for this station.

Figure 34 shows the Eh measurements from the cage of ROPOS at station 15-1 (Dive 341). A slight Eh drop between 21:38 and 21:45 may be due to cage movement resulting from ship movement. Figure 35 shows the Eh measurements at EXPLOS station 17-1. Eh drops at 6:08 and at 6:10, which correspond with the temperature anomalies, might be indicative of some fluid emission from the seafloor, where some bacterial mats were observed through the TV image.

Part II
Cruise Report
SONNE 110, Leg 1b and 2

16 July - 4 August, 1996 (Victoria - Kodiak)
5 August - 19 August, 1996 (Kodiak - Victoria)

Table of contents **Page**

1 The Gulf of Alaska accretionary complex and fluid venting

E. Suess, D. Orange, G. Bohrmann

1.1 Tectonic setting

The 3,000 km Aleutian trench is the surface expression of the active subduction zone between the Pacific and North American plates (Fig. 36). The eastern Aleutian trench separates continental from oceanic crust, and has been active since at least early Jurassic time (Plafker et al., 1989); conversely, the western trench (west of Shumagin Island) represents ocean-ocean subduction that initiated after the Bering Sea margin became sutured to the North American margin in Eocene time (Scholl et al., 1987).

From east to west along the present-day trench, the subducting Pacific plate is older (colder) and dips more steeply beneath the overriding plate (subduction angle increases), and is filled with less terrigenous trench-fill sediments (von Huene, 1989). The thickness of sediment entering the subduction zone varies from 3-5 km in the northeast to approximately 1.5 km off SHUMAGIN. In both areas, however, multi-channel seismic data display 1-3 km of sediment being subducted below the décollement; these subducted sediments may be accreted to the margin by underplating farther from the toe (and may be responsible for the uplift in the mid- to upper slope region; von Huene, 1989).

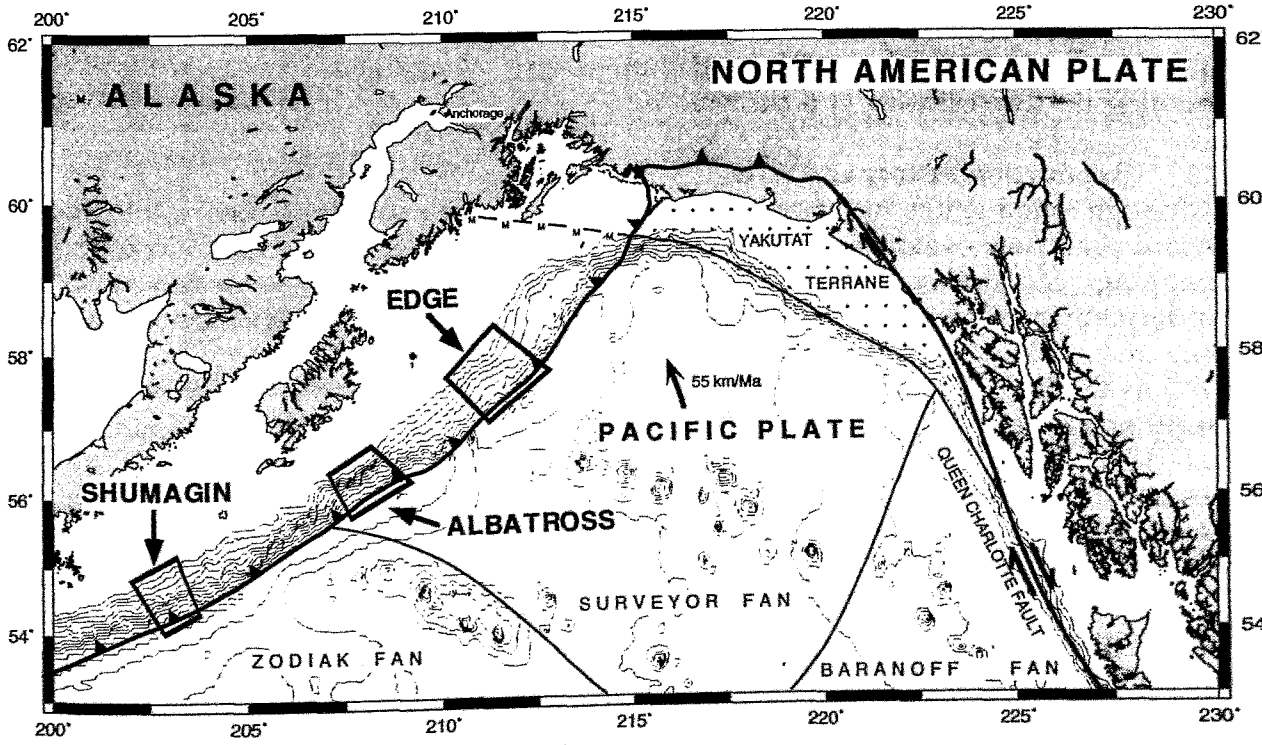

Fig. 36: Bathymetric map of the Gulf of Alaska showing major plate boundaries, fan deposits and the main areas of investigation during R.V. SONNE cruise 97.

1.2 Three fans

Three large fan systems are present on the northeastern pacific plate (Fig. 36). They are, from oldest to youngest, the Zodiac Fan, the Suveyor Fan, and the Baranoff Fan (von Huene, 1989). Plate reconstructions and microfaunal studies suggest that the Zodiak Fan, of 40-32 My age, was deposited far to the south, and transported north into the subduction zone along with the Pacific plate. Subduction of the Zodiac Fan began approximately 3-5 Ma. Sediments of the Zodiac Fan were drilled at DSDP Site 183 (von Huene and Kulm, 1973) and are composed of terrigenous sedimentary debris deposited by turbidity currents. However there was also reported a carbonate-rich upper horizon within the Zodiac Fan sequence. The Zodiac Fan is presently entering the subduction zone from Kodiak Island west to Sanak Island.

The Surveyor Fan was deposited on Pacific crust from 20 Ma, and has since been transported into the subduction zone in northeastern and central Alaska. The continentally derived glacial sediments of the Surveyor Fan are clastic and porous, and provide an abundant source of fluid during accretion (offscraping and underplating). The Surveyor Fan entered the subduction zone behind the Yakutat Terrane approximately at 3 Ma at Kodiak Island with the subduction of fan sediments progressing east as the Yakutat Terrane swept through the subduction zone.

Sedimentation of the Baranoff Fan began in the uppermost Miocene and continues today. These glacial sediments are similar to the Surveyor Fan, although this fan has yet to be subducted; instead, it currently sits astride the Queen Charlotte Transverse Fault off southeastern Alaska and British Columbia (moving north-northwest at 6 cm/yr).

1.3 Subduction history and style

Although subduction has been continuous since Mesozoic time, the geologic record preserves evidence of dramatically different accretionary styles. Geologic mapping of Kodiak Island indicates Jurassic to Paleocene accretion and underplating of trench and trench-slope sediments (Byrne, 1986; Moore and Allwardt, 1980). A regional unconformity in Oligocene to mid-Miocene time, as well as the immense volume of Eocene accretionary rocks, indicate a period of uplift and erosion at the surface and coincident underplating at depth (Moore et al., 1991b). This abrupt change in tectonic style may have been triggerred by the cessation of Kula-Pacific spreading, which would have decreased the convergence rate markedly from 200 to 40 mm/yr.

The present-day margin from the SHUMAGIN-sector to Kodiak Island contains an abrupt mid-slope topographic step at approximately 3,500 m. Seismic imaging and dredge samples indicate that this topographic step is the surface expression of an active out-of-sequence thrust fault that juxtaposes a landward Eocene accretionary/forearc basin sequence against a seaward Plio-Pleistocene to Recent accretionary complex. In fact, off Shumagin, the Oligocene-Miocene unconformity is presently at a depth of 2 km. The lack of a Miocene accretionary complex throughout the margin led von Huene (1989) and Lewis et al. (1988) to suggest that a period of tectonic erosion occurred as either the relict Kula-Pacific

spreading center, or the Yakutat Terrane, entered the subduction zone. Alternatively, the lower sedimentation rate before 6.5 Ma may have starved the accretionary complex and led to tectonic erosion.

The lower slope section, seaward of the topographic break, is comprised of an accretionary complex 3 Ma and younger. The subsidence of shelf basins off Shumagin, and the lack of compressional structures, demonstrate that in this region there has been no convergence landward of the upper slope since 3-5 Ma. Sediment accretion at the toe of the slope occurs by both landward and seaward vergence, although landward vergence is rare and increases in frequency toward the northeast. Furthermore, west of Kodiak Island high-angle cross faults appear to accommodate a significant amount of shortening.

1.4 Fluid venting in the Aleutian subduction zone

Fluid venting and dewatering of sediments along the global subduction zones have been recognised over the past ten years as a process of first order importance for marine geo- and ocean sciences (COSOD-2, 1987; Moore and Vrolijk, 1992). In the circum-Pacific subduction zones such processes are well documented in the Nankai trough (Sibuet et al. 1988), the Kurile trench (Sakai et al., 1992), at the Oregon margin (Suess et al., 1985; Kulm et al., 1986), at Costa Rica continental margin (McAdoo et al. 1996), within the Peru subduction zone (Bourgois et al., 1993) etc.

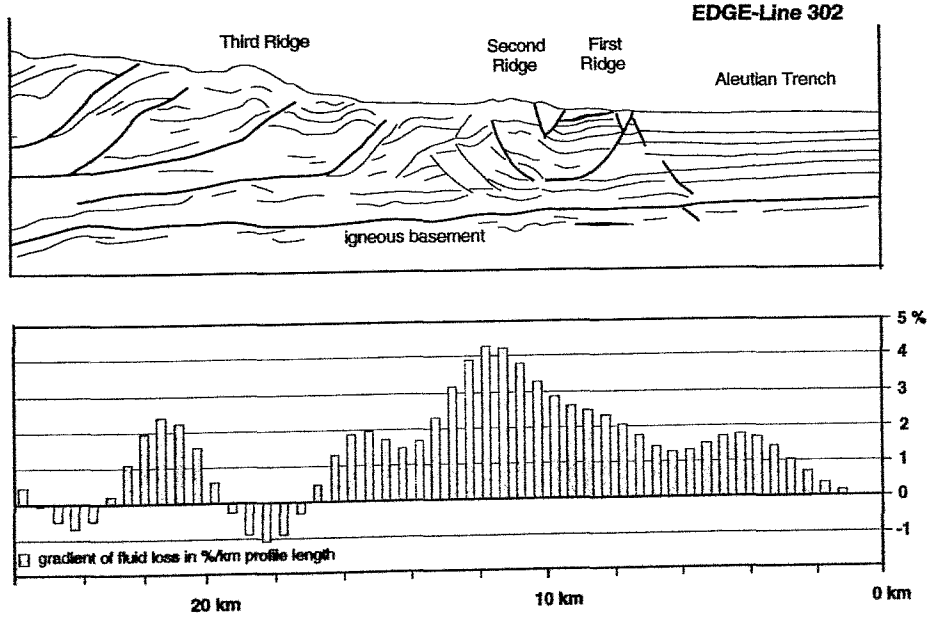

Fig. 37: Line drawing from the southeastern part of EDGE transect Line 302 and the fluid loss of dewatering calculated on porosity reduction after Huene et al. (1997).

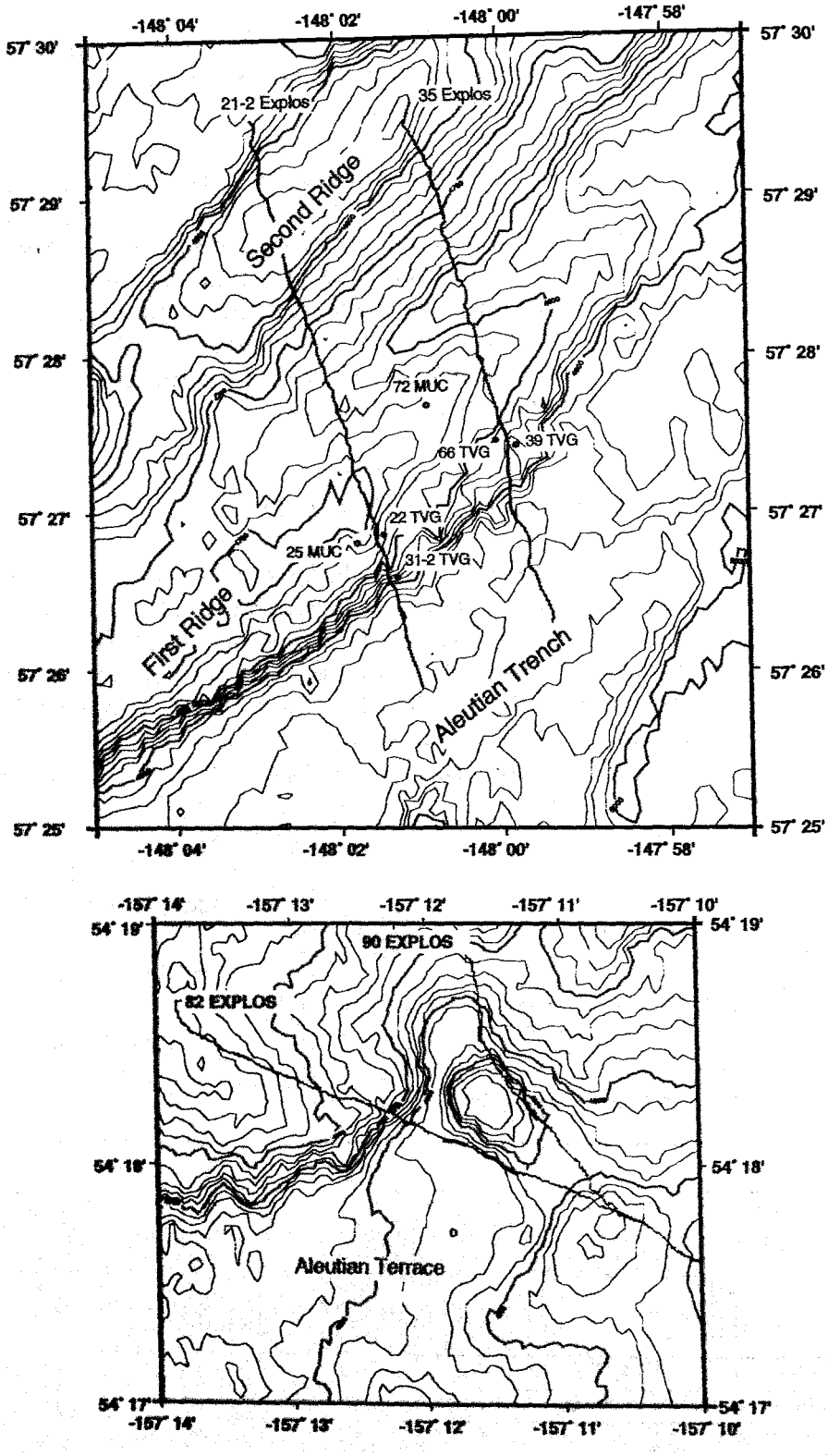

Fig. 38: Location maps of the vent sites from the EDGE-sector (a) and SHUMAGIN-sector (b) 20 m contour lines. The bold lines along the TV-sled tracks of the EXPLOS surveys indicate sites where active venting was found. Station numbers of the TV-guided box corer (TV-G) and the multiple corer (MUC) are also indicated.

In the Gulf of Alaska area, Frühn (1995), Kunert (1995) and von Huene et al. (1997) have derived a detailed dewatering scenario for several USGS seismic lines. Their convergence reconstruction and the velocity/porosity analysis of the EDGE multi-channel seismic lines demonstrate that 50% of the total net fluid loss occurs within the first 14 km of the toe of the accretionary complex (Fig. 37).

However, first evidence for active fluid venting within the Aleutian trench were found during the SONNE 97 cruise (Suess, 1994). Active vent areas were identified by mapping anomalies of dissolved methane and temperatures in the near-bottom water column and by conducting video-serveys in selected areas. This strategy assumed that the vents presently are emitting methane and other reduced chemical species (dominantly H_2S), maintain collonies of characteristic vent biota as well as create the environment conducive to the formation of vent precipitates. Active vent sites were found in all three sectors (Fig. 36) that were investigated (EDGE-, ALBATROSS- and SHUMAGIN-sectors) documenting that fluid venting is a common process within the Aleutian accretionary prism.

In the EDGE-sector the youngest tectonic structures, forming the deformation front, consist of two relatively gentle but structurally oversteepened folds with their flanks facing the trench (Figs. 38a and 39). These structures are parallel to and situated just off the trench axis at about 5,000 m water depth. Towards the southwest they terminate against a steep scar, believed to be the trace of a subducted seamount. The folds consist of subrecent trench fill; their relief reaches about 300 m above the trench floor; and their steepened flanks exhibit many small slumps visible in the high-resolution swathmapping (Fig. 38a). The oversteepened slopes expose horizontal to gently trenchward-dipping strata which form a series of escarpments (Fig. 39). Invariably at the base of these escarpments, but also higher up at intermediate steps in the morphology, colonies of characteristic vent biota and carbonate and barite precipitation within the sediments were found that are typical manifestations of fluid escape (Suess, 1994).

In the ALBATROSS-sector the deformation front consists of a growing anticlinal fold on the 5,000 m deep trench axial floor with a relief of up to 400 m. Sediment in the trench is probably distal glacial material channeled from southern Kodiak Island by a well-defined glacial trough extending from the island to the upper slope above the surveyed sector. Where it is crossed by a seismic line, the structure includes a blind backthrust with a landward verging fold (von Huene, 1989). The steeper slope facing the trench is also sculpted by slumps but generally they are not as numerous or as extensively developed as those in the EDGE-sector. The failed slopes expose horizontal strata in the strike direction along which fluids escape, apparently rapidly enough to support the vent colonies observed here (Fig. 39).

The SHUMAGIN-sector, where the trench axis is 6,000 m deep, receives most of its axial fill by lateral transport from the northeast. The folds at the deformation front show little evidence of slumping and are discontinuous along strike. Due to the more oblique subduction direction in this part of the survey, the lateral

component on convergence becomes larger than to the northeast and hence a set of shear faults develops diagonal to the axial trend (Lewis et al, 1988). Little evidence for venting was found along the folds at the deformation front, instead more active vents and extensive carbonate crusts were observed along the crestal regions of ridges further upslope, where they were cut by canyons (Fig. 38b). The vent biota were in colonies similar to those in the EDGE- and ALBATROSS-sectors.

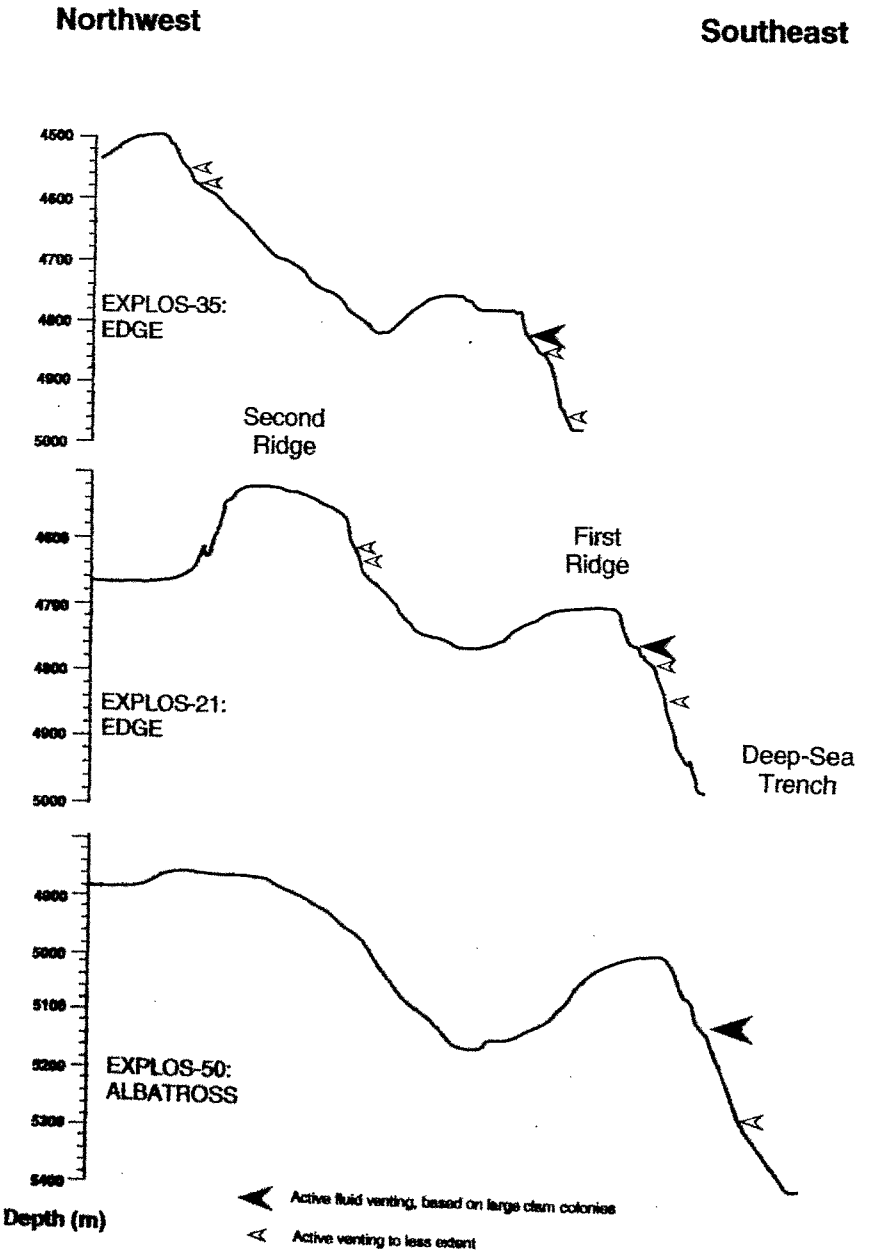

Fig. 39: Depth profiles taken by CTD-measurements along EXPLOS tracks during R.V. *Sonne* cruise 97. Sites of active fluid venting are indicated.

2 Cruise narrative and preliminary results

E. Suess and G. Bohrmann

Week of 17 - 24 July 1996

After mounting the new glass-fibre cable and necessary adjustments of the cable drum and the new ROPOS winch, R.V. SONNE departed Victoria on July 17 at 2030 local time heading for the working area EDGE at the eastern end of the Aleutian Trench. In exceptionally good weather and calm seas we covered more than 1,000 nm in a transit in only 90 hours including a four-hour stop for testing the ROPOS system by lowering the cage and diving to 600 m on July 20 at around noon.

The transponder net was deployed in the working area on July 13 at 13:30. Following a brief hydrosweep survey and recording of hydroacoustical velocity structure in the upper water column six transponder were dropped. An EXPLOS survey was taken west of the vent fields found during SO 97. After completion of the calibration of the net on July 22 at 11:00 the first ROPOS deployment began. At a depth of 3,200 m, almost 800 m deeper than the device had been brought into action previously, two of the 6 hydraulic systems showed a pressure drop which requiered compensation. This delayed the deployment of the system by 4 more hours. However, at 19:00 the same day a record diving depth of 4,960 m was reached with all systems operating.

After only 20 minutes of bottom time in the vicinity of the previous sighting of vent communities during SO97 numerous clam fields, pogonophoran colonies of substantial size as well as individual specimens of vent organisms were found. Thanks to the highly maneuverable camera system of ROPOS a fascinating and so far unique visual documentation of deep subduction zone vents and their biological communities was possible. The survey was conducted uphill across the seaward flank of the first accretionary ridge (Figs. 40 and 41). On several steep terraces and in narrow canyons dozens of vent fields were observed. Several profiles were run at an angle to the slope and one along strike. Here vent fields were almost continuously lined up. The ROPOS deployment lasted until late afternoon of July 23; reaching a record time of 17.5 hours for deployment at the bottom and also a record for the longest continuous system deployment of over 28 hours. The entire deployment at the bottom took place at water depths between 4,960 and 4,830 m, more than doubling the previous maximum deployment depth. During the entire operation not one single device of the numerous observation, sampling, sensor, and navigation systems of ROPOS failed. In addition to the technical highlights associated with the deep deployment there were the following scientific highlights recorded: Detailed and unique visual documentation of the vent communities and associated fauna; systematic surveying of the seeward flank of the first accretionary ridge defining topographic units at which dewatering occurs preferentially; clarification of the ridge´s structure as an oversteepened fold with a fracture system; sampling macrofauna, bacterial mats and bottom water in the vent area.

On July 23 at 18:30 in deteriorating weather conditions and rain ROPOS was returned back on deck. The routine check showed that after the system´s absolutely magnificent operation at 5,000 m another problem had developed: the failure of the glass-fibre cable. Eight optical fibres broke between 100 m and 500 m from the drum´s end. After assessing the extent of the damage and the alternatives it was clear that this problem could not be fixed at sea during SO110 considering time and logistics. The decision to discontinue the ROPOS operation was made in agreement with BMBF and all partners involved. Hence, the ROPOS team and equipment were unloaded in Port Valdez. Work on the scientific objectives in the areas EDGE, ALBATROSS, and SHUMAGIN continued as far as possible without ROPOS.

Week of 24 July - 5 August 1996

On July 24 in the late afternoon R.V. SONNE left the working area EDGE to disembark the ROPOS team and equipment in Port Valdez as planned. After passing the impressive scenery of Prince William Sound R.V. SONNE anchored the following night outside the harbour and proceeded in the morning of July 27 to dock and immediately began to demobilize and unload the ROPOS system. Unloading was completed in the evening of the same day and the vessel departed Valdez at 20:30 local time to return again to the working area EDGE where she arrived on July 28.

The scientific programme was changed to rely more on VESP and TV-grab deployments at the vent localities of the first accretionary ridge and on EXPLOS-surveys. The VESP/TV-grab deployments where along the seismic profile EDGE and documented active dewatering at two sections when crossing the accretionary ridges. Though the first ridge does not have a morphological expression here but it is characterized by prolific vent communities.

In the evening of July 29 R.V. SONNE transited to the westernmost area SHUMAGIN. In transit near the Island of Ugak a successful survey was conducted by EXPLOS. Here again active vent colonies were found on the seeward flank of the accretionary ridge. No sampling was conducted in order to reach the area SHUMAGIN without further delay. On July 30 an EXPLOS survey was carried out on the second accretionary ridge but yielded only slight indications of vent activity. From earlier investigations during SO97 along a transversel fault on the third ridge prominent fluid vents were known which were to be sampled subsequently. However, the first two deployments failed: water penetrated into the camera housing of the TV-grab and the release mechanism of the TV-guided box corer sheared off when penetrating the sediment.

A methane plume centered between 3,500 - 4,960 m with maximum concentrations around 4,750 m was again found just like two years ago. The concentration however reached only 42 nl/l and was, thus, clearly less developed than 2 years ago. On August 2 a new attempt with the TV-guided box corer was successful, although the box was slightly damaged when it hit a carbonate crust

and the major part of the content was washed out. Nevertheless, a rich vent fauna was retrieved (Solemyas, Calyptogenas, Pogonophorans, tubes of vestimentiferans, gastropods and others) in an amazing range of sizes. Also fragments of the carbonate crust underlying the sediment were recovered. The crust was peculiarly porous caused by penetrating pogonophorans. On August 3 a successful VESP-deployment with recording flow data was carried out. This was

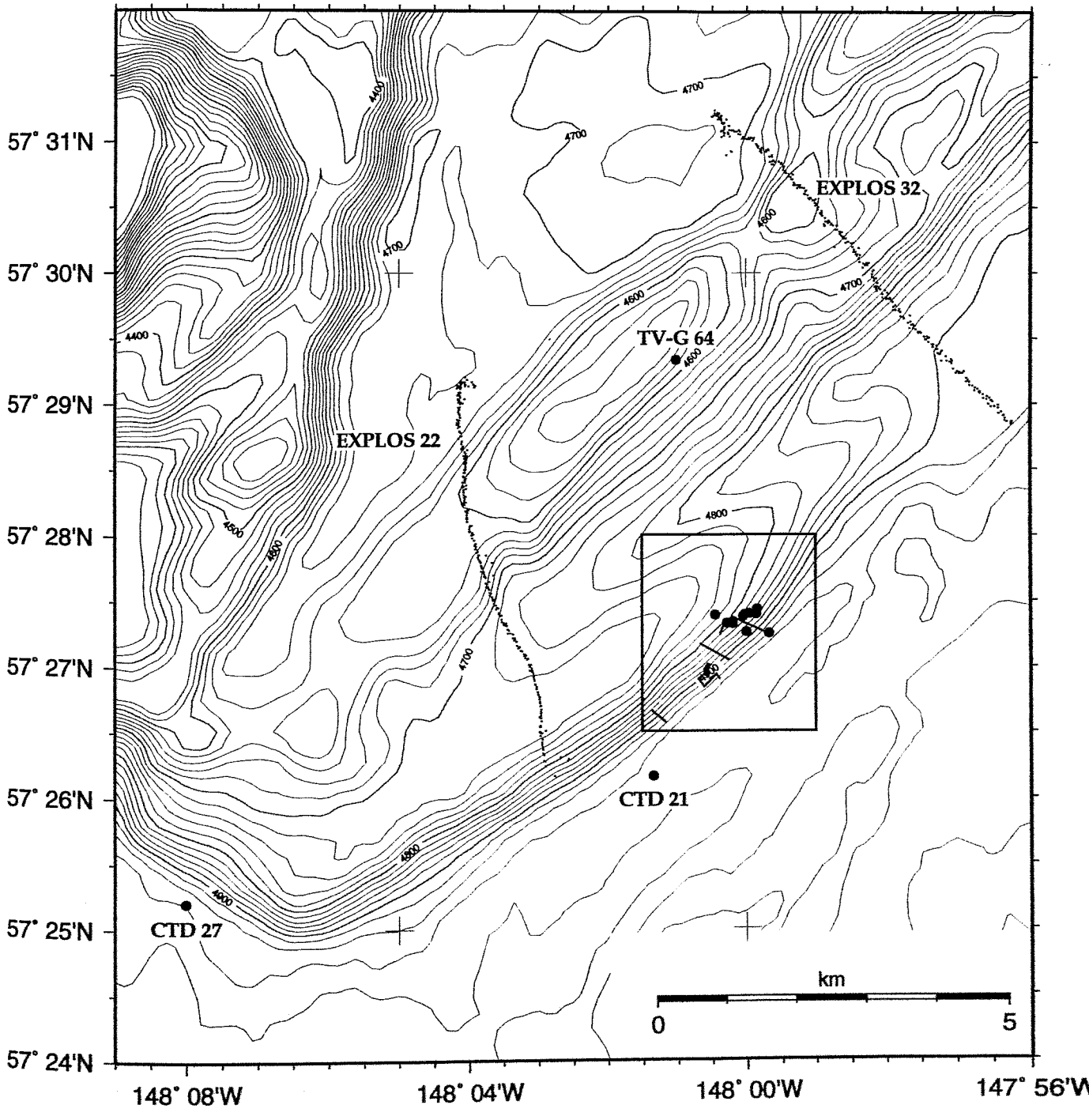

Fig. 40: Station work at the EDGE-sector during Legs 110-1b and 110-2. The box area is shown in greater detail (Fig. 41).

followed by a renewed failure of the TV-guided box corer when the release mechnism was again sheard off. In water depths of around 5,000 m failures such as these clearly affected the available station time.

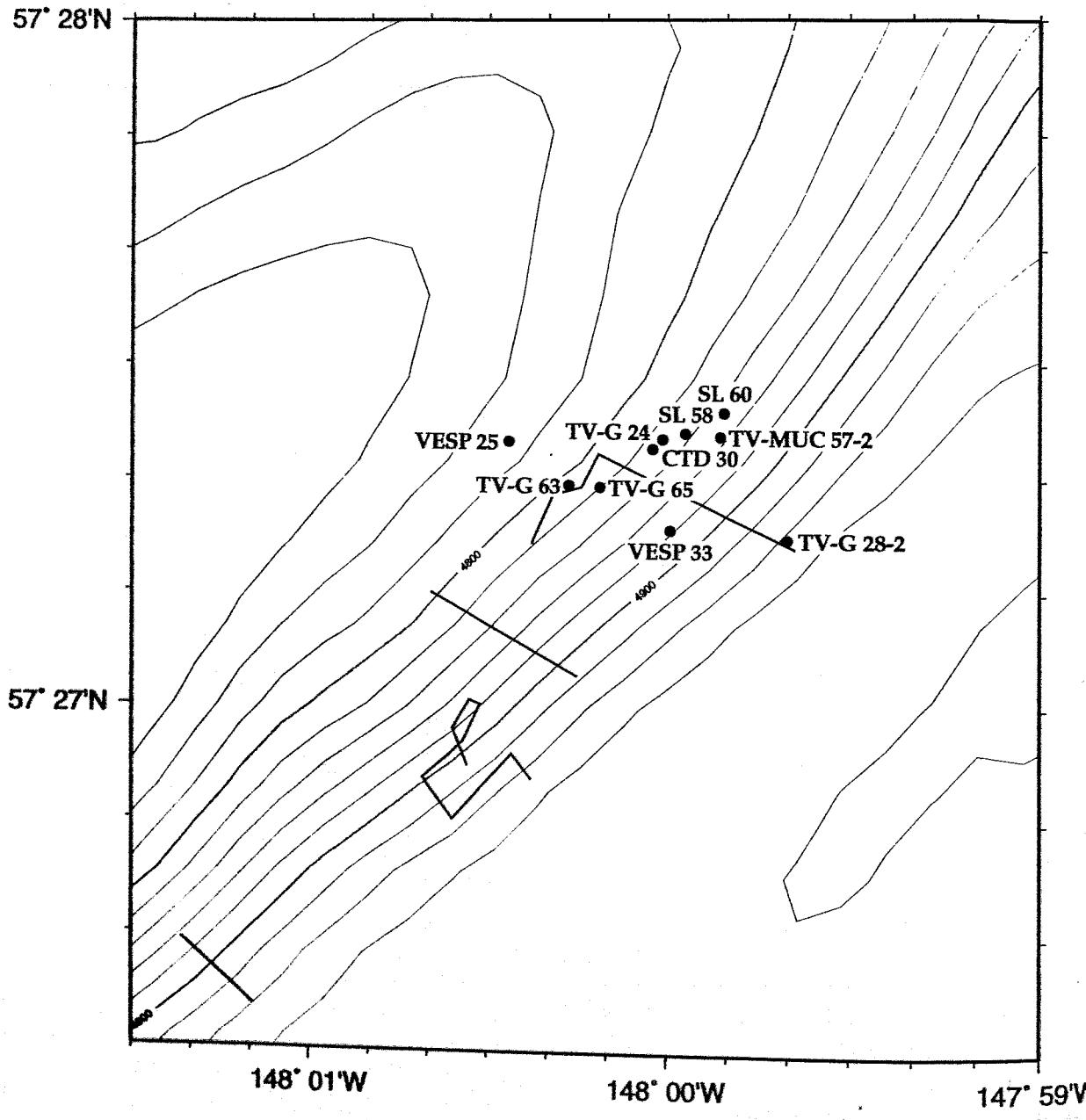

Fig. 41: Detail area from the southeastern flank of the first accretionary ridge (box area of Fig. 40). ROPOS survey is indicated by track lines in black.

We succeeded in placing a TV-grab directly on a field of pogonophorans after almost 8 hours of search. This core yielded sample material for pore water-sediments and gas-analyses as well as hundreds of individuals of Pogonophorans, Calyptogenas, and Solemyas. To complete work in SHUMAGIN the vent sampler was deployed in a new free-return configuration for the first time. All systems

operated without problems and the device was put down at 4,780 m. The frame, telemetry, video cameras, lights and CTD-probe were then separated from the *in situ* device and brought back onboard. The *in situ* device equipped with long-term recorder for flow data and sequential water sampling was actuated to return to the surface after 6 hours. However, this attempt failed for as yet unknown reasons. We left the device at its original position and departed SHUMAGIN on 4 August in the morning. Twentyfour hours later on 5 August R.V. SONNE tied up at Kodiak to exchange several groups of scientists.

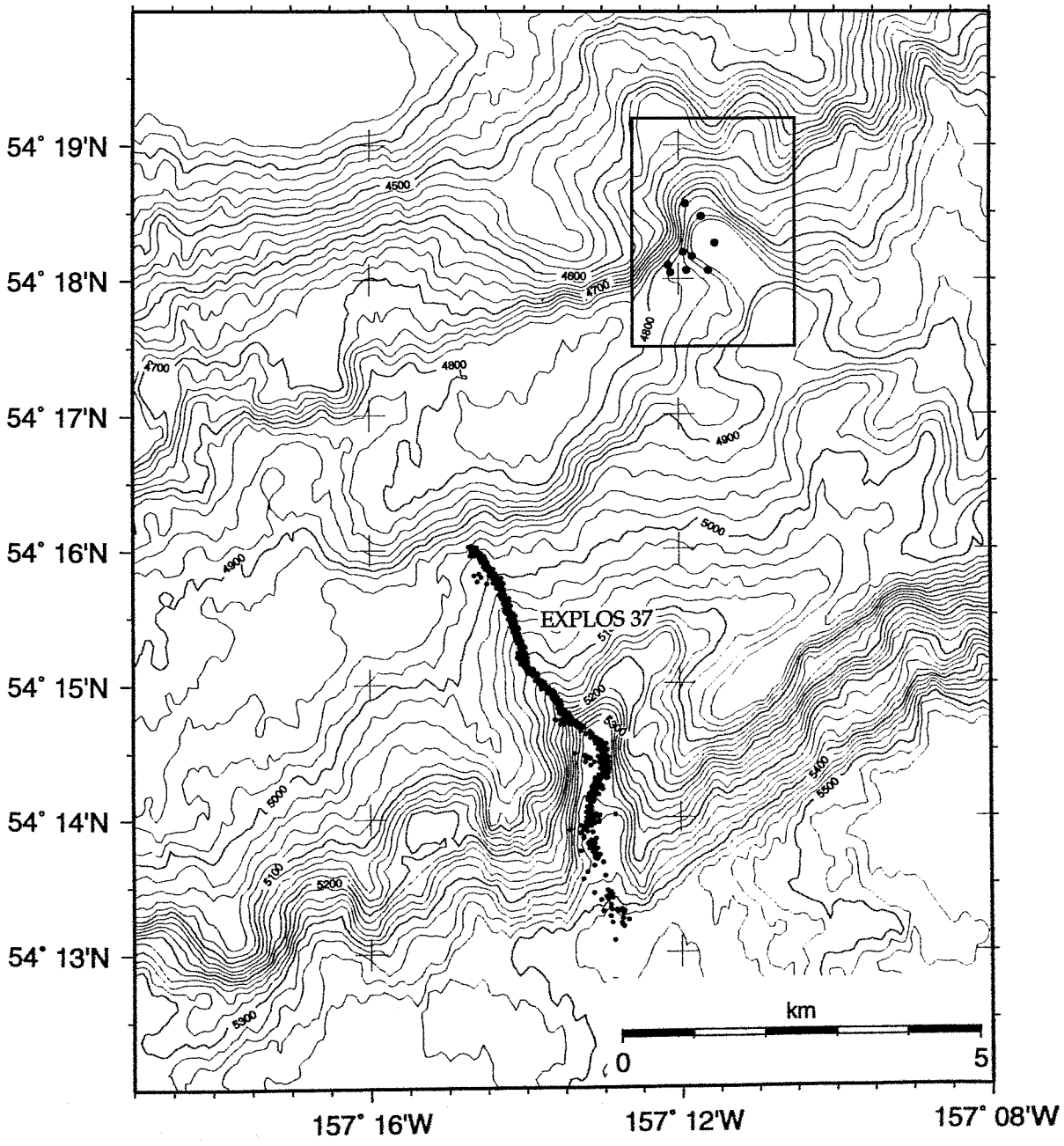

Fig. 42: Station work in the SHUMAGIN-sector. The box area is shown in greater detail (Fig. 43.)

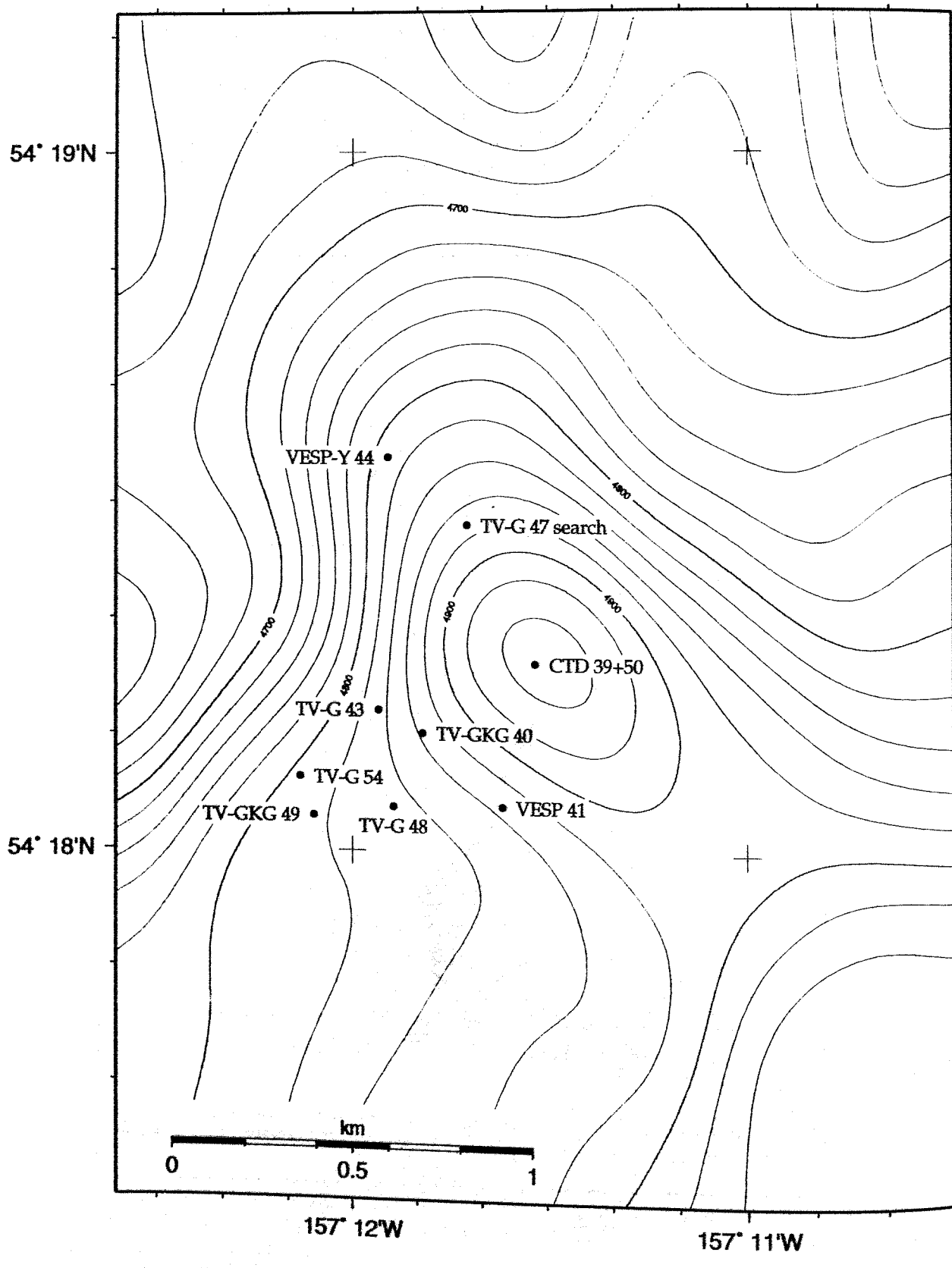

Fig. 43: Station work in the SHUMAGIN canyon (box area of Fig. 42).

Week of 6 - 18 August 1996

The last leg of the SONNE 110 cruise (SO110-2) started on 5 August after an exchange of the scientific crew in the habour of Kodiak. During this leg investigations of subduction-induced fluid venting in the Aleutian accretionary prism were planned without the use of the canadian remotely operated vehicle. R.V. SONNE departed Kodiak at 18:00 p.m. local time in exceptionally good weather. During transit to the working area SHUMAGIN large areas parallel to the trench axis were covered by HYDROSWEEP mapping. Station work began at the following morning in the SHUMAGIN-sector.

Work started with the search for the new vent sampler in the SHUMAGIN canyon (Fig. 43). This instrument was lost on the last day of the previous leg. A large fish-hook was mounted on the TV-grab to get hold of the device. Based on acoustic measurements of the transponders we were able to approach up to 18 m but were never able to see it with the TV-grab camera or even to recover it. After twenty hours of search this operation was stopped in order to save the rest of the ship time in the SHUMAGIN-sector for vent sampling.

During the remaining two and a half days we tried to use all TV-guided sampling instruments.The most successful instrument in obtaining vent samples was the TV-grab. TV-G 48, 54 and TV-GKG 49 (Fig. 43) recovered numerous important sediment cores as well as clams and several specimen of pogonophorans from vent field areas on the southwestern terrace of the NW/SE trending SHUMAGIN canyon. Unfortunately no additional carbonate precipitates could be sampled, as recovered during SO97 cruise. CTD station 50 (Fig. 43) completed the hydrocast sampling of CTD 39 from leg SO110-1b for the upper water column and showed an additional methane peak of 70 nL/L at the bottom of the canyon. Sampling in this area revealed the overal higher methane contents in the SHUMAGIN-sector than in other fluid venting areas of the Aleutian trench.

During the evening of August 10 we finished our station work in the SHUMAGIN-sector and transited to the easternmost area the EDGE-sector. During this 30 hour long transit additional HYDROSWEEP tracks along the trench axis parallel to the older profiles filled gaps in crucial areas of the swathmapping. As a result of this a 20-30 km wide bathymetric map of the Aleutian trench over a distance of 800 km was produced. This map shows us the morphology in great detail which is very important for future work in this area. At this point it is important to notice that the major part of the HYDROSWEEP measurements were achieved during transit times which did not consume valuable station time. Unfortunately a planned EXPLOS survey in the CHIRIKOF-sector could not be conducred due to time restriction.

During 11 - 14 August an intensive programme of vent sampling was carried out in the EDGE-sector (Figs. 40 and 41). In this area active vent sites were found during SO97 and the ROPOS dive during SO110-1b. The vent sites are restricted to seaward dipping slopes of the first and second anticlinal ridge at the frontal thrust. Here a series of escarpments and steps mark outcrops of dipping beds as well as thrust faults which serve as conduits for expelled pore fluids and gases.

Although it was difficult to sample vent fields in 5,000 m depth using the TV-guided instruments several complete pore water profiles of vent sediments as well as a rich vent fauna could be retrieved. TV-multicorer and TV-box cores were less successful than the TV-grab sampling. All instruments were navigated with a Super-Short-Baseline transponder system by Simrad. In addition to the previous sampling of the first ridge we sampled vent sites of the second ridge in order to compare the geochemical differences of two separate dewatering systems. The analysis of all the pore water profiles as well as the vent communities will allow to give answers on numerous scientific questions.

Scientific program of SO110 in the Gulf of Alaska ended on August 14. During the night a small HYDROSWEEP survey recorded details of the Kodiak Seamount bathymetry. R.V. SONNE headed for Victoria, where she tied up at Odgen Pier on August 18 at 7:00 a.m. local time.

3 Swathmapping and sidescan sonar imaging

3.1 HYDROSWEEP survey

W. Weinrebe, F. Heeren

The swath mapping system HYDROSWEEP (HYDROgraphic multi-beam SWEEPing survey echosounder, by Atlas Elektronik GmbH, Bremen) was used to continuously map the seafloor. With 59 acoustic beams at an angle of 90° a swath width of about twice the water depth is achieved. The working frequency of the system is 15.5 kHz.

The HYDROSWEEP data were processed onboard using the MBSystem software developed at Lamont-Doherty Earth Observatory by Caress and Chayes. The raw data were first converted to depth using the sound velocity profile measured in this area by the CTD probe. Sweeps including all 59 beams were displayed in profile on a screen and edited to eliminate erratic points. Edited sweeps were then assembled, gridded, and contoured with the GMT software (Wessel and Smith, 1991). No filters were applied to smooth the edited data. Thus more small tectonic features, but also more noise, are visible in the maps; however, the viewer can distinguish between small tectonic features and map artifacts.

During SO96 and SO97 a large part of the Alaskan continental margin was mapped (Flueh and von Huene, 1994, Suess, 1994), and during SO110 the surveyed area was extended considerably. Transits between sampling stations were carefully planned to optimize mapping and to systematically fill the gaps, with HYDROSWEEP measurements concentrated on the lower part of the continental margin. Now a complete coverage of the lower margin over a length of more than 800 km could be achieved (Fig. 44) and combined with seabeam data gathered by NOAA ship SURVEYOR in 1986.

The swathmapping data document two contrasting continental margin morphologies. In the western Gulf, a trench-parallel ridge and trough morphology characterizes the accretionary terrain along the Aleutian subduction zone. Along the northern Gulf, the slope is sculpted by large canyons and a pervasive system of small canyons and rills. This morphology characterizes the trailing edge of the Yakutat Terrane and parts of the slope beneath which the trailing edge of the Terrane subducts.

Three parts of the mapped areas which are based mainly on data gathered during SO110 are discussed in more detail below.

3.1.1 SHUMAGIN-sector

The area off Shumagin Island was the westernmost region investigated. Several sampling sites are situated here. An area of roughly 80 km to 40 km comprising the depth region from the mid slope (2,500 m) to the trench (5,500 m) was completely mapped (Fig. 45). This part of the continental margin is characterized by two steep cliffs, from 3,000 m to 4,000 m and from 5,000 m to 5,500 m and the gentle Aleutian terrace 30 km to 40 km wide inbetween. A prominent canyon in

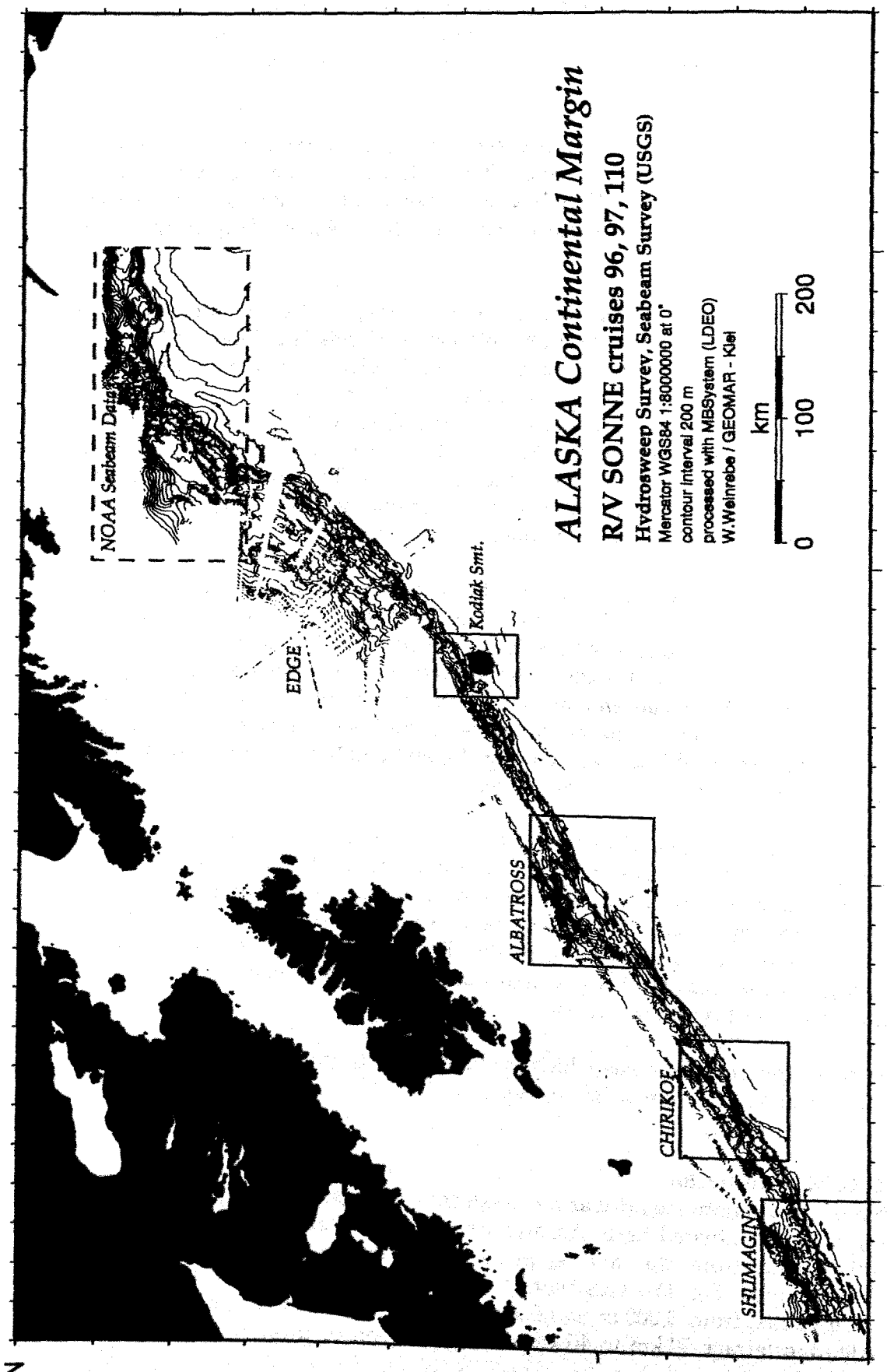

Fig. 44: Bathymetry of the Alaska continental margin from the HYDROSWEEP survey during SO96, SO97, SO110 and NOAA-SURVEYOR-1986 (dashed box). Areas shown in greater detail are indicated by boxes.

the middle part cuts both steep walls. A sedimentary fan at the mouth of the canyon in the trench documents considerable sediment transport from the mountains and glaciers of the adjacent Alaska Peninsula (Figs. 46 and 47).

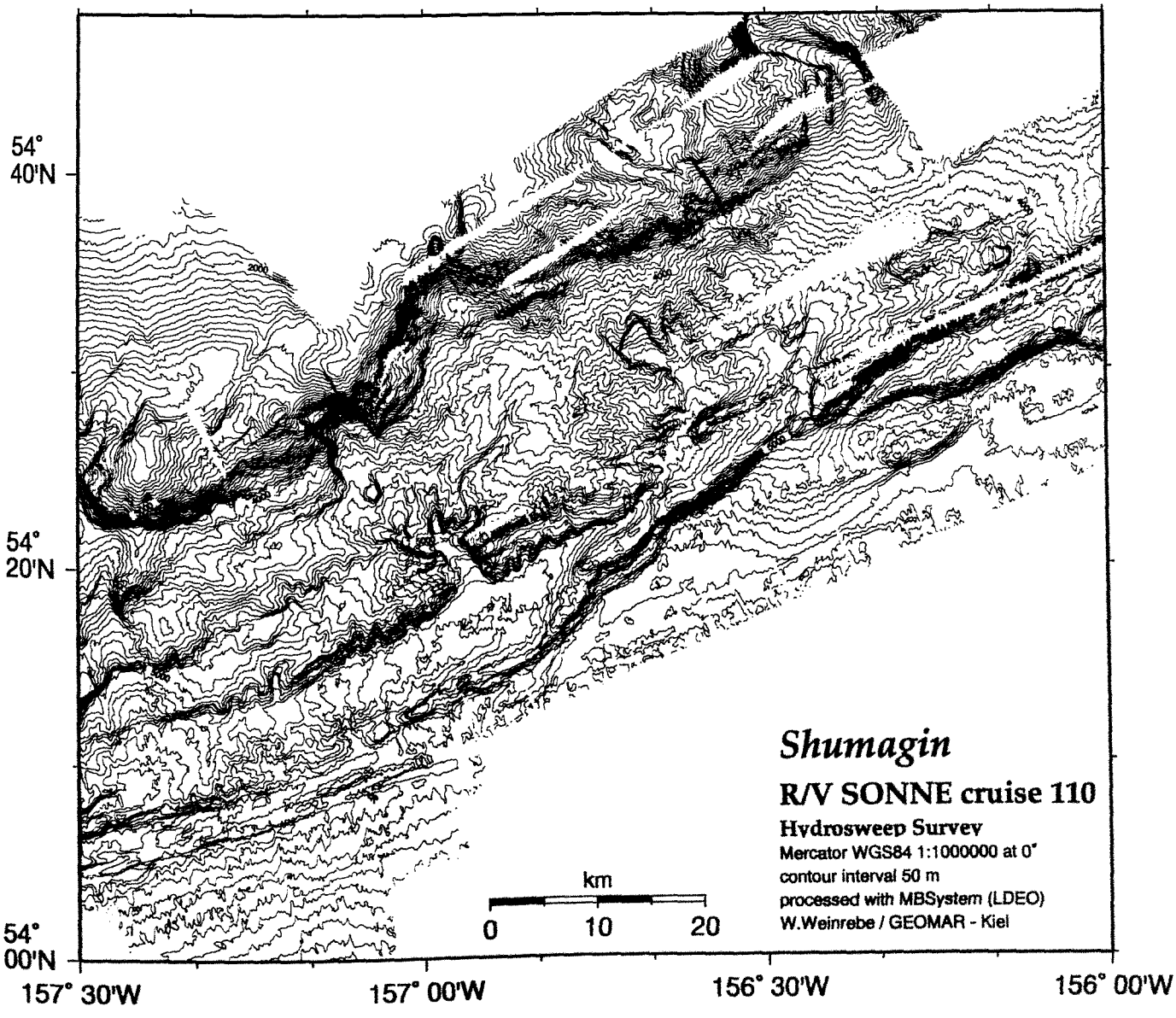

Fig. 45: Bathymetry of the SHUMAGIN area from the HYDROSWEEP survey during SO96, SO97, SO110.

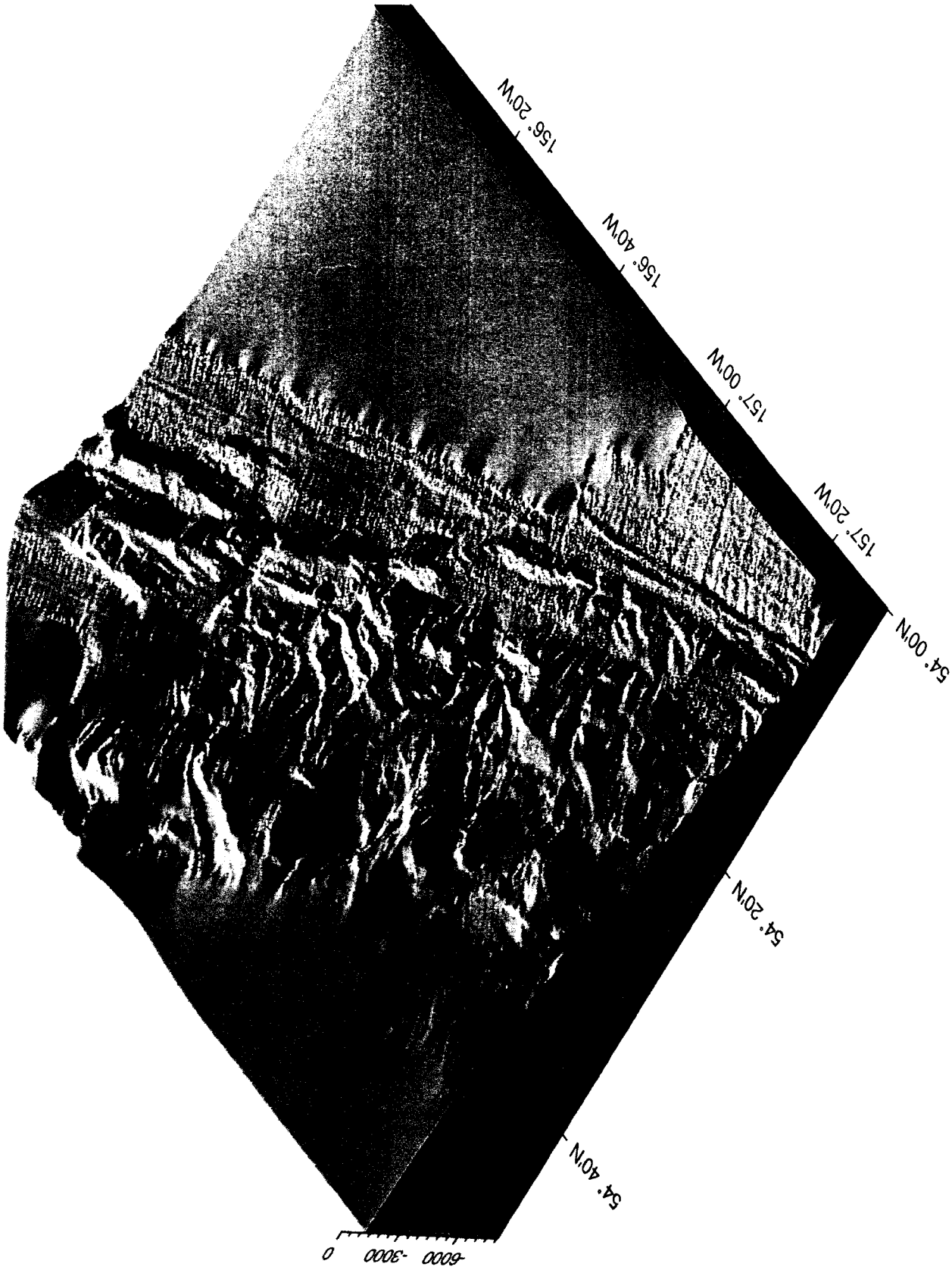

Fig. 46: Perspective view of the SHUMAGIN area. View from the southwest, elevation 45°, illumination from the northeast.

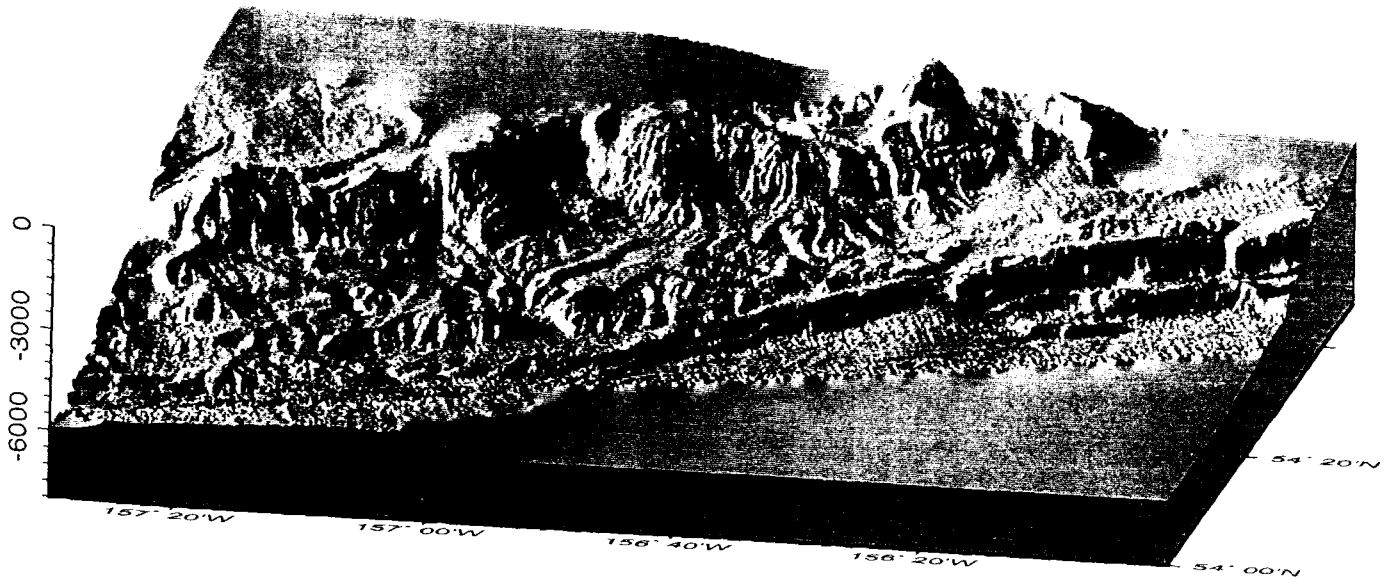

Fig. 47: Perspective view of the SHUMAGIN area. View from the south, elevation 15°, illumination from the west.

3.1.2 CHIRIKOF-sector

The area off Chirikof Island (Fig. 48) is characterized by a steep scarp in the lower slope, the middle terrace is uplifted, and the frontline of the lower slope is indented at this place. On the oceanic plate this is marked by a fault with an angle of approximately 35 degrees (Fig. 49). Obviously a topographic irregularity on the oceanic plate, maybe a seamount, caused this structure during subduction, as it is also in line with the Patton Seamounts on the plate.

3.1.3 ALBATROSS-sector

The Albatross area south of Kodiak Island was mapped from around 1000 m depth to the trench at 5,200 m depth (Fig. 50). The mid-slope Aleutian terrace, found here at two levels at about 4,000 m and 4,900 m respectively, each about 10 km wide, divides the area into two tectonic provinces (Fig. 51). The upper slope has a steep and rugged morphology dominated by canyons and rills. The lower margin is characterized by elongated trench parallel ridges and troughs, a typical subduction and accretion morphology.

3.1.4 Kodiak seamount

The Kodiak Seamount southeast of Kodiak Island is the one closest to the subduction zone in the chain of the Kodiak - Bowie seamounts, and the next one to collide with the Aleutian continental margin (Fig. 52). This seamount with a diameter of 20 km rises nearly 2,500 m above the surrounding ocean floor. It is much higher and steeper than the lower continental margin with which it collides. The lower slope of the margin is shifted about 5 km to the northwest along a transverse fault (Fig. 53).

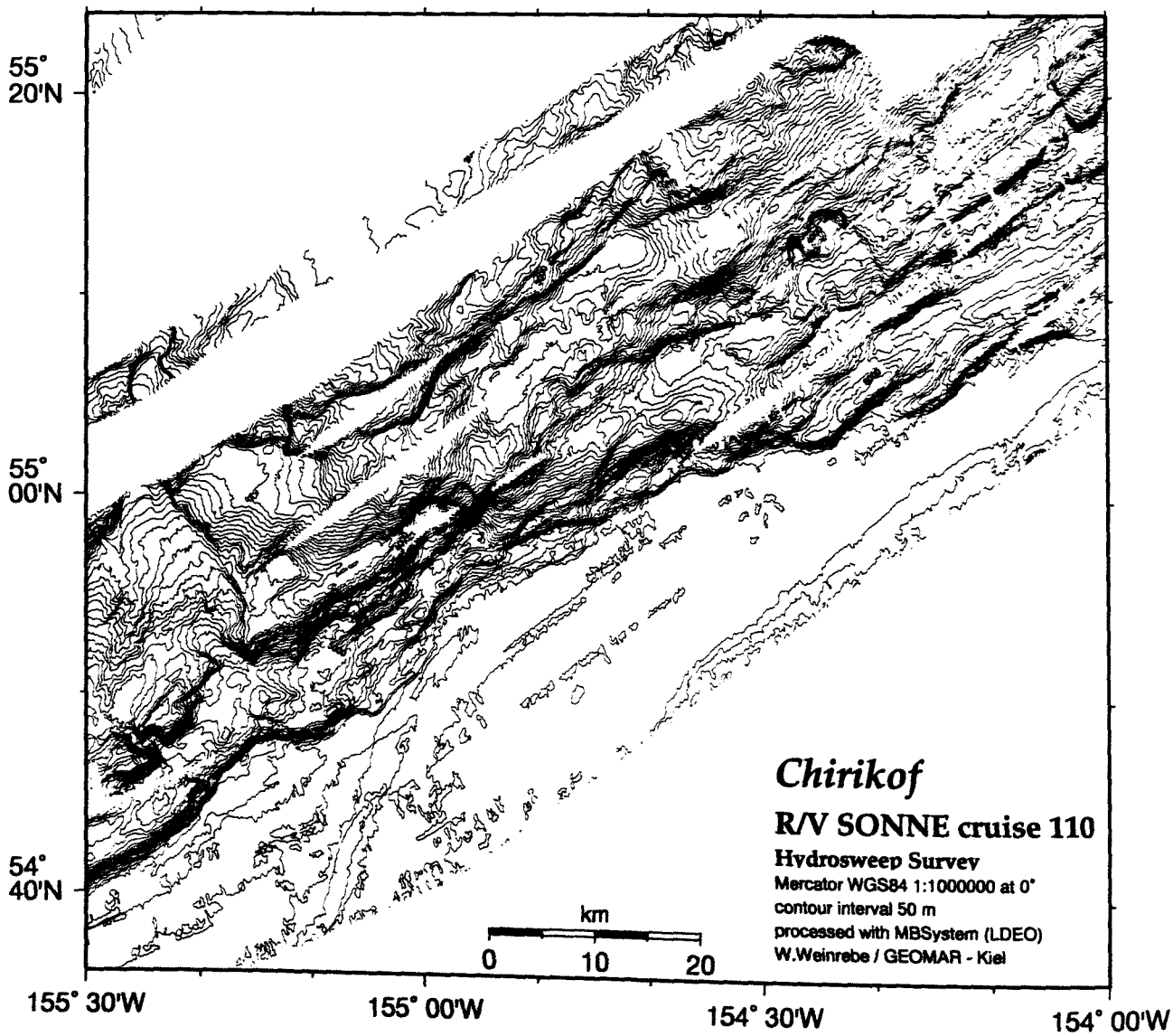

Fig. 48: Bathymetry of the CHIRIKOF area from the HYDROSWEEP survey during SO96, SO97, SO110.

Fig. 49: Perspective view of the CHIRIKOF area. View from the east, elevation 55°, illumination from the west.

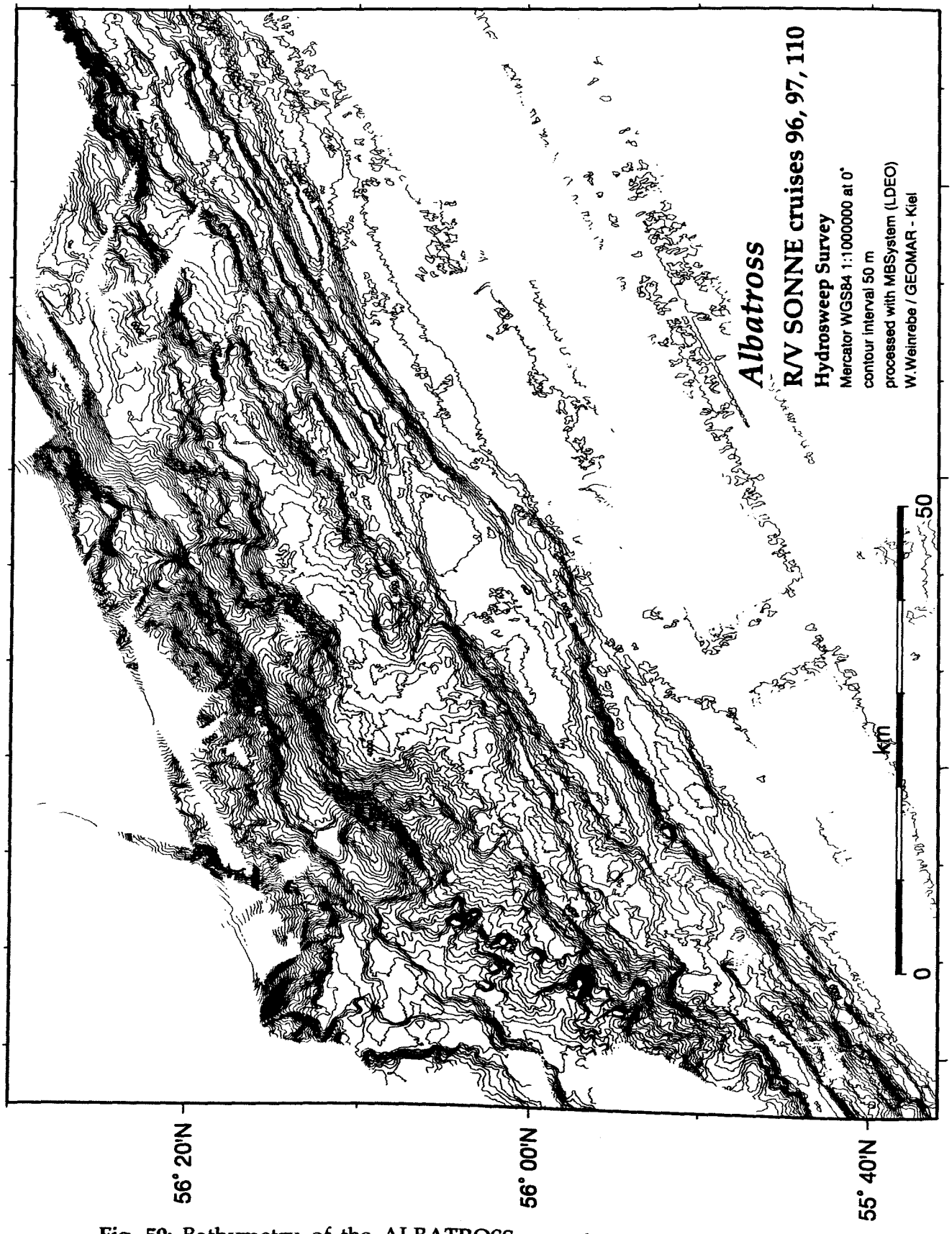

Fig. 50: Bathymetry of the ALBATROSS area from the HYDROSWEEP survey during SO96, SO97, SO110.

Fig. 51: Perspective view of the ALBATROSS area. View from the southeast, elevation 35°, illumination from the west.

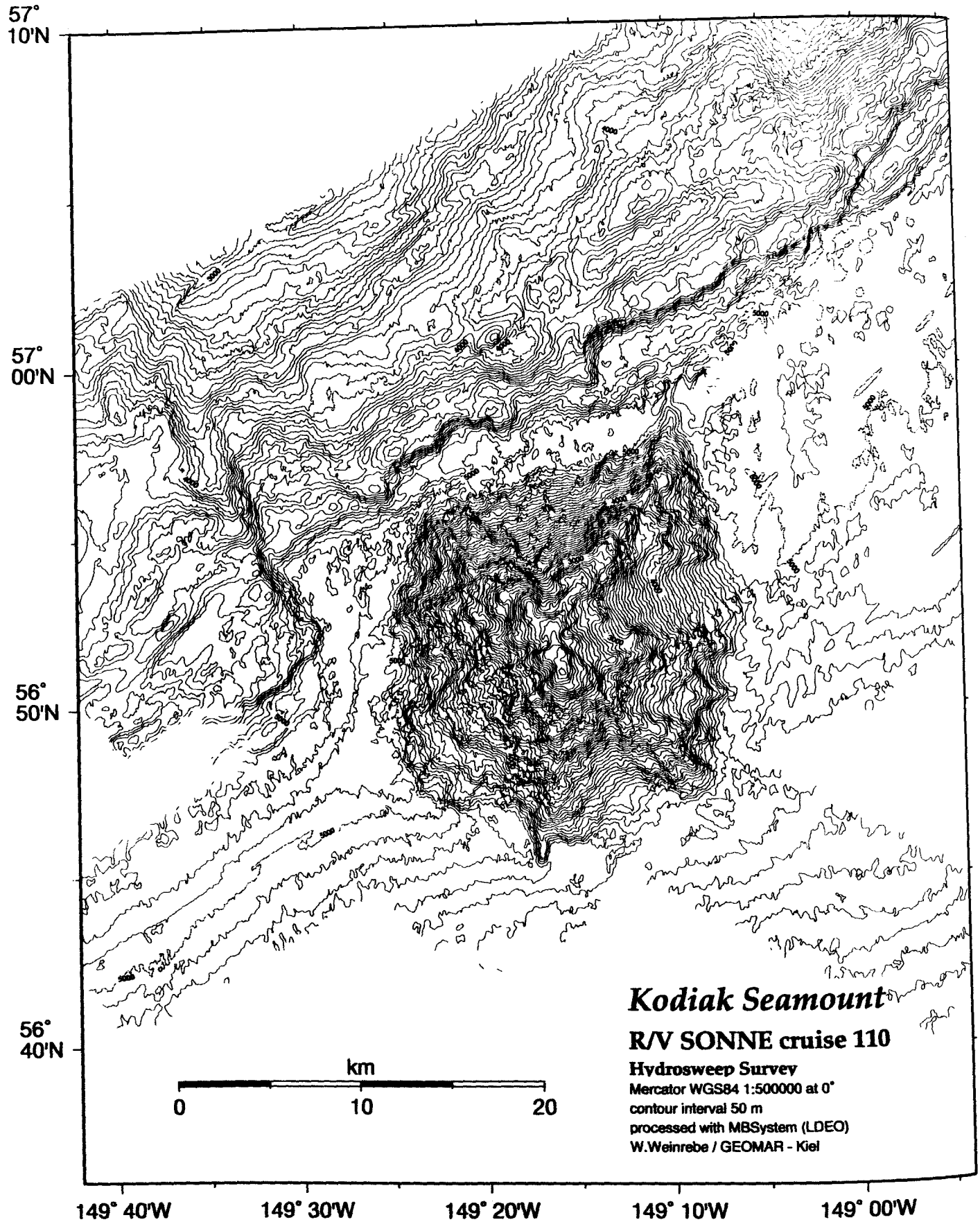

Fig. 52: Bathymetry of the Kodiak seamount area from the HYDROSWEEP survey during SO96, SO97, SO110.

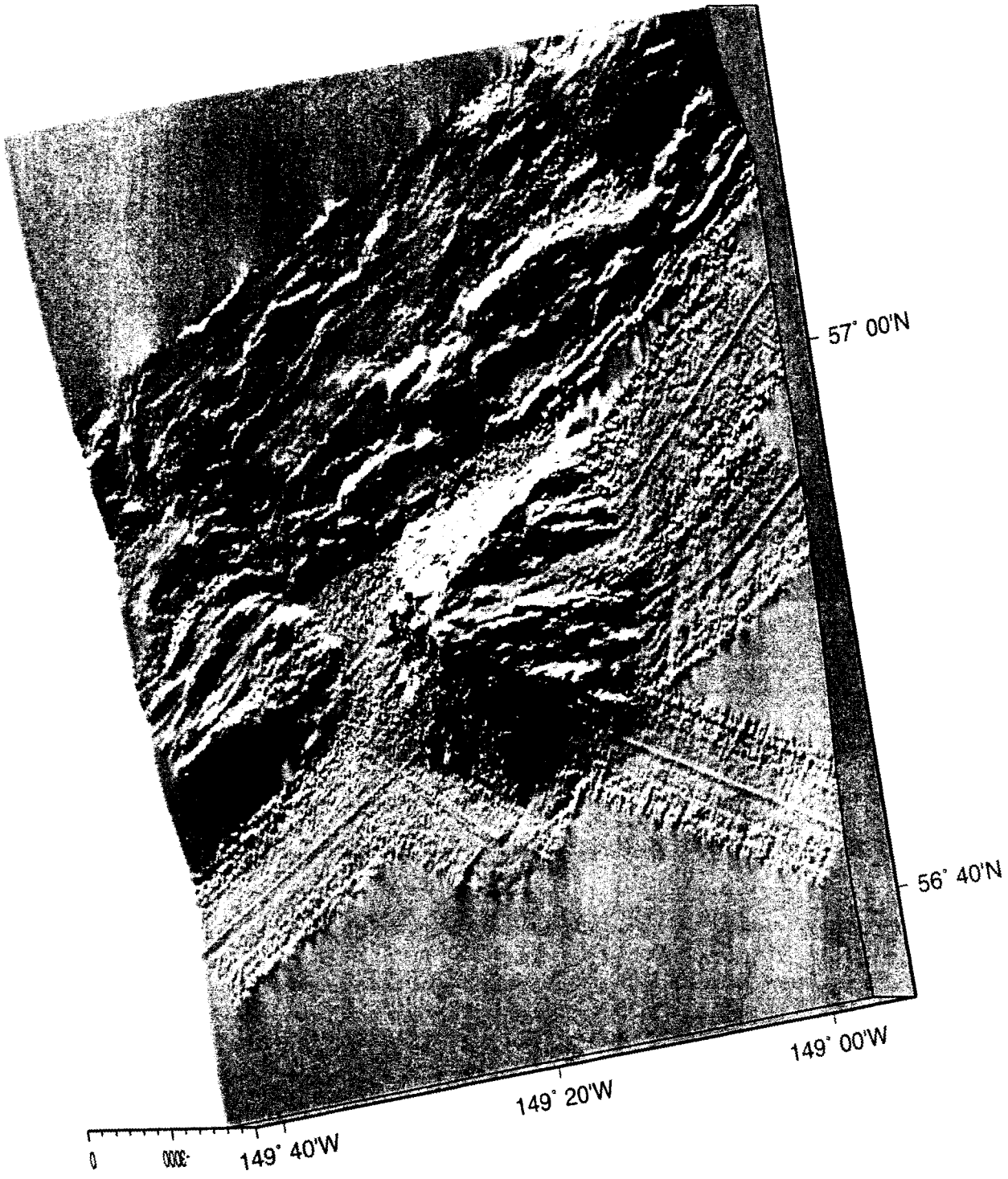

Fig. 53: Perspective view of the Kodiak seamount area. View from the east, elevation 65°, illumination from the west.

3.2 GLORIA imaging

N. Maher

Sidescan Sonar imagery collected by the U.S. Geological Survey with the GLORIA (Geologic LOng Range Inclined Asdic) system was used for locating geologic features in the EDGE and UGAK study areas. Two processed and mosaicked images each covering an area of about 40,000 km^2 and having a pixel resolution of 100 meters were used. At this resolution large geologic features several kilometers or more across are discernable. While not well suited for locating smaller targets such as features less than 1-2 kilometers and clam beds, the imagery may be useful for finding areas with a high potential for seep activities such as areas of widespread exposed outcrops. We looked at the occurrence of exposed outcrop, rubble and talus, and sedimented seafloor along one EXPLOS transect to see if there were any direct correlations between bottom type and reflectivity. Areas of high acoustic reflectivity show up as light gray to white while areas of low reflectivity are dark gray to black. GLORIA quad 43 covers much of the Edge study area and quad 40 covers the UGAK area between EDGE and ALBATROSS. Basemaps were created by merging GLORIA imagery with contoured Hydrosweep bathymetry collected by GEOMAR in 1994 and contoured ETOPO5 data where hydrosweep has not been collected.

EXPLOS 32, a 6.5 kilometer transect, was run from the northwest to the southeast across the first and second anticlinal ridges (Fig. 54) parallel and to the north of EXPLOS transects 21, 22-2, and 35. The transect begins just inboard of the second ridge crest at 4,700 meters and, heading seaward to the southwest, climbs up the back slope of the second ridge to 4,600 meters, continues across a broad ridge crest and then down a moderately steep sedimented slope to 4,900 meters and back up a low sedimented ridge just inboard from the trench. Most of the transect is over featureless bioturbated sediments. Outcrops of subhorizontal to gently NW dipping strata form step-like scarps near the base of the inboard slope of the second ridge and just below the crest on the inboard slope of the second ridge. A series of small, steep, step-like bedding scarps were found near the end of the transect on the leading edge of the first ridge. Clams were noted in five locations along the transect. Four of the clam occurrences were associated with the steep outcrop areas and one was on a steep sedimented slope on the back side of the second ridge.

Bottom features were plotted on the merged GLORIA image and hydrosweep bathymetry. The largest area of outcrops correlates with a narrow band of high reflectivity on the GLORIA image. The other two outcrops, however, occur on more subdued reflectivity and have no obvious correlation to features on the image. The GLORIA sidescan most likely is unable to resolve the smaller outcrops. The broader bands of moderately high and low of reflectivity area function of angle of ensonification to the slope (i.e. slope facing sidescan beam is high reflectivity and slope facing away is low reflectivity) while narrow bands of very high reflectivity are probably showing areas of extensive outcropping.

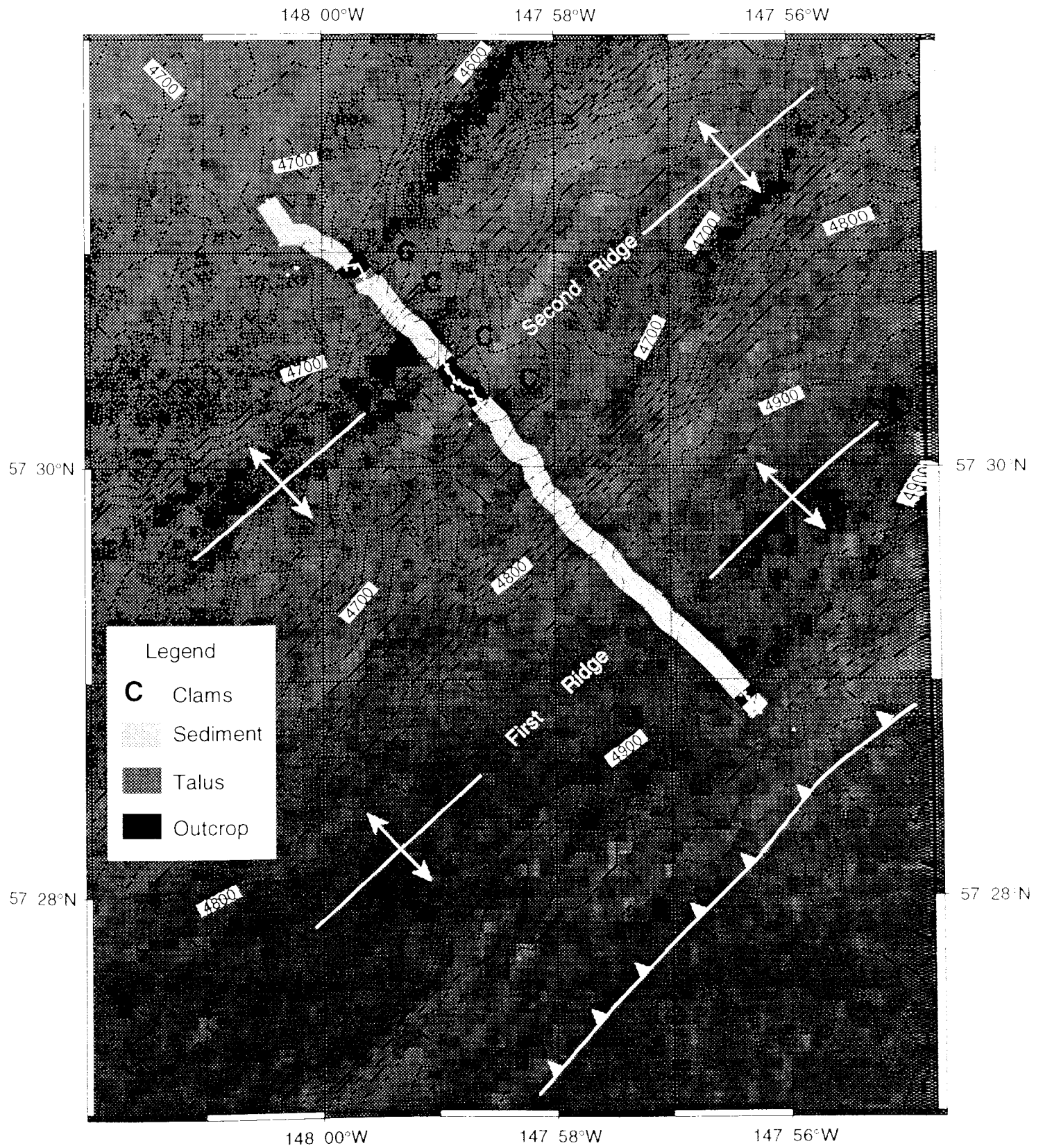

Fig. 54: Occurrence of clams, sediment, talus, and outcrops plotted along EXPLOS transect 32. Basemap is GLORIA imagery merged with contoured HYDROSWEEP data. Light areas are high reflectivity; dark areas are low reflectivity.

4 Water column sampling

4.1 CTD program

J. Schiller, G. Winckler, E. Zuleger,

Water column sampling was carried out using the CTD (Conductivity-Temperature-Depth) -Rosette sampling system described below. CTD locations are shown in Figs. 40-43 and listed in Tab. 15 . Three CTD (21-1, 27-1, 30-1) were taken in the EDGE-sector at the first ridge near observed vents, whereas CTD 39-1 and 50-1were taken at the SHUMAGIN-sector (54°18.28 N, 157°11.54 W) in a canyon intensively studied during this cruise.

Table 15: Locations of CTD stations measured during SO 110/1b+2.

Station	Area	Date	Latitude	Longitude	Water depth (m)
21-1	EDGE	21.07.1996	57°26.16 N	148°01.34 W	4974
27-1	EDGE	25.07.1996	57°25.21 N	148°08.01 W	4958
30-1	EDGE	28.07.1996	57°27.38 N	148°00.04 W	4770
39-1	SHUMAGIN	02.08.1996	54°18.28 N	157°11.53 W	4889 (4952 pressure)
50-1	SHUMAGIN	09.08.1996	54°18.27 N	157°11.54 W	4910 (4951 pressure)

The CTD program was conducted as described in Part 1, chapter 4 using the GEOMAR CTD and associated rosette water sampling system. The instrumentation package included a Sea-Bird 911plus CTD (S/N 09P10108-0410) with temperature, conductivity, and pressure sensors. The instrument also logged data from a Datasonics altimeter and a SeaTech 25 cm transmissometer. Unfortunately the transmissometer was not providing data after CTD 30-1. The rosette system is a Sea-Bird model 32 twelve-position rosette pylon (software controlled) with 10-L Niskin-type water samplers.

The calibration coefficients in the seasoft.con file are the same as used in SO109 and will need correction to the transmissometer coefficients post-cruise. Downcasts proceeded continuously at about 50 meters/minute until the bottom-trigger alarm sounded and the altimeter was brought to within 6-15 meters above bottom. The first water sample was generally collected at this point; the balance collected on the upcast. Separate data files were collected and processed for each down and up cast and are stored and processed with the file-naming format: STN#-1.* and STN#-1UP.*.

Water samples were collected for helium isotopes and tritium (Winckler, Schiller), methane and methane isotopes (Zuleger), nutrients and trace elements (Dählmann and Domeyer), and oxygen (Greinert). Methane, some nutrients, and oxygen concentration analyses were performed onboard and are discussed below. The other chemical species will follow from post-cruise laboratory analyses.

Table 16: Samples collected from CTD site 21-1.

Sample ID bottle	depth (m)	CH4 conc. GEOMAR	CH4 conc. VBC	CH4 isotope analysis VBC	3He/4He Uni HD	O_2	nutrients GEOMAR
1	601	x	x	x	-	-	x
2	495	x	x	x	-	-	x
3	373	x	x	x	-	-	x
4	250	x	x	x	-	-	x
5	201	x	x	x	-	-	x
6	150	x	x	x	-	-	x
7	101	x	x	x	-	-	x
8	74	x	x	x	-	-	x
9	50	x	x	x	-	-	x
10	25	x	x	x	-	-	x
11	10	x	x	x	-	-	x
12	5	x	x	x	-	-	x

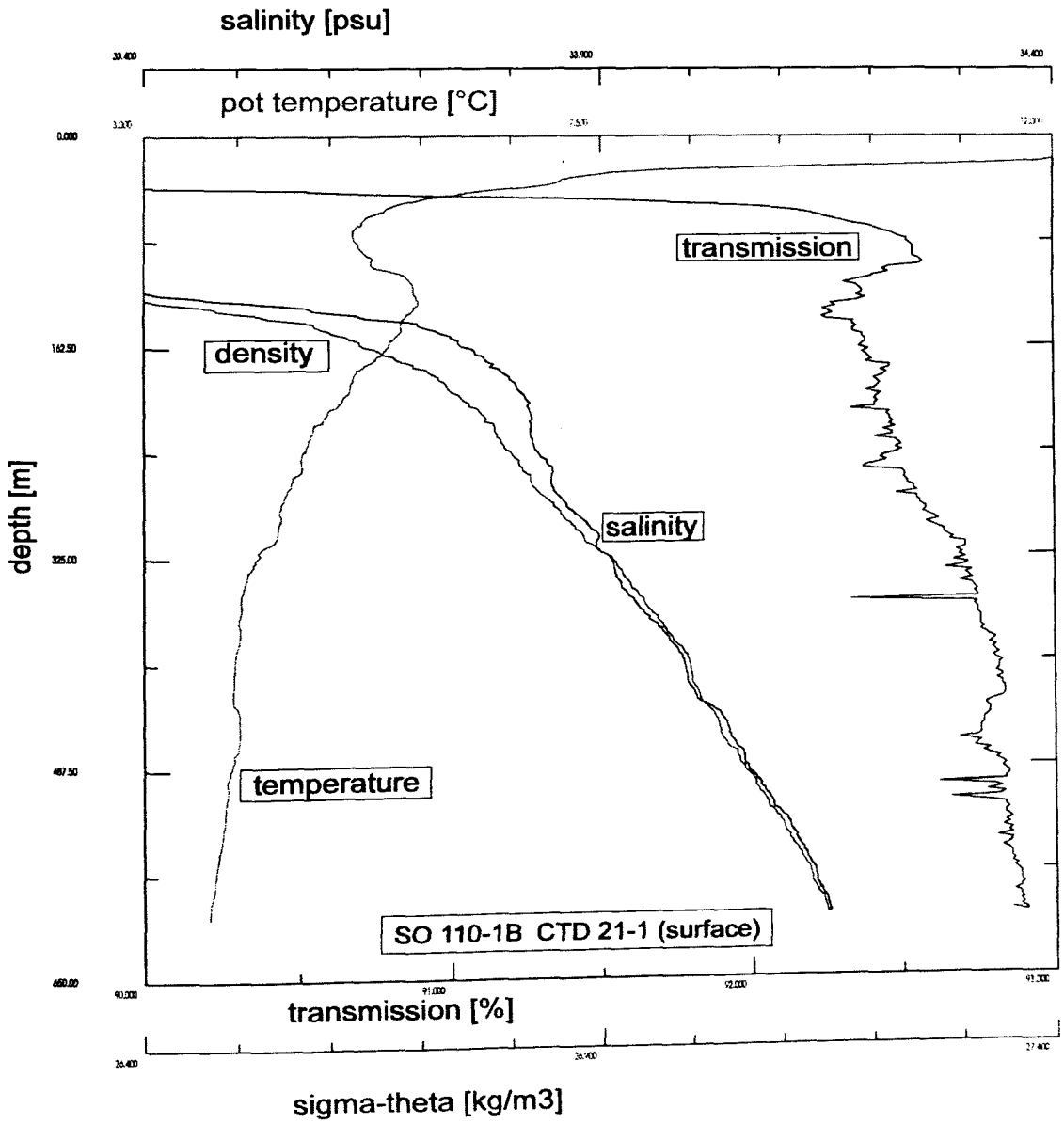

Fig. 55: Hydrographic data from CTD site 21-1.

Table 17: Samples collected from CTD site 27-1.

Sample ID bottle	depth (m)	CH4 conc. GEOMAR	CH4 conc. VBC	CH4 isotope analysis VBC	3He/4He Uni HD	O_2	nutrients GEOMAR
1	4948	-	x	-	-	-	-
2	4900	x	x	x	-	-	-
3	4849	x	x	x	-	-	-
4	4801	x	x	x	-	-	-
5	4750	x	x	x	-	-	-
6	4646	x	x	x	-	-	-
7	4501	x	x	x	-	-	-
8	4401	x	x	x	-	-	-
9	4301	x	x	x	-	-	-
10	3999	x	x	x	-	-	-
11	3500	x	x	x	-	-	-
12	2500	x	x	-	-	-	-

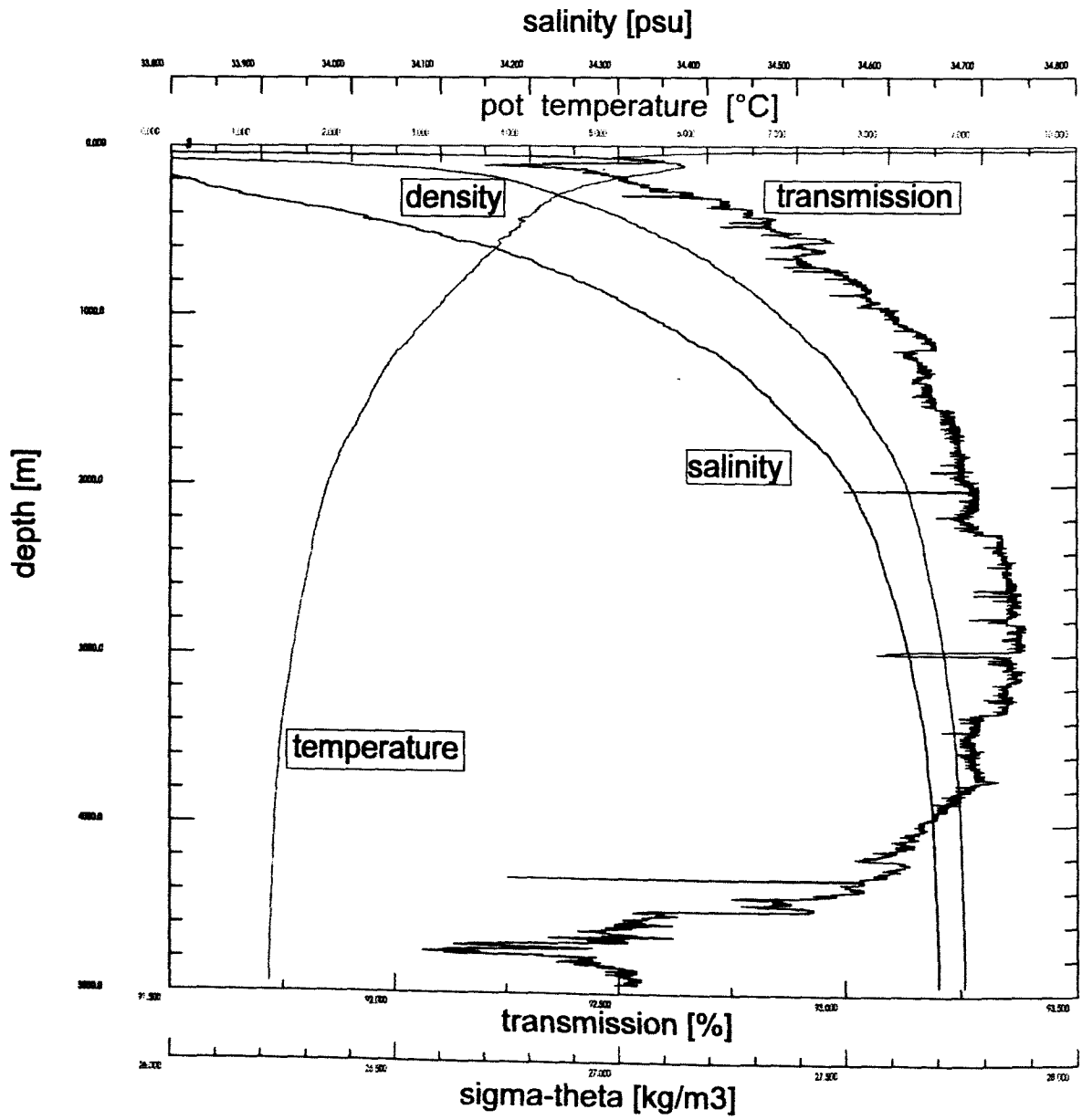

Fig. 56: Hydrographic data from CTD site 27-1.

Table 18: Samples collected from CTD site 30-1.

Sample ID bottle	depth (m)	CH4 conc. GEOMAR	CH4 conc. VBC	CH4 isotope analysis VBC	3He/4He Uni HD	O_2	nutrients GEOMAR
1	4807	x	x	-	x	x	x
2	4779	x	x	x	x	x	x
3	4749	x	x	x	x	x	x
4	4720	x	x	x	x	x	x
5	4689	x	x	x	-	x	x
6	4660	x	x	x	-	-	x
7	4630	x	x	x	x	x	x
8	4600	x	x	x	-	-	x
9	4570	x	x	x	x	x	x
10	4539	x	x	x	-	-	x
11	4509	x	x	x	x	x	x
12	4478	x	x	-	-	-	x

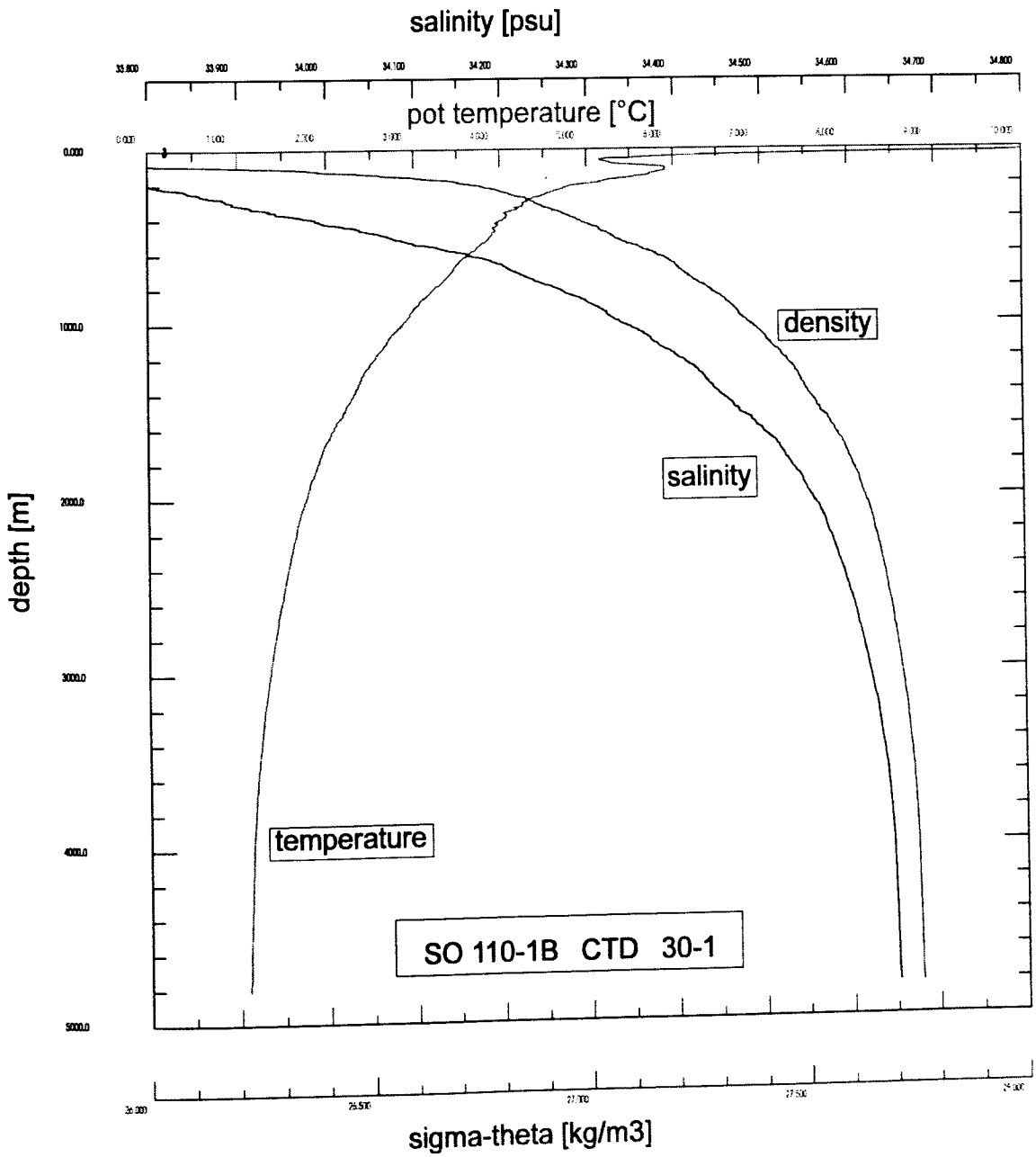

Fig. 57: Hydrographic data from CTD site 30-1.

Table 19: Samples collected from CTD site 39-1.

Sample ID bottle	depth (m)	CH4 conc. GEOMAR	CH4 conc. VBC	CH4 isotope analysis VBC	3He/4He Uni HD	O_2	nutrients GEOMAR
1	4953	x	x	x	x	x	x
2	4899	x	x	x	x	x	x
3	4851	x	x	x	x	x	x
4	4802	x	x	x	x	x	x
5	4750	x	x	x	-	x	x
6	4700	x	x	x	x	-	x
7	4650	x	x	x	-	x	x
8	4600	x	x	x	-	-	x
9	4549	x	x	x	-	x	x
10	4500	x	x	x	-	-	x
11	4400	x	x	x	-	x	x
12	4301	x	x	x	-	-	x

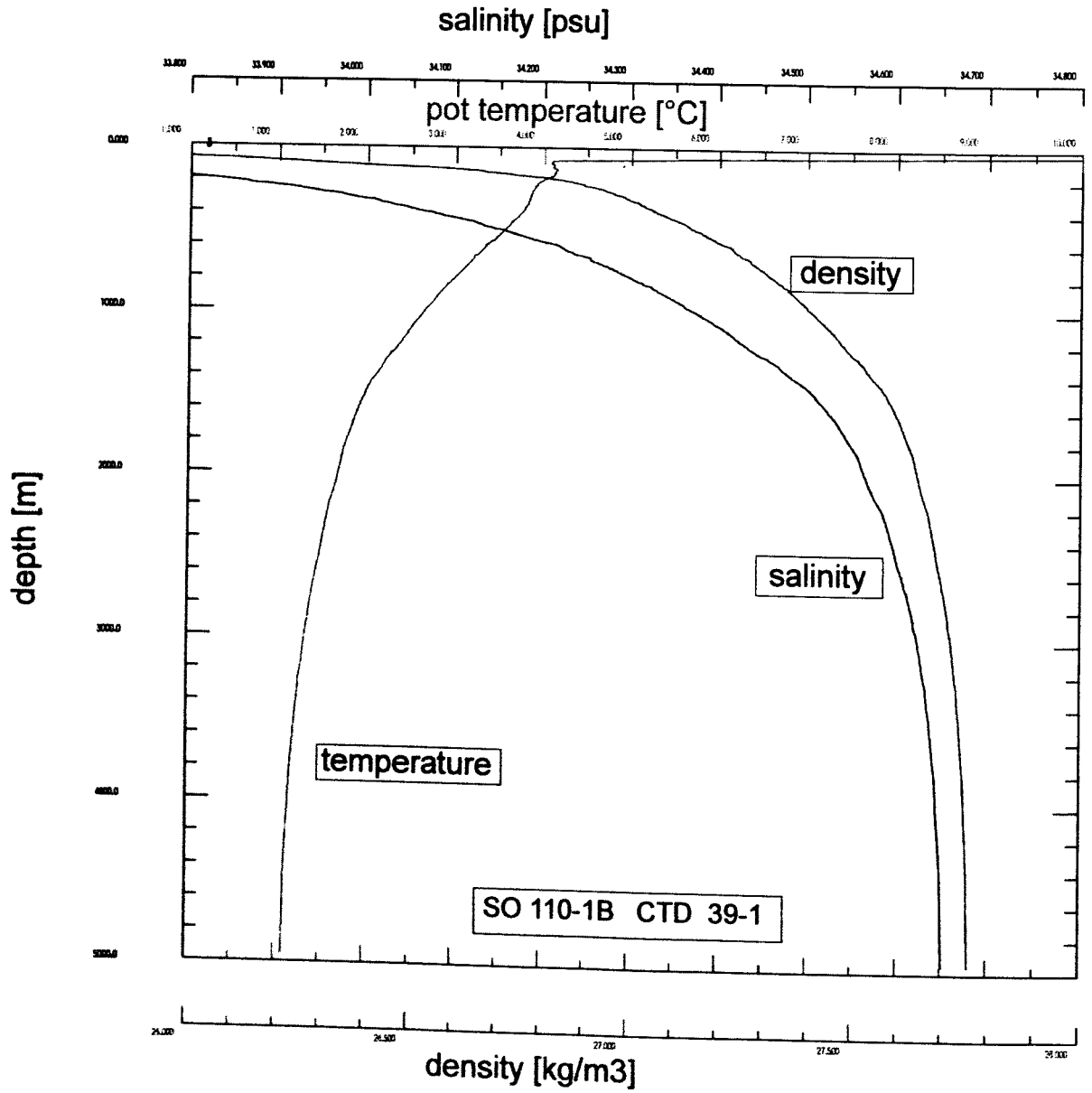

Fig. 58: Hydrographic data from CTD site 39-1.

Table 20: Samples collected from CTD site 50-1.

Sample ID	depth	CH4 conc.	CH4 conc.	CH4 isotope analysis	3He/4He	Tritium	O_2	Nutrients
(bottle)	(m)	GEOMAR	VBC	VBC	Uni HD	Uni HD		GEOMAR
1	4952	X	X	X	-	-	X	-
2	4750	X	X	-	-	-	X	-
3	4549	X	X	X	X	X	X	-
4	4251	X	X	X	X	X	X	-
5	4000	X	X	X	X	X	X	-
6	3000	X	X	-	X	X	X	-
7	1999	X	X	-	X	X	X	-
8	999	X	X	-	X	X	X	-
9	750	X	X	-	-	X	X	-
10	499	X	X	-	-	X	X	-
11	100	X	X	X	-	X	X	-
12	49	X	X	-	-	X	X	-

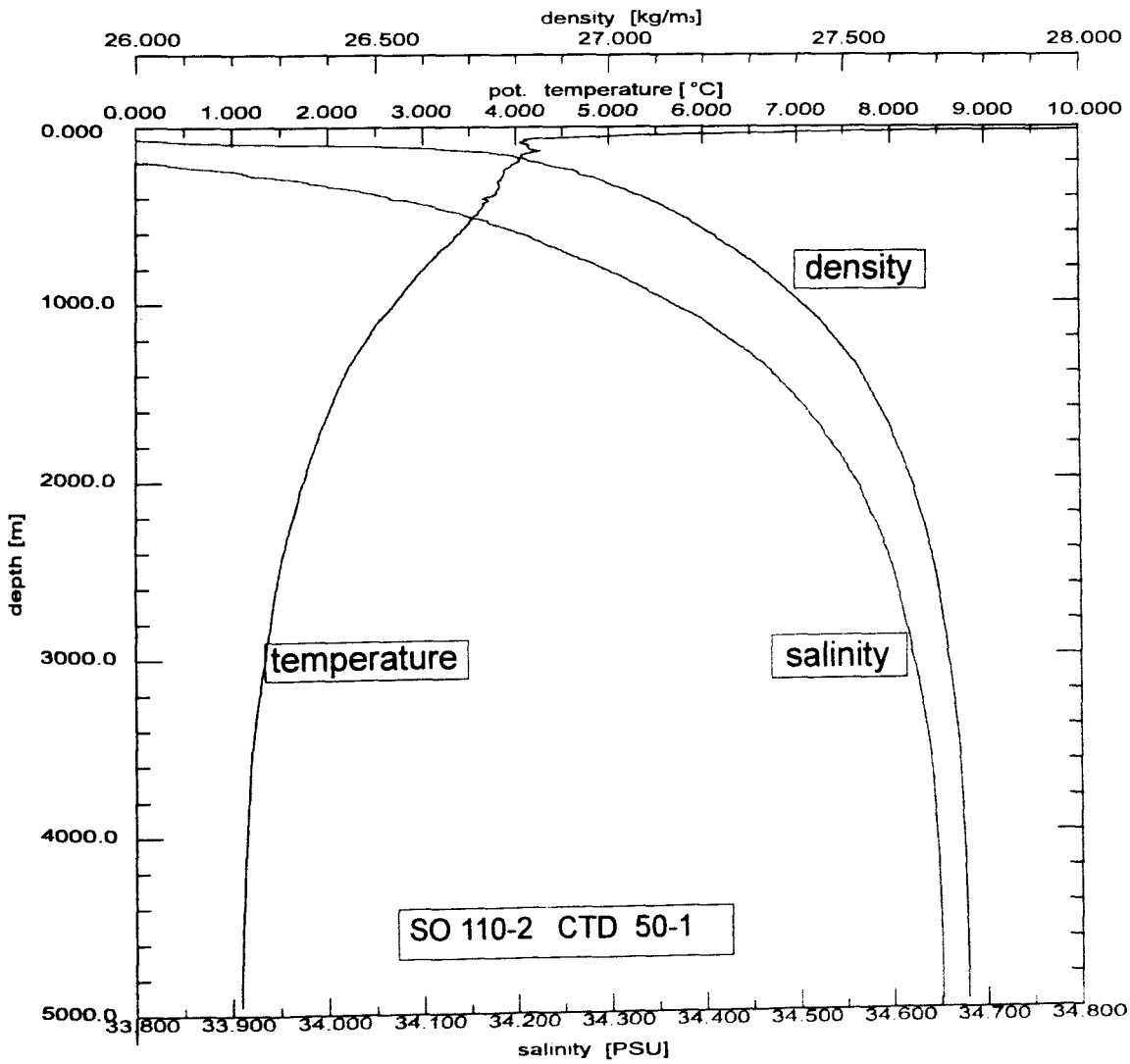

Fig. 59: Hydrographic data from CTD site 50-1.

4.2 Helium sampling

J. Schiller

During SO110-1b and SO110-2 five CTD stations were carried out (Tab. 15).
Three of them (stations 21-1, 27-1 and 30-1) were located in the EDGE-sector and stations 39-1 and 50-1 were conducted at the same position in the SHUMAGIN-sector.

4.2.1 EGDE-sector

CTD station 21-1 is located at the bottom of the first anticlinal ridge (for position see Tab. 15) and was intended to aquire data for the determination of sound velocity as well as methane data in the surface area (top 600 m) of the water column. Station 30-1 is located on the ridge in an area of several vent sites, which were also investigated by numerous VESP and TV-grab stations, whereas station 27-1 is further west at the bottom of the first ridge. Both stations 27-1 and 30-1 were run throughout the entire water column.
For all three stations the hydrographic data obtained (potential temperature, salinity and density sigma-theta) show very similar features (see Figs. 55-57): There is a local maximum in potential temperature at a depth of approximately 140 to 150 meters, which corresponds to a local minimum in transmission at stations 21-1 and 27-1 (no transmission data available for station 30-1) and also to a maximum in methane concentration of 80 nL/L at station 21-1.

Data from station 27-1 also show a significantly reduced transmission in the deepest 500 m of the water column with a minimum 200 m above the ground (Fig. 56), which can also be seen as a small maximum in methane concentration (35 nL/L; background is approximately 10-15 nL/L). This deep anomaly can easily be understood in terms of its proximity (in depth and geographical) to the venting sites. Due to missing transmission data for station 30-1 (Fig. 57) we cannot establish a similar correspondence between transmission and methane concentration at that station. Apart from that, all profiles are characterised by an absence of anomalies and by a remarkable smoothness with respect to hydrographic data in the entire water column.
Seven samples were taken (Winckler) for 3He/4He isotopic analysis at the station nearest to known venting activity (30-1).

4.2.2 SHUMAGIN-sector

The only two CTD stations in the SHUMAGIN-sector (stations 39-1 during SO110-1b and 50-1 during SO110-2) are located at the same position in an area of strong venting activity, as seen in several preceeding VESP and TV-grab sites (see Tab. 15 for exact positions). The objective being to provide an overall, but sufficiently detailed characterisation of the entire water column, station 39-1 covered the deepest 600 m in detail, whereas at station 50-1 water samples taken were evenly distributed throughout the water column (Figs. 58 and 59).

Hydrographic data (salinity, potential temperature, density sigma-theta, there was no transmission data available) generally show the same pattern as in the EDGE area (Figs. 58 and 59): i. e., the typical non perturbated pycnocline below approximately 500 m and the small local maximum in potential temperature

around 150 m. Again this maximum can also be found in the corresponding methane concentration data (see below).
Samples were taken for a tritium concentration analyis throughout the water column and for helium isotope analysis in layers deeper than 1,000 m (G. Winckler, J. Schiller).

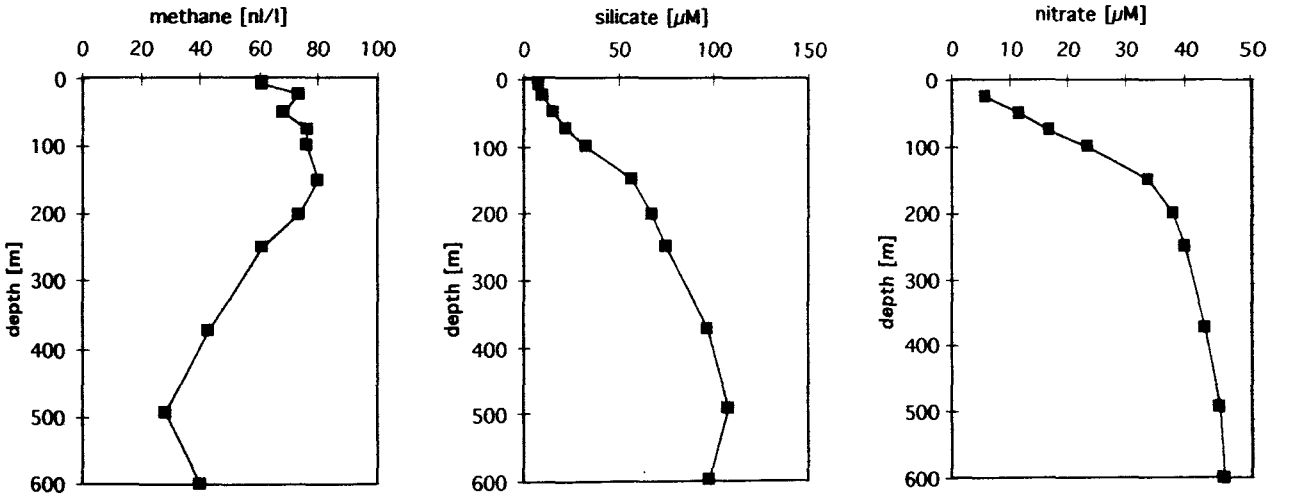

Fig. 60: Methane, silicate, and nitrate in the water column of CTD station 21-1.

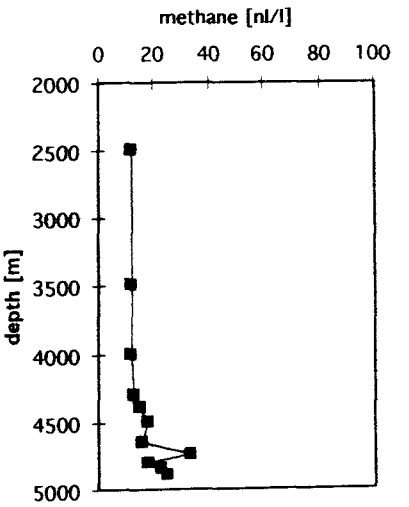

Fig. 61: Methane in the water column of CTD station 27-1.

4.3 Methane analyses

E. Zuleger

On-board analysis of methane in water samples serves as a quick and simple means of acquiring information about both the methane distribution in the water column and the flow rates of methane from cold seeps into the ocean. Dissolved methane in the water column is a known indicator of both hydrothermal and cold vent activity, allowing methane analysis to serve as a useful means of determining further site locations.
Therefore immediately after sampling, water samples from the hydrocast were degassed by a headspace vacuum-ultrasonication method and analysed by GC as

described in detail in part I, chapter 4.3. Additionally, samples were taken for high precision shore determination of CH_4 and $\delta^{13}CH_4$ by helium stripping and GC/GC-C-IRMS analysis.

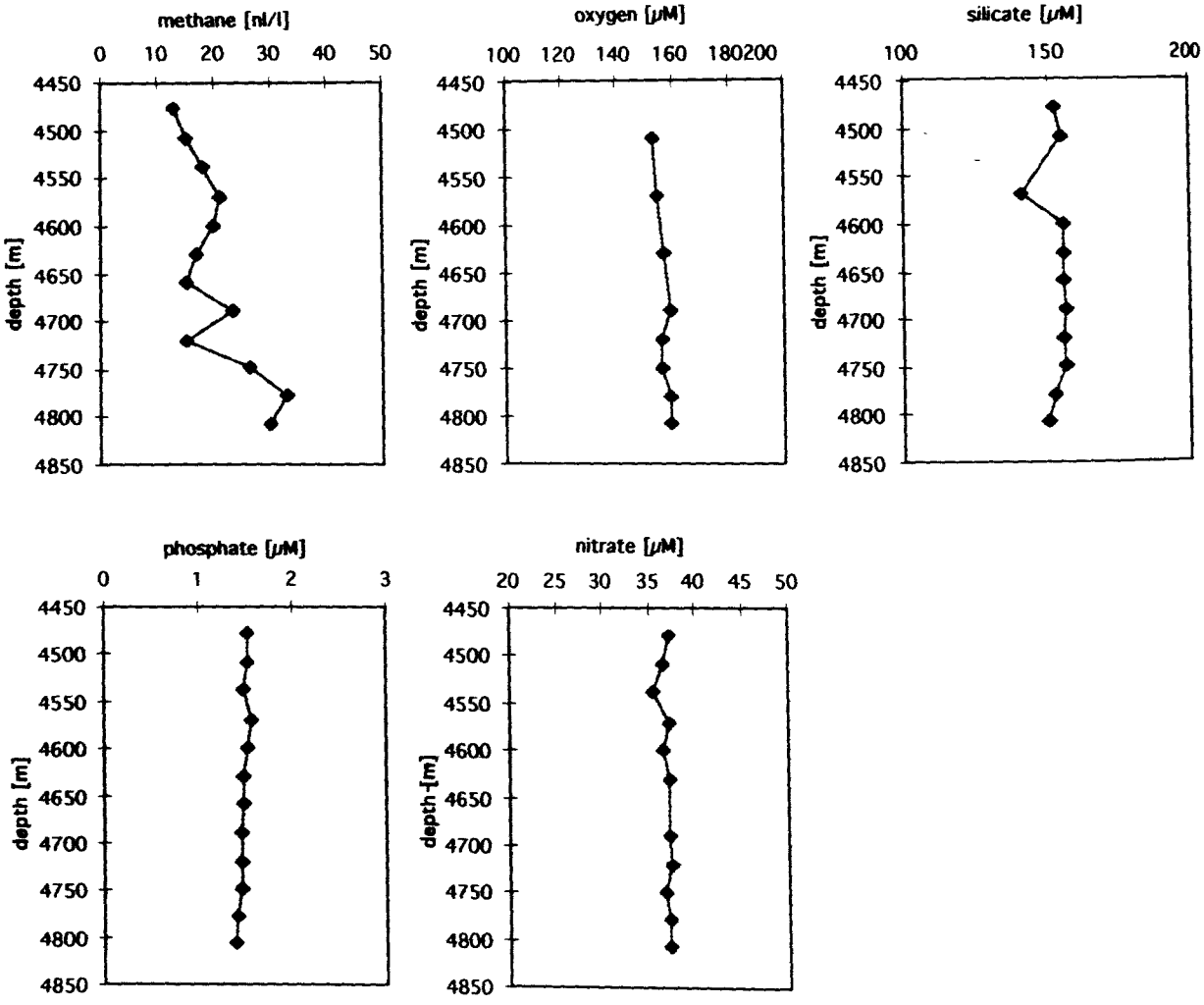

Fig. 62a: Methane, silicate, phosphate, nitrate, and oxygen in the water column of CTD station 30-1.

During the SONNE 110-1b and 2 expeditions, 60 water samples from 5 hydrocast stations were taken in the EDGE- and SHUMAGIN-sector at the Aleutian subduction margin to carry out methane analysis. The methane concentration data from these five CTD casts are listed in the appendix.

The objective for CTD 21-1 in the **EDGE**-sector was to obtain the CTD data for sound velocity and the methane concentration in the upper 600 m of the water column. In addition the location was more or less the location of CTD SO97 20, 23-1 and 2. At the surface the profile shows a methane concentration of 60 nL/L , reflecting the expected value of this area. After a slight increase to about 80 nL/L at 150 m the methane concentration drops to about 20-40 nL/L at 600 m as seen at SO97.

Water samples of CTD 27-1 and 30-1 (Fig. 56) were taken in the lower 2,500 m and 500 m, respectively. CTD 27-1 is located right in front of the first ridge, whereas CTD 30-1 is located on the first ridge in the close vicinity of ROPOS, VESP and TV-grab sites described in the following chapters. Both profiles show the usual background concentration of about 10 nL/L, except for a slight increase at the near bottom to about 35 nL/L as seen in CTD location SO97-73.

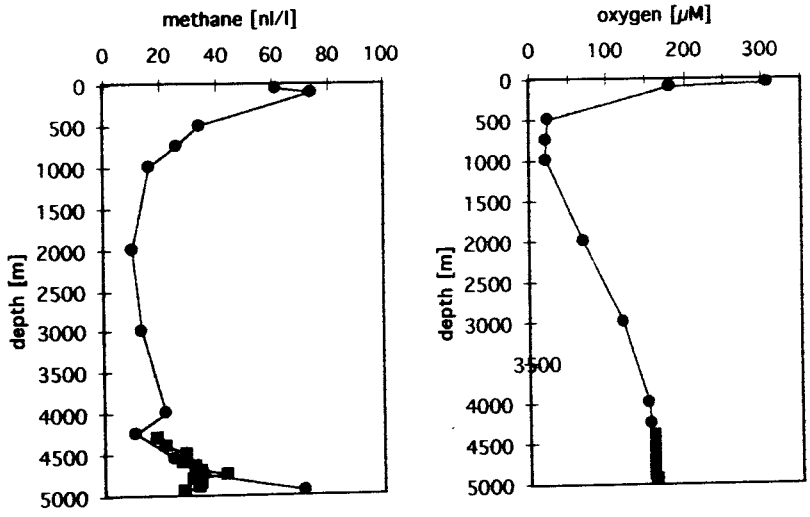

Fig. 62b: Methane and oxygen in the water column of CTD stations 39-1 and 50-1.

At the **SHUMAGIN**-sector only two CTDs were carried out, 39-1 and 50-1 (Figs. 58 and 59) at one location to receive a complete profile throughout the water column in the close vicinity of observed vents. The upper part shows the usual 60 nL/L at the surface, the slight increase to about 80 nL/L in the upper 200 m and the decrease to the background of about 10 nL/L. As seen in the EDGE-sector the near bottom samples are slightly increased to about 40- 70 nL/L.

Additionally, several water samples were taken by VESP, and by ROPOS during dive 344. Further details and the results from these samples can be found in the apropriate section of this report.

4.4 Nutrients and oxygen

A. Dählmann, J. Greinert, B. Domeyer

Oxygen analyses were carried out by Winkler titration on water samples of 3 CTD casts (30-1, 39-1 and 50-1). The reproducibility, determined by measuring two replicates was less than 1 µmoL/L.
Samples of CTD 39-1 and 50-1 represent one location at the Shumigan-sector. Water samples were taken in even distribution throughout the water column. The profile is typical with the oxygen minimum zone at about 750 m and bottom water values of about 160 µmoL/L (Fig. 62b).
In contrast, water samples of CTD 30-1 were taken near bottom and show a typical decrease from the bottom to 4,500 m (160 to 153 µmoL/L). In both cases oxygen values are slightly higher than expected for North Pacific bottom water.

Nutrients (silicate, nitrate, and phosphate) were analyzed at CTD station 21-1 and 30-1 (Figs. 60 and 62a). The analytical procedures are described in chapter 9 of part I. Water samples at 21-1 were taken at the upper 600 m of the water column, whereas samples of CTD 30-1 were collected near bottom, in 4,450 to 4,850 m water depth.

Silicate and nitrate show low values at the sea surface and increase to values of about 100 µM and 46 µM, respectively in 600 m water depth. Nutrient data are rather constant in the CTD samples taken near bottom, representing the expected values for North Pacific bottom water.

5 ROPOS and VESP operations

5.1. Background and summary

P. Linke, F. Appel

5.1.1 Transponder navigation

The long-baseline transponder net in working area EDGE was established during SONNE cruise 110-1b using an array of 6 SONARTRACK transponders and GEOMAR's MORS RM301 deckset (Fig. 63). For accurate navigation in the net the ROPOS system is equipped with an EDGETECH PS8000 deep-sea range meter linked through the fiber optic cable with the on-board navigation PC and a DATASONICS transponder on the vehicle.

5.1.2 ROPOS operations

Dive 344 was started in the morning of July 13 in calm weather. This condition permitted video shots of the ROPOS system at the sea surface by snorkeling from a Zodiak after the ROV was launched for its deepest mission so far. At a depth of 3,200 m, almost 800 m deeper than the device had been brought into action previously, two of the 6 hydraulic systems showed a pressure drop which required compensation in shallower water depths, hence the system was brought up again. After a delay of 4 hours ROPOS reached its record diving depth of 4,960 m with all systems operating.

After only 20 minutes of bottom time in the vicinity of the vent sites which had been located during the previous SONNE cruise 97 in 1994 numerous clam fields surrounded by pogonophorans were found and investigated in much more detail as possible before with conventional towed camera systems. The ROPOS deployment lasted until late afternoon of July 23; deteriorating weather conditions forced us to interrupt the diving operation.

Nevertheless, ROPOS had reached a record time of 17.5 hours at the bottom and also a record for the longest continuous system deployment of over 28 hours. On the way back to the surface the SIT camera cut out, then came back on, then cut out for good. Then we lost the 3 chip colour camera and the telemetry, and powered down completely for recovery.

The routine check after recovery showed that 8 of the 9 optical fibres were broken between 100 and 500 m from the drum's end. After assessing the extent of the damage it became clear that this problem could not be solved at sea considering time and logistics. The decision to terminate ROPOS operation was made in agreement with BMBF and all partners involved. Hence, the ROPOS system was dissassembled and the ROPOS team and equipment were unloaded in Valdez.

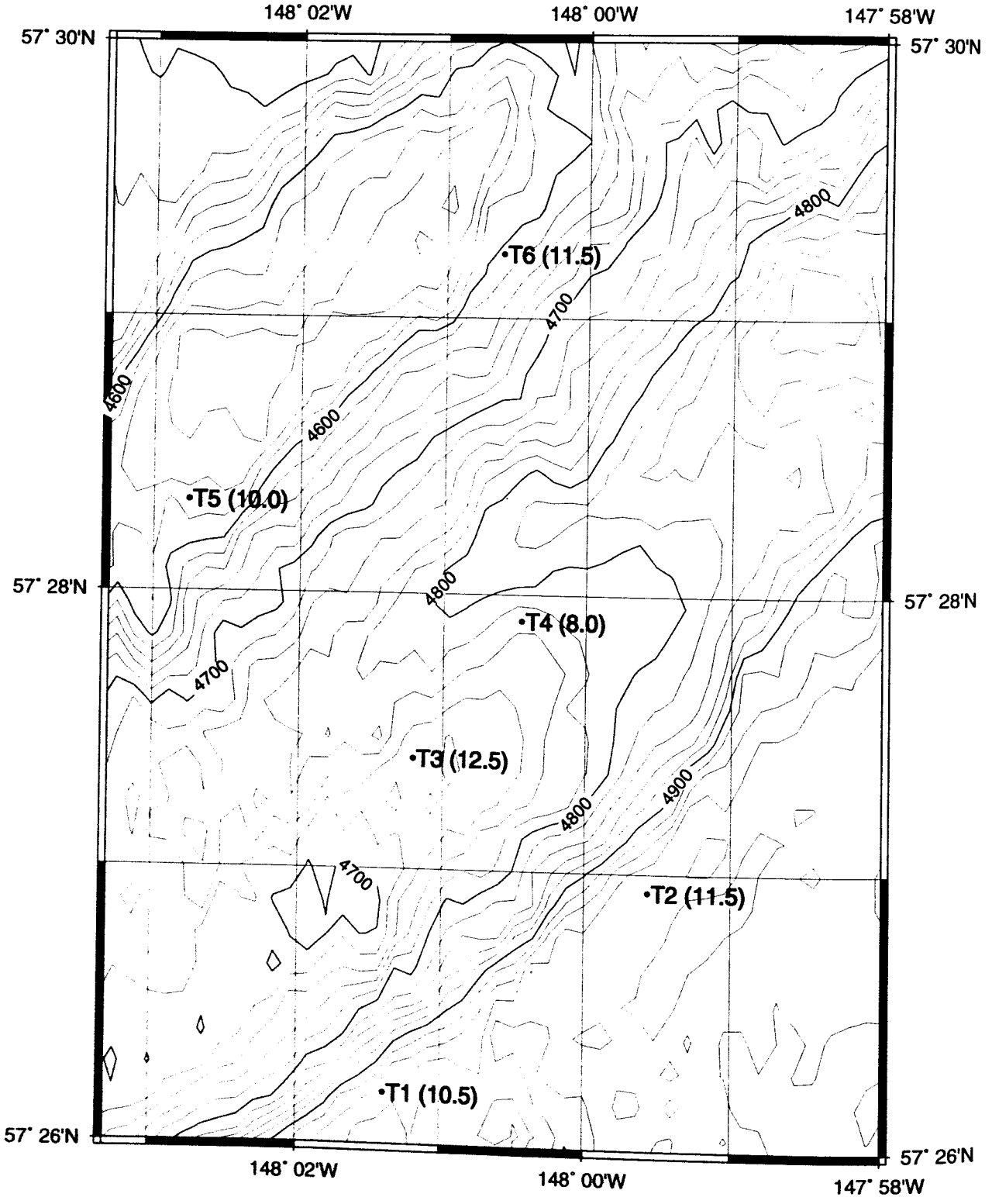

Fig. 63: Position and frequencies of the SONARTRACK transponder net deployed in the EDGE-sector.

5.2 Geological and hydrological observations of ROPOS dive

D. Orange, N. Maher

ROPOS dive 344 covered 5 partial transects of the seaward limb of the frontal anticline in the EDGE research area. Three transects proceeded from the lower portion of the slope upward, while the two others traversed the slope. From north to south, these will be termed transects A, B, C, D and E (Figs. 64 and 65).

5.2.1 Description of transects

Transect A began at a depth of 4,947 m (03:58 UTC) on bioturbated sediment (cross-section A-A'; Fig. 66a). The first outcrops encountered, at a depth of 4,932 m, were clearly seaward dipping, and were cut by high angle fractures that gave the outcrop face an angular, blocky appearance. From the top of this scarp to 4,921 m was an expanse of sediment talus covered with numerous cold seeps. Toward the lower portion there were a number of clams with tracks; higher up on this slope the clams were clustered in groups of 1-2 m diameter. At least one of the clusters was situated along a linear trend of N30E. Two distinct seaward dipping beds cropped out above this seep area up to 4,908 m, with some small seeps occurring on the talus slope and in pockets of the outcrop (4,912 m).

Above 4,908 m the slope levelled off, and was relatively monotonous and bioturbated. At 4,880 m, however, we encountered an interesting feature when we crested a local rise and descended to 4,885 m. This swale may be related to bedding slip mass-wasting, although that interpretation is purely conjectural and based only on the morphology.

Above this mid-slope swale we again climbed up a continuous bioturbated sedimented slope. At 4,855 m we entered an area of extensive cold seep communities which showed the scars of VESP and TV-G sampling (from the 1994 SO97). These seeps occurred in clusters of 1-2 m across, and up to 3-5 m long. At the first seep we encountered numerous clams at the margins and away from the seep clam trails radiated away from them. We followed a trend of seeps N40E to another large seepage area at 4,859 m.

Due to tether concerns we left the seafloor to check on the ROPOS cage; we returned to the seafloor at a depth of 4,875 m, again on monotonous sedimented seafloor. With tether out, ROV headings, and navigation placed us in the neighborhood of where we left the seafloor. At 4,870 m we encountered another linear cold seep, this time trending N30W. Leaving this seep behind we again traversed a sedimented slope, although bedding scarps cropped out at 4,849 and 4,824 m. These beds were shallowly seaward dipping. From 4,824 to 4813 m we proceeded up a near continuous outcrop of beds 30-50cm thick, that appeared to be coarsening upward. Above 4,813 m the seafloor sloped more gradually and was sedimented and bioturbated. This transect ended at 4,809 m (08:18 UTC).

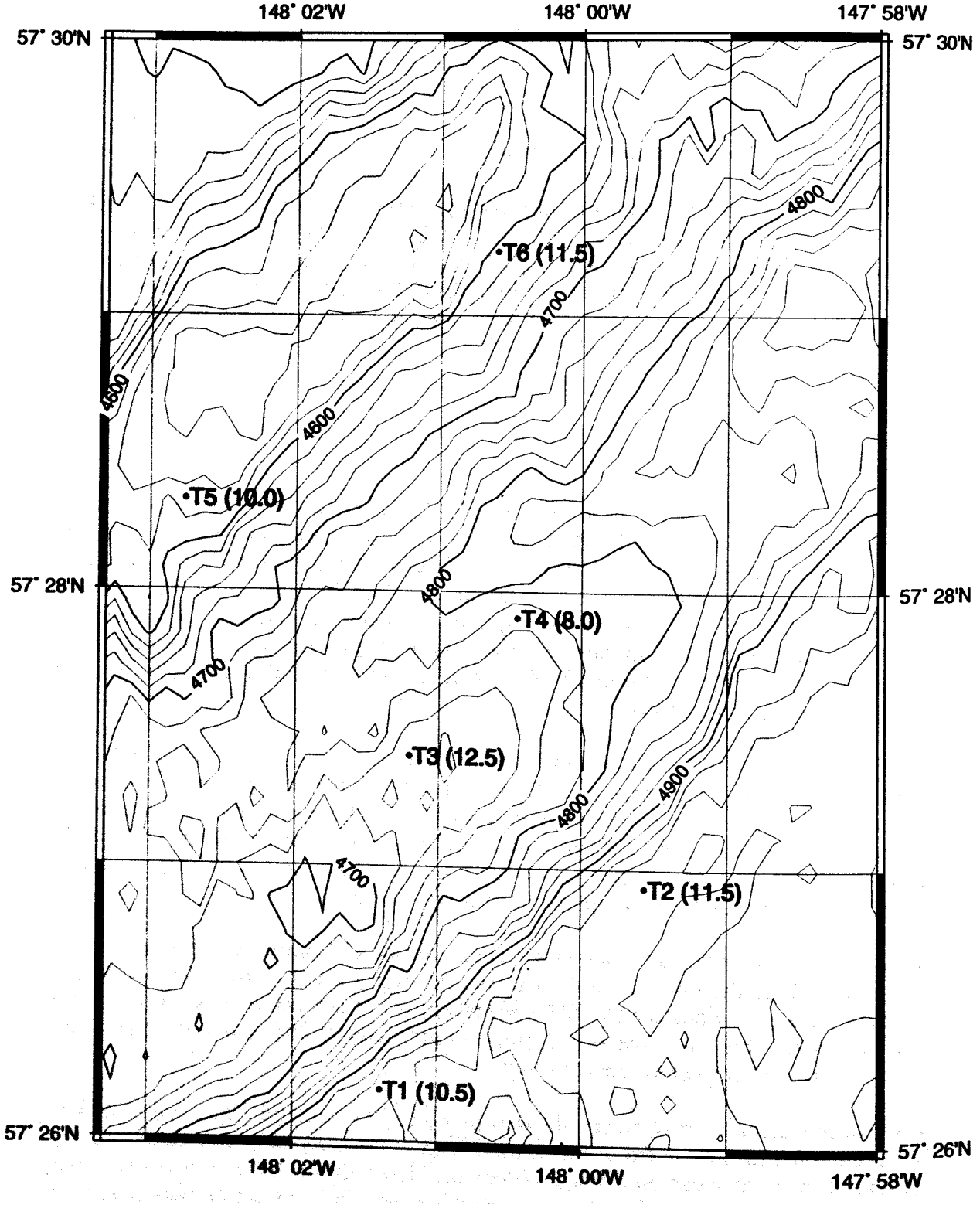

Fig. 63: Position and frequencies of the SONARTRACK transponder net deployed in the EDGE-sector.

5.2 Geological and hydrological observations of ROPOS dive

D. Orange, N. Maher

ROPOS dive 344 covered 5 partial transects of the seaward limb of the frontal anticline in the EDGE research area. Three transects proceeded from the lower portion of the slope upward, while the two others traversed the slope. From north to south, these will be termed transects A, B, C, D and E (Figs. 64 and 65).

5.2.1 Description of transects

Transect A began at a depth of 4,947 m (03:58 UTC) on bioturbated sediment (cross-section A-A'; Fig. 66a). The first outcrops encountered, at a depth of 4,932 m, were clearly seaward dipping, and were cut by high angle fractures that gave the outcrop face an angular, blocky appearance. From the top of this scarp to 4,921 m was an expanse of sediment talus covered with numerous cold seeps. Toward the lower portion there were a number of clams with tracks; higher up on this slope the clams were clustered in groups of 1-2 m diameter. At least one of the clusters was situated along a linear trend of N30E. Two distinct seaward dipping beds cropped out above this seep area up to 4,908 m, with some small seeps occurring on the talus slope and in pockets of the outcrop (4,912 m).

Above 4,908 m the slope levelled off, and was relatively monotonous and bioturbated. At 4,880 m, however, we encountered an interesting feature when we crested a local rise and descended to 4,885 m. This swale may be related to bedding slip mass-wasting, although that interpretation is purely conjectural and based only on the morphology.

Above this mid-slope swale we again climbed up a continuous bioturbated sedimented slope. At 4,855 m we entered an area of extensive cold seep communities which showed the scars of VESP and TV-G sampling (from the 1994 SO97). These seeps occurred in clusters of 1-2 m across, and up to 3-5 m long. At the first seep we encountered numerous clams at the margins and away from the seep clam trails radiated away from them. We followed a trend of seeps N40E to another large seepage area at 4,859 m.

Due to tether concerns we left the seafloor to check on the ROPOS cage; we returned to the seafloor at a depth of 4,875 m, again on monotonous sedimented seafloor. With tether out, ROV headings, and navigation placed us in the neighborhood of where we left the seafloor. At 4,870 m we encountered another linear cold seep, this time trending N30W. Leaving this seep behind we again traversed a sedimented slope, although bedding scarps cropped out at 4,849 and 4,824 m. These beds were shallowly seaward dipping. From 4,824 to 4813 m we proceeded up a near continuous outcrop of beds 30-50cm thick, that appeared to be coarsening upward. Above 4,813 m the seafloor sloped more gradually and was sedimented and bioturbated. This transect ended at 4,809 m (08:18 UTC).

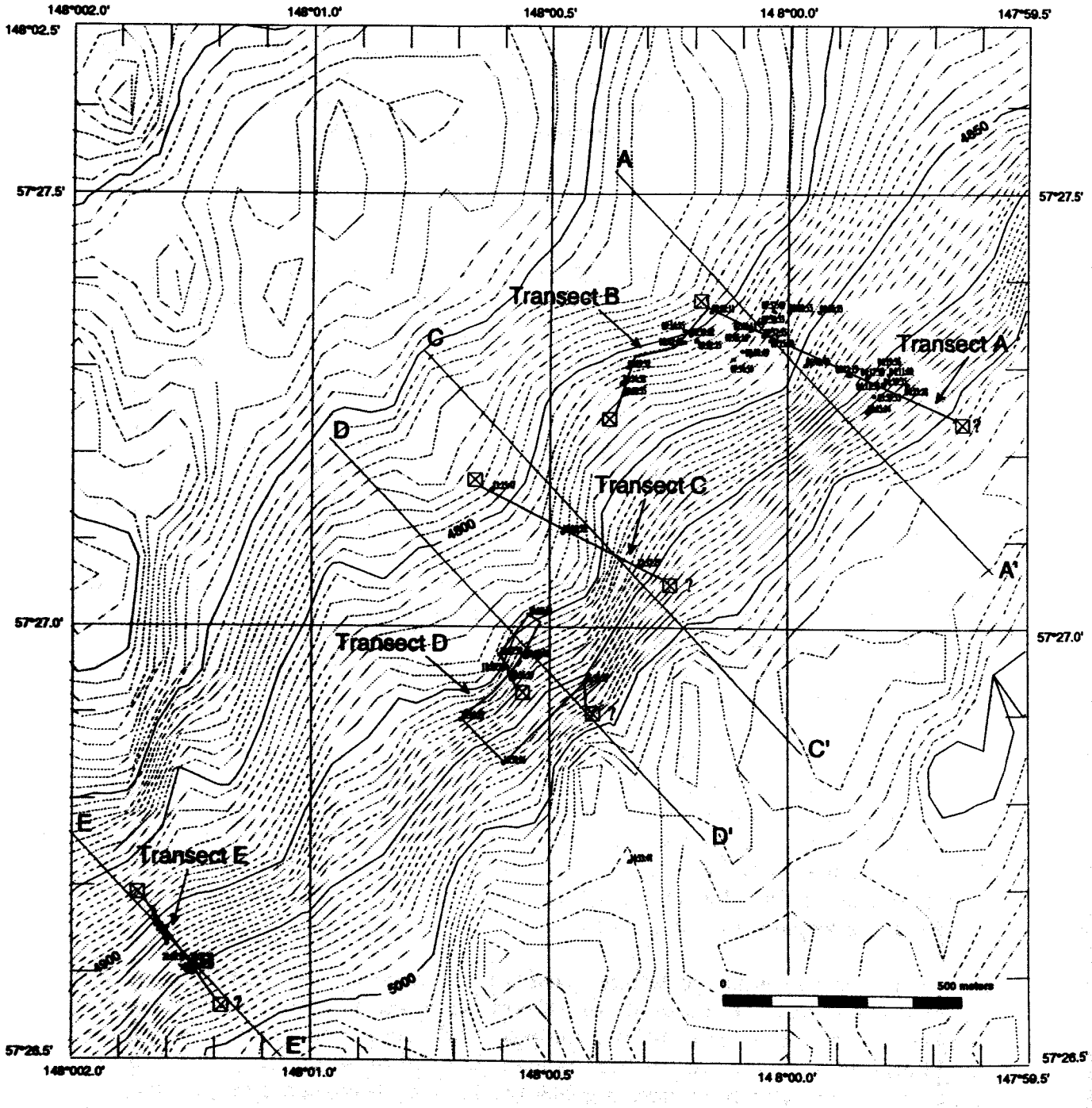

Fig. 64: ROPOS dive 344 tracklines showing location of transects on HYDROSWEEP base map. ROPOS navigation determined using ROV fixes (select fixes shown), cage fixes (shown for transect E), ROV heading and R/V Sonne ship tracks. Between transects ROPOS transitted in its cage, and off bottom. Boxes indicate beginning and end of each transect. A-A', C-C', D-D' and E-E' correspond to cross-sections (Figs. 66).

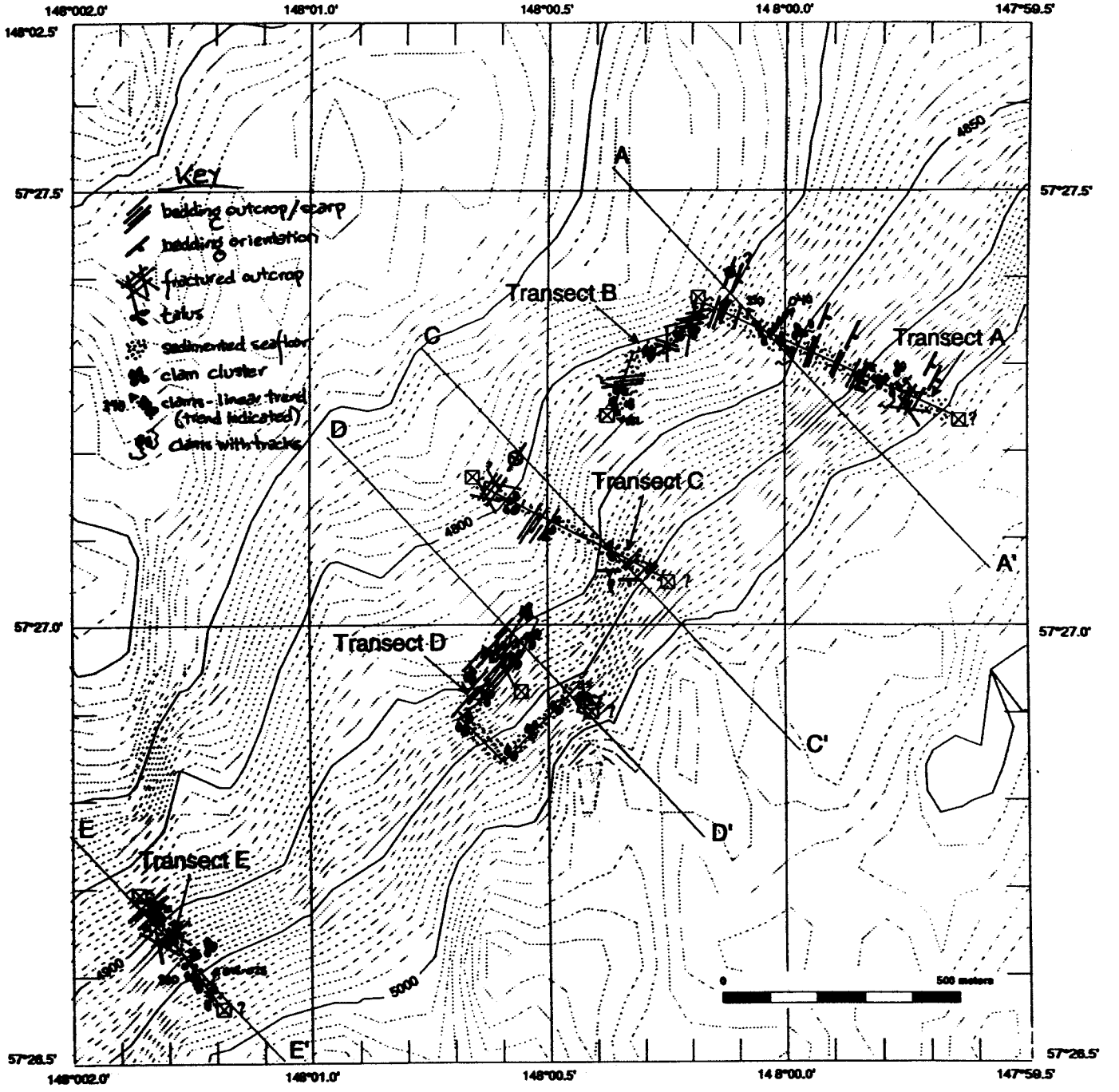

Fig. 65: Composite geologic map of ROPOS dive 344, indicating sedimented seafloor, prominent bedding scarps, talus, the location of cold seeps, and fracturing. Seeps occurred at a variety of depths as both circular colonies as well as lines of clams oriented either northeast or northwest. Approximate location of anticlinal ridge crest and frontal thrust shown.

Transect B: At 4,809 m (08:18 UTC) we changed course to 200 to traverse downslope while examining bedrock features (Fig. 66). We didn't have long to wait before things got exciting. At 4,803 m we went over an abrupt scarp that was extensively fractured. SIT camera images clearly showed a conjugate set of fractures bisected along a trend of N50E (Fig. 65). This scarp was several meters high. At 4,829 m we encountered the top of a fairly large seep field. These seeps were in approximately circular clusters 1-2 m in diameter, and occurred on a sedimented debris/talus slope below the bedding scarp region. Between 4,829 and 4,863 m the seafloor was smooth and sedimented, except for a bedding scarp at 4,843 m. Talus littered the seafloor below this scarp, but gave way below to bioturbated sediment. Another bedding outcrop occurred at 4,863 m, although this scarp was cross-cut by high angle fractures. A cold seep occurred below this scarp on a sedimented slope at 4,871 m. ROPOS came off the bottom at 08:49 UTC, and touched down again on a bedding scarp at a depth of 4,839 m (09:05 UTC). We found seeps at 4,847 and 4,863 m, with a small bedding scarp between. The shape of this scarp indicated that the bedding was sub-parallel to the slope, indicating seaward dips. At 4,867 m we crossed over a smoothed scarp (bedding?), with a linear seep nestled in a groove in the lower portion of the outcrop trending N19W. The sedimented seafloor levelled off at 4,880 m and we encountered another seep, and completed this transect (due to ship/cage problems) at 4,878 m (09:38 UTC).

During Transect B we found that ROPOS did not traverse downhill very well. This was due to a combination of difficulties with viewing (forward looking while going downhill), driving (dragging the tail), and most importantly, the cage (the cage was behind - and uphill - ROPOS, and kept colliding with the bottom twice (the second and third time the cage has hit the seafloor). We returned to the cage and transitted downslope. The mate, however, was unable to keep on station, and wandered as much as 350 m off site, dragging the cage (and ROPOS) with it. These cage-ship difficulties continued to 12:25 UTC.

Transect C: This transect began at a depth of 4,938 m on sedimented seafloor (cross-section C-C', Fig. 66b). Bedding scarps cropped out at 4,935 and 4,920 m. The 4,935 m scarp was overhanging (!), and indicated a seaward (south-southwest?) dip. The 4,920 m outcrop also had a southwest dip. If these dips are correct, they are significantly oblique to the regional north-northeast strike, and may indicate a high angle fault zone in this region. Talus blocks littered the sedimented slope between these scarps; we also saw one open, articulated Solemya shell. From 4,920 to 4,865 m we covered a monotonous, bioturbated smooth seafloor. At 4,865 m we saw small white fragments among the debris, but no active seeps. We then came up a large bedding scarp, topping out at 4,841 m. Talus littered the above scarp area from 4,841 to 4,832 m. At 4,798 m we encountered a small seep cluster among talus fragments below a shallowly dipping/subhorizontal outcrop that appeared blocky (due to fracturing?). After cresting this scarp we completed the transect at 4,787 m (13:23 UTC).

Transect D: ROPOS left its cage at 15:30 UTC, and at 15:37 picked up the bottom on the Mesotech sonar at a range of 40 m. Due to ship/cage problems, and tugging on ROPOS, we did not reach the seafloor until 16:28 UTC, at a depth of 4,960 m

(cross-section D-D', Fig. 66c). After traversing northeast for several minutes we changed course to 250 (still at 4,960 m). Between 4,960 and 4,950 m we saw scattered clam clusters, and numerous dead clams. We observed more clusters at 4,945 m, and changed course to 040 to head into the current. For the next several hours we traversed a very steep and apparently unstable wall inhabited by a large number of small clam clusters in pockets on the cliff face. Small-scale slumping was rampant, leaving scars and scarps across the face of the outcrop. We traversed up (top of this scarp at 4,900 m) and down slope on a number of occasions, and found that the seepage activity died off in both directions. All of the clam colonies were located between 4,940 and 4,950 m. We returned to the cage to transit to a new location at 20:26 UTC.

Transect E: This traverse began at a depth of 4,947 m on relatively shallowly sloping sedimented seafloor with a linear patch of cold seep clams oriented N15-25E (cross-section E-E', Fig. 66d). The slope gradient began to increase at 4941m, although we encountered no outcrop until 4,922 m. We did, however, encounter a number of seep fields. The first field, at 4,934 m, had several linear seeps oriented N30W on hummocky, sedimented seafloor. The next field, at 4,931 m, was characterized by circular seep colonies up to 1m in diameter nestled in pockets in the slope. We returned to a seep at 4,939 m for extensive fluid sampling in and around one of the clam clusters. The seafloor was smooth and sedimented until we encountered talus and isolated bedding scarps at 4,922 m. Between 4,922 m and the end of the transect at 4,900 m we passed a clear outcrop of southeast (seaward) dipping beds, with talus fields both above and below.

End of dive: At 22:14 UTC the power distribution unit in the ROPOS control room kicked out, and the wind had increased from 15 to 25 knots (gusts), and the dive was terminated. On the way to the surface (23:00 UTC, depth = 4,440 m) the SIT camera cut out, then came back on, then cut out for good. We then lost the 3 chip camera and telemetry, and powered down completely for recovery.

5.2.2 Additional observations from TV-guided sampling

D. Saffer

In addition to ROPOS transects in the EDGE area, two EXPLOS tracks from SONNE Leg 97 in 1994 and numerous TV-guided sample runs during leg 110-2 provide information on the location of features such as clam fields, scarps, and crusts within the sediment. Records from EXPLOS-35 and EXPLOS-21 in 1994 include cold seep communities clustered on the seaward facing limbs of both the first and second anticlinal ridges, at depths of ~4,700-4,800 m and 4,600 m, respectively. These seep locations are generally associated with well developed and steep seaward facing scarps which expose landward dipping beds. The landward limbs of both anticlines are essentially free of seep communities.

TV-guided sampling records from SONNE Leg 110-2, including TV-MUC 57, 59, TV-GKG 61, 62, and TV-G 63, 65 are generally consistent with the observations from EXPLOS and ROPOS. Seep communities are found generally on the seaward facing limb of the first anticlinal ridge near scarps. The orientation of

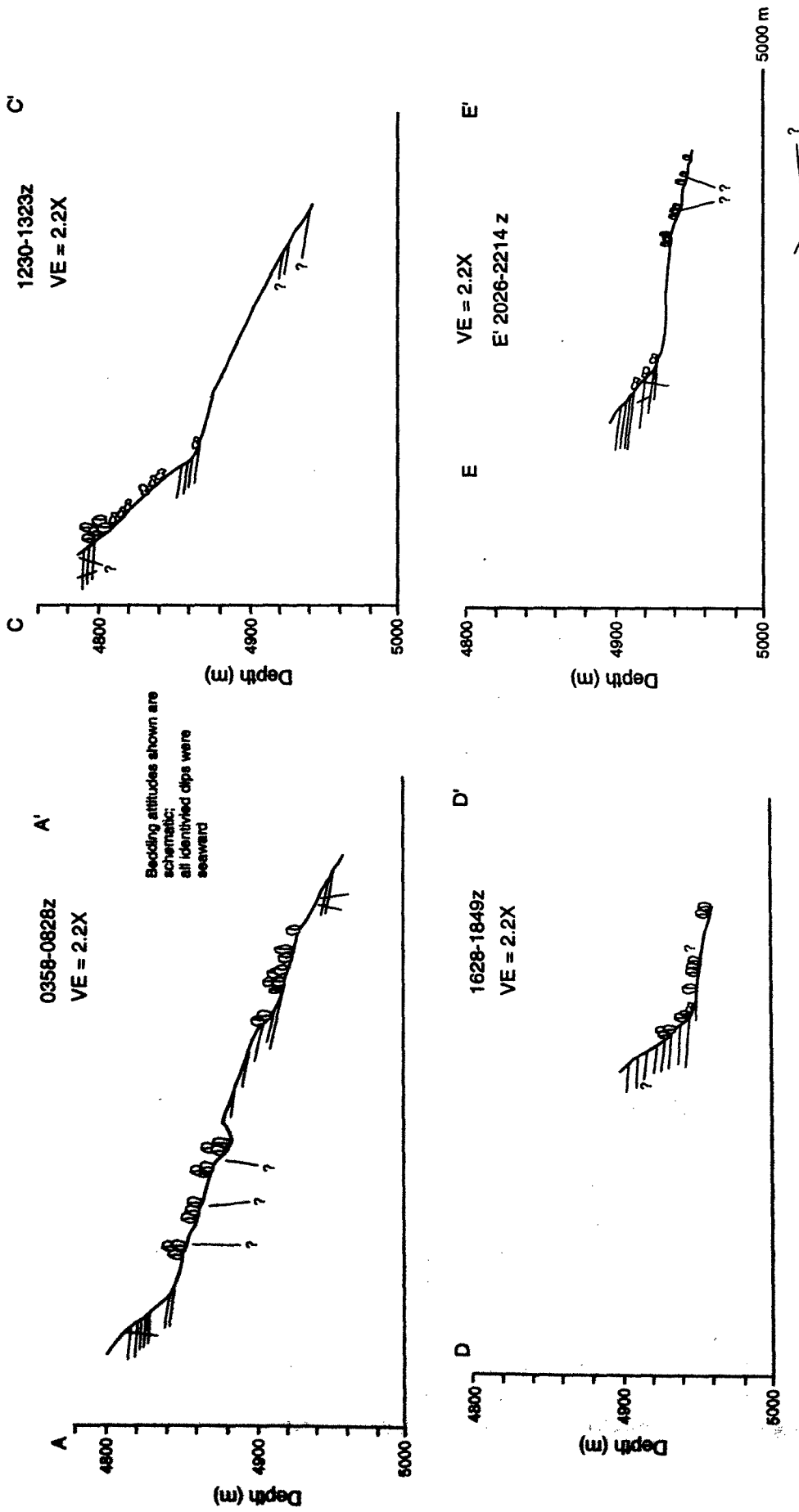

Fig. 66: NW-SE cross-sections: A = A-A', C = C-C', D= D-D', E = E-E'. Vertical exaggeration = 2.2; Lat./long. position from ROV navigation (see Fig. 63); depths directly from ROV.

scarps is unknown because the TV-guided sampling devices do not provide directional information. No linear trending seeps were observed.

5.2.3 Summary of observations

- All reliable bedding orientations on the seaward limb of the first anticlinal ridge were clearly seaward dipping, although beds higher upslope had shallower dips, and at the base of transect C the strike may be oblique to the regional trend.
- Seeps were encountered on all transects and at a variety of depths; no one depth horizon should preferred seep occurrence.
- Seeps occurred as both circular clusters and as linear trends; linear seeps were oriented N15-40E (n=3) or N19-30W (n=3).
- Seeps occurred near scarps; the orientation of these scarps could not be ascertained.
- Several outcrops showed clear evidence of high angle fracturing; the best example of this was at the beginning of transect B, where a conjugate fracture pattern had a bisector of N50E.
- EXPLOS video/camera sled runs in the area showed no evidence of seepage activity on the landward limb of the anticline, although several clam colonies were seen from the upper portions of the seaward limb to near the frontal thrust.

5.2.4 Preliminary interpretations

Scenario 1: Leakage through the hanging wall
Given the presence of cold seeps at a variety of depths across the seaward limb of the anticline, and their apparent absence on the seaward limb, we suggest that the fluids charging from these seeps originate in the basal thrust fault or in the underthrust section. These fluids could migrate along the thrust fault (utilizing its fracture permeability) or below it (contained by a permeability cap of sheared clays). The fluids could then escape through the overthrust section near the toe of the anticline where the ever-thinning overburden would be too small to contain the fluids. This decrease in overburden pressure would then allow the fluids to leak out into the hanging wall near the toe of the thrust (Fig. 67a).

This hypothesis adequately addresses the scatterring of seeps at a variety of depths on the seaward limb of the anticline, but it does not explain the linear trends of some seeps or the contour-limited aspect of others.

Scenario 2: Leaking along high-angle fractures
We observed a number of linear clam tracks oriented NE and NW, and a dramatic conjugate fracture pattern in outcrop bisected about an angle of N50E. Other outcrops were obviously fractured, although we did not have exposure to determine their orientation. Finally, the EDGE dive area occurs northeast of a major embayment in the thrust front. This embayment is the scar left behind the subduction of a seamount. The seamount collision would have had a major effect on the surrounding structures, and may have caused significant

deformation proximal to its direct path. In addition, the embayment in the frontal thrust requires a large amount of lateral strain, which may also have led to high angle fracturing in the frontal anticline proximal to this shear zone. Furthermore, small-scale extensional fractures probably form during large-scale fault driven folding of the anticline. Any or all of these mechanisms could produce significant shear strains in this ridge, resulting in high-angle faulting and fracture. These high-angle fractures may cut the entire over-riding section, and would provide an efficient conduit for over-pressured fluids to escape (Fig. 67b).

This hypothesis explains the linear seeps and fractures, but fails to explain why we detected no seepage on the landward limb of the anticline. If there were enough strain to cause high-angle fracturing, it should not be limited to the seaward limb of the anticline. In addition, this hypothesis does not address the seeps limited to a contour.

Scenario 3: Leaking along splay faults or geomorphically controlled by scarps
The extensive seepage limited to the 4,940-4,950 m contour along 300 m of strike of transect D-D' do no fit either of the above models. Note that we also encountered seeps at approximately this depth on A-A' and E-E'. These observations suggest that a splay fault may cut upsection from the décollement through the hanging wall to crop out at the 4,940 depth interval (Fig. 67c). Alternatively, the presence of a scarp itself can affect the flow field and lead to fluid focussing (Orange and Breen, 1992; Orange et al., 1994). We have a number of concerns with both hypotheses (Fig. 67d).

If a splay fault cut up section we would expect to see more deformation in outcrops near the fault in both the hanging wall and footwall. For the geomorphic control, the scarp is not continuous at this depth, nor is it large, nor is it the largest scarp encountered in the ROPOS program, and therefore we are uncomfortable with a geomorphic control on these seeps.

The Lockian View: Life is nasty, cruel, brutish and short
Given the above scenarios and the loss of ROPOS as a field vehicle during our field program it is difficult to differentiate between the hypotheses above. We would suggest, therefore, that during the subsequent leg a few judicious EXPLOS runs be carried out from the base of the second ridge, across the forearc basin and landward limb of the first ridge, across the seaward limb and frontal thrust and into the trench. This would provide further constraint on the regional distibution of venting. Features to be especially watchful for would be any venting at all on the landward limb, high-angle fracturing throughout the section, and venting/scarps at or near the toe. Additionally, we would recommend a run to the southwest across the high-angle embayment separating the first ridge from the trench behind the seamount. This would clearly show whether there were an increase in strain/fracturing as this boundary was approached, and might indicate whether this were a region of copious fluid venting. This run should be done as close as comfortable to the frontal thrust seaward of the subducting seamount.

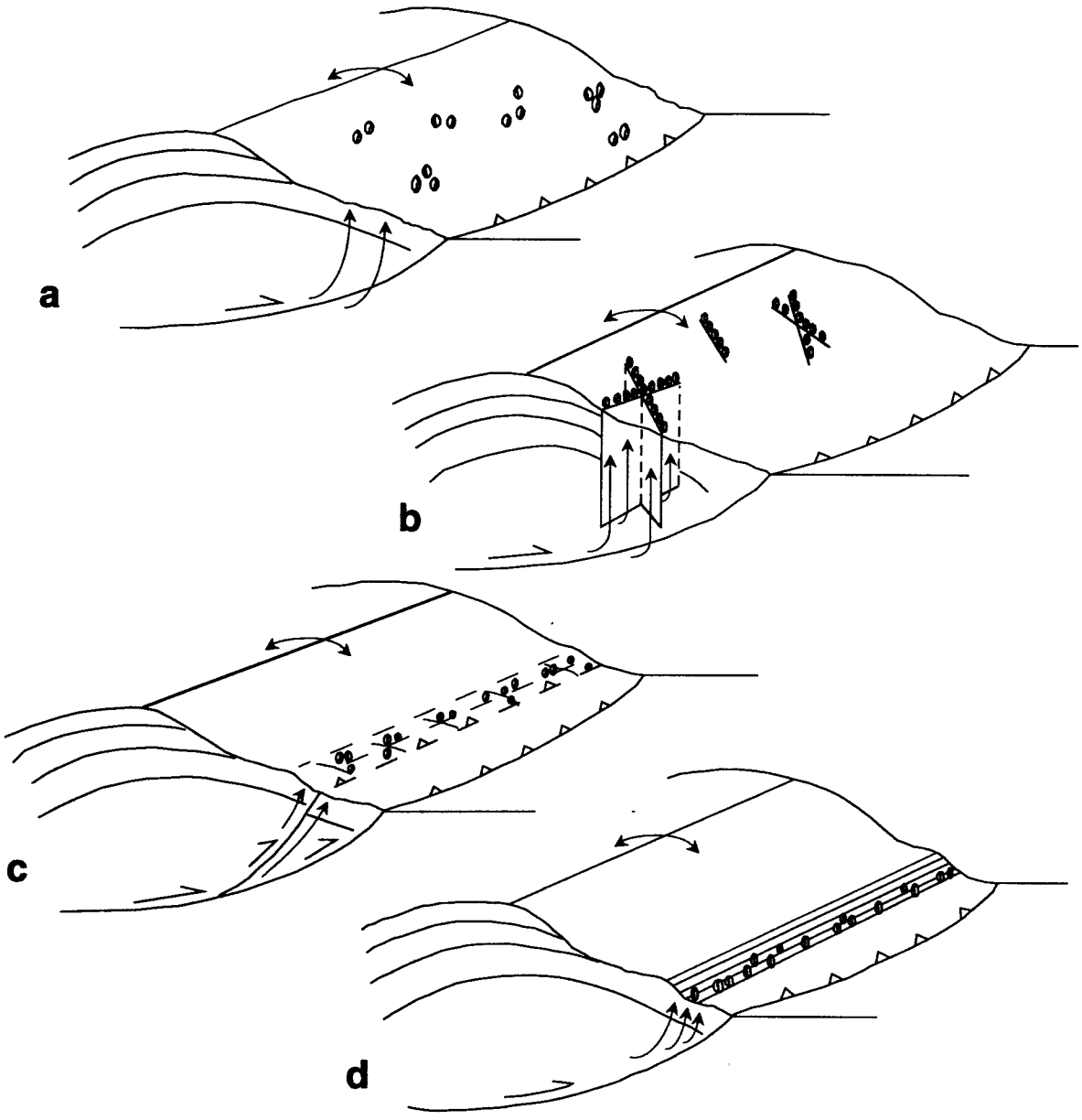

Fig. 67: (a) The presence of fluid venting at a variety of depths along the landward limb of the frontal anticline suggests that the decrease in overburden may be allowing fluids previously trapped within or below the frontal thrust to leak out. (b) Numerous seep communities occurred along either northeast or northwest trends, and bedding outcrops with high angle fractures are present throughout the field area - these observations suggest a link between high-angle fracturing and fluid expulsion. The passing of a seamount into the subduction zone, or the differences in how far the thrust front projects into the trench, can both produce significant amounts of lateral strain in the wedge that may manifest as high angle faulting and fracturing. These fractures can in turn allow fluid expulsion from depth. The presence of some seeps along a restricted depth, and along a scarp, suggests that either a splay fault steps up through the hanging wall (c; allowing fliud migration), or a bedding scarp itself can control fluid flow from depth (d). See text for discussion.

The Hobbsian View: This is the best of all possible worlds

Even without additional EXPLOS runs, we feel comfortable interpreting the structural and fluid features as a hybrid of the scenarios laid out above. Namely, the wide distribution of cold seep depths indicates that there is extensive leakage out of the landward limb, whereas the presence of linear seeps and obvious fracturing implies some fracture control. The presence of seeps in close proximity to scarps suggests that either flow is focussed by the presence of scarps, or that the scarps themselves mark structural horizons such as faults or bedding, which focus flow through increased hydraulic conductivity. We suggest that some combination of decreasing overburden - allowing fluid leakage into the hanging wall - and high-angle fracturing - controlling some but not all of the seepage - is responsible for the tectono-hydrogeology evident on the first seaward vergent anticlinal ridge of the Aleutian accretionary complex in the EDGE research area.

5.3. VESP deployment

P. Linke, F. Appel, F. Kulescha

To obtain water samples and *in situ* flow rates from cold seeps we used a TV-controlled device for the deployment of a Benthic Barrel from a conventional surface research vessel (Linke et al., 1994). The barrel is attached to the central piston of a modified multicorer frame, which operates on a water hydraulic basis and assures gentle deployment of the barrel once the frame settles on the sea floor. The **VEnt SamPler (VESP)** is equipped with five 5L water bottles and a storage CTD probe which is used to activate the water-sampling cycle and to continuously record conductivity, temperature, pressure and flow data.

The benthic barrel is a commercially available 55-gallon polyethylene barrel with a large opening at the bottom and a small exhaust port at the top. The barrel encloses 0.238 m^2 of the sediment surface and has an internal displacement volume of 284 L. The chamber is deployed over a suspected vent site with the purpose of channelling the effluent from the sea floor into a semi-enclosed environment. The internal volume of the chamber is initially flooded with ambient seawater and is then slowly replaced by vented fluids. In this way a water mixture develops within the chamber with increasing amounts of vent fluid. Sequentially timed water samples are collected during deployment by Niskin bottles (5 L) mounted inside the chamber. The sampling cycle is activated by the telemetry unit on board the ship. Changes in the concentration of dissolved components among these bottles are then used to calculate their flux rates (Carson et al., 1990). The exhaust port at the top of the chamber carries a thermistor flowmeter which directly records the flow rate from the chamber (Linke et al., 1994).

During VESP-operation an additional SONARTRACK transponder was mounted with brackets on the cable and was used as a relay transponder in the ship's SONARTRACK transponder net. The operation of VESP had been hampered by the flooding of the CTD-pressure case during deployment on station 14 on the previous leg SO110-1A. In order to gain nevertheless water samples and flow

rates the damaged electronic boards were replaced by new circuits which were build during the transit times.

Table 21: VESP stations during SO110-1b.

Station	Device	Sector	Date	Latitude °N	Longitude °W	Water depth (m)	Description
25-1	VESP	EDGE	24 July	57°27.38	147°59.95	4876	water samples
29-1	VESP	EDGE	28 July				no bottom contact
33-1	VESP	EDGE	29 July	57°27.26	147°59.99	4844	water samples
41-1	VESP	SHUMAGIN	03 July	54°18.07	157°11.61	4839	water samples and flow measurements

Since the old VESP system (Linke et al., 1994) has a permanent cable connection to the ship for bidirectional power, video and data transmission which limits the deployment time (up to 2 hours) we developed a concept (Fig. 68) to disconnect a lander system from the ship's coaxial cable after its video-guided deployment with a launcher on a suspected vent site (Cremer, 1995). The launcher carries the telemetry, lights and 2 cameras (a survey camera and a second one which observes the lander during deployment) and has the permanent cable connection to the ship. After deployment the lander is mechanically released from the launcher by an electric releaser which is activated by the telemetry unit on board the ship. The launcher is brought back to the surface vessel, whereas the lander stays on the seafloor for long-term measurements independent from the ship's cable and power supply. The lander is equipped with an improved chamber to obtain both direct water flow and samples expelled from active sites and is designed as an instrument carrier for a variety of different measurements which could be integrated within this system. The lander is designed to stay on the seafloor for several days recording the different parameters (e.g. temperature, transmission, fluid flow), could take photographs and would take syringe samples prior to the recovery of the instrument by acoustic release of the additional weight. The obtained data can be checked and downloaded during deployment with an acoustic data link through an acoustic modem (DATASONICS ATM880).

This new prototype was assembled on board and tested several times at the sea surface for it's various functions (e.g. floatation of the synthatic foam, function of the electric and acoustic releasers). To complete work in SHUMAGIN the new vent sampler was deployed in this free-return configuration for the first time (44-1). All systems operated without problems and the device was put down at 4,780 m. Video observation of the lander revealed a perfect deployment and after a check of the acoustic releasers the laucher was separated from the lander and brought back onboard. The lander equipped with long-term recorder for flow data and sequential water sampling was actuated by acoustic command to drop weights and return to the surface after 6 hours. However, this attempt failed for as yet unknown reasons. Acoustic measurements revealed that the device did not leave it's original position despite the confirmation of the paired releasers that they had executed the aucoustic release command.

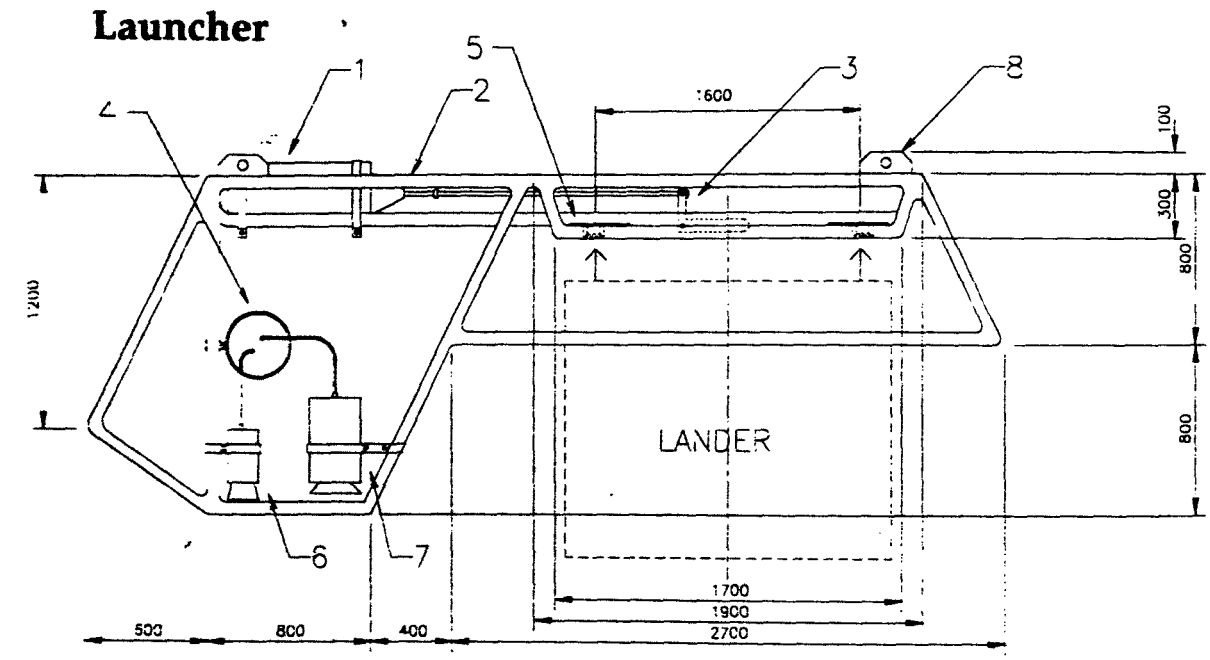

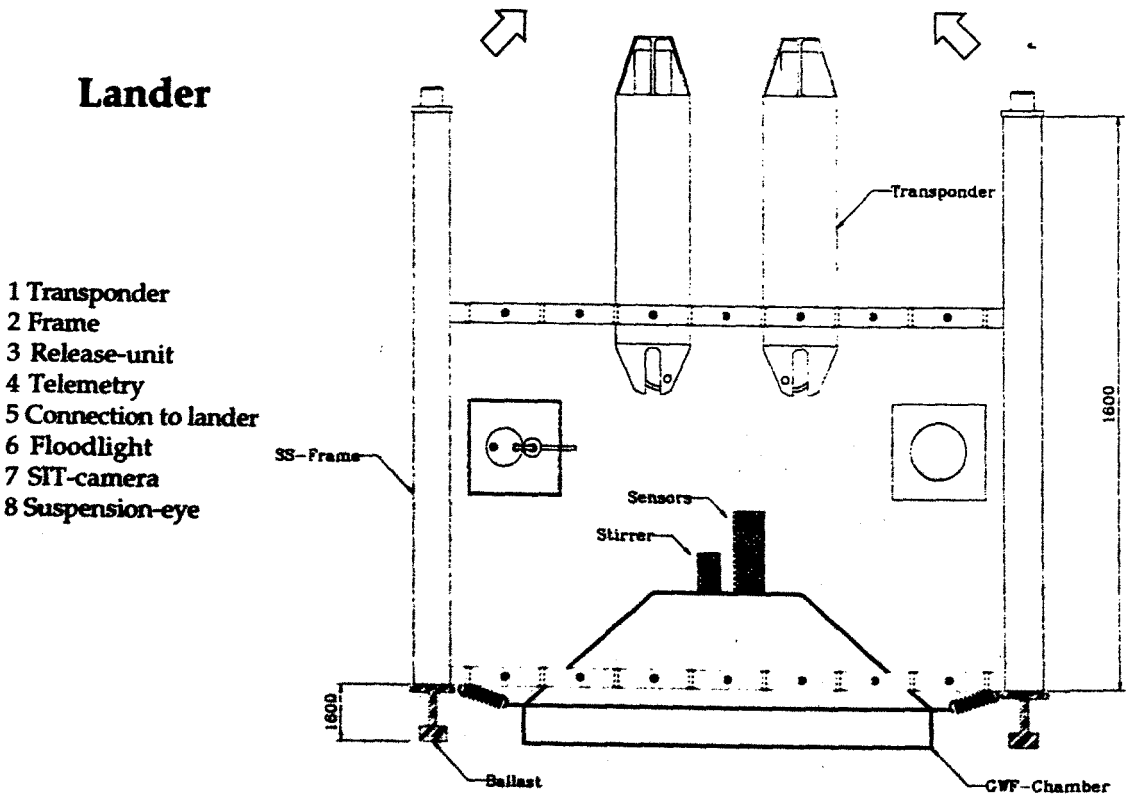

Fig. 68: Schematics of the new VESP prototype.

5.4 Fluid chemistry of VESP and ROPOS

5.4.1 Introduction

A. Dählmann, J. Greinert, E. Suess, E. Zuleger

During SO110-1b water samples were taken from areas of vent activity, indicated by the presence of clam fields. Sampling during ROPOS dive 344 (station 23-2) and VESP stations 25-1, 29-1 and 33-1 took place at the EDGE area, at the first ridge of the Aleutian accretionary prism. VESP 41-1 was taken at SHUMAGIN in a canyon located at the third accretionary ridge. All samples were taken video-controlled directly above clam fields. Sample locations are reported in Tab. 22 and are shown in Figs. 41 and 43.

Table 22: ROPOS and VESP stations during SO110-1b.

Station	Device	Sector	Date	Latitude °N	Longitude °W	Water depth (m)	Description
23-2	ROPOS	EDGE	23 July	57°27.37	147°59.19	4939	clam cluster
25-1	VESP	EDGE	24 July	57°27.38	147°59.95	4876	clam cluster
29-1	VESP	EDGE	28 July				no samples
33-1	VESP	EDGE	29 July	57°27.26	147°59.99	4844	clam cluster
41-1	VESP	SHUMAGIN	03 July	54°18.07	157°11.61	4839	pogos & clams

Table 23: Methane, nutrients, and oxygen data of stations 23, 25, 33 and 41 (n.d.= not detected, bdl = below detection limit).

Station	Bottle No.	Time of deployment [min]	Silicate [µM]	Phosphate [µM]	Nitrate [µM]	Ammonia [µM]	Methane [nl/l]	Oxygen [µM]	Sulfide [µM]
ROPOS 23	1		135	2,06	37,4	2,25	n.d.	n.d.	n.d.
	2		130	1,15	34,1	0,69	45	n.d.	n.d.
	3		139	1,40	37,0	0,52	193	n.d.	n.d.
	4		145	1,24	36,9	0,52	56	n.d.	n.d.
	7		140	1,24	37,3	bdl	n.d.	n.d.	n.d.
VESP 25	1	10	151	2,10	37,4	11,4	41	163	n.d.
	2	25	152	2,56	36,5	11,1	62	158	n.d.
	3	40	152	2,33	38,1	11,1	32	158	n.d.
	4	55	157	2,33	38,5	10,8	56	159	n.d.
	5	70	156	2,33	37,5	10,8	59	155	n.d.
VESP 33	1	10	156	1,87	35,2	bdl	40	160	bdl
	2	25	157	1,87	38,5	bdl	29	159	bdl
	3	45	156	1,74	37,5	bdl	37	158	bdl
	4	75	156	1,87	36,6	bdl	44	157	bdl
	5	120	155	2,24	37,5	bdl	37	159	bdl
VESP 41	3	11	148	n.d.	n.d.	17,3	96	161	bdl
	4	26	151	n.d.	n.d.	n.d.	92	161	bdl
	5	46	152	n.d.	n.d.	15,5	102	161	bdl

Analyses of methane, oxygen and nutrients were carried out onboard. The methods are described in the appropriate sections of cruise report SO110, part I, chapter 4. The data are listed in Tab. 23 and plotted in Figs. 69 and 70.

In addition, samples were collected for helium isotopes and tritium (Heidelberg, Potsdam), methane and carbon isotopes and deuterium of methane (University Victoria), methane oxidation rates (Humboldt State), and trace elements (GEOMAR) for post-cruise laboratory analyses.

5.4.2 Methane

E. Zuleger

During Leg 110-1b dissolved methane in cold seeps of the Aleutian subduction zone system was completed on 18 samples taken by video controlled VESP and ROPOS directly from vent fields, as indicated by the presence of clam colonies. During VESP deployment 3 to 5 samples were taken in a time serie to gain knowledge about the fluid flow out of the seep as well as the composition of the fluids. ROPOS samples were taken by sucking water into 5 L PE-buckets. Methane serves as a good indicator for seep fluids due to its low concentration in the ambient water column and is relatively enriched in fluids.

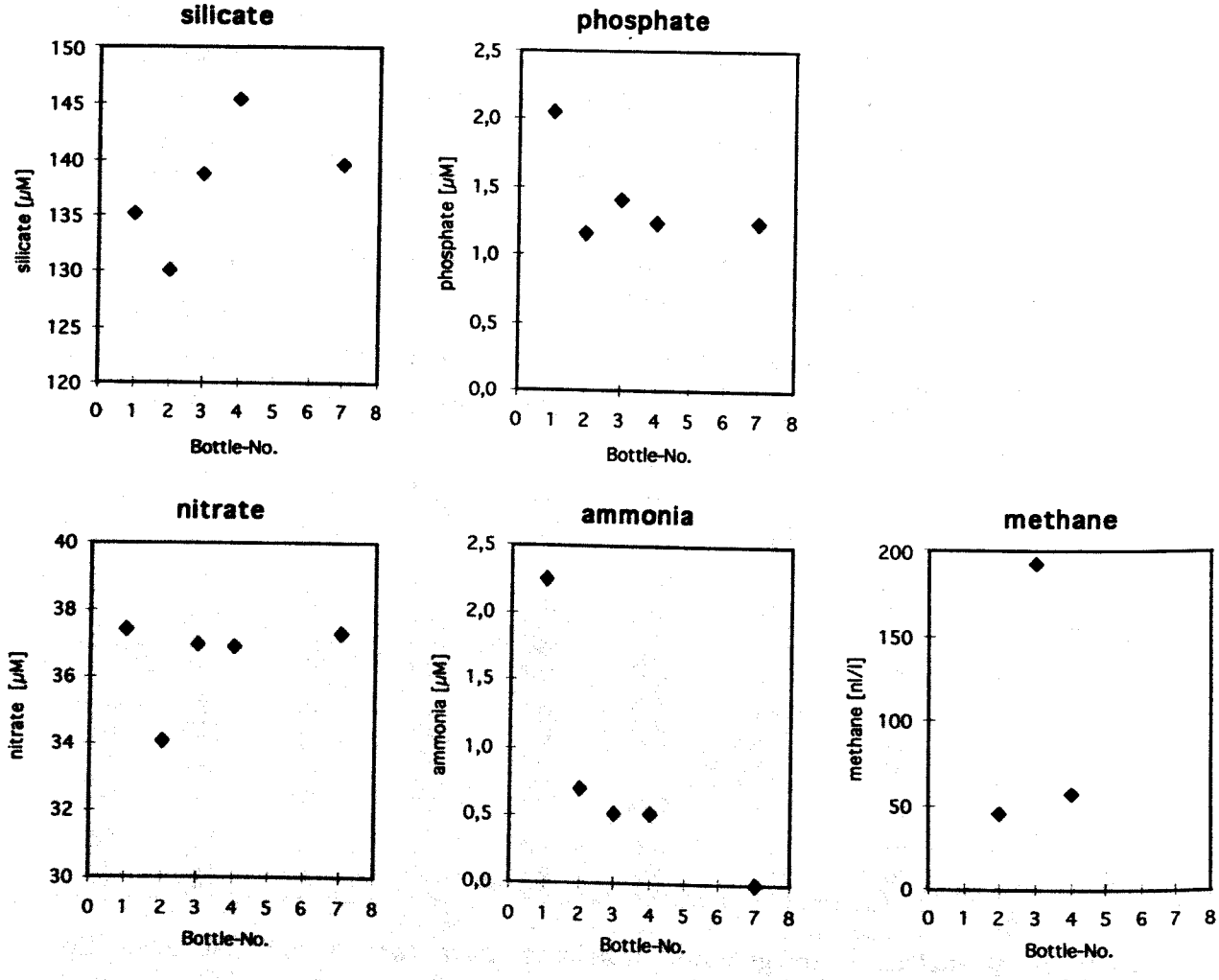

Fig. 69: Methane, silicate, phosphate, nitrate, and ammonia of ROPOS dive 344 (Station 23-2).

On-board analyses of dissolved methane were performed using a vacuum-ultrasonication degassing method (Schmitt et al., 1991, Lammers & Suess, 1994) and subsequent determination with a Shimadzu GC 14A gas-chromatograph. For further details see part I, chapter 4.3.

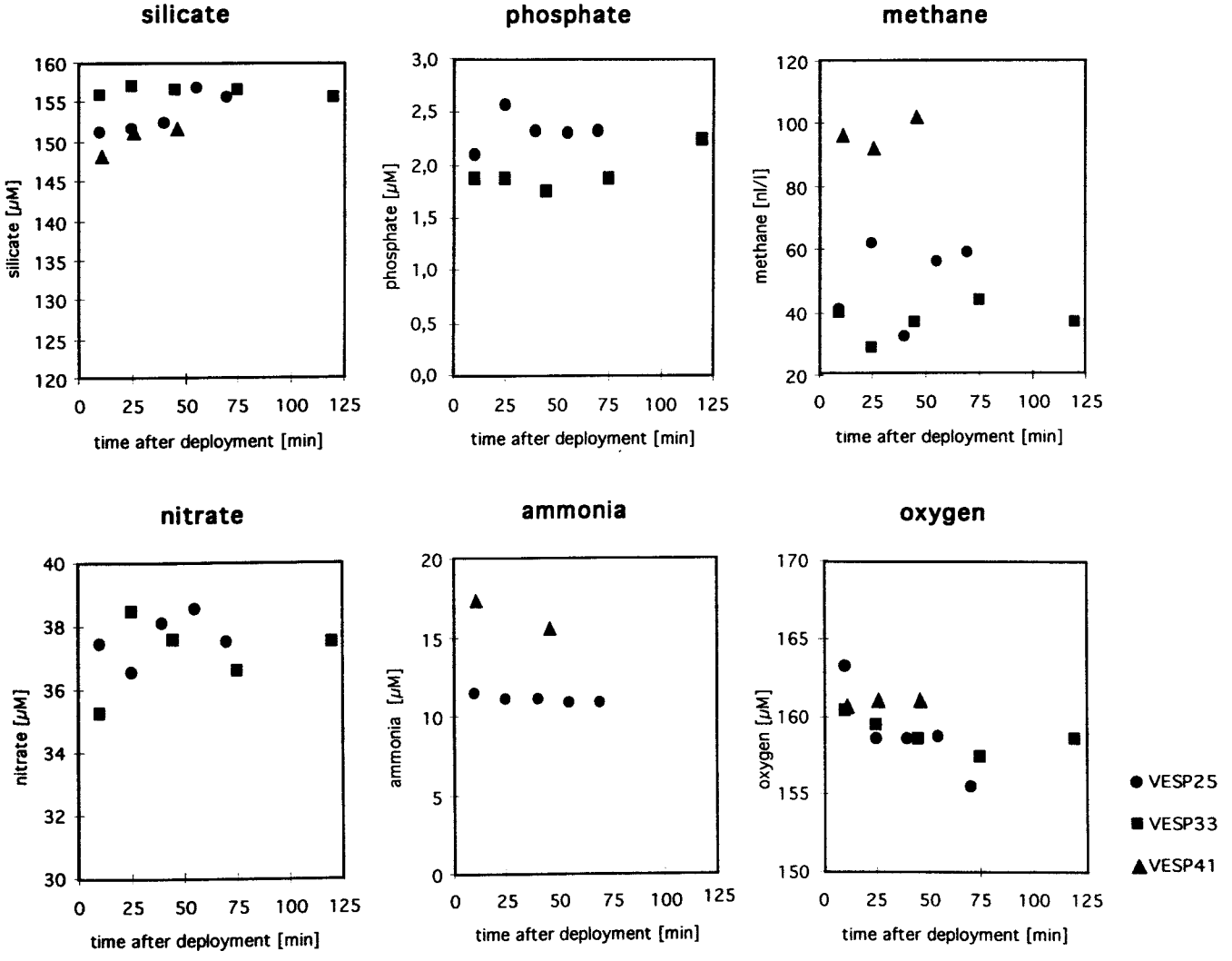

Fig. 70: Methane, silicate, phosphate, nitrate, ammonia and oxygen versus time of VESP deployment (Station 25-1, 33-1, and 41-1).

Five water samples were taken during ROPOS Dive 344 at the EDGE area. Methane could be analyzed in only three of these samples due to their small volume. However, the methane concentration in two of the samples with about 50 nL/L is only slightly increased relative to the background concentration of the water column in this area (see CTD stations for comparison). In contrast bottle 3 shows high methane content of about 200 nL/L.

VESP deployment was carried out at the EDGE area as well as in the SHUMAGIN-sector. At all stations the expected increase of methane due to the time dependent sampling was not detectable. However, VESP 41-1 deployed at

SHUMAGIN showed the highest values with about 100 nL/L. The methane value at EDGE for VESP 33-1 and 25-1 is 60 nL/L and 40 nL/L, respectively and therefore only slightly higher than bottom water in this area.

5.4.3 Oxygen

J. Greinert, E. Zuleger

Oxygen was determined by Winkler titration with 0.01n $Na_2S_2O_3$ on all water samples collected by VESP. The reproducibility, determined by measuring replicates was less than 1 µM. Station 41-1 shows no time dependence for oxygen with values of 160 µM. As for the methane, these values are representative of near bottom water values (see CTD data for comparison). However, station 25-1 and 33-1 showed a slight decrease (161 to 155 µM).

5.4.4 Nutrients

A. Dählmann, B. Domeyer

As silicate is usúally not effected by the metabolism of vent organisms and therefore used to estimate fluid flow. The concentration of silicate in pore water is much higher than in bottom water, so an increase in the VESP-samples is expected with the time of deployment. In contrast, oxygen concentration should decrease due to consumption by vent biota. The data for VESP 25 show these trends, whereas the data for VESP 33 and 41 are not that clear. A decrease in oxygen concentration indicates fluid flow for site VESP 33, however silicate does not show any changes. VESP 41 shows rather stable oxygen values, whereas silicate increases. Therefore, the fluid flow is calculated only for station VESP 25. The time-dependent change in concentration is given by the slope of linear regression.

$$d[Si]/dt = 5{,}70\ \mu M * h^{-1} = 5{,}7 * 103\ \mu mol * m^{-3} * h^{-1} \qquad (r^2 = 0{,}77)$$
$$d[O_2]/dt = -6{,}17\ \mu M * h^{-1} = -6{,}17 * 103\ \mu mol * m^{-3} * h^{-1} \qquad (r^2 = 0{,}76)$$

The flow is calculated by taking into account the volume (0,15 m^3) and the area of the sediment surface enclosed by the VESP barrel (0,234 m^2).

$$F(Si) = 3654\ \mu mol * h^{-1} * m^{-2}$$
$$F(O_2) = -3955\ \mu mol * h^{-1} * m^{-2}$$

The vent fluid flow is calculated using the following mass balance equation:

$$F(Si) = F(VF) * [SiVF] + F(SiDiff) - F(VF) * [SiBW]$$

with:
- F(Si) — flow of Si calculated from VESP data [µmol * h^{-1} * m^{-2}]
- F(VF) — vent fluid flow [m^3 * h^{-1} * m^{-2}]
- [SiVF] — silicate concentration in vent fluids [µmol * m^{-3}] mean value of TVG 63 (0-1 cm): 344 µM
- [SiBW] — silicate concentration in bottom water [µmol * m^{-3}]

data from MUC 57: 170 µM

F(SiDiff) diffusion flow of Si [$m^{3*} h^{-1} * m^{-2}$]
can be neglected, because it is two orders of magnitude smaller than F(Si)

After transformation the flow results as:

$$F(VF) = 21 * 10^{-3} m^{3*} h^{-1} * m^{-2}$$

For a 70 minutes deployment 5,7 L fluid penetrate into the barrel and the same amount of bottom water leaves the barrel at the top. Considering that such a small volume does not fully mix the barrel the oxygen consumption is calculated using the following mass balance equation. This is based on the assumption of a piston-like system where fluid displaces the bottom water and maintains horizontal layering:

$$F(O_2) = F(VF) * [O_2VF] - F(VF) * [O_2BW] - C(O_2)$$

with: F(O2) flow of O_2 calculated from VESP data [µmol * $h^{-1} * m^{-2}$]
F(VF) vent fluid flow [$m^{3*} h^{-1} * m^{-2}$]
$[O_2VF]$ oxygen concentration in vent fluids [µmol * m^{-3}]
since pore water analysis show an anoxic environment, it is set to zero
$[O_2BW]$ oxygen concentration in bottom water [µmol * m^{-3}]
data from MUC 57: 164 µM
$C(O_2)$ consumption of oxygen in the VESP barrel [µmol * $h^{-1} * m^{-2}$]

The resulting oxygen consumption of vent biota is:

$$C(O_2) = 511 \text{ µmol} * h^{-1} * m^{-2} = 0{,}5 \text{ mmol} * h^{-1} * m^{-2}$$

This value for oxygen consumption is slightly lower than the results obtained on the cruise SO97 (0,6 and 2,5 mmol * h^{-1} * m^{-2}). This is in reasonably good agreement with a higher fluid (SO 97: 8 and 3 * 10^{-3} $m^{3*} h^{-1} * m^{-2}$). The other nutrients do not show a time-depending change in concentration. Comparing the composition of nutrients in VESP-Niskin bottles with vent fluids sampled by ROPOS, shows that the latter are characterised by lower values of silicate, phosphate and ammonia, whereas CTD data are comparable to VESP concentrations.

6 Biology of cold-seep communities

6.1 Biological observations with ROPOS

R. Lutz, P. Linke

During the course of the ROPOS dive to the EDGE site, extremely high quality 3-chip camera video footage was recorded on a BETA SP format (RGB and YRB component), with extensive footage taken of geological features and biological communities associated with fluid seepage. Upon return to the laboratory, selected images were frame-grabbed using a spectrum of state-of-the-art video analysis equipment. Fig. 71 depicts a series of frame-grabbed video prints (from the BETA SP footage) of biological communities at the EDGE sites.

The *in situ* observations and video footage of numerous organism communities within the region include wide-field and close-up images of a variety of constituent organisms including vesicomyid clams, sea anemones (present on the ventral margins of the vesicomyids), galatheid crabs, 2 species of pogonophorans (of which many of the tubes have attached gastropod egg capsules), crinoids and buccinid gastropods. The partially infaunal vesicomyid clams, whose biomass dominates the community, are „bean-shaped", morphologically resembling both *Calyptogena phaseoliformis* from the Japan Trench and *Calyptogena (Ectenagena) extenta* from Monterey Bay, California.

6.2 Biological samples from TV-G, TV-GKG, TV-MUC, and ROPOS

P. Linke, N. von Mirbach, G. Lévai, H. Sahling

The main biological objective in the use of ROPOS and other sampling devices such as the TV-G (TV-guided grab), TV-GKG (TV-guided box corer), VESP (VEnt SPider) and TV-MUC (TV-MUltiCorer) was the recovery of undisturbed samples. Organisms of interest covering a wide range of size classes, from bacteria to macrofauna, were brought to the surface. Water samples from VESP and sediment subsamples from the TV-G and TV-MUC were preserved for enumeration of bacteria and determination of meiofauna. Subsamples of TV-G squeeze cakes from Shumagin and Edge up to a sediment depth of 10 cm were frozen at -20 °C for determination of chlorophyll-a and isotope analysis of ^{210}Pb. These analyses will be conducted at GEOMAR in Kiel. Despite the large quantity of sediment recovered by the TV-G, only the larger and heavier macrofauna was recovered. Similarly, the ROPOS manipulator yielded only small distinct samples, omitting an understanding of the surrounding community. Therefore, the TV-GKG, designed to take a section of undisturbed sediment within the community provided the greatest variety of fauna, since sea water-sediment interface is the habitat of most organisms. Although there were only two successful boxcorer deployments, each yielding a small amount of sediment, the specimens that were recovered provided quite a different understanding of the community structure. Table 23 gives a summary of the biological samples retrieved.

Fig 71: Cold seep communities at the EDGE site in the Aleutian subduction zone. (a) extensive populations of vesicomyid clams, buccinid gastropods (lower left), and anemones; (b, c, d) higher magnification of populations seen in a; (e) pogonophorans amongst clams and gastropods; (f) higher magnification of pogonophorans seen in e (gastropod egg cases present on pogonophoran tubes).

A great number of large Calyptogena (#1), Solemya and the very thin Pogonophorans (#1) were preserved for genetic studies, stable isotopes and other further investigations. Some of the larger Pogonophorans or Vestimentifera (#2) were also found, on which genetic and morphological studies will be conducted by the laboratory group of G. Lévai (New Jersey) and species specialist E. Southward (Plymouth).

New in this area is a small, up to 1 cm long, white bivalve with a red coloured foot and enlarged gills termed Clam #2. This size class, which has not been seen before, was first recovered by the TV-GKG. The small clam individuals in the mm range may be the juveniles of the Solemya and elongated Calyptogena #1 clam.

The symbiont harbouring cold-seep fauna in the Aleutian-trench consists of at least two different species of Pogonophorans and three different clam species present in a wide size spectrum. Anemones attached to the upper part of the Calyptogena #1 shells and commensal (?) polychaetes in the mantle cavity in the same species were not found elsewhere within the community and may have a strong relationship with the clam. Protobranch bivalves, buccinid and other gastropods and polychaetes are common parts of the community. The occurrence of two galatheid crabs and some different epibenthic crustacea are new to this environment.

Differences in the community structure from the different areas of EDGE and SHUMAGIN can, so far, only be observed visually. The extension of the colonies in SHUMAGIN and on the second ridge in the EDGE area is much bigger and less densely inhabited by clams than the highly packed small clusters on the first ridge in EDGE.
All clams yielded by the TV-guided sampling tools were dead when they came on deck. When the clams came on deck the valves of their shells were tightly closed but the bleeding was an unmistakable indication of death. The huge pressure difference from around 400 bars up to 1 bar was too great, thus no cultivation experiments were carried out during these two legs. All clams were dissected directly after retrieval and the different tissues, like foot, mantle, adductor and gill, were stored at -20 °C and also fixed in liquid nitrogen. Also shell length measurements were performed if the shells were intact. Independent of the two different Calyptogena species present, the clams in the Edge area were over twice as long as the clams from Shumagin: mean shell-length Edge: 170.3 mm (SD 17 mm); mean length Shumagin: 64.0 mm (SD 49.6 mm).

As an indicator for bioturbation sediment samples were taken for chlorophyll-a measurements. These samples were either taken from the squeeze cake or in the case of the TV-G 63 and 64 plastic syringes were taken in clam bed and also in the vicinity of the clams in the same grab. The analysis of the chlorophyll a content will be conducted on shore.

Table 23: Summary of the biological samples from Leg SO110-1b and Leg SO110-2.

Date 1996	Stat. No.	Device	Remarks	Symbionts harbouring fauna	Macro-fauna	Other samples
23 July	EDGE 23/1	ROPOS	dive 344	18 Calyptogena sp. # 1, Pogonoph. #1, Pogonoph. #2,	an, pb, bg, gc, po,	
24 July	EDGE 24/1	TV-G	57° 27.39' N 148° 00.01' W 4890 m	5 Calyptogena sp. # 1, Pogonophora #1, 1 Solemya	an, pb, bg, po, si ?	
28 July	EDGE 28/2	TV-G	57° 27.25' N 147° 59.67' W 4867 m	2 Calyptogena sp. # 1, Pogonophora #1, Pogonophora #2, 1 Solemya	si?, an, po, sp?	
29 July	EDGE 33/1	VESP	54° 27.26' N 147° 59.99' W 4844 m			1
2 August	EDGE 40/1	TV-GKG	54° 18.17' N 157° 11.82' W 4808 m	11 Calyptogena sp. # 1, 2 Calyptogena # 2, Pogonophora # 1,	an, pb, bg, gc, po, sp, oph	2
3 August	EDGE 41/1	VESP				1
3 August	EDGE 43/1	TV-G	54° 18.19' N 157° 11.93' W 4810 m	4 Calyptogena sp. # 1, Calyptogena # 2, Pogo.#1, Solemya	an, pb, bg, po	3
8 August	SHUM. 48/1	TV-G	54° 18.06' N 157° 11.89' W 4877 m	9 Calyptogena sp. # 1, 1 Calyptogena # 2, Pogo.#1, 52 Solemya	an, pb, bg, po, sp	2
8 August	SHUM. 49/1	TV-GKG	54° 18.05' N 157° 12.11' W 4809 m	2 Calyptogena sp. # 1, 1 Calyptogena # 2, Pogo. # 1, 26 small Solemya	an, pb, bg, gc, po, sp	2
10 August	SHUM. 54/1	TV-G	54° 18.11' N 157° 12.13' W 4796 m	Pogonophora #1	an, pb, bg, gc, si, po, sp	
12 August	57/2	TV-MUC	57° 27.40' N 147° 59.85' W 4856 m			2, 3
12 August	EDGE 59/1	TV-MUC	not tightly closed			3
13 August	EDGE 63/1	TV-G	57° 27.33' N 148° 0.27' 4774 m	20 Calyptogena sp. # 1, Pogonophora #1, Pogonophora #2	an, pb, bg, gc, po, sp, oph	2, 3
14 August	EDGE 64/1	TV-G	57° 29.34' N 148° 01.01' W 4550 m	3 Calyp. sp. # 1, 2 Calyp. # 2, Pogo. #1, Pogo. #2, 12 Solemya	an, po,	2, 3
14 August	EDGE 65/1	TV-G	57° 27.32' N 148° 00.19' W 4764 m	Pogonophora # 1, Pogonophora #2		2

Macrofauna:

anemones	= an
protobranch bivalve	= pb
buccinid gastropod	= bg
galatheid crab	= gc
sipunculida	= si
polychaetes	= po
sponge	= sp
stalked sponge	= stsp
crustacea	= cr
ophiuroidae	= oph

Other Samples

250 ml water samples for bacterial counts = 1
subsamples of squeeze cake for chlorophyll a = 2
sediment for meiofauna and bacterial counts = 3

6.3 Genetic investigations

R. A. Lutz, G. Levai

6.3.1 Objectives

A spectrum of seep-endemic organisms from two separate areas (EDGE and SHUMAGIN) of methane seepage was sampled along the Aleutian subduction zone. Collected organisms are to be subjected to a variety of allozyme and molecular genetic analyses which should shed considerable light on: (1) rates of gene flow between geographically separated populations of organisms along the Aleutian Subduction Zone; and (2) evolutionary relationships between cold seep organisms inhabiting the Aleutian Subduction Zone and similar taxa (within cryopreserved collections at Rutgers University) previously collected from other deep-sea methane/sulfide seeps and hydrothermal vents throughout the eastern and western Pacific Ocean basins.

To accomplish our objectives during SONNE Cruise 110, organisms were collected using: (1) the Canadian ROV ROPOS during the course of a 17-hour dive to the EDGE area; and (2) the TV Grab (standard SONNE equipment) at both the EDGE and SHUMAGIN sites. Upon retrieval of the samples on board the ship, selected tissue samples from the majority of organisms were immediately frozen in liquid nitrogen and several whole organisms of each species were preserved in 80 % methanol (non-denatured) to be kept as voucher specimens for subsequent studies. Table 1 presents a summary of the organisms collected and subsequently frozen and/or preserved for genetic and associated taxonomic studies.

Table 24: Organisms collected at two separate sites (EDGE and SHUMAGIN) in the Aleutian Subduction Zone during July/August, 1996 (SONNE cruise 110).

Location	Organism	Total Number
EDGE (57°27.3'N 147°59.7'W Depth: 4,950 m	vesicomyid clams	48
	sea anemones	16
	galatheid crabs	1
	protobranch bivalves	3
	buccinid gastropods	1
	polychaetes	19
	pogonophorans (2-3 species)	33
	Solemya sp.	6
SHUMAGIN (54°18.3'N 157°12.8'W) Depth: 3,550m	vesicomyid clams	38
	pogonophorans (2-3 species)	70
	Solemya sp.	34
	polychaetes	69

In the coming months, the collected organisms will be subjected to a variety of allozyme and molecular genetic analyses in our laboratory at Rutgers University. A summary of the techniques to be utilized in our analyses of these specimens is presented below.

6.3.2 Molecular techniques

Allozyme techniques are the most cost-effective way to get multi-locus genetic data for studies of gene flow (Vrijenhoek 1997). We have developed allozyme techniques for more than 35 species of invertebrates (e.g. gastropods, bivalves, vestimentiferans, and arthropods) inhabiting vent or seep environments. We have also used restriction analysis of mtDNA in our studies of gene flow (Craddock, et al. 1995) and obtained estimates of gene flow essentially identical to those found with allozymes. We examined single-copy nuclear DNAs in our study of gene flow in *Calyptogena magnifica* (Karl, et al. 1996). We are currently applying this technique to vestimentiferan populations from various vent and seep environments in the eastern Pacific. We will use genealogical methods (where applicable) with DNA-based data to provide robust estimates of gene flow and population parameters relevant to the dispersal and phylogeography of the collected seep-endemic organisms. A strength of the phylogeographic approach lies in the parallel analysis of several species that share a common biogeographic history or traverse similar ecological boundaries (reviewed by Avise 1994). Shared population structures and patterns of gene flow across boundaries (such as gaps between ridge or subduction systems) can provide significant insight into the spatial and temporal dynamics of the boundaries themselves.

Molecular systematic analyses require robust estimates of divergence, so we have turned instead to automated sequence analysis of specific mitochondrial genes. We have become proficient at analyzing DNA sequences from a variety of mitochondrial genes; COI, Cyt b, 16S rRNA. To assure that we are sequencing a single DNA fragment (i.e. amplicon) in species that exhibit evidence for heteroplasmy (e.g. some bivalve mollusks, see Zouros, et al. 1994), we clone PCR amplified DNA prior to sequencing. Standard DNA cloning techniques are routinely used in our laboratory (see Karl, et al. 1996).

6.3.3 Statistical methods for analysis of gene flow

If dispersal occurs predominantly in a stepwise manner (i.e. along roughly linear systems as would be expected for seep species along continental margins), it should be possible to identify the genetic signature associated with the "stepping-stone model". If long-distance dispersal events are rare, and dispersal occurs predominantly between neighboring colonies, gene flow will decline monotonically as the number of steps between colonies increases (Kimura and Weiss 1964). A similar negative relationship is expected under "isolation-by-distance" in continuously distributed species with limited dispersal capability (Wright 1943). However, if dispersal is dominated by long-distance events, individuals founding new colonies and those dispersing between existing colonies may be drawn from a relatively well-mixed pool of migrants, then population structure is best described by the classical "island model" (Wright 1931). Rates of gene flow between these island-like colonies will be independent of geographic distance.

In our studies of gene flow hydrothermal vent organisms, we have primarily used Slatkin's DIST program to discriminate between "island model" vs.

"stepping-stone" patterns of dispersal. DIST estimates migration rates between pairs of populations and regresses these estimates on geographical distance. Other methods (e.g. private alleles) are available, but have not been applicable for most studies of vent organisms (Vrijenhoek 1997). The confidence one can place in estimates of gene flow depends mostly on the number of independent polymorphic loci examined (Slatkin and Barton 1989). Multilocus allozymes still provide the most economical method for obtaining such data; however, we also use restriction analysis of mitochondrial DNA (mtDNA), anonymous single-copy nuclear DNAs (nDNA), and sequence analysis to expand the sample of loci. To date, we have examined rates of gene flow in 11 vent-or seep-endemic species (Vrijenhoek 1997).

6.3.4 Phylogenetic analysis

Phylogenetics (molecular or otherwise) are hypotheses that require independent tests. A measure of the robustness of a phylogenetic hypothesis is its consistency under different methods of analyses. We have experimented with most methods of phylogenetic inference including distance-based, parsimony, and maximum likelihood methods. Graduate students and post-doctoral fellows associated with our ongoing studies (Andy Peek, Robert Feldman, Tim Shank, Michael Black, and Otis Sanjur) completed the recent MOLECULAR PHYLOGENETICS workshop at Woods Hole using a variety of methods.. Although we can employ a variety of phylogeny reconstruction methods (e.g. parsimony, neighbor-joining, etc.) we prefer maximum likelihood (ML) methods as they are less sensitive to rate heterogeneity (Huelsenbeck 1995) and offer a rigorous statistical basis for evaluating alternative phylogenetic hypotheses (Hasegawa and Yano 1984). ML is computationally intensive, but our present computers (i.e. SPARC 4, and SUN Ultra-I 170 MHz), provide usable platforms for this method. We used the DNAML algorithm of PHYLIP (Felsenstein 1990) in several studies of vent organisms (Black, et al. in press; Hoeh, et al. in rev.), however, DNAML assumes a relatively simple model of sequence evolution (e.g. Jukes and Cantor 1969). The ML method will be used to evaluate alternative phylogenetic hypotheses and test assumptions about the evolutionary relationships among vent and seep organisms.

6.4 Microbiological sampling

C. L. Moyer

6.4.1 Introduction

One of the greatest challenges in microbial ecology is the accurate identification and description of microbial populations within their respective communities. This information is central to determining the extent of global microbial diversity, which remains the least understood of all the biological size classes. To address this challenge, molecular biological techniques using small-subunit ribosomal RNA (SSU rRNA) gene sequences have been applied to describe the

structure and diversity of different microbial communities (Giovannoni et al., 1990; Ward et al., 1990). The overall endeavor is to examine habitats with specific biogeochemical activities to learn more about the dominant microorganisms residing therein. The primary focus of this study is to estimate the microbial community structure and diversity to assess the degree of commonality and uniqueness between different deep-sea cold seep habitats and to compare these results with other hydrothermal vent habitats. This study will also allow for the enhanced development of a comprehensive global perspective regarding the diversity of deep-sea microbial communities.

The initial discovery of deep-sea hydrothermal vent systems and the unexpected presence of dense, but spatially-restricted microbial and animal communities within the fields of hydrothermal fluid discharge first occurred at the Galapagos Rift zone (Lonsdale, 1977). This discovery has been followed by nearly two decades of submersible-based exploration and experimentation. Numerous additional discoveries of hydrothermal vents and cold seeps around the world's ocean basins clearly established the importance of these systems as sources of mantle-derived gases and solutes, and as loci for heat dissipation, polymetallic sulfide mineral deposition, geochemical exchange, and microbial activity. These oases of life have drastically changed the long-standing paradigm of a deep-sea desert, yet the examination of the in situ or naturally-occurring microbial community structure at deep-sea seeps and vents has gone virtually unexplored due to the limitations imposed by culture enrichment techniques and by a previous lack of applicable alternative methods.

Selective enrichment culture has severe limitations as an approach to the cultivation of naturally-occurring microorganisms (Ward et al., 1992). The majority (typically >90-99%) of bacteria in nature cannot be cultivated using traditional techniques (Brock, 1987; Jannasch and Jones, 1959). Consequently, it is very unlikely that collections of bacterial isolates are representative of in situ diversity and community structure. Furthermore, because relatively nutrient-rich media are generally used for isolations, copiotrophic bacteria may be selected rather than those dominant in the natural community. My approach, herein, is to ascertain a microbial community's primary members through molecular (i.e., cell component) means and then to more wisely attempt their culture to further characterize their respective physiologies. Obtaining a better representation of bacterial community structure and diversity is crucial to aspects of microbial ecology where bacteria interact with one another and with their environment, e.g., global biogeochemical cycling of matter, succession and disturbance responses, predator-prey relationships, and trophic-level interactions.

Cell component analyses provide a culture-independent means of investigating microorganisms as they occur in nature (Ward et al., 1992). While several types of cell components have been analyzed, the SSU rRNA molecule offers an amount and type of information that makes it one of the best culture-independent descriptors or biomarkers of microorganisms. For example, each SSU rRNA gene contains highly conserved regions found among all living organisms as well as diagnostic variable regions unique to particular organisms or closely related groups. Additionally, each SSU rRNA gene contains about 1,500 nucleotides of

sequence information that can be obtained and utilized to differentiate among closely-related and distantly-related groups of microorganisms. Therefore, this information has phylogenetic implications and can be analyzed in the context of a large and growing database of SSU rRNA sequences of cultivated and uncultivated microorganisms. This type of molecular approach allows the autecology of microorganisms to be studied whether or not they can be cultivated. In addition, the phylogenetically described taxa or "phylotypes" can be placed in a synecology context through the examination of SSU rRNA clone libraries generated from a microbial community.

In recent years a detailed theory of evolutionary relationships among the domains Bacteria, Archaea and Eucarya has emerged from comparisons of SSU rRNA "signature" sequences (Figure 72; Olsen et al., 1994; Woese, 1994). Ribosomal RNAs have been the most widely used biomolecules for phylogenetic comparisons for the following reasons: (i) they are essential components of the protein synthesis machinery and therefore, are ubiquitously distributed and functionally conserved in all organisms, (ii) they lack the interspecies horizontal gene transfer found with many prokaryotic genes, (iii) they are readily isolated and identified, and (iv) they contain variable regions interspersed among highly conserved regions of primary and secondary structure, permitting phylogenies to be inferred over a broad range of evolutionary distance. These features make rRNAs particularly useful for studies of microbial community ecology, where a broad and unknown diversity of microorganisms is likely to exist. Currently, over 3,000 SSU rRNA sequences have been made available for study from the Ribosomal Database Project (Maidak et al., 1994), which provides these data in an aligned and phylogenetically ordered format.

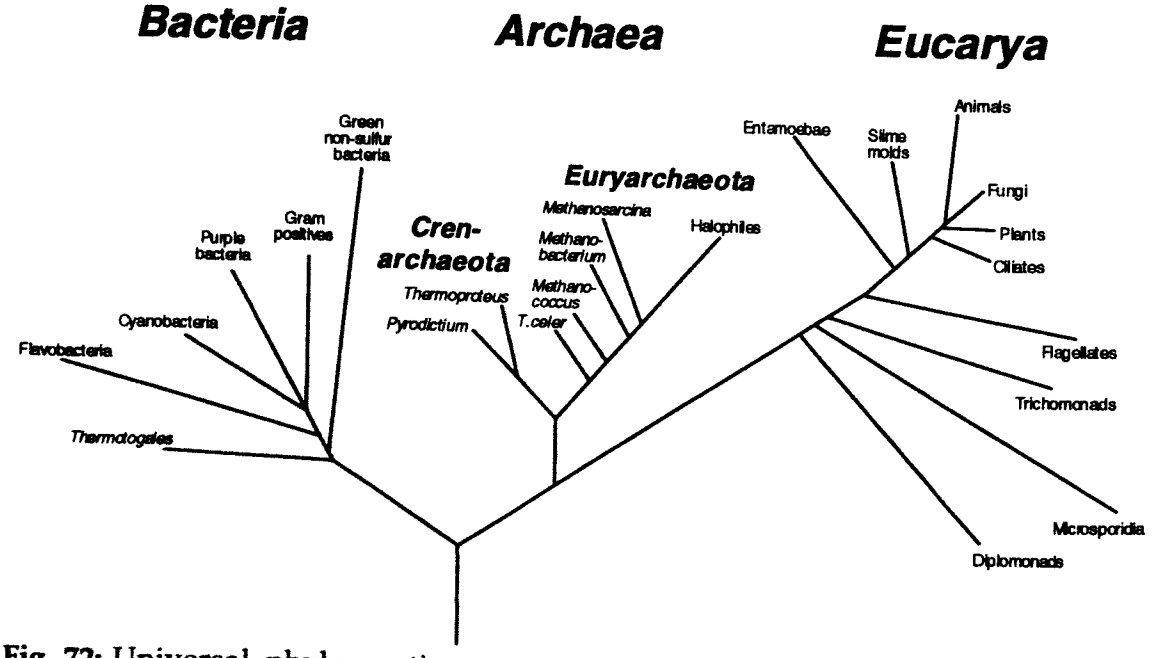

Fig. 72: Universal phylogenetic tree in rooted form, showing the three domains, *Archaea*, *Bacteria*, and *Eucarya*; adapted from Woese (1994). The position of the root was determined using the paralogous gene couple, translation elongation factors EFTu and EFG (Iwabe et al. 1989).

6.4.2 Experimental design and methods

Shipboard processing and storage of samples

Cold seep sediment samples collected by ROPOS, TV-GKG, and TV-G were each independently processed. Microbial biomass preservation was achieved by quick-freezing in liquid nitrogen and storing on dry ice until return to the laboratory. These samples will be used for the direct extraction of nucleic acids. A series of sub-samples were also (i) cryo-preserved (again using liquid nitrogen) with 40% glycerol for enrichment culture selection of aerobes, and (ii) stored at 4°C in gas-tight vials (head-space purged with N2) for enrichment culture selection of anaerobes. Another series of sub-samples was fixed with 2.5% EM grade glutaraldehyde for examination with SEM and epifluorescence microscopy.

Laboratory processing and molecular biological analysis

Initially, all samples will be examined by SEM and epifluorescence microscopy in an effort to ascertain biomass estimates and examine morphological diversity. The molecular biological strategy used will be essentially that of Moyer et al. (1994, 1995). The first step will be the efficient and direct extraction of high molecular weight nucleic acids from quick-frozen sediment samples. This will be followed by the polymerase chain reaction (PCR), where the specific amplification of SSU rRNA gene sequences occurs when using previously defined conditions to maximize the equal representation of each population contained within the respective community.

The concept, here, is to proportionally amplify or make several copies using the total genomic DNA from a natural community serving as the template for oligonucleotide primers that are complementary to universally conserved SSU rRNA sequence positions. Representative SSU rRNA gene amplification products are cloned into a plasmid vector and from this process a clone library is generated. The clone library is examined through the use of a restriction fragment length polymorphism (RFLP) distribution analysis. This approach, using tetrameric restriction enzymes, has been shown to detect >99% of the taxa (i.e., phylotypes) present within a model dataset with maximized diversity (Moyer et al., 1996). RFLP distribution data will be further analyzed through rarefaction analysis to estimate the genetic diversity of the microbial community. SSU rRNA gene sequences will be subjected to phylogenetic analysis to estimate the affiliated ancestral lineage for each dominant community member thereby yielding clues as to their respective evolutionary histories and potential physiologies. Access to the Ribosomal Database Project (RDP) as well as software and computer facilities are readily available at NSF's Center for Microbial Ecology.

6.5 Rates of methane oxidation

M. de Angelis, M. Large

6.5.1 Background

Methane, in large excess to that found in ambient seawater, enters ocean bottom water at deep-sea hydrothermal vents, hydrocarbon seeps and cold seeps associated with subduction zones. The fate of this methane is of interest as it represents a potentially significant source of methane to the atmosphere, where it acts as a greenhouse gas and plays a key role in controlling atmospheric chemistry. Bacterial methane oxidation is the only process known to occur under seawater conditions that can prevent the eventual diffusion and convection of vent and seep methane to surface waters and across the air/water interface into the atmosphere. Simple calculations and methane oxidation rate measurements taken throughout the world's oceans indicate that methane is not being oxidized to any significant degree within the water column. In addition, most of the methane does not reach the atmosphere. This suggests that methane oxidation is efficient and highly localized. A main focus of our research has been to determine the sites of vent and seep methane oxidation and understand what controls the location and rate of this process.

Previous studies at hydrothermal vents at the Juan de Fuca Ridge and hydrocarbon seeps in the Gulf of Mexico have indicated that surfaces exposed to seawater containing elevated levels of methane are important sites of methane oxidation. Such surfaces include mussel, clam, limpet and snail shells, carbonate rocks, tubeworm tubes, and surface sediments. At hydrothermal vent sites, where sulfide concentrations are orders of magnitude higher than methane levels, endosymbiotic associations have been found to be primarily based on sulfide oxidation. At such sites, non-endosymbiotic methane oxidation on external surfaces appears to be the major site of methane oxidation in the immediate vicinity of venting. At hydrocarbon seeps where we have carried out my studies and where methane levels are orders of magnitude higher than at vent sites, methane-oxidizer based endosymbioses have been found to be the major site of seep methane-oxidation. At such sites, methane oxidation on surfaces represents <10% of the methane oxidation activity, but represents an important mechanism for removing methane that escapes from endosymbiotic methane oxidizers.

In addition to the above-mentioned sites of methane injection into bottom ocean water, we have examined methane oxidation activity at dead whale falls where methane may be injected into seawater, but at low enough rates that elevated methane levels in seawater have not been detected. At this site, despite low ambient methane levels, we again found elevated methane oxidation rates on external surfaces of invertebrates sampled off the dead whale bones.

At all of these sites at which we have measured methane oxidation rates, the seawater methane levels have ranged over 3 orders of magnitude. Despite this, at all sites we found extremely low methane oxidation rates within the water column, even when methane concentrations were present at mM levels. This suggests that surfaces are sites where methane oxidizing bacteria can localize

themselves within optimum methane concentrations without being advected away or it may indicate that these bacteria require surfaces to be active. The locations and potential removal rates of methane at these sites are important in determining the capacity of methane oxidation to remove methane being added to the ocean at present rates and also in helping to determine if methane oxidation can handle additional methane release that may result from future exploitation of methane reserves, particularly in the coastal ocean.

6.5.2 Objectives

The major objective of this cruise for our research was to obtain additional data from a site different from those we had previously sampled and that was likely to have methane release from sediments associated with it. This would allow us to verify that elevated methane oxidation rates are found on surfaces exposed to seawater and that rates in ambient seawater were essentially equal to background deep seawater levels. These sites were also expected to provide a methane concentration intermediate between those found at hydrocarbon seeps and hydrothermal vents. Our cruise objectives were as follows:

(a) to collect surfaces (external animal hard parts, sediment, rocks) at subduction zone seeps and to measure methane oxidation activity associated with such surfaces using $^{14}CH_4$ methodology.

(b) to collect seawater samples from the same vicinity from which solid samples were collected and measure methane oxidation activity within such samples.

(c)to measure methane oxidation activity in sediment cores at several depths to obtain an idea of methane oxidation rate gradients within sediments at seep sites.

6.5.3 Methods

C-14 labeled CH_4 was used to determine methane oxidation activity. Approximately 0.001 mCi of $^{14}CH_4$ (g) was added to 5- or 10-ml gas-tight syringes containing filter-sterilized seawater. The gaseous $^{14}CH_4$ was allowed to equilibrate with the sterile seawater overnight at deep seawater ambient temperatures. This resulted in final $^{14}CH_4$ concentrations ranging from 800 to 1,200 nM CH_4 (approximate values) in most cases and up to 10 uM $^{14}CH_4$ in selected samples.

Animal samples were dissected and all internal organs discarded. Surfaces were cut or divided into approximately equal sizes (~1cm^2 for surfaces and 0.5 cc for sediment) and placed in 7- or 14-ml septum vials. The vials were filled with prechilled filter-sterilized seawater and sealed with no headspace using teflon/silicone septa. For sediment samples only, seawater that had been deoxygenated with N_2 was used. Once all vials were filled and sealed, the remaining gaseous CH_4 was expelled from the gastight syringes into the hood. A 0.25 or 0.5 ml aliquot of $^{14}CH_4$-equilibrated seawater was then injected into each vial using a sideport needle. Samples were incubated in the cold room between 5 and 7° C for up to 8 hours. Samples were run in replicate over 4 time periods (0,

2, 4, 8 hours). Seawater samples were added to fill the septum vials to capacity and then treated as described for surface samples. Samples were killed, including a killed control, immediately after injection of the label, by addition of 0.2 ml 6N NaOH which converted any $^{14}CO_2$ produced by methane oxidation to insoluble C-14 carbonate. After a minimum of one hour after addition of NaOH, samples were transferred to 20 ml sample vials for transport back to shore for analysis. Samples for methane oxidation rates are expected to be run by mid-October using an acidification and $^{14}CO_2$ trapping method followed by liquid scintillation counting. Samples will also be filtered to obtain estimates of the amount of $^{14}CH_4$ incorporated into cell carbon.

7 Vent site survey by TV-sled EXPLOS

7.1 Introduction

D. Saffer, J. Greinert, D. Orange, N. Maher, J. Yun, H. Sahling, G. Levai, M. Schumann, E. Suess, G. Bohrmann

The EXPLOS camera sled (Ocean Floor EXPLOration System) was used to map the distribution of biological vent communities and geologic features across the first (most seaward) and second anticlinal ridges of the Shumigan, Ugak, and EDGE areas of the Aleutian accretionary complex. EXPLOS is equipped with a black and white video camera (OSPREY 0111-6006), a color video camera (MSC 2000-D), 4 halogen lamps, and 2 still cameras to take color slides of features on the seafloor. EXPLOS uses an SIMRAD SSBL transponder for online navigation. Unfortunately, the fiber optic cable used for color video transmission was damaged during TV-GKG 31, and color video was not available for EXPLOS tracks 32, 35, and 37. Black and white video was maintained using a coaxial cable, although the video quality was compromised without fiber optics. EXPLOS was used in three areas of the Aleutian trench during cruise 100-1b: EDGE-sector (EXPLOS 22, 32), UGAK-sector (EXPLOS 35), and SHUMIGAN-sector (EXPLOS 37).

Table 25: Summary data of EXPLOS tracks.

Date	Station	Latitude begin Latitude end	Longitude begin Longitude end	Cable length begin Cable length end
22 July	22	57° 29.12′ N 57° 25.52′ N	148°03.99′ W 148°02.12′ W	4662 m 4991 m
29 July	32	57°31.22′ N 57°28.76′ N	148°00.47′ W 147°55.97′ W	4693 m 5003 m
30 July	35	56°40.42′ N 56°36.71′ N	150°10.58′ W 150°07.58′ W	4844 m 5229 m
1 Aug	37	54°16.02′ N 54°13.09′ N	157°14.68′ W 157°12.86′ W	4889 m 5405 m

7.2 EDGE-sector

D. Saffer, J. Greinert

EXPLOS tracks 22 and 32 in the EDGE are parallel to EXPLOS tracks 21-2 and 35 from Sonne cruise 97 (1994), oriented N-NW to S-SE, and extend the coverage of the older tracks to the Northeast and Southwest (Figs. 73 and 74). EXPLOS dive tracks 22, 21-2, and 35 cross the first and second anticlinal ridges of the accretionary complex, while track 32 crosses only one ridge farther to the Northeast where the topographic expression of the first ridge is less pronounced. Bedding orientations measured during ROPOS dive 344 indicate that the first anticline plunges to the Northeast, parallel to the trench, which may explain its decreasing topographic expression to the Northeast.

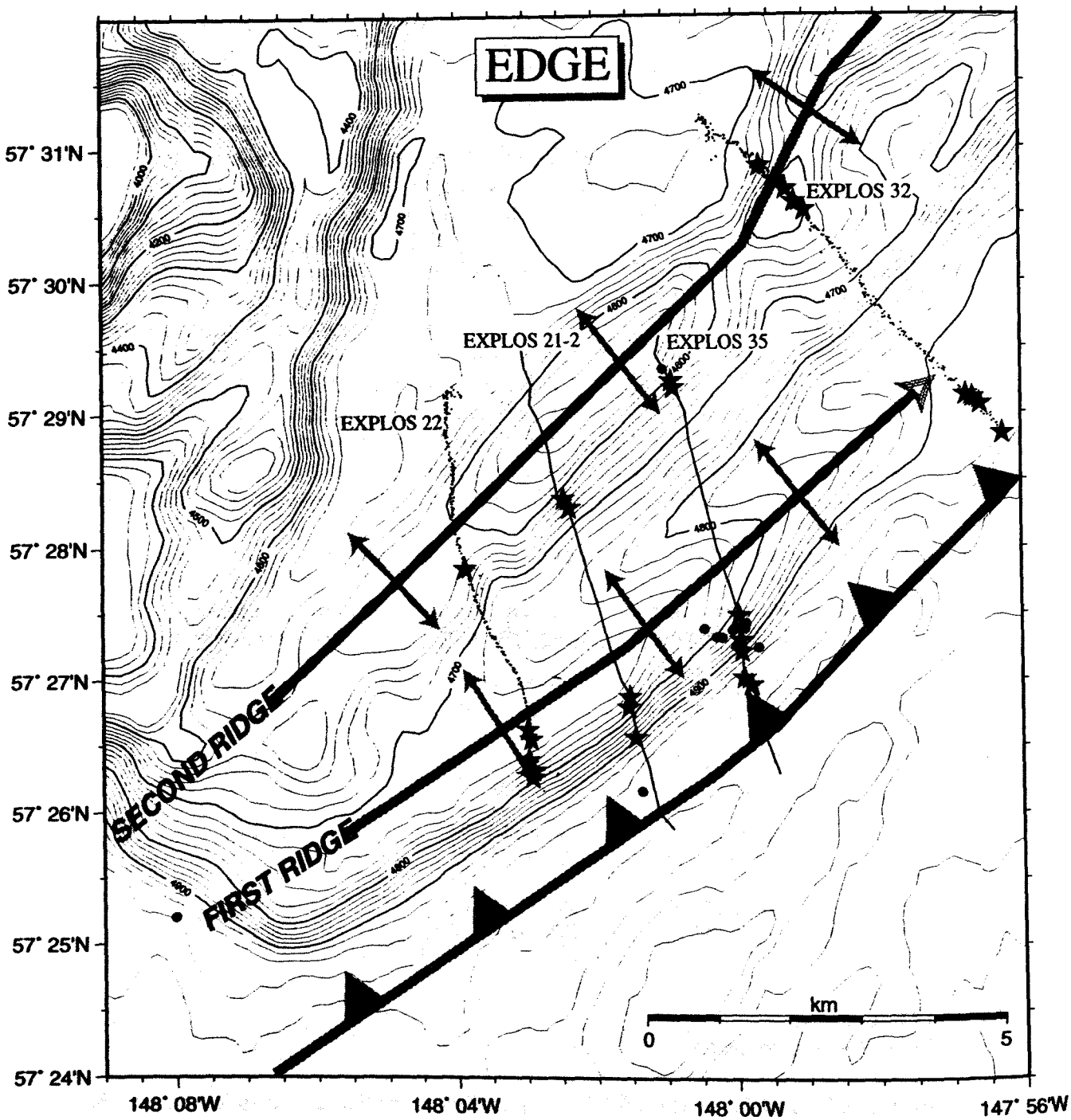

Fig. 73: Overview map of the EDGE area, showing EXPLOS 21-2 and 35 from Sonne cruise 97 (1994) and EXPLOS 22 and 32 from Sonne 110-1b. The approximate location of the first and second anticlinal ridges with dip direction, as well as the plate boundary, are drawn in grey. Stars indicate the location of clam beds; black circles mark device positions. Note that the track of EXPLOS 22 includes a navigation error and should be shifted along the track to the South.

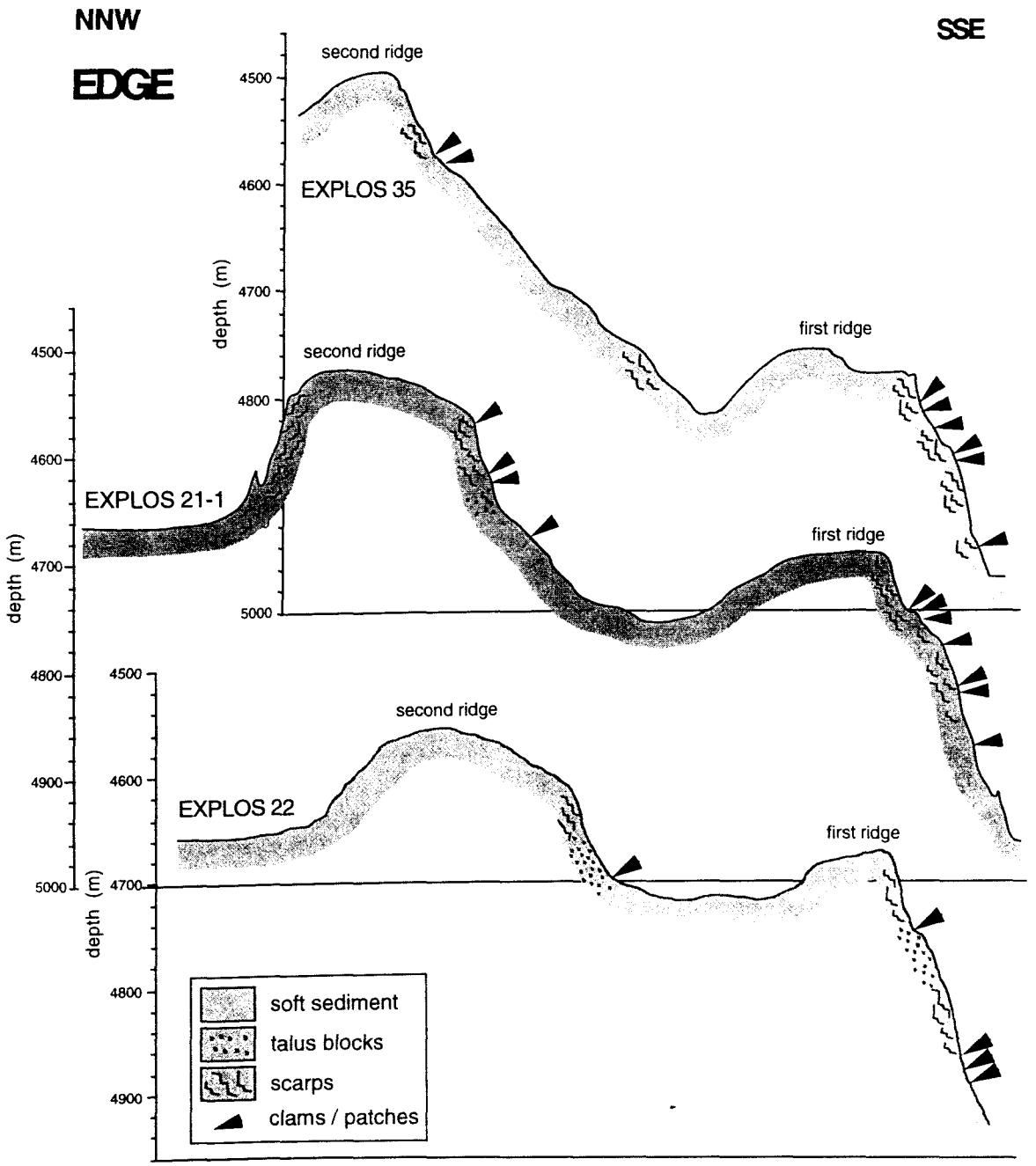

Fig. 74: Perspective plot of CTD depth profiles from three southernmost EXPLOS tracks in EDGE (21-2, 22, 35). Clam positions are marked by arrows.

A systematic error in navigation appears to have occurred during EXPLOS 22, resulting in a shift of the actual track approximately 650 m to the North and 250 m to the West. Fig. 74 shows topographic profiles plotted from CTD depth measurements for the three southernmost EXPLOS dives (21-2, 22, 35), and indicates the distribution of vent sites, scarps, and soft sediment.

EXPLOS track 22 began at a depth of 4,662 m on a smooth sediment covered slope North of the top of the second anticlinal ridge. The entire landward limb of the second ridge exhibited no signs of venting or erosion, but was characterized by a smooth sediment cover. The first scarps were observed on the seaward limb of the second ridge at a depth of about 4,620 m. These scarps were generally steep and bedding was clearly visible in some cases. Below these scarps, smooth sediment and talus blocks were observed. Starting at depth of 4,680 m, clams appeared, increasing in density from a few lone clams to several patches 0.5 m in diameter. These clam patches coincide with the base of the second anticlinal ridge. The flat depression between the first and second ridges was covered with smooth sediment and occasional talus blocks. The landward limb of the first ridge, like the second, was covered in smooth sediment. The steeper seaward face of the first ridge was marked by scarps which exposed seaward dipping beds. Mounds of slumped sediment were found at the bases of some scarps. Three separate clam beds were found along the lower portion of the seaward face, beginning at a depth of 4,740 m. These clam beds were separated by steep sediment covered slopes and scarps. Track 22 ended at the base of the first ridge, at a depth of 4,930 m.

EXPLOS track 32 was completed without CTD data to constrain water depths, due to technical problems. The dive began northwest of the landward limb of the first ridge, and encountered only soft sediment with occasional blocky sediment and rubble in the depression landward of the ridge. The bottom portion of the landward limb of the first ridge is a steep slope dominated by scarps, talus blocks, and vertical sheets. Exposed bedding dips to the Northwest. Above this area, clams beds were found where the slope flattens and is covered by smooth sediment. The slope increases above the first clam beds, and is covered by rubble and blocky sediment. On the Northwest side of the summit, the slope steepens again, and is characterized by interspersed clam beds and scarps. Some of the scarps are large single features, while others appear as a series of 1-2 m steps.
The top portion of the seaward limb is gently sloping and covered with smooth sediment. Near the base of the seaward limb, step-like series of freshly broken 1-2 m scarps are interspersed with clam beds. Below the clam beds, a large steep fractured outcrop was encountered. Downward from this outcrop, we found only soft sediment.

Implications for fluid flow
In the EDGE area, seep communities were found only on the seaward limbs of the first and second anticlinal ridges, with the exception of EXPLOS 32, where some clam beds were observed on both sides of an isolated summit atop the second ridge. The depth of seep communities on the second ridge increases systematically from Northeast to the Southwest, from 4600 m (EXPLOS 32) to 4680 m (EXPLOS 22, from CTD). Seep communities on the first ridge occur mostly on the upper 150 m, just below a 40 m high scarp, on EXPLOS 21-2, 22, and 35.

Fluid seeping at the EDGE site may be controlled by flow along low angle faults, diffuse seepage through the toe of the prism, flow along high angle fractures, geomorphically focussed flow, or flow through high permeability beds. The systematic decrease in elevation of seeps along the seaward face of the second

anticlinal ridge is consistent with aquifer flow controlled by a high permeability bedding layer within a Northeasterly plunging fold. In this case, seep communities would be observed where the permeable bed contacts the seafloor. This hypothesis can also explain the seep communities found at ~4,600 m on the landward face of the anticlinal ridge. Alternatively, these seeps may be associated with a dipping fault surface which controls flow either through high fracture permeability, or by acting as a permeability cap for sediments below. The association of vent communities on the first anticlinal ridge with a large scarp suggests that flow is either controlled geomorphically by a major break in slope, or more likely, that a major structural feature (fault or bedding) controls both the scarp and the fluid expulsion. In the latter case, geomorphically driven seepage may add to the structurally controlled flow and further influence erosion.

7.3 UGAK-sector

D. Saffer, J. Greinert

EXPLOS track 35 crossed both the first and second anticlinal ridges, beginning just below a small summit between the second and third ridges (Figs. 75 and 76). For this dive, the CTD was used to track depth, but this profile shows a similar systematic error in navigation to EXPLOS track 22. The dive began at a depth of 4,840 m, and progressed upslope for approximately 40 m over smoothly sedimented terrain. The seaward face of this summit is dominated by scarps and outcrops occurring in 2-6 m steps. A cluster of clams and clam tracks were found on soft sediment approximately 100 m below the summit. A clam field ~40 m across, with single patches as large as 4 m in diameter, was found on a flat area covered by sediment in a small distance from the first cluster. Below the clam field, the slope increases and is covered by smooth sediment interrupted by an occasional small scarp. The landward limb of the second anticlinal ridge is steep in places and is sediment covered; no scarps or clam fields were encountered. The top of the second ridge was reached at a water depth of 4,875 m. Several scarps, some as high as 13 m, were found interspersed with flat sediment covered areas and talus on the seaward limb of the second ridge. In many cases, the scarps expose fractured bedding. At a water depth of 5,130 m, the slope decreases and is covered primarily by soft sediment, with occasional scarps. No clam fields were found on the second ridge, although a single clam shell was observed at 5,225 m just before the end of the dive.

Implications for fluid flow

Seep communities on EXPLOS track 35 were found only on the seaward slope of the summit between the second and third ridges. Like the EDGE area, the clam fields in UGAK were located below scarps, on flat areas covered by soft sediment. The presence of vent sites with scarps suggests again that either flow is geomorphically controlled, or scarps mark structural features. Because only two vent sites have been found in the UGAK area on a single EXPLOS dive, it is difficult to make interpretations about fluid flow in this area.

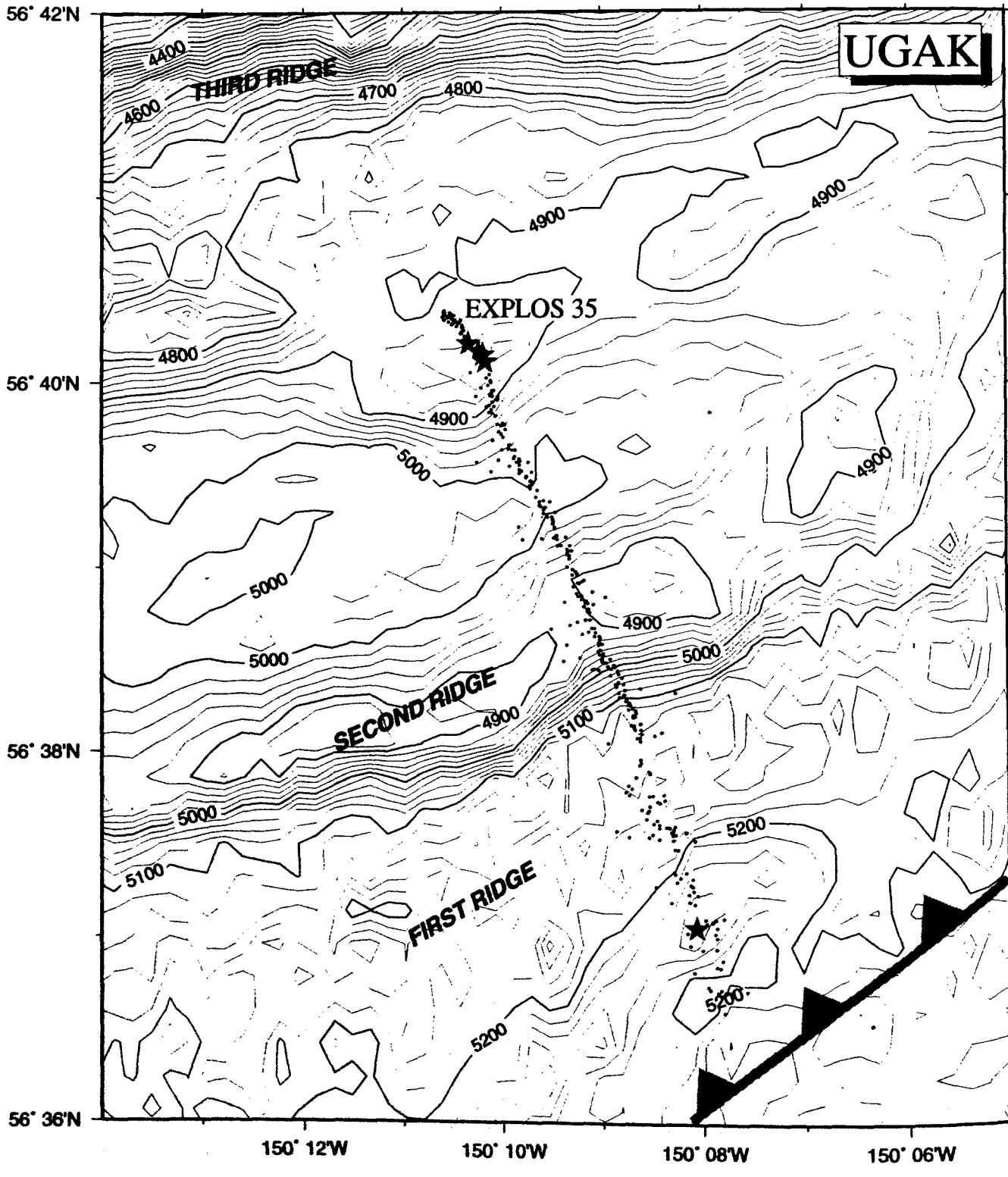

Fig. 75: Map of UGAK area showing EXPLOS positions during dive 35. Stars mark the location of observed clam beds. The approximate trace of the subduction zone is drawn in grey. Note that this track also includes a navigation error and should be shifted along the track to the South-Southeast.

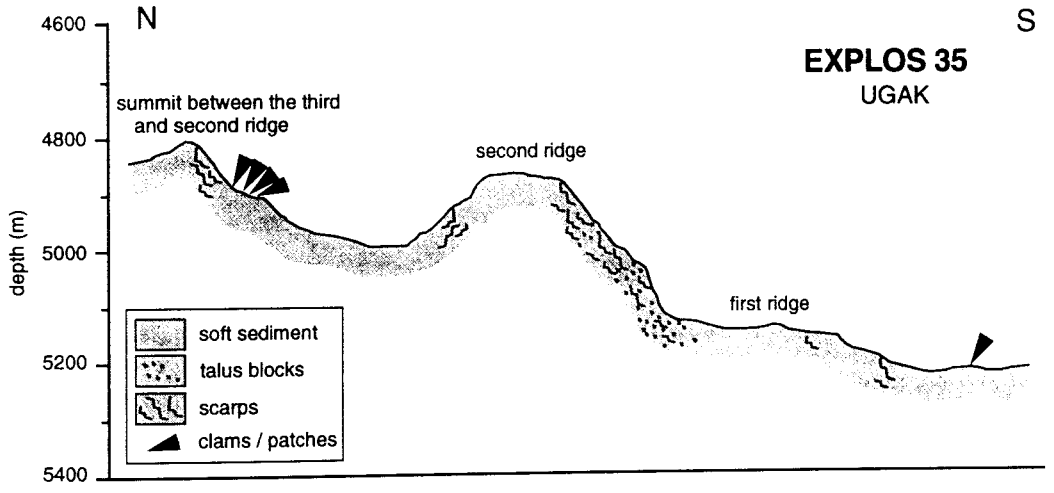

Fig. 76: Profile from EXPLOS 35 in the UGAK area; arrows mark the location of clam beds.

7.4 SHUMIGAN-sector

D. Saffer, J. Greinert

The track of **EXPLOS 37** (Fig. 77) followed a large headless submarine canyon in the westernmost portion of the Shumigan area. The canyon is oriented approximately North-South on the seaward limb of the first anticline, and is located at approximately 157°13' W longitude. Because of it's location, this EXPLOS dive not only allowed mapping of vent distribution across the ridge, but also allowed a direct investigation of the role that fluid seeping may play in the formation and maintenance of submarine canyons (Orange et al., 1994). During this track, the CTD was flooded, and data recovery was impossible.

In general, scarps were visible along the northernmost part of the EXPLOS 37 track, near the steeper upper reaches of the canyon (Fig. 77). Often these scarps were clustered together in a series of steps, while in other cases the scarps were single features as high as 8 meters. Some of the scarps also exhibited fractured bedding of unknown orientation. Talus blocks, fallen sediment, and talus fields were observed primarily in the lower reaches of the canyon, where slopes are shallower. No vent communities were seen until the end of the EXPLOS track, near the base of the anticlinal ridge.

These observations suggest that the canyon erodes northward at its head mainly as a result of slumping, which forms scarps. This material is probably transported down the canyon either by currents, transient events like earthquakes, storms, or turbidity flows, or by some combination of these. Although biological vent sites were not found in the upper portion of the canyon, some focussed seepage may occur at scarps and facilitate erosion (Orange et al., 1994). The talus found in the lower reaches of the canyon is probably derived from erosion of the steep canyon walls, although transport from the eroding canyon head cannot be ruled out.

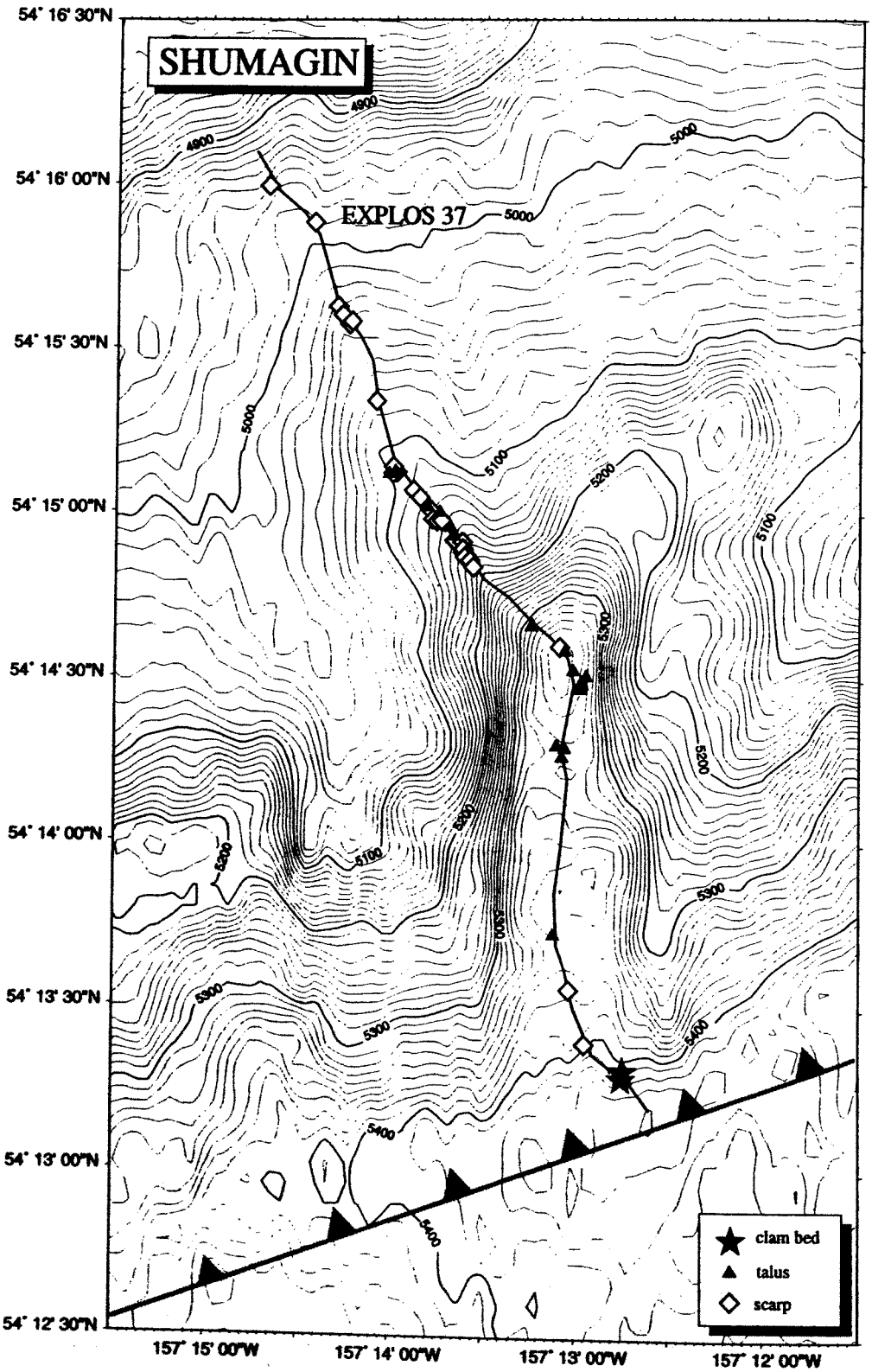

Fig. 77: Map of EXPLOS 35 track in the southern SHUMIGAN area. Open squares indicate scarps, black triangles indicate talus blocks, and stars mark the location of clam beds.

Implications for fluid flow

The absence of vent communities everywhere along the canyon where scarps and erosional remnants are present can be explained in a couple of ways. The lack of a spatial correlation between scarps and venting sites implies that geomorphically focussed aquifer flow is unimportant in supporting vent communities. The data may also suggest that fluid flow is not important in facilitating the canyon erosion, as Orange et al. (1994) argue is the case for other headless submarine canyons. Alternatively, these observations may simply mean that the flux of expelled fluid is high enough to support vent communities only in selected areas near the frontal thrust or where the prism sediments are thin, but flow below this threshold may still occur at scarps. In this scenario, fluid flow would be derived from a widespread source (compacting accreted sediments below), but expulsion from the most seaward part of the accretionary complex would be scattered at several sites along the seaward limb of the first anticlinal ridge.

Like the observations made by ROPOS and during TV-guided sampling at the EDGE area, the location of clam beds on EXPLOS 37 suggests that the highest fluxes occur on the seaward limb. The observations made here are also consistent with all of the hypotheses offered to explain venting in the EDGE area, except that of geomorphically focussed flow. Because of the small number of vent sites observed, it is difficult to further differentiate between fracture controlled seepage and diffuse seeping from underthrust sediments in areas where the overlying prism is sufficiently thin. (No linear trending clam beds were observed but the total number found was only two). The absence of a relationship between vent sites and scarps does seem to rule out the hypothesis that geomorphically focussed fluid flow is enough to support vent communities, at least at this location. However, these observations do not discount the contribution of seepage to erosional processes which form the scarps.

8 Geological sampling

M. Schumann, F. Kulescha, A. Petersen

Geologic and hydrographic sampling were essential activities aboard R.V. SONNE in support of in-itu observations and remotely operated sampling. The main objective was to place the sampling equipment as close as possible to previously determined targets; another objective was to optimize sample recovery from the highly variable bottom conditions.

8.1 Performance of equipment

In order to collect sediments, precipitates as well as fauna and pore water from vent sites a wide variety of coring devices was used. All instruments were deployed with the SONNE's own SSBL-transponder navigation (*SIMRAD*). These devices include:

- Kastencorer (KAL): gravity corer with a square box of 30 x 30 cm, a weight of 4.5 tons and a length of 575 cm for the core barrel segments.

- Gravity corer (SL) with a weight of 3 t and a core barrel segment of 3 m length and 10 cm in diameter.

- TV-box corer (TV-GKG): box-corer, weight 1 ton, square boxes of 50 x 50 cm in diameter and 50 cm high. TV-equipment contained a telemetry-unit, a *Simrad OE 1358* camera, and two lights of 250 watts.

- TV-multicorer (TV-MUC): the multicorer used fibre-tubes with a 10 cm inner diameter, 50 cm long. Because of the TV-equipment we could only use six tubes. The TV-equipment consists of a videocamera, two lights of 150 watts and a telemetry-unit. Total weight was 1 t.

- TV-Grab (TV-G): the TV-Grab of RV SONNE was built by *Preussag*. The instrument contains an *OSPREY* videocamera, two lights of 150 watts, and a telemetry-unit. Spades of the grab are controlled on deck from the geology laboratory. Sample size is 100 x 170 cm.

Both the gravity corer (SL) and the Kastencorer (KAL) were unable to achieve the expected sample sizes, either due to rough morphology or indurated sediments on the seafloor. At station 52 the 3 m KAL-box penetrated 2 m deep into the sediment, but could not tear off the core. The box was entirely folded by the underpressure when pulled out of the sediment. At stations 58 and 60 cores could be recovered by the SL, despite a damaged corecatcher.

In general the TV-guided box corer as well as the TV-MUC had problems in penetrating the sediments because of their small weights. Due to technical problems with the TV-unit station 31 had been canceled. Wave-movements and sideward dragging cable caused relaeasing-failure at stations 38, 42, 53 and 61. To increase penetration the TV-MUC was used with only 4 sampling-tubes only. At

station 57-1 the cable got twisted around one foot of the frame und pulled it up upside down, washing out the sediment from the tubes. At station 59 the sediment was washed out during heaving.

Due to its weight, the TV-grab was the instrument with the most success. Stations 26 and 38 had to be canceled due to camera problems. Sediments, precipitates and vent biota could be sampled using the TV-grab.

8.2 Sampling program and preliminary sedimentological results

N. Biebow, J. Greinert, J. Yun, C. Didié, J. Heinze, C. Jung

The main objective of the sediment sampling during cruise SO110 was to obtain complete undisturbed sediment cores from vent sites. Video-operated instruments, like the TV-box corer and the TV-multicorer were used for the first time in an attempt to locate and directly sample these sites. In the SHUMIGAN and EDGE study areas, sediment was sampled by 3 kastencorers (KAL), 2 gravity corers (SL), 7 TV-box corers (TV-GKG), 3 TV-multicorers (TV-MUC) and 12 TV-grabs (TV-G).
Positions, water depths, successful core recovery and sample types are documented in Table 26., Sediment samples were taken from each core for pore water chemistry and determination of the physical properties

Table 26: Sedimentological sampling during SO110 cruise (P = porewater, M = methane, Fe = iron, I = S-isotopes, S = sedimentology samples, PP = physical property samples, B = barite, Pb = lead, Su= sulfide).

Stat. No.	Instr.	Lat. N°	Long. W°	Water depth (m)	Rec.	P	M	Fe	I	S	PP	B	Pb	Su
24-1	TV-G	57°27.4	148°00.0	4890	50 %	--	--	--	--	25	25	--	--	--
26-1	TV-G	57°27.3	147°59.8	4796	------	--	--	--	--	--	--	--	--	--
28-1	TV-G	57°27.3	147°58.9	4954	------	--	--	--	--	--	--	--	--	--
28-2	TV-G	57°27.2	147°59.7	4867	25 %	--	--	--	--	1	--	--	--	--
31-1	TV-GKG	57°27.4	148°00.1	4761	------	--	--	--	--	--	--	--	--	--
38-1	TV-G	54°18.3	157°12.9	4536	------	--	--	--	--	--	--	--	--	--
38-2	TV-GKG	54°18.1	157°12.2	4647	------	--	--	--	--	--	--	--	--	--
40-1	TV-GKG	54°18.2	157°11.8	4808	5 cm	--	--	--	--	--	3	--	--	--
42-1	TV-GKG	54°17.9	157°11.8	4813	------	--	--	--	--	--	--	--	--	--
43-1	TV-G	54°18.2	157°11.9	4810	100 %	--	--	--	--	40	40	--	--	--
46-1	KAL	54°18.1	157°11.7	4827	------	3	--	--	--	1	--	--	--	--
48-1	TV-G	54°18.1	157°11.9	4877	50 %	12	3	--	--	19	17	--	--	--
49-1	TV-GKG	54°18.1	157°12.1	4809	10 cm	--	--	--	--	3	7	--	--	--
52-1	KAL	54°17.9	157°12.0	4829	------	--	--	--	--	1	--	--	--	--
53-1	TV-GKG	54°18.1	157°12.1	4789	------	--	--	--	--	--	--	--	--	--
54-1	TV-G	54°18.1	157°12.1	4796	100 %	--	--	--	--	40	40	--	--	--
56-1	KAL	57°27.4	148°00.1	4775	------	--	--	--	--	--	--	--	--	--
57-1	TV-MUC	57°27.3	147°59.9	4860	------	--	--	--	--	--	--	--	--	--
57-2	TV-MUC	57°27.4	147°59.8	4856	32 cm	17	16	16	16	--	16	--	--	16
58-1	SL	57°27.4	147°59.9	4791	129 cm	7	--	7	--	--	27	--	--	--
59-1	TV-MUC	57°27.5	147°59.9	4833	------	--	--	--	--	--	--	--	--	--
60-1	SL	57°27.4	147°59.8	4800	47 cm	3	--	3	--	--	11	--	--	--
61-1	TV-GKG	57°27.5	147°59.5	4550	------	--	--	--	--	--	--	--	--	--
62-1	TV-G	57°27.2	147°59.8	4920	------	--	--	--	--	--	--	--	--	--
63-1	TV-G	57°27.3	148°00.3	4774	100 %	58	55	55	14	33	70	2	4	--
64-1	TV-G	57°29.3	148°01.0	4550	100 %	81	83	79	25	35	93	--	4	--
65-1	TV-G	57°27.3	148°00.2	4764	100 %	23	23	23	--	--	23	--	--	--

In the **SHUMIGAN**-sector, 2 TV-GKG's and 3 TV-G's were deployed. Unfortunately the kasten corer operation was unsuccessful at every location.
TV-GKG 40-1 was dropped at a vent site, but contained only 5 cm of sediment. The sediment consisted of greenish gray terrigenous mud containing some mudstones and carbonate precipitates. The carbonate precipitates are gray coloured, small and contain several pogonophoran tubes, indicating the precipitates were cemented after the pogonophorans had built their tubes. Several samples of clams and pogonophorans were taken for biological studies.
TV-G 43-1 was also dropped at a vent site. The surface sediment is a greenish gray terrigenous mud, changing into a dark gray terrigenous mud with increasing depth. Several samples of mudstones, clams and pogonophorans were taken for sedimentological and biological studies.
In TV-G 48-1, a rich fauna of living *Solemya* clams, *Calyptogena* clams and pogonophorans were collected and investigated. The sediment was composed of greenish gray terrigenous muds. Several fragments of mudstones, slightly indurated sandstones and carbonate precipitates were collected.
Although TV-GKG 49-1 was also dropped at a vent site, no vent fauna or carbonate precipitates were observed. The sediment was characterized as a gray terrigenous mud. TV-G 54-1 was dropped beside a vent site and contained brownish gray terrigenous muds with several lenses of indurated sand.

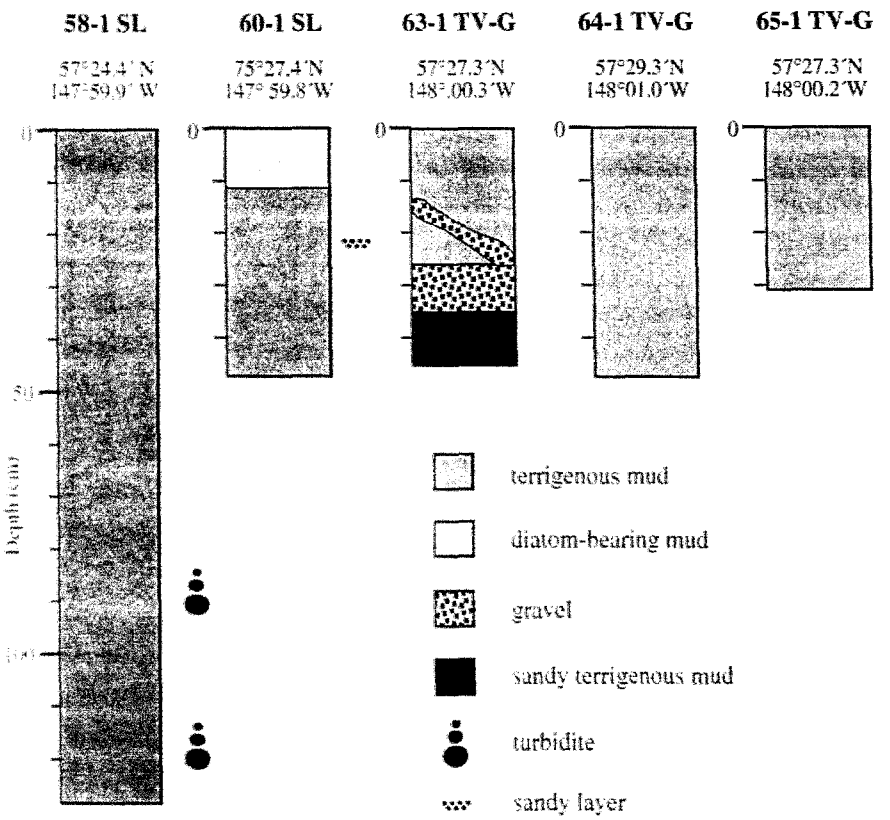

Fig. 78: Lithological composition of the sediment cores from the EDGE-sector.

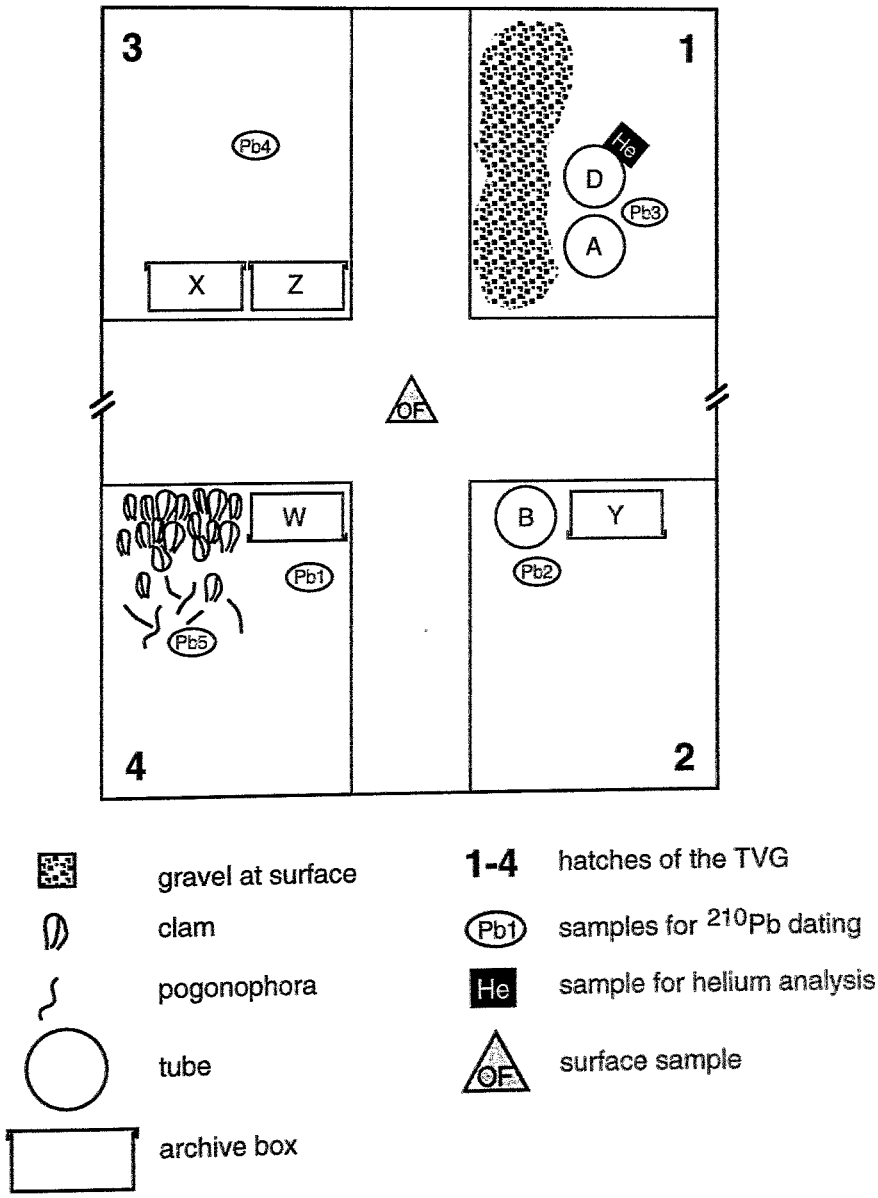

Fig. 79: Surface structures and sampling strategy of TV-G 63-1.

In the **EDGE-sector**, two gravity corers, one TV-MUC and five TV-G's were deployed on the first accretionary ridge. TV-G 64-1 was dropped at the second accretionary ridge. The sediments of TV-G 24-1 from the first accretionary ridge are dark gray terrigenous muds, containing abundant mudstones. At depth of 16 cm below the sediment surface, a layer of gravel was observed, and we hypothesize this may be the transport medium of the vent fluids. Several samples of clams and pogonophorans were taken for biological studies. TV-G 28-2 was dropped at a vent site on the first accretionary ridge. The sediment was composed of dark gray slightly indurated terrigenous muds, containing several mudstones. Clams and pogonophorans were observed and sampled.

Gravity corer 58-1 provided 1.29 m of sediment for study. The lithological composition of the core is documented in Fig. 78. The sediment consists of alternating sequences of dark greenish gray and greenish gray terrigenous muds. Two turbidity sequences are encountered at depth intervals of 84-93 cm and 115-123 cm. These sequences are characterized by a soupy matrix and a sand layer at the bottom. Gravity corer 60-1 provided only 47 cm of sediment. The upper 11 cm of the core is composed of diatom-bearing muds. With increasing depth the sediment changes to greenish gray terrigenous muds with dark gray streaks of organic material. TV-G 63-1 was dropped at a vent site and contained a rich fauna of living *Calyptogena* clams and pogonophorans. The sediments are greenish gray terrigenous muds, with a gravel layer of irregular thickness, as in TV-G 24-1. The gravel layer domes up beneath the clam beds. Yellow coloured barite precipitates are also present and were sampled. The surface structure of the core and the sampling strategy is documented in Fig. 79. Four archive boxes and 3 tubes were taken out of this TV-grab and each was sampled for pore water chemistry and physical properties to produce a three dimensional picture of the sediment properties and the chemistry at this vent site. The same sampling strategy was used for the subsequent TV-G´s.

TV-G 64-1 was dropped at a vent site on the second accretionary ridge. It contained dark greenish gray terrigenous mud with several clams and pogonophorans. In contrast to TV-G 24-1 and 63-1 from the first accretionary ridge, no evidence of a gravel layer was observed. TV-G 65- 1 was dropped beside a vent site. The sediment was composed of greenish gray terrigenous mud with lenses of black mud. The sediment is more indurated at the bottom of the core than at the top.

9 Pore water studies

A. Dählmann, K. Wallmann, B. Domeyer, D. Beck,
A. Schäfer-Pinto, A. Käding

During cruise SO110 sediment samples were collected with a TV-grab (TV-G), a TV-guided box corer (TV-GKG), a kasten corer (KAL), a TV-guided multicorer (TV-MUC) and a gravity corer (SL). Subcores were pushed into the sediment taken by the TV-grab. They were segmented in the cold room (4°C) and pore water was collected with a polypropylene squeezer.

9.1 Sampling strategies

The TV-grabs provide relatively undisturbed sediments. Plexiglass tubes (10 cm diameter) were cut out of the retrieved loads and the core was cut into slices of 1 cm. All of the slices were squeezed for pore water. Bottom water from TV-MUC was also analysed for oxygen and filtered through a 0,45 µm membrane filter.

The highest number of pore water samples was derived from the last three TV-G deployments (63, 64 and 65). Both TVG 63 and 64 were successfully placed in the center of a vent field. To obtain a three dimensional view, subsamples were taken in a special procedure: Four box cores (15 x 7,5 x 40/60 cm) were cut out from each quadrant of the TV-G to gain both a vertical and a lateral picture of nutrient and element distribution in the sediment of a vent site (see Fig. 79). Just one subcore was sampled from TV-G 65 which serves as a reference location (no vent site).

Each subcore from TV-G 63, 64, 65 and TV-MUC 57 was cut into 1 cm slices. Every other slice was used for porewater sampling, alternating with a slice that was used for various subsamples, starting with the first cm used for pore water extraction (see table1). Half of the following slice was frozen in perforated oil sample bags for measuring methane (stored in liquid nitrogen). The other is divided into five subsamples: 5 cm^3 for physical properties analysis, 1 cm^3 for S-isotopes analysis, 1cm^3 for Fe-extraction in diluted Hcl. The pH and S^{2-} were measured in the remaining part of the slice using electrodes. This method provides a high interlocking of all data collected from one core, which provides a good base for interpretation.

Because TV-GKG and KAL only recovered small amounts of sediments, only three pore water samples without any definite depth could be taken from each of these cores. The SL were cut along their longitudinal axes and sediment samples were taken every 20 cm with 50 ml syringes.

9.2 Squeezing procedure

Each sediment sample used for pore water extraction was placed on a thick plastic plate which could hold a maximum of 157 cm^3 of sediment (10 cm diameter x 1 cm hight). Using a piece of parafilm, the sediment was spread carefully on the filter so as not to tear it. The plate was then completely covered with the parafilm. The filled segments were placed on top of each other, separated by rubber gaskets and stored in a press. Plastic tubes connected each glass plate to HDPE-vials

receiving the pore water. The chambers were pressurized with argon at a constant pressure of 2 to 3 atm for almost an hour. A maximum of 20 ml pore water can be received from each sediment sample. The remaining squeeze cakes were packed into plastic bags and stored for further analysis. All procedures described had to be undertaken in a cold room at 4°C.

9.3 Analytical methods

After collecting the pore water samples the pH of the sediment, the alkalinity and the sulfide concentration were measured immediately .Subsequently, silicate, phosphate and ammonia were analysed. Some samples were analysed for chloride, calcium and magnesium. A certain volume (1-5 ml) was acidified with 65% HCl suprapur (10 µl / ml sample) for trace element analysis. For further details see the description in chapter 9 of part I.

Some analyses of sulfide were done with an ion selective electrode (Ag/S-electrode, Methrom) using an Ag/AgCl-electrode as reference.
The calibration is carried out with sodium sulfide in buffer solutions of different pH at 4°C (cold room). Buffers are used to keep the pH constant when adding various amounts of sulfide. They are either made of Na_2HPO_4 / KH_2PO_4 (200 mM) or $Na_2B_4O_7$ (100mM) / 0,2N HCl in NaCl-solution, resulting in a pH of 7,0 to 8,6. The NaCl-solution is half concentrated referred to seawater, so that the total ionic strength of the buffer substances and NaCl is about that of seawater. The pH of the solution is measured before and after the addition of sulfide to control the efficiency of the buffer. All solutions have to be oxygen-free (N_2-bubbled for 1 hour). The vessel used is light protected and covered with a lid with two holes for the electrodes. Increasing amounts of 10 µl to 5 ml of a concentrated sodium sulfide solution (125 mM) are added stepwise to 75 ml of the buffer and stirred smoothly. After each addition the potential of the voltmeter is registered when constant.

For Fe-extraction 1 cm^3 sediment was put into 30 ml 1M HCl and shaken for 24 hours. After centrifugation the solution was decanted and analysed for ferric and ferrous ions: TRIS buffer and ferrozine reagent were added to an aliquote of the extract and Fe II was measured photometrically (Grasshoff et al., 1983). After adding the reduction agent hydroxylamine hydrochloride to another aliquote of the extract, the sample was analysed for total Fe content as described above.

9.4 Results and discussion

A synopsis of cores, numbers of samples, subsampling, sampling strategy and geochemical analysis performed on board is given in the appendix. A comparative diagram of silicate, ammonia, and sulfide of the TV-grabs in **SHUMIGAN** is given in Fig. 80.

The first evidence for bioirrigation is the decrease of Si in the upper centimeters if many individuals settle on/into the sediment. The gradient is so slight (e.g. TV-G 48) that it cannot be explained by diffusion alone (reference core TV-G 54).

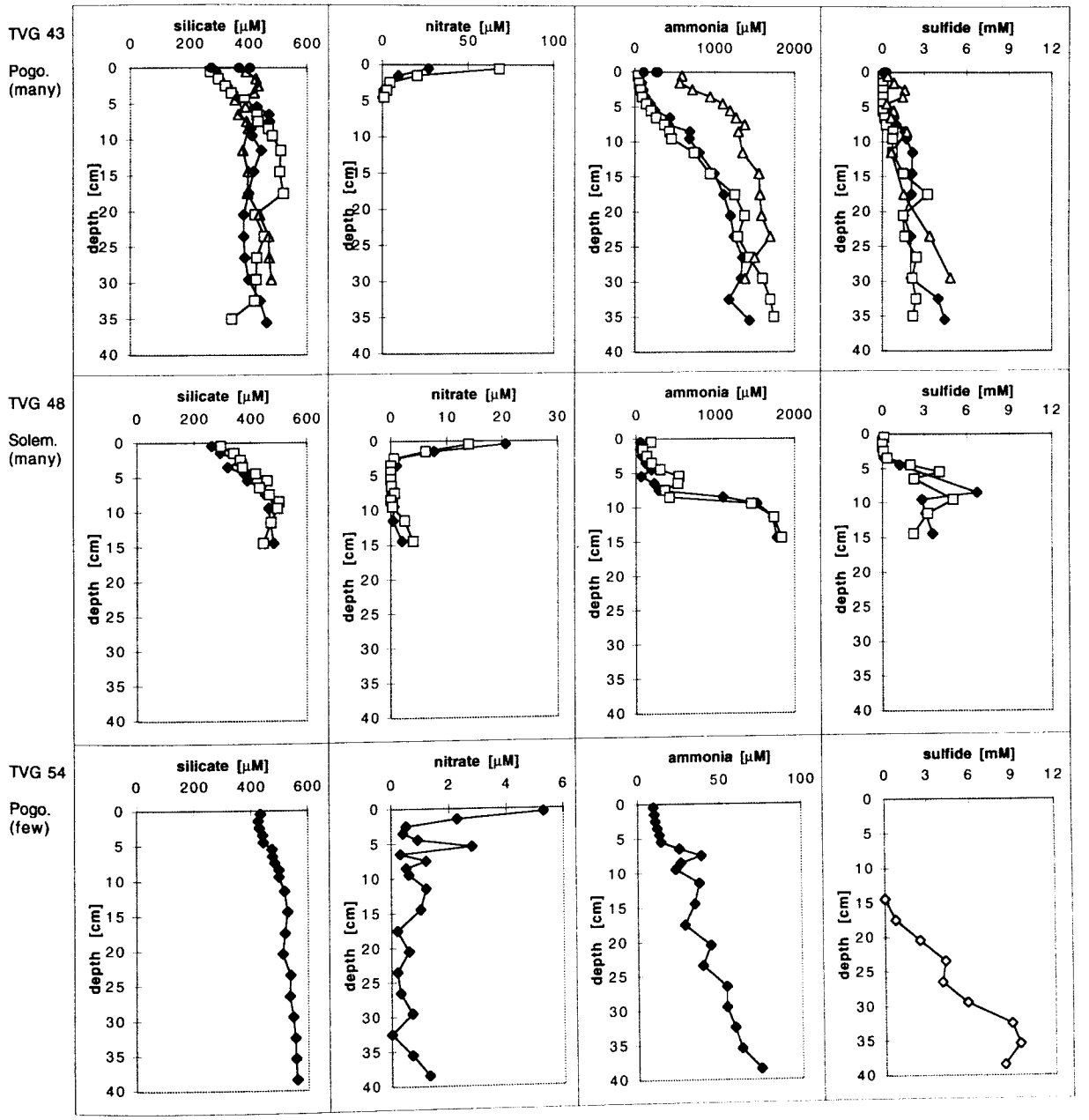

Fig. 80: Synopsis of nutrient data from TV grabs in SHUMIGAN, different symbols indicate subcores (Pogo.: pogonophora; Solem.: *Solemya*)

Comparison of ammonia profiles show evidence for macro fauna influence as well. The profile is very steep at station TVG 48, where many solemya were found, whereas at station TV-G 43 (pogonophora) the highest amounts analysed were below 35 cm. Additionally, both the ammonia and silicate profiles from one of the subcores of TV-G 43 (triangles) show evidence for a small scale heterogenity in fluid composition that might be caused by the biota as well, if it is not due to missing surface sediment.

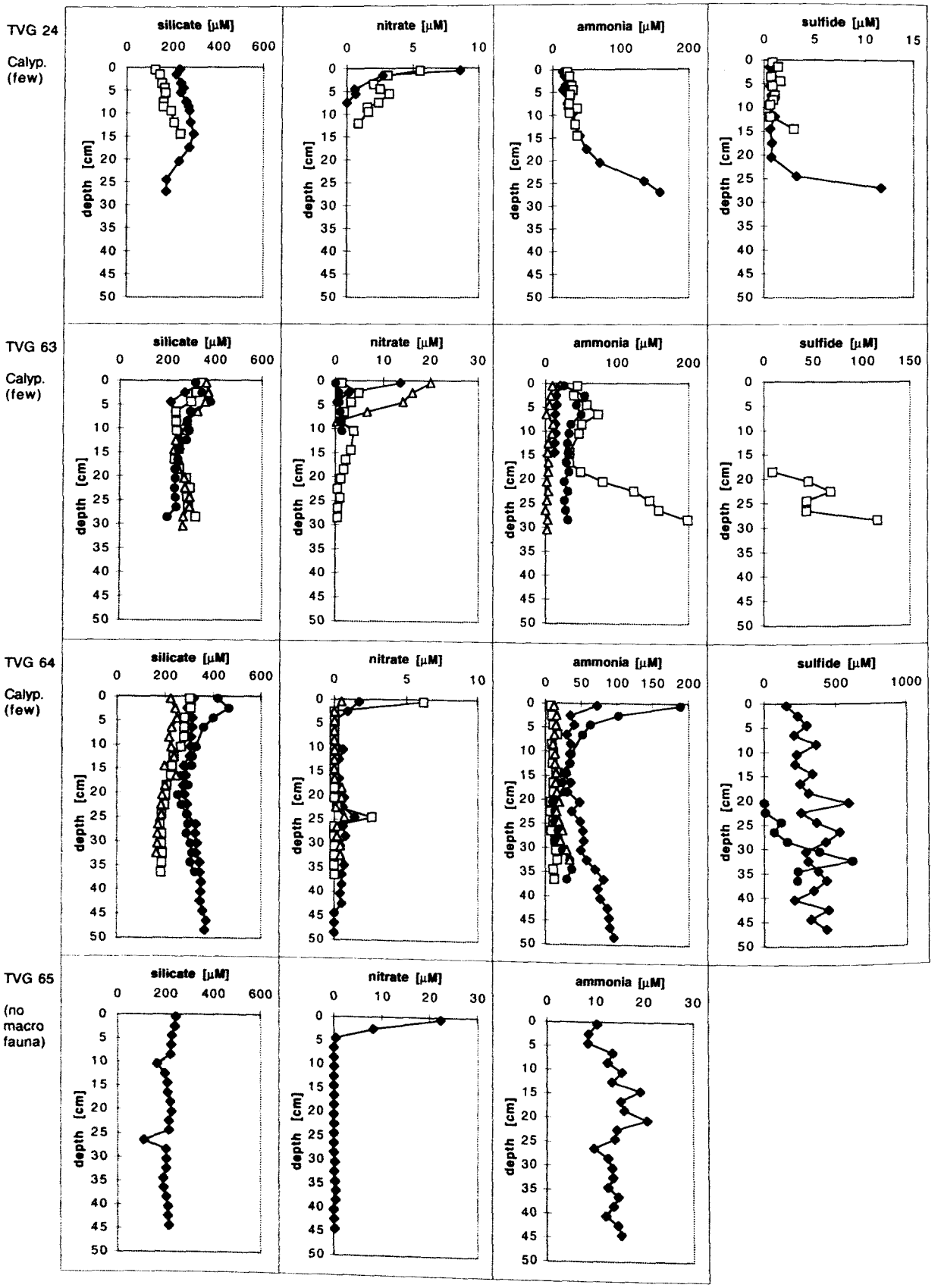

Fig. 81: Synopsis of nutrient data from TV grabs in EDGE; different symbols indicate subcores (Calyp.: *Calyptogena*).

High amounts of ammonia in greater depths are due to degradating organic material:

$$(C(H_2O)_{106}(NH_3)_{16}H_3PO_4 + 53SO_4^{2-} \text{ -->} 106HCO_3^- + 16NH_4+ + HPO_4^{2-} + 53HS^- + 39H^+$$

The Redfield Ratio of sulfide to ammonia is 53/16. Exemplarily calculated for TVG 43 and 48 (deepest depth, subcore 1), the ratio is 3,1 and 2,0 respectively, which is quite near to the theoretical value (3,3). As the organic carbon degradation produces phosphate as well as ammonia, Redfield Ratios for sulfide/phosphate can also be calculated. For TVG 43 and 48 (as above) the resulting values are 257 and 204 respectively, which exceeds the Redfield Ratio (53) by a factor of 5. This can be explained by a diminished concentration of phosphate in the pore water because phosphate anions are subject to adsorption at particle surfaces and precipitate as secondary minerals (with Fe, Ca, Mn). It can be concluded then, that organic carbon degradation is the process responsible for sulfide formation in vent sites of the Aleutian Trench. Methane oxidation as occurs at Cascadia Margin is less important in the Aleutian subduction zone (see cruise report SO110-1a).

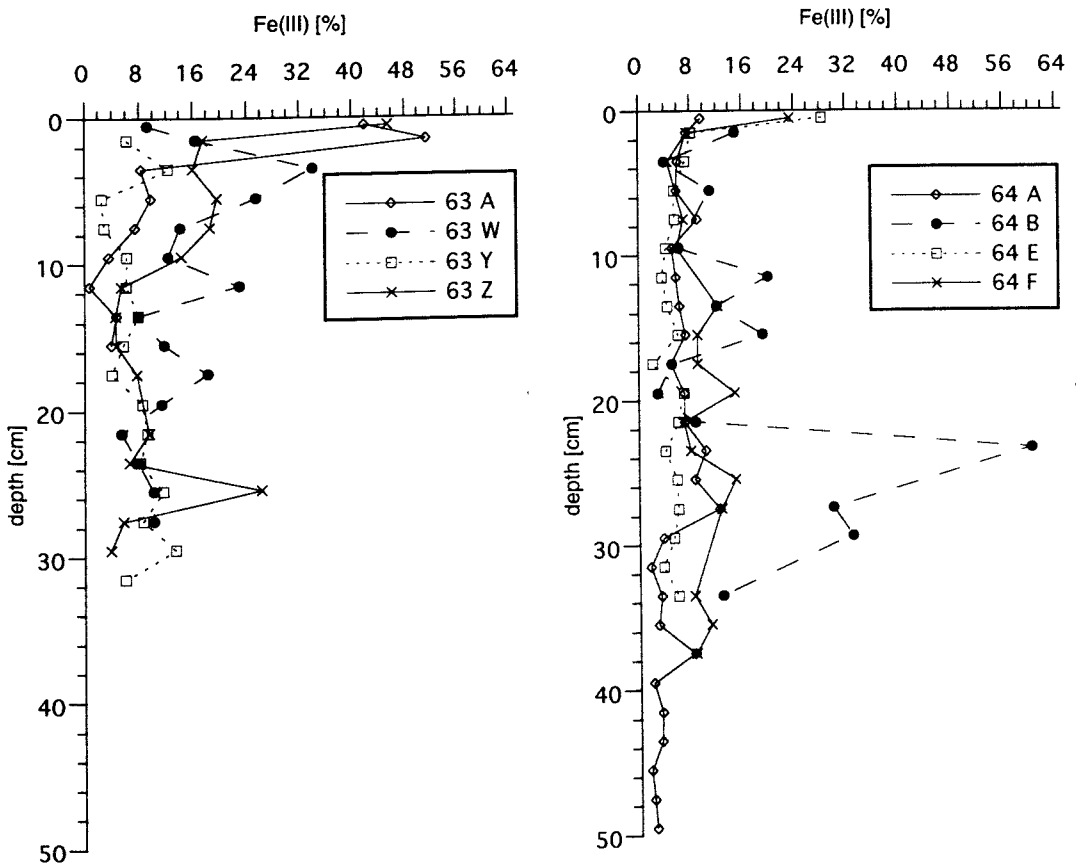

Fig. 82: Fe III in HCl extract of sediment samples, in percentage of total Fe content.

Concentration diagrams of **EDGE** TV-grabs, plotted in Fig. 81, differ from those of SHUMIGAN in their lower concentration of all nutrients. But not just the nutrients that are subject to biological processes (metabolism, consumption) are of generally low concentration, pore water is even depleted in silicate (about 250, max. 400 mM; compare 400-500 mM for SHUMIGAN, Fig. 80) which might be due to penetrating bottom water.

Corresponding to a small amount of biomass (biogenic particles), the ammonia content in pore water is pretty low (max. 100-200 µM; compare max. 1800 µM for SHUMIGAN). The more clams are found the more the ammonia concentration increases with depth (up to 200 µM; reference location: 20 µM).

Fig. 82 illustrates the results of the Fe extraction. At present, only the ferric / ferrous ratio is available, however, for the evaluation total iron contents of the sediment are necessary.

Appendix **Page**

A1 References

Avise JC (1994). Molecular markers, natural history and evolution, Chapman and Hall, New York, NY.

Black MB, Hoeh WR, Hashimoto J, Desbruyères D, Lutz R, Vrijenhoek RC (in press). Molecular systematics of deep-sea tube worms (Vestimentifera), Marine Biology.

Bourgois J, Lagabrielle Y, De Wever P, Suess E, and NAUTIPERC Team (1993). Tectonic history of a non-accreting active margin during the past 400 ka, Geology 21: 531-534.

Brock TD (1987). The study of microorganisms in situ: progress and problems, Symp Soc Gen Microbiol 41: 1-17.

Byrne T (1986). Eocene underplating along the Kodiak shelf, Alaska: Implications and regional correlations, Tectonics 5: 403-421.

Carson B, Suess E, and Strasser JC (1990). Fluid flow and mass flux Determinations at vent sites on the Cascadia margin accretionary prism. Journal of Geophysical Research, 95(B6): 8891-8897.

Carson B, Holmes M L, Umstatts K, Strasser J C, and Johnson H P (1994). Fluid expulsion from the Cascadia accretionary prism: Evidence from porosity distribution, direct measurements, and GLORIA imagery, in: Tarney J, Pickering KT, Knipe RJ, and Dewey JF, eds.: The behavior and influence of fluids in subduction zones, the royal society, London, 105-114.

Craddock C, Hoeh WR, Lutz RA, Vrijenhoek RC (1995). Extensive gene flow in the deep-sea hydrothermal vent mytilid *Bathymodiolus thermophilus*. Marine Biology 124: 137-146.

Cremer A (1995). Maßnahmen zur Realisierung eines videogeführten Lander-Systems für die Langzeitmesssung und Beprobung submariner Quellen. Diplomarbeit an der Fachhochschule Kiel, 1-69.

DeMets C, Gordon, RG, Argus, DF & Stein (1990). Current plate motions: Geophysical Journal International, 101: 425-478.

Dickson AG (1993). pH buffers for sea water media based on the total hydrogen ion concentration scale, Deep-Sea Research I, 40: 107-118.

Felsenstein J (1990). PHYLIP Manual, version 3.3. University Herbarium, university of California, Berkeley, CA.

Flueh E and von Huene R (1994). FS SONNE Fahrtbericht SO96 KODIAK SEIS, GEOMAR Forschungszentrum Kiel.

Frühn J (1995). Tektonik und Entwässerung des aktiven Kontinentalrandes südöstlich der Kenai-Halbinsel, Alaska. GEOMAR Report, 39.

Gieskes J Garno H and Brumsack H (1991). Chemical methods for interstitial water analysis aboard Joides Resolution, Ocean Drilling Program technical note No. 15.

Giovannoni SJ, Britschgi T B, Moyer CL, and Field K G (1990). Genetic diversity in Sargasso Sea bacterioplankton, Nature (London) 345: 60-63.

Grasshoff K, Ehrhardt M, and Kremling K (1983). Methods of seawater analysis, VCH Weinheim.

Hasegawa M, Yano T (1984). Maximum likelihood methods of phylogenetic inference from DNA sequence data. Bull Biometr Soc Japan 5: 1-7.

Hoeh WR, Black MB, Gustafson RG, Bogan AE, Lutz R, Vrijenhoek RC (in rev.). Convergent body plan evolution within the Mollusca: polyphyly of the Diasoma and Bivalvia, Science.

Huelsenbeck JP (1995). Performance of phylogenetic methods in simulation. Systematic Biology 44: 17-48.

Iwabe N, Kuma K, Hasegawa M, Osaw, S, and Miyata T (1989). Evolutionary relationship of archaebacteria, eubacteria and eukaryotes inferred from phylogenetic trees of duplicate genes, Proc Natl Acad Sci USA 86: 9355-9359.

Jannasch HW, and Jones GE (1959). Bacterial populations in seawater as determined by different methods of enumeration, Limnol Oceanogr 4:128-139.

Jukes TH, Cantor CR (1969). Evolution of protein molecules. In: Munro HNM (ed) Mammalian protein metabolism. Academic Press, New York.

Karl SA, Schulz SJ, Desbruyères D, Lutz RA, Vrijenhoek RC (in press). Mollecular analysis of gene flow in the hydrothermal-vent clam *Calyptogena magnifica.*, Molecular Marine Biology and Biotechnology 5.

Kimura M, Weiss WH (1964). The stepping stone model of genetic structure and the decrease of genetic correlation with distance. Genetics 49: 561-576.

Kleinrock MC, Humphris SE, Shaw P, Bowen A, Crook T, Davis C, Elder R, Gleason D, Goff J, Goldstein L, Handley W, Howland J, Hussenoeder S, Koga K, Lerner S, Nakamura K, Rashid M, Reiser, Wetzel L, Sellers W, Sulanowska M, Van Dover C, and Whitcomb L, (1995). Detailed structure and morphology of the TAG active hydrothermal mound and its geotectonic environment. In Humphris SE, Herzig PM , Miller DJ, et al. Proc ODP Init Repts 158: 5-21, College Station, TX (Ocean Drilling Program).

Kulm LD, von Huene, R, et al. (1973). Initial Reports of the Deep Sea Drilling Project, U.S. Government Printing Office, 1077.

Kulm LD, and Suess E (1990). Relationship between carbonate deposits and fluid venting: Oregon accretionary prism: Journal of Geophysical Research, 95 (B6): 8899-8915.

Kulm LD, Suess E, Moore JC, Carson B, Lewis BT, Ritger S, Kadko DC,. Thornberg TM, Embley RW, Rugh WD, Massoth GJ, Lanseth MG, Cochrane GR, and Scamman RL (1986). Oregon subduction zone: venting, fauna, and carbonates. Science 231: 561-566.

Kunert J (1995). Untersuchungen zu Massen- und Fluidtransport anhand der Bearbeitung reflexionsseismischer Daten aus der Kodiak-Subduktionszone, Alaska. GEOMAR Report, 36.

Lewis SD, Ladd JW, and Bruns TR (1988). Structural development of an accretionary prism by thrust and strike-slip faulting: Shumagin region, Aleutian Trench, Geological Society of America Bulletin, 100 : 767-782.

Lammers S, and Suess E (1994). An improved head-space analysis method for methane in seawater. Mar Chem 47: 115-125.

Linke P, Suess E, Torres M, et al. (1994). In situ measurement of fluid flow from cold seeps at active continental margins. Deep-Sea Res 41(4): 721-739.

Lonsdale P (1977). Clustering of suspension-feeding macrobenthos near abyssal hydrothermal vents at oceanic spreading centers. Deep-Sea Res, 24: 857-863.

MacKay ME, Moore GF, Cochrane GR, Moore JC and Kulm LD (1992). Landward vengence and oblique structural trends in the Oregon margin accretionary prism: implications and effect on fluid flow: Earth Planet, Sci Let 109.

Maidak BL, Larsen N, McCaughey MJ, Overbeek R, Olsen GJ, Fogel K, Blandy J, and Woese CR (1994). The ribosomal database project. Nucl Acids Res 22: 3485-3487.

McAdoo BG, Orange DL, Silver EA, et al. (1996). Seafloor structural observations, Costa Rica accretinary prism. Geophysical Research Letters, 23(8): 883-886.

Moore J C, and Vrolijk P (1992). Fluids in accretionary prisms, Rev in Geophys 30, 113-135.

Moore JC, Orange D, and Kulm LD (1990). Interrelationship of fluid venting and structural evolution: ALVIN observations from the frontal accretionary prism, Oregon. Journal of Geophysical Research, 85: 4741-4756.

Moore JC and Allwardt, A (1980). Progressive deformation of a Tertiary trench slope, Kodiak Islands, Alaska. Journal of Geophysical Research, 95: 8795-8808.

Moore, JC, Dieblod J, Fisher MA, Sample J, Brocher T, Talwani M, Ewing J, von Huene R, Rowe C, Stone D, Stevens C, and Sawyer D (1991b). EDGE deep seismic reflection transect of the eastern Aleutian arc-trench layered lower crust reveals underplating and continental growth. Geology 19: 420-424.

Moyer CL, Dobbs FC, and Karl DM (1994). Estimation of diversity and community structure through restriction fragment length polymorphism distribution analysis of bacterial 16S rRNA genes from a microbial mat at an active, hydrothermal vent system, Loihi Seamount, Hawaii. Appl Environ Microbiol 60: 871-879.

Moyer CL, Dobbs FC, and Karl MD (1995). Phylogenetic diversity of the bacterial community from a microbial mat at an active, hydrothermal vent system, Loihi Seamount, Hawaii. Appl Environ Microbiol 61: 1555-1562.

Moyer CL, Tiedje JM, Dobbs FC and Karl DM (1996). A computer-simulatedrestriction fragment length polymorphism analysis of bacterial SSU rRNA genes: effacacy of selected tetrameric restriction enzymes. Appl Environ Microbiol 62: 2501-2507.

Nakamura K, Baker ET, and Ridge Flux / R.V. Melville Westward Expedition Leg 1 onboard scientific party (1994). Characterization of hydrothermal plumes in the East Pacific Rise by in-situ Eh measurements during tow yo surveys. abstracts of 1994 Joint Meeting of Japan. Earth and Planetary Science, 167.

Nakamura K, Maeda K, Murayama N, Saito N, and Ito M (1996). Mapping active hydrothermal sites in the Izena Hole in the Okinawa Trough by Eh and CTD in-situ measurements and its implication for future hydrothermal prospecting. Abstracts, Annual Meeting of the Japan Society for Marine Surveys and Technology.

Orange DL, Greene HG, Barry J, Kochevar R (1994). ROV investigations of cold seeps along fault zones and mud volcanoes in the Monterey Bay, EOS (Transactions, American Geophysical Union), 75, 32.

Olsen GJ, Woese CR, and Overbeek R (1994). The winds of (evolutionary) change: breathing new life into microbiology. Microbiol Rev 176: 1-6.

Paull CK and Newmann AC (1987). Continental margin brine seeps: Their geological consequences, Geology 15: 545-548.

Plafker G, Nokelberg WJ, and Lull JS (1989). Bedrock geology and tectonic evolution of the Wrangellia, Peninsular, and Chugach terrans along the Trans-Alaska Crustal Transect in the Chugach Mountains and southern Copper River basin, Alaska, Journal of Geophysical Research 94: 4255-4296.

Ritger S, Carson B, and Suess E (1987). Methane-derived authigenic carbonates formed by subduction-induced pore water expulsion along the Oregon/Washington margin: Geol Soc Amer Bull 98: 147-156.

Sakai H, Gamo T, Ogawa Y, and Boulègue, J (1992). Stable isotopic ratios and origin of the carbonates associated with cold seapage at the eastern Nankai Trough. Earth and Planetary Science Letters, 109: 391-4404.

Schmitt M, Faber E, Botz R, and Stoffers P (1991). Extraction of methane from seawater using ultrasonic vacuum degassing. Anal Chem 63: 529-531.

Scholl DW, Vallier TL, and Stevenson AJ (1987). Geologic evolution and petroleum geology of the Aleutian Ridge, in Scholl DW, Grantz A, and Vedder JG eds. Geology and Resource Potential of the Continental Margin of Western North America and Adjacent Oceans - Beaufort Sea to Baja California: Houston, Texas, Circum-Pacific Council for Energy and Mineral Resources Earth Science Series6 : 191-212.

Sibuet M, Juniper SK, and Pautot G (1988). Cold-seep benthic communities in the Japan subduction zones: Geological control of community developement. J Mar Res, 46: 333-348.

Suess E, Carson B, Ritger S, Moore JC, Jones M, Kulm LD and Cochrane G (1985). Biological communities at vent sites along the subduction zones off Oregon, Bull Biol Soc Wash 6 : 475-484.

Suess E (1992). FS Sonne. Fahrtbericht SO 78 Peruvent. Balboa, Panama - Balboa, Panama 28.2.1992-16.4.1992. GEOMAR Report, 14.

Suess E (1994). FS SONNE Fahrtbericht SO97 KODIAK VENT, GEOMAR Forschungszentrum Kiel, Report No. 29.

Suess, E, Bohrmann, G, von Huene, R, et al. (submitted). Fluid venting in Aleutian subduction zone. Journal of Geophysical Research.

Slatkin M, Barton NH (1989). A comparison of three indirect methods for estimating average levels of gene flow. Evolution 43: 1349-1368.

Stumm W, and Morgan JJ (1996). Aquatic Chemistry, Wiley, New York.

Torres M, Bohrmann G, and Suess E (1996). Authigenic barites and fluxes of barium associated with fluid seeps in the Peru subduction zone. Earth and Planetary Science Letters, 144: 469-481.

Urabe T, Baker ET, Ishibashi J, Feely RA, Marumo K, Massoth GJ, Maruyama A, Shitashima K, Okamura K, Lupton JE, Sonoda A, Yamazaki T, Aoki M, Gendron J, Greene R, Kaiho Y, Kisimoto K, Lebon G, Matsumoto T, Nakamura K, Nishizawa A, Okano O, Paradis G, Ro K, Shibata T, Tennant D, Vance T, Walker SL, Yabuki T, and Ytow N (1995). The effect of magamatic activity on hydrothermal venting along the superfast-spreading East Pacific Rise. Science 269: 1092-1095.

von Huene R (1989). Continental margins around the Gulf of Alaska, in Winterer EL, Hussong DM, and Decker RW eds. The Eastern Pacific Ocean and Hawaii: Boulder, Colorado, Geological Society of America, The geology of north america: 383-401.

von Huene R, Klaeschen D, Gutscher M, and Fruehn J (submitted). Mass and fluid flux during accretion at Alaska Margin. Journal of Geophysical Research.

Vrijenhoek RC (1997). Gene flow and genetic diversity in naturally fragmented metapopulations of deep-sea hydrothermal vent animals. Journal of

Heredity in special symposium issue dedicated to the "Genetics of Fragmented Populations".

Ward DM, Bateson M M, Weller R, and Ruff-Roberts AL (1992). Ribosomal RNA analysis of microorganisms as they occur in nature. Adv Microb Ecol 12: 219-286.

Ward DM, Weller R, and Bateson MM (1990). 16S rRNA sequences reveal numerous uncultured microorganisms in a natural community. Nature 345: 63-65.

Wessel P, and Smith WHF (1991). Free Software helps map and display data", EOS Trans Am Geoph U vol 72 : 445-446.

Westbrook GK, Carson B, Musgrave RT, and Suess E (1995). Proc. ODP Sci. Results 146. 611. College Station Texas: Ocean Drilling Program.

Wright S (1931). Evolution in Mendelian populations. Genetics 16: 97-159.

Wright S (1943). Isolation by distance. Genetics 28: 114-138.

Woese CR (1994). There must be a prokaryote somewhere: microbiology's search for itself. Microbiol Rev 58: 1-9.

Zouros E, Ball,AO, Saavedra C, Freeman KR (1994). An unusual mitochondrial DNA inheritance in the blue mussel *Mytilus*. Proceedings of the National Academy of Sciences, USA 91: 7463-7467.

A2 Station list SO110-1a.

SO110-1a Gas Hydrate Ridge

Date 1996	Stat. No	Instrument	Begin (UTC)	at seafloor max. depth	off seafloor	End (UTC)	Duration hh:mm	Latitude N° Begin; at sf. / End; off sf.	Longitude W° Begin; at sf. / End; off sf.	Water depth (m)	Recovery	Remarks
10. Jul	1 - 1 a	CM	4:20			4:26	0:06	44:39.35	125:06.35			in the water
10. Jul	2 - 1	HS	8:06			8:26	0:20	44:39.0 / 44:36.3	125:06.0 / 125:06.8			
10. Jul	2 - 2	HS	9:15			9:39	0:24	44:35.4 / 44:34.3	125:07.7 / 125:02.9			
10. Jul	2 - 3	HS	9:49			10:33	0:44	44:33.2 / 44.34.8	125:03.4 / 125:12.7			
10. Jul	2 - 4	HS	10:42			11:07	0:25	44:33.6 / 44:33.9	125:13.8 / 125:08.7			
10. Jul	2 - 5	HS	11:24			11:54	0:30	44:36.0 / 44:39.4	125:10.1 / 125:06.1			
10. Jul	3 - 1	CTD	12:15	12:36		13:11	0:56	44:39.40	125:06.30	626	12 bottles	same position like CM 1 / 1a
10. Jul	4 - 1	ROPOS	14:03			23:40	9:37	44:40.4 / 44:40.2	125:6.5 / 125:6.5	635 / 632		*ROPOS Dive #339*
11. Jul	5 - 1	EXPLOS	0:22	1:12	6:04	6:22	6:00	44:40.072 / 44:40.214	125:05.423 / 125:07.872	617 / 745		
11. Jul	6 - 1	CTD	7:05	7:23		7:54	0:49	44:39.30	125:06.29	633	12 bottles	same position like CM 1 / 1a
11. Jul	7 - 1	HS	8:32			8:57	0:25	44:33.866 / 44:32.394	125:08.697 / 125:04.858			
11. Jul	7 - 2	HS	9:07			9:56	0:49	44:31.399 / 44:32.281	125:04.503 / 125:14.381			
11. Jul	7 - 3	HS	10:07			10:36	0:29	44:31.071 / 44:32.395	125:15.981 / 125:09.399			
11. Jul	7 - 4	HS	11:10			11:49	0:39	44:30.391 / 44:30.609	125:04.954 / 125:13.495			
11. Jul	7 - 5	HS	12:03			12:23	0:20	44:31.293 / 44:30.687	125:11.602 / 125:07.538			
11. Jul	7 - 6	HS	12:33			12:41	0:08	44:31.427 / 44:31.818	125:08.807 / 125:10.541			
11. Jul	8 - 1	ROPOS	15:15			23:40	8:25	44:40.169 / 44:40.451	125:05.867 / 125:05.947	592 / 615		*ROPOS Dive #340*
12. Jul	9 - 1	TV-G	0:36	1:12	1:48	2:30	1:54	44:39.997 / 44:40.167	125:05.855 / 125:05.873	604 / 596	100%, Summit vent site	dropped at 44:40.167/125:05.873
12. Jul	10 - 1	CTD	3:55	4:14		4:42	0:47	44:39.30	125:06.24	630	12 bottles	same position like CM 1 / 1a
12. Jul	11 - 1	TV-G	4:59	5:20	6:44	7:26	2:27	44:40.090 / 44:40.134	125:06.506 / 125:06.503	628 / 524	100%, Bioherm vent site	dropped at 44:40.134/125:06.503
12. Jul	12 - 1	CTD	8:33	8:52		9:20	0:47	44:40.15	125:05.86	594	12 bottles	
12. Jul	13 - 1	HS	10:21			10:34	0:13	44:45.30 / 44:45.30	125:15.10 / 125:12.40			
12. Jul	13 - 2	HS	11:04			11:29	0:25	44:45.30 / 44:45.30	125:04.70 / 124:59.30			
12. Jul	13 - 3	HS	11:33			11:55	0:22	44:45.00 / 44:45.00	124:58.40 / 124:53.40			
12. Jul	1 - 1 b	CM	13:00			14:30	1:30	44:39.12	125:06.35			out of the water
12. Jul	14 - 1	VESP	15:25			18:30	3:05	44:40.187	125:05.916	595		
12. Jul	15 - 1	ROPOS	19:50			23:00	3:10	44:40.15 / 44:40.14	125:05.81 / 125:05.72			*ROPOS Dive #341*
13. Jul	16 - 1	CTD	0:10	0:28		0:59	0:49	44:40.11	125:05.81	595	12 bottles	
13. Jul	17 - 1	EXPLOS	4:50	5:11	6:18	6:30	1:40	44:34.047 / 44:34.236	125:08.328 / 125:08.920	810 / 763		
13. Jul	18 - 1	TV-G	7:37	7:59	8:22	8:55	1:18	44:34.158 / 44:34.235	125:08.756 / 125:08.891	778 / 785	100%, Gas-Hydrate site	dropped at 44:34.235/125:08.891

Latitude / Longitude : TV-G, EXPLOS is at seafloor and off seafloor
VESP is drop position
CTD is max. depth
HS / PS is Begin and End

Sample devices : TV-G : TV-Grab
EXPLOS : TV-sled (Exploration System)
ROPOS : Remotely Operating Observation System
HS : Hydrosweep ; PS : Parasound

CTD : Multisonde and hydrocasts
VESP : Vent Sampler
CM : Current Meter

SO110-1b Alaska

Date 1998	Stat. No	Instrument	Begin (UTC)	at seafloor max. depth	off seafloor	End (UTC)	Duration hh:mm	Latitude N° Begin; at sf. / End; off sf.	Longitude W° Begin; at sf. / End; off sf.	Water depth (m)	Recovery	Remarks
EDGE												
18. Jul	19 - 1	HS/PS	19:47			20:47	1:00	49:09.600 / 49:12.065	128:49.650 / 129:01.098	2423 / 2434		
18. Jul	19 - 2	HS/PS	20:47			22:35	1:48	49:12.065 / 49:16.480	129:01.098 / 129:22.522	2434 / 2462		
18. Jul	19 - 3	HS/PS	22:35			23:30	0:55	49:16.480 / 49:19.343	129:22.522 /129:32.635	2462 / 2379		
21. Jul	20 - 1	HS	21:31			21:57	0:26	57:26.014 / 57:30.040	147:59.942 / 148:02.410	4944 / 4677		
22. Jul	21 - 1	CTD	1:16	1:32		2:10	0:54	57:26.16	148:01.34	4974	12 bottles	CTD down to 600 m
22. Jul	22 - 1	EXPLOS	2:42	4:26	9:44	11:30	8:48	57:29.124 / 57:25.516	148:03.992 / 148:02.122	4662 / 4991		
23. Jul	23 - 1	ROPOS	0:28	3:57	22:29	30 (24.Ju	25:02	57:27.316 / 57:26.631	147:59.732 / 148:01.321	4947 / 4919		ROPOS Dive #344
24. Jul	24 - 1	TV-G	3:17	4:53	7:51	9:43	6:26	57:27.281 / 57:27.394	148:00.933 / 148:00.013	4743 / 4890	50%, vent site	dropped at 57:27.394 / 148:00.013 4890m
24. Jul	25 - 1	VESP	13:20	15:28	17:36	19:33	6:13	57:27.389	148:00.470	4876	5 bottles	
24. Jul	26 - 1	TV-G	20:01	21:31	22:56	0:49	4:48	57:27.351 / 57:27.336	148:00.537 / 147:59.781	4774 / 4796	not dropped	camera/ hydraulic problems
25. Jul	27 - 1	CTD	1:47	3:31		6:58	5:11	57:25.21	148:08.01	4958	12 bottles	
27. Jul	28 - 1	TV-G	23:43	1:15	4:18	5:03	5:20	57:27.445 / 57:27.311	148:00.146 / 147:58.891	4752 / 4954	not dropped	
28. Jul	28 - 2	TV-G	5:06	6:50	7:00	10:10	5:04	57:27.178 / 57:27.249	147:59.625 / 147:59.668	4954 / 4867	25%, vent site	at 57:27.249 / 147:59.668 4867m (fall over)
28. Jul	29 - 1	VESP	11:30			15:00	3:30	57:27.373	148:00.323	4487	no bottom contact	
28. Jul	30 - 1	CTD	15:10	17:00		19:46	4:36	57:27.380	148:00.040	4770	12 bottles	
28. Jul	31 - 1	TV-GKG	20:34			0:30	3:56	57:27.383	148:00.191	4761	no bottom contact	telemetry problems
29. Jul	32 - 1	EXPLOS	6:19	7:37	13:03	14:39	8:20	57:31.218 / 57:28.764	148:00.468 / 147:55.968	4693 / 5004		
29. Jul	33 - 1	VESP	16:00	17:56	23:19	3:30	11:30	57:27.262	147:59.990	4844	5 bottles	
30. Jul	34 - 1	HS	6:28			12:50	6:22	57:21.80 / 56:42.80	148:32.80 / 150.15.80	4837 / 4188		
30. Jul	34 - 2	HS	13:05			13:55	0:50	56:42.80 / 56:34.00	150.15.80 / 150:09.00	3815 / 5157		
30. Jul	34 - 3	HS	14:18			15:00	0:42	56:36.00 / 56:42.00	150:03.00 / 150:08.70	5146 / 4611		
UGAK												
30. Jul	35 - 1	EXPLOS	15:18	17:13	23:28	1:47	10:29	56:40.42 / 56:36.71	150:10.58 / 150:07.58	4844 / 5229		
31. Jul	36 - 1	HS	2:15			5:26 (1.Aug.)	27:11	56:42.74 / 54:17.48	150:15.60 / 157:01.22	4161 / 5073		VESP-Y tested
SHUMAGIN												
01. Aug	37 - 1	EXPLOS	6:13	7:57	14:14	16:12	9:59	54:16.015 / 54:13.093	157:14.680 / 157:12.858	4889 / 5405		
01. Aug	38 - 1	TV-G	17:51			18:57	1:06	54:18.278 / 54:18.292	157:12.805 / 157:12.851	4556 / 4536	no bottom contact	camera flooded
01. Aug	38 - 2	TV-GKG	20:33	22:21	0:24	2:02	5:29	54:18.378 / 54:18.097	157:12.766 / 157:12.188	4576 / 4647	not closed	
02. Aug	39 - 1	CTD	3:06	4:51		7:31	4:25	54:18.277	157:11.528	4952	12 bottles	
02. Aug	40 - 1	TV-GKG	8:07	10:07	14:34	16:34	8:27	54:18.17 / 54:18.17	157:11.82 / 157:11.82	4583 / 4808	5 cm, vent site	dropped at 54:18.17 / 157:11.82 4808m
03. Aug	41 - 1	VESP	18:30	0:04	2:21	4:09	9:39	54:18.065	157:11.614	4839	3 bottles	
03. Aug	42 - 1	TV-GKG	5:56	7:42	15:29	17:46	11:50	54:18.055 / 54:17.892	157:11.602 / 157:11.757	4845 / 4813	not closed	
03. Aug	43 - 1	TV-G	18:23	19:57	0:02	2:05	7:42	54:18.284 / 54:18.196	157:12.510 / 157:11.936	4591 / 4810	100%, vent site	dropped at 54:18.196 / 157:11.936 4810m
04. Aug	44 - 1	VESP-Y	4:45	7:15	10:58	16:06	11:21	54:18.561	157:11.907	4865		still on the bottom

Latitude / Longitude : TV-G, TV-GKG, EXPLOS is at seafloor and off seafloor
VESP, VESP-Y is drop position
CTD is max. depth
HS / PS is Begin and End

Sample devices : TV-G : TV-Grab
TV-GKG : TV-Boxcorer
EXPLOS : TV-sled (Exploration System)
ROPOS : Remotely Operating Observation System
HS : Hydrosweep ; PS : Parasound
CTD : Multisonde and hydrocasts
VESP : Vent Sampler
VESP-Y : The new Vent Sampler in Yellow

A4 Station list SO110-2.

SO110-2 Alaska

Date 1996	Stat. No	Instrument	Begin (UTC)	at seafloor max. depth	off seafloor	End (UTC)	Duration hh:mm	Latitude N° Begin; at sf. / End; off sf.	Longitude W° Begin; at sf. / End; off sf.	Water depth (m)	Recovery	Remarks
Shumagin												
06. Aug	45 - 1	HS / PS	13:25			21:53	8:28	55:42.80 / 54:46.70	153:03.00 / 155:29.00	4408 / 4210		
06. Aug	45 - 2	HS	22:27			2:58	4:31	54:53.00 / 55:20.00	155:34.00 / 154:22.00	3517 / 2882		
07. Aug	45 - 3	HS	3:19			7:39	4:20	55:22.00 / 54:54.00	154:25.00 / 155:40.80	2270 / 2572		
07. Aug	45 - 4	HS	8:35			13:10	4:35	54:45.00 / 54:23.80	155:54:00 / 156:58.00	4253 / 4617		
07. Aug	46 - 1	KAL	14:45	16:30		18:16	3:31	54:18.129	157:11.896	4827	empty	
07. Aug	47 - 1	TV-G search	19:05	20:51	12:08	13:55	18:50	54:18.413 / 54:18.432	157:11.702 / 157:11.690	4779 / 4799		VESP-Y pos. 54:18.468 / 157:11.708 4799m
08. Aug	48 - 1	TV-G	14:55	16:40	19:00	21:03	6:08	54:17.847 / 54:18.064	157:11.968 / 157:11.895	4885 / 4877	50%, vent site	dropped at 54:18.064 / 157:11.895 4877m
08. Aug	49 - 1	TV-GKG	22:34	0:13	0:54	3:09	4:35	54:18.039 / 54:18.056	157:12.170 / 157:12.107	4785 / 4809	10 cm, vent site	dropped at 54:18.056 / 157:12.107 4809m
09. Aug	50 - 1	CTD	3:38	5:25		7:33	3:55	54:18.270	157:11.535	4951	12 bottles	
09. Aug	51 - 1	HS	8:47			10:44	1:57	54:30.000 / 54:41.725	157:00.000 / 156:25.346	3894 / 3519		
09. Aug	51 - 2	HS	11:01			12:11	1:10	54:38.584 / 54:32.000	156:22.586 / 156:43.000	3864 / 4285		
09. Aug	52 - 1	KAL	14:25	16:36		18:24	3:59	54:17.929	157:12.060	4829	empty	
09. Aug	53 - 1	TV-GKG	18:46	20:28	0:10	2:13	7:27	54:18.098 / 54:18.121	157:12.320 / 157:12.139	4766 / 4789	empty	dropped at 54:18.121 / 157:12.139 4789m
10. Aug	54 - 1	TV-G	2:41	5:01	9:59	11:47	9:06	54:18.036 / 54:18.106	157:11.735 / 157:12.135	4792 / 4796	100%, no vent site	dropped at 54:18.106 / 157:12.135 4796m
10. Aug	55 - 1	HS	14:16			0:54	10:38	54:18.070 / 55:25.000	157:12.300 / 153:58.000	4720 / 3944		
11. Aug	55 - 2	HS	0:54			22:42	21:48	55:25.000 / 57:27.400	153:58.000 / 148:00.200	3944 / 4821		
EDGE												
11. Aug	56 - 1	KAL	23:00	0:51		2:41	3:41	57:27.428	148:00.123	4775	0%	
12. Aug	57 - 1	TV-MUC	2:53	4:45	5:16	7:04	4:11	57:27.357 / 57:27.342	147:59.882 / 147:59.890	4834 / 4860	0%, vent site	dropped but fall over
12. Aug	57 - 2	TV-MUC	7:31	9:21	9:56	11:43	4:12	57:27.344 / 57:27.398	147:59.677 / 147:59.852	4874 / 4856	1 core 32 cm, vent site	dropped at 57:27.398 / 147:59.852 4856m
12. Aug	58 - 1	SL	12:02	13:30		15:15	3:13	57:27.402	147:59.946	4791	130cm	
12. Aug	59 - 1	TV-MUC	15:25	17:06	18:55	21:02	5:37	57:27.352 / 57:27.498	147:59.824 / 147:59.998	4896 / 4833	0%, vent site	not tightly closed
12. Aug	60 - 1	SL	21:15	23:12		0:49	3:34	57:27.432	147:59.841	4800	47 cm	
13. Aug	61 - 1	TV-GKG	1:23	2:55	5:38	7:28	6:05	57:27.310 / 57:27.457	148:00.045 / 147:59.507	4814 / 4910	not closed	no vent site
13. Aug	62 - 1	TV-G	7:55	9:29	11:21	13:15	5:20	57:27.660 / 57:27.169	148:00.104 / 147:59.800	4760 / 4920	not dropped	no vent site
13. Aug	63 - 1	TV-G	20:51	22:29	22:46	0:20	3:29	57:27.390 / 57:27.326	148:00.261 / 148:00.275	4812 / 4774	100%, vent site	dropped at 57:27.326 / 148:00.275 4774m
14. Aug	64 - 1	TV-G	2:01	3:32	4:40	6:23	4:22	57:29.396 / 57:29.336	148:01.185 / 148:01.009	4482 / 4550	100%, vent site	dropped at 57:29.336 / 148:01.009 4550m
14. Aug	65 - 1	TV-G	7:32	9:12	11:31	12:35	5:03	57:27.281 / 57:27.324	148:00.391 / 148:00.187	4733 / 4764	100%, vent site	dropped at 57:27.324 / 148:00.187 4764m
14. Aug	66 - 1	HS	12:42			17:33	4:51	57:27.300 / 56:44.292	148:00.000 / 149:19.076	4855 / 4767		
14. Aug	66 - 2	HS	17:34			18:17	0:43	56:44.292 / 56:50.000	149:19.076 / 149:31.883	4767 / 5026		
14. Aug	66 - 3	HS	18:18			19:28	1:10	56:50.000 / 56.58.000	149:31.883 / 149:10.538	5026 / 4914		
14. Aug	66 - 4	HS	19:29			20:18	0:49	56:58.000 / 56:51.752	149:10.538 / 149:24.000	4914 / 4831		

Latitude / Longitude : TV-G, TV-GKG, TV-MUC, EXPLOS is at seafloor and off seafloor
KAL, SL is drop position
CTD is max. depth
HS / PS is Begin and End

Sample devices : TV-G : TV-Grab
TV-GKG : TV-Boxcorer
TV-MUC : TV-Multicorer
EXPLOS : TV-sled (Exploration System)

HS : Hydrosweep ; PS : Parasound
CTD : Multisonde and hydrocasts
KAL : Kastencorer
SL : Gravity Corer

Sample List : So110-1a Oregon Margin

CTD	CTD 3 / 1	CTD 6 / 1	CTD 10 / 1	CTD 12 / 1	CTD 16 / 1
GEOMAR Forschungszentrum, Kiel	12 water samples CH4 conc. * 7 water samples metals + 12 water samples nutrients	12 water samples CH4 conc. * 8 water samples metals + 12 water samples nutrients	12 water samples CH4 conc. * 12 water samples metals + -	12 water samples CH4 conc. * 12 water samples metals + 12 water samples nutrients	12 water samples CH4 conc. * 12 water samples metals + 12 water samples nutrients
Oregon State University, Corvallis	7 water samples metals	8 water samples metals	12 water samples metals	12 water samples metals	12 water samples metals
Umweltphysik, Universität Heidelberg	6 water samples 3He/4He	-	-	9 water samples 3He/4He	12 water samples 3He/4He
University Victoria	12 water samples CH4 conc. (120 ml) 7 gas samples CH4 isotope	12 water samples CH4 conc. (120 ml) 12 gas samples CH4 isotope	- 6 gas samples CH4 isotope		12 water samples CH4 conc. (120 ml) 11 gas samples CH4 isotope

ROPOS + VESP	ROPOS 4 / 1	ROPOS 8 / 1	ROPOS 15 / 1	VESP 14 / 1
GEOMAR Forschungszentrum, Kiel	video + slides 7 water samples CH4 conc. (120 ml) 7 water samples nutrients 7 water samples metals biology	video + slides 4 water samples CH4 conc. (120 ml) 6 water samples nutrients 6 water samples metals biology	video + slides 1 water samples CH4 conc. (120 ml) 3 water samples nutrients 3 water samples metals biology	video + slides 5 water samples CH4 conc. (120 ml) 5 water samples nutrients 5 water samples metals -
Institute of Ocean Sciences, Sidney	Documentation	Documentation	Documentation	-
Oregon State University, Corvallis	7 water samples metals 2 calyptogena	6 water samples metals 4 calyptogena	3 water samples metals -	5 water samples metals -
Umweltphysik, Universität Heidelberg	-	4 water samples 3He/4He	3 water samples 3He/4He	5 water samples 3He/4He
University Victoria	- - sediment #	6 water samples CH4 conc. (120 ml) 4 gas samples CH4 isotope -	3 water samples CH4 conc. (120 ml) 1 gas samples CH4 isotope -	5 water samples CH4 conc. (120 ml) 5 gas samples CH4 isotope -
University of Victoria	macrofauna	macrofauna	macrofauna	

TV-G	TV-G 9 / 1	TV-G 11 / 1	TVG 18 / 1
GEOMAR Forschungszentrum, Kiel	video core A : 7 pore water samples core B : 5 pore water samples - biology 24 Sediment and PP samples Carbonate preciptates -	video core A : 6 pore water samples core B : 5 pore water samples - biology 24 Sediment and PP samples Carbonate preciptates -	video core 1 : 9 pore water samples core 2 : 7 pore water samples core 3: 8 pore water samples biology 24 Sediment and PP samples Carbonate preciptates Gas hydrates
Oregon State University, Corvallis	core A : 6 pore water samples $ core B : 4 pore water samples $ 4 calyptogena -	core A : 5 pore water samples $ core B : 4 pore water samples $ 4 calyptogena -	core 2 : 7 pore water samples § core 3: 8 pore water samples § 2 calyptogena Gas hydrates
University Victoria	sediment # -	sediment # -	sediment # Gas hydrates
University Victoria	macrofauna	-	macrofauna

keynotes: * = not available for further analysis, + = splits from Oregon, # = analyzed onboard, § = same samples than Geomar, $ = alternating to Geomar samples, PP = physical properties

SO110-1b + 2 Aleutian Trench, Alaska

CTD	CTD 21 / 1	CTD 27 / 1	CTD 30 / 1	CTD 39 / 1	CTD 50/ 1
GEOMAR Forschungszentrum, Kiel	12 water samples CH4 conc. *# 12 water samples metals 12 water samples nutrients - -	11 water samples CH4 conc. *# - - - -	12 water samples CH4 conc. *# 12 water samples metals 12 water samples nutrients 8 water samples oxygen *# -	12 water samples CH4 conc. *# 12 water samples metals 12 water samples nutrients 8 water samples oxygen *# 12 water samples bacterial counting	12 water samples CH4 conc. *# - 5 water samples pH 12 water samples oxygen *# -
Humboldt State University	-	-	-	12 water samples CH4 oxidation *	-
Umweltphysik, Universität Heidelberg	- -	- -	7 water samples 3He/4He -	6 water samples 3He/4He 9 water samples tritium	8 water samples 3He/4He 9 water samples tritium
University Victoria	12 water samples CH4 conc. (120 ml) 12 gas samples CH4 isotope	12 water samples CH4 conc. (120 ml) 10 gas samples CH4 isotope	12 water samples CH4 conc. (120 ml) 12 gas samples CH4 isotope	12 water samples CH4 conc. (120 ml) 12 gas samples CH4 isotope	12 water samples CH4 conc. (120 ml) 5 gas samples CH4 isotope

ROPOS + VESP	ROPOS 23 / 2	VESP 25 / 1	VESP 33 / 1	VESP 41 / 1	VESP-NEU 44 / 1
GEOMAR Forschungszentrum, Kiel	video + slides 3 water samples CH4 conc. (120 ml) 5 water samples nutrients 5 water samples metals macrofauna sediment biology	video + slides 5 water samples CH4 conc. (120 ml) 5 water samples nutrients 5 water samples metals 5 water samples oxygen *# -	video + slides 5 water samples CH4 conc. (120 ml) 5 water samples nutrients 5 water samples metals 5 water samples oxygen *# 5 water samples bacterial counting	video + slides 3 water samples CH4 conc. (120 ml) 3 water samples nutrients 3 water samples metals 3 water samples oxygen *# 3 water samples bacterial counting	video - - - - -
Institute of Ocean Sciences, Sidney	Documentation	-	-	-	-
Humboldt State University	3 clams CH4 oxid.	-	2 water samples CH4 oxidation *	2 water samples CH4 oxidation *	-
Rutgers University	46 biology samples	-	-	-	-
GFZ Potsdam	-	2 water samples noble gases	5 water samples noble gases	3 water samples noble gases	-
Umweltphysik, Universität Heidelberg	5 water samples 3He/4He	8 water samples 3He/4He	2 x 5 water samples 3He/4He	5 water samples 3He/4He	-
University Victoria	5 water samples CH4 conc. (120 ml) 3 gas samples CH4 isotope	5 water samples CH4 conc. (120 ml) 5 gas samples CH4 isotope	5 water samples CH4 conc. (120 ml) 5 gas samples CH4 isotope	3 water samples CH4 conc. (120 ml) 3 gas samples CH4 isotope	- -
Michigan State University	2 sediment samples	-	-	-	-

TV-G	TV-G 24 / 1	TV-G 26 / 1	TV-G 28 / 1	TV-G 28 / 2	TV-G 43 / 1
GEOMAR Forschungszentrum, Kiel	video core 1 : 14 pore water samples core 2 : 10 pore water samples core 1 : 4 CH4 samples - 25 sediment and 24 PP samples core 2 : 4 CH4 samples macrofauna sediment biology	video - - - - - - - -	video - - - - - - - -	- - - - - 1 sediment sample - macrofauna sediment biology	video core 1 : 19 pore water samples core 2 : 19 pore water samples core 3 : 17 pore water samples core 4 : 15 sediment samples CH4 40 sediment and PP samples bacteria macrofauna sediment biology
Humboldt State University	core 1 ; 3 CH4 samples 1 poganophoran sample CH4 oxid.	- -	- -	- 2 poganophoran + 1 clam sample CH4 oxid.	core 4 : 7 sediment samples CH4 2 poganophoran samples CH4 oxid.
Rutgers University	29 biology samples	-	-	9 pogonophorans	56 biology samples
Michigan State University	-	-	-	-	1 sediment sample

TV-G	**TV-G 48 / 1**	**TV-G 54 / 1**	**TV-G 62 / 1**	**TV-G 63 / 1**	**TV-G 64 / 1**	**TV-G 65 / 1**
GEOMAR Forschungszentrum, Kiel	video core A: 12 pore water samples core B: ? - 3 sediment samples methane 19 sediment and 17 PP samples macrofauna sediment biology	video core A: 21 pore water samples - - - 40 sediment and 40 PP samples macrofauna sediment biology	video - - - - - - -	video 58 pore water samples 55 Fe, 14 isotope sediment samples 55 methane sediment samples precipitates 26 sediment and 70 PP samples macrofauna sediment biology 4 Pb 210	video 81 pore water samples 79 Fe, 25 isotope sediment samples 83 methane sediment samples - 35 sediment and 93 PP samples macrofauna bacteria 4 Pb 210	video 3 sediment cores archive 23 pore water samples 23 Fe sediment samples 23 methane sediment samples 23 PP sediment samples macrofauna - -
Humboldt State University	- -	- -	- -	- -	- -	- -
Rutgers University	52 biology samples	5 pogonophorans	- -	7 pogonophorans 19 calyptogena	6 solyemya 4 calyptogena	6 pogonophorans -
University of Victoria			-	-	9 pogonophorans	4 pogonophorans
Michigan State University	-	-	-	-	-	-
TV-GKG	**TV-GKG 38 / 2**	**TV-GKG 40 / 1**	**TV-GKG 42 / 1**	**TV-GKG 49 / 1**	**TV-GKG 53 / 1**	**TV-GKG 61 / 1**
GEOMAR Forschungszentrum, Kiel	video - - - -	video 3 pore water samples precipitates macrofauna sediment biology	video - - - -	video 1dinoflag. sediment sample 3 sediment and 7 PP samples macrofauna sediment biology	video - - - -	video - - - -
Humboldt State University	- -	1 clam, 2 poganophoran CH4 oxid. 1 sediment sample CH4 oxid.	- -	- -	- -	- -
Rutgers University	-	69 biology samples	-	23 biology samples	-	-
Michigan State University	-	sediment samples	-	-	-	-
EXPLOS	**EXPLOS 22 / 1**	**EXPLOS 32 / 1**	**EXPLOS 35 / 1**	**EXPLOS 37 / 1**		
GEOMAR Forschungszentrum, Kiel	video + slides	video + slides	video + slides	video + slides		
Kasteniote	**KAL 46 / 1**	**KAL 52 / 1**	**KAL 56 / 1**	**SL 58 / 1**	**SL 60 / 1**	
GEOMAR Forschungszentrum, Kiel	3 pore water samples 1 sediment sample	- 1 sediment sample	- -	7 pore water samples 7 Fe and 27 PP samples	3 pore water samples 3 Fe and 11 PP samples	
TV-MUC	**TV-MUC 57 / 1**	**TV-MUC 57 / 2**	**TV-MUC 59/ 1**			
GEOMAR Forschungszentrum, Kiel	video - - - - -	17 pore water samples 16 Fe samples 16 sediment methane 16 sediment and 16 PP samples bacteria sediment biology macrofauna	video - - - - sediment biology -			

keynotes: * = not available for further analysis, # = analyzed onboard, Fe = iron extraction, PP = physical properties, further abbrevations see station list

A7 Chemical data from CTD stations: 3, 6, 12, 16.

CTD3

depth [m]	SiO2 [µM]	PO4 [µM]	NO3 [µM]	NH4 [µM]	CH4 [nl/l]
625	86	3,55	39,0	bdl	112
609	85	3,31	39,8	bdl	85
595	82	3,43	40,7	bdl	82
582	73	3,43	37,1	bdl	128
564	83	3,43	39,9	bdl	77
550	79	3,43	38,6	bdl	49
535	80	3,43	37,5	bdl	58
516	83	3,43	38,5	bdl	58
499	85	3,43	39,3	bdl	62
485	91	3,31	38,9	bdl	nd
468	62	3,31	36,7	bdl	269
449	64	3,31	39,0	bdl	119

CTD6

depth [m]	SiO2 [µM]	PO4 [µM]	NO3 [µM]	NH4 [µM]	CH4 [nl/l]
634	83	3,55	35,3	bdl	121
599	93	3,55	39,0	bdl	91
575	94	3,55	39,7	bdl	94
556	103	3,43	40,8	bdl	83
534	86	3,67	41,0	bdl	58
517	78	3,43	40,8	bdl	113
506	83	3,43	39,1	bdl	153
489	77	3,43	38,2	bdl	143
475	77	3,43	37,1	bdl	74
475	74	3,43	37,2	bdl	72
460	72	3,31	39,9	bdl	42
445	72	3,31	38,8	bdl	27

CTD12

depth [m]	SiO2 [µM]	PO4 [µM]	NO3 [µM]	NH4 [µM]	CH4 [nl/l]	Cl [mM]	Ca [mM]	Mg [mM]
584	87	3,27	37,5	bdl	146	546	10,4	53,5
575	80	3,16	37,2	bdl	166			
565	85	3,16	38,3	bdl	98			
550	81	3,16	37,3	bdl	154			
535	81	3,04	39,7	bdl	196			
520	81	3,16	38,4	bdl	214			
504	73	3,16	35,1	bdl	nd	548	10,3	53,9
490	73	3,16	38,5	bdl	73586	547	10,4	53,7
475	70	3,16	34,8	bdl	1585			
450	71	3,04	35,2	bdl	1770			
418	66	3,04	36,0	bdl	355			
355	56	2,92	34,9	bdl	513			

CTD16

depth [m]	SiO2 [µM]	PO4 [µM]	NO3 [µM]	NH4 [µM]	CH4 [nl/l]	Cl [mM]	Ca [mM]	Mg [mM]
590	92	3,59	38,2	bdl	1001	533	10,4	52,8
565	88	3,36	40,3	bdl	19259	544	10,4	53,4
545	90	3,24	38,7	bdl	1071			
524	85	3,24	36,9	bdl	79			
510	78	3,24	37,5	bdl	210			
495	83	3,13	35,7	bdl	557			
480	78	3,94	36,6	bdl	246			
468	79	3,59	37,8	bdl	93			
457	74	3,13	38,4	bdl	102			
444	72	3,13	32,5	bdl	nd			
430	65	3,01	33,6	bdl	104			
409	63	2,89	34,9	bdl	42			

A7 Chemical data from CTD stations: 21, 27, 30, 39, 50.

station	depth [m]	silicate [µM]	phosphate [µM]	nitrate [µM]	ammonia [µM]	methane [nl/l]	oxygen [µM]
CTD21	600	97	n.d.	46,0	n.d.	40	n.d.
	494	107	n.d.	45,5	n.d.	28	n.d.
	374	97	n.d.	43,2	n.d.	43	n.d.
	250	75	n.d.	40,0	n.d.	61	n.d.
	201	67	n.d.	37,9	n.d.	73	n.d.
	150	56	n.d.	33,9	n.d.	80	n.d.
	100	32	n.d.	23,7	n.d.	76	n.d.
	74	21	n.d.	16,9	n.d.	76	n.d.
	50	15	n.d.	11,7	n.d.	68	n.d.
	25	9	n.d.	5,7	n.d.	73	n.d.
	10	7	n.d.	bdl	n.d.	61	n.d.
	5	8	n.d.	bdl	n.d.	61	n.d.
CTD27	4948	n.d.	n.d.	n.d.	n.d.	n.d.	n.d.
	4900	n.d.	n.d.	n.d.	n.d.	25	n.d.
	4849	n.d.	n.d.	n.d.	n.d.	23	n.d.
	4801	n.d.	n.d.	n.d.	n.d.	18	n.d.
	4750	n.d.	n.d.	n.d.	n.d.	33	n.d.
	4646	n.d.	n.d.	n.d.	n.d.	16	n.d.
	4501	n.d.	n.d.	n.d.	n.d.	18	n.d.
	4401	n.d.	n.d.	n.d.	n.d.	15	n.d.
	4301	n.d.	n.d.	n.d.	n.d.	13	n.d.
	3999	n.d.	n.d.	n.d.	n.d.	12	n.d.
	3500	n.d.	n.d.	n.d.	n.d.	12	n.d.
	2500	n.d.	n.d.	n.d.	n.d.	12	n.d.
CTD30	4807	150	1,39	37,3	n.d.	30	159
	4779	152	1,42	37,3	n.d.	33	160
	4749	156	1,45	36,9	n.d.	26	157
	4720	155	1,45	37,6	n.d.	15	157
	4689	156	1,45	37,3	n.d.	23	160
	4660	155	1,49	n.d.	n.d.	15	n.d.
	4630	155	1,49	37,3	n.d.	17	157
	4600	155	1,52	36,7	n.d.	20	n.d.
	4570	141	1,55	37,3	n.d.	21	155
	4539	n.d.	1,49	35,5	n.d.	18	n.d.
	4509	154	1,52	36,6	n.d.	15	154
	4478	152	1,52	37,4	n.d.	13	n.d.
CTD39	4953	n.d.	n.d.	n.d.	n.d.	28	164
	4899	n.d.	n.d.	n.d.	n.d.	33	161
	4851	n.d.	n.d.	n.d.	n.d.	34	160
	4802	n.d.	n.d.	n.d.	n.d.	31	161
	4750	n.d.	n.d.	n.d.	n.d.	43	161
	4700	n.d.	n.d.	n.d.	n.d.	34	n.d.
	4650	n.d.	n.d.	n.d.	n.d.	32	159
	4600	n.d.	n.d.	n.d.	n.d.	27	n.d.
	4549	n.d.	n.d.	n.d.	n.d.	29	159
	4500	n.d.	n.d.	n.d.	n.d.	29	n.d.
	4400	n.d.	n.d.	n.d.	n.d.	21	159
	4301	n.d.	n.d.	n.d.	n.d.	18	n.d.
CTD50	4951	n.d.	n.d.	n.d.	n.d.	71	163
	4750	n.d.	n.d.	n.d.	n.d.	35	161
	4549	n.d.	n.d.	n.d.	n.d.	24	159
	4250	n.d.	n.d.	n.d.	n.d.	11	155
	4000	n.d.	n.d.	n.d.	n.d.	21	151
	3000	n.d.	n.d.	n.d.	n.d.	13	120
	2000	n.d.	n.d.	n.d.	n.d.	10	69
	999	n.d.	n.d.	n.d.	n.d.	16	22
	750	n.d.	n.d.	n.d.	n.d.	26	21
	500	n.d.	n.d.	n.d.	n.d.	34	25
	100	n.d.	n.d.	n.d.	n.d.	74	181
	49	n.d.	n.d.	n.d.	n.d.	61	307

A8 Pore water sample list.

leg	station	no of sub-cores	core depth [cm]	no of pore water samples	analysis aboard	subsampling	strategy of sampling
1a	TV-G 9	2	34 / 22	7 / 5	pH, TA, H_2S, SiO_2, PO_4, NO_3, NH_4	PW ac.	2cm slices; every other PW sample to Oregon State University
	TV-G 11	2	28 / 22	6 / 5	pH, TA, H_2S, SiO_2, PO_4, NO_3, NH_4	PW ac.	2cm slices; every other PW sample to Oregon State University
	TV-G 18	3	22 / 16 / 19	9 / 7 / 8	pH, TA, H_2S, SiO_2, PO_4, NO_3, NH_4, Cl, Ca, Mg	PW ac.	2cm slices
1b	TV-G 24	2	28 / 16	14 / 10	pH, TA, H_2S, SiO_2, PO_4, NO_3, NH_4	CH_4, PW ac.	≤10cm: 1cm slices; > 10cm: 3cm slices; CH4: every 4th cm
	GKG 40	-	-	3	pH, TA, H_2S, SiO_2, NH_4		random
	TV-G 43	3	37 / 36 / 31	19 / 19 / 17 + 3	pH, TA, H_2S, SiO_2, PO_4, NO_3, NH_4	CH_4, PW ac.	≤10cm: 1cm slices; > 10cm: 3cm slices; CH4: core 4
2	KAL 46	-	-	3	pH, TA, H_2S, SiO_2, PO_4, NO_3, NH_4	PW ac.	random
	TV-G 48	2	16 / 16	12 / 12	pH, TA, H_2S, SiO_2, PO_4, NO_3, NH_4	PW ac.	≤10cm: 1cm slices; > 10cm: 3cm slices
	TV-G 54	1	43	21	pH, TA, H_2S, SiO_2, PO_4, NO_3, NH_4	PW ac.	≤10cm: 1cm slices; > 10cm: 3cm slices
	MUC 57	1	31	16 + 1	pH, TA, H_2S, SiO_2, PO_4, NO_3, NH_4, Fe, O_2	PW ac.	1 cm slices, alternating for PW sqeezing and subsampling, resp.
	SL 58	1	124	7	pH, TA, H_2S, SiO_2, PO_4, NO_3, NH_4, Fe	PW ac.	50cm3 syringes, every 20 cm
	SL 60	1	47	3	pH, TA, Fe	PW ac.	50cm3 syringes, every 20 cm
	TV-G 63	4	16 / 28 / 30 / 30	8 / 15 / 15 / 16 + 3	pH, TA, H_2S, SiO_2, PO_4, NO_3, NH_4, Fe	PP, CH_4, SI, PW ac.	1 cm slices, alternating for PW sqeezing and subsampling, resp.
	TV-G 64	4	50 / 37 / 38 / 35	25 / 19 / 19 / 18	pH, TA, H_2S, SiO_2, PO_4, NO_3, NH_4, Fe	PP, CH_4, SI, PW ac.	1 cm slices, alternating for PW sqeezing and subsampling, resp.
	TV-G 65	1	45	23	pH, TA, H_2S, SiO_2, PO_4, NO_3, NH_4, Fe	PP, CH_4, PW ac.	1 cm slices, alternating for PW sqeezing and subsampling, resp.

Keywords

pH determination of sediment pH
TA total alkalinity of pore water
H_2S sulfide concentration in pore water
SiO_2, PO_4, NO_3, NH_4 nutrient analysis in pore water
Cl, Ca, Mg titration
Fe ferric / ferrous ions in sediment extract (HCl)
O_2 oxygen concentration in bottom water
PP sediment sample for physical properties analysis
CH_4 sediment sample for methane analysis
SI sediment sample for S-isotopes
PW ac acidified pore water sample

A9 Chemical data of pore water.

TVG9 / core A

depth [cm]	SiO2 [µM]	PO4 [µM]	NH4 [µM]	TA [mM]	pH	H2S [mM]
0-2	148	6,2	25,5	3,2	7,61	0,1
4-6	181	5,3	3,2	10,3	7,72	2,0
8-10	231	7,9	bdl	21,3	7,93	4,8
13-16	302	13,5	bdl	27,0	8,15	13,3
19-22	308	9,3	28,4	27,5	8,27	44,6
25-28	342	10,6	70,3	30,4	8,15	43,7
31-34	329	5,4	38,3	29,0	8,13	42,3

TVG9 / core B

depth [cm]	SiO2 [µM]	PO4 [µM]	NH4 [µM]	TA [mM]	pH	H2S [mM]
0-2	250	6,8	bdl	21,2	7,61	5,5
4-6	221	10,1	bdl	15,4	7,39	4,0
8-10	206	8,9	bdl	12,9	7,76	3,2
13-16	288	12,5	bdl	26,2	7,74	38,1
19-22	321	7,2	87,2	30,5	8,15	46,8

TVG11 / core A

depth [cm]	SiO2 [µM]	PO4 [µM]	NH4 [µM]	TA [mM]	pH	H2S [mM]
0-2	180	6,0	58,2	3,3	8,06	0,1
4-6	158	5,0	32,3	3,3	7,82	bdl
8-10	125	2,9	19,4	nd	7,91	bdl
13-16	125	6,2	bdl	16,6	7,60	40,7
19-22	214	8,2	74,9	32,4	7,78	39,5
25-28	214	2,8	203,2	34,0	7,73	36,7

TVG11 / core B

depth [cm]	SiO2 [µM]	PO4 [µM]	NH4 [µM]	TA [mM]	pH	H2S [mM]
0-2	nd	nd	69,4	nd	7,86	0,1
4-6	nd	nd	nd	nd	7,82	nd
8-10	nd	nd	71,1	4,2	7,84	0,1
13-16	182	6,8	bdl	17,0	7,60	41,4
19-22	nd	nd	0,0	nd	7,60	nd

TVG18 / core 1

depth [cm]	SiO2 [µM]	PO4 [µM]	NH4 [µM]	TA [mM]	pH	H2S [mM]	Cl [mM]	Ca [mM]	Mg [mM]
0-2	228	5,2	125	34,2	7,92	7,5	553	nd	nd
2-4	239	3,7	99	35,9	7,94	20,6	554	nd	nd
4-6	251	5,7	80	35,4	7,77	17,2	559	nd	nd
6-8	241	8,7	192	35,0	7,74	18,8	556	nd	nd
8-10	261	10,6	160	36,8	7,65	21,2	542	nd	nd
10-13	260	5,6	93	37,1	7,77	22,0	549	nd	nd
13-16	259	7,9	bdl	36,0	7,99	19,0	551	nd	nd
16-19	258	12,9	24	39,5	7,88	22,8	556	nd	nd
19-22	261	12,3	202	38,5	7,65	20,5	546	nd	nd

TVG18 / core 2

depth [cm]	SiO2 [µM]	PO4 [µM]	NH4 [µM]	TA [mM]	pH	H2S [mM]	Cl [mM]	Ca [mM]	Mg [mM]
0-2	nd	nd	nd	31,2	8,08	11,0	555	nd	nd
2-4	nd	nd	nd	32,2	7,65	14,4	554	nd	nd
4-6	nd	nd	nd	35,4	7,65	16,4	556	nd	nd
6-8	nd	nd	nd	34,5	7,65	16,2	550	nd	nd
8-10	nd	nd	nd	36,3	7,57	16,5	559	nd	nd
10-13	nd	nd	nd	34,7	7,79	14,0	553	nd	nd
13-16	nd	nd	nd	32,0	7,54	18,7	482	nd	nd

TVG18 / core 3

depth [cm]	SiO2 [µM]	PO4 [µM]	NH4 [µM]	TA [mM]	pH	H2S [mM]	Cl [mM]	Ca [mM]	Mg [mM]
0-2	268	nd	144	34,4	7,61	16,0	549	4,3	49,8
2-4	273	nd	170	34,3	7,70	18,1	549	4,0	49,7
4-6	274	nd	181	33,0	7,85	17,9	531	3,9	49,4
6-8	284	nd	226	33,1	7,66	16,8	536	3,8	49,2
8-10	285	nd	197	33,7	7,66	14,4	543	4,0	49,7
10-13	277	nd	255	36,6	7,68	15,9	544	3,7	49,8
13-16	283	nd	115	34,8	7,57	17,5	548	3,8	50,7
16-19	273	nd	204	34,3	7,68	16,0	544	3,6	49,5

A9 Chemical data of pore water.

TVG 24 / core 1

depth [cm]	SiO2 [µM]	PO4 [µM]	NO3 [µM]	NH4 [µM]	H2S [µM]	TA [mM]	pH
0-1	230	1,40	8,61	14,5	0,80	2,54	7,49
1-2	215	1,17	2,68	17,2	0,55	2,72	7,35
3-4	235	0,58	nd	19,1	0,80	2,83	7,48
4-5	247	0,35	0,57	15,1	1,04	2,83	7,42
5-6	234	0,70	0,66	21,6	0,63	2,93	7,33
7-8	259	0,35	bdl	21,2	0,71	2,93	7,27
8-9	268	0,35	nd	23,1	0,71	2,97	7,40
9-10	272	0,47	nd	30,2	0,63	2,93	7,60
11-13	276	0,35	nd	33,3	1,04	3,10	7,46
13-16	290	1,05	nd	40,4	0,63	3,02	7,84
16-19	273	1,40	nd	49,5	0,80	3,14	7,55
19-22	228	3,03	nd	69,5	0,71	3,31	7,48
23-26	173	5,24	nd	134,4	3,20	3,63	7,42
26-28	173	bdl	nd	157,8	11,65	3,99	7,40

TVG 24 / core 2

depth [cm]	SiO2 [µM]	PO4 [µM]	NO3 [µM]	NH4 [µM]	H2S [µM]	TA [mM]	pH
0-1	124	0,58	5,55	21,6	0,80	2,77	7,81
1-2	144	0,47	3,06	24,6	1,38	2,88	7,77
3-4	153	0,58	2,01	28,0	0,71	3,18	7,68
4-5	165	0,70	2,49	29,6	1,62	3,10	7,82
5-6	168	0,35	3,16	25,2	0,80	3,21	7,31
7-8	160	0,82	2,39	24,3	1,04	3,18	7,75
8-9	159	0,93	1,53	36,0	0,88	3,21	7,82
9-10	194	1,40	1,63	24,6	0,63	3,14	7,38
11-13	207	2,68	0,86	32,6	0,63	2,97	7,29
13-16	235	4,31	nd	36,3	2,95	2,88	7,29

GKG40

SampleNo.	SiO2 [µM]	PO4 [µM]	NO3 [µM]	NH4 [µM]	H2S [mM]	TA [mM]	pH	comment
1	244	nd	nd	27	bdl	2,5	7,20	surface, light
2	375	nd	nd	332	7,39	19,2	7,91	subsurface, dark
3	312	nd	nd	216	4,91	13,8	7,89	subsurface, dark

KAL46

Sample No.	SiO2 [µM]	PO4 [µM]	NO3 [µM]	NH4 [µM]	TA [mM]	H2S [µM]	pH
1	455	8,52	2,5	26,0	3,31	85,2	MW
2	468	8,03	3,4	20,2	2,66	37,6	(n=7)
3	447	7,21	2,0	59,4	3,21	38,1	7,85

MUC57

depth [cm]	SiO2 [µM]	PO4 [µM]	NO3 [µM]	NH4 [µM]	TA [mM]	H2S [µM]
0-1	244	4,00	41,9	37,9	2,21	bdl
2-3	280	4,00	33,0	21,7	2,21	bdl
4-5	305	2,22	17,0	34,5	2,41	bdl
6-7	287	1,48	4,0	24,0	0,56	bdl
8-9	251	2,37	bdl	26,1	1,45	bdl
10-11	251	4,15	bdl	29,9	1,69	bdl
12-13	267	2,67	bdl	22,9	2,96	bdl
14-15	278	2,22	bdl	22,7	2,60	bdl
16-17	290	2,22	bdl	23,7	1,91	bdl
18-19	307	2,37	bdl	21,8	1,28	bdl
20-21	324	2,52	bdl	21,6	1,68	bdl
22-23	305	3,26	bdl	22,0	2,76	bdl
24-25	316	2,82	bdl	21,6	1,85	bdl
26-27	321	2,37	bdl	23,4	2,35	bdl
28-29	227	2,37	bdl	22,6	1,28	bdl
30-31	213	nd	0,8	21,6	2,41	bdl
bottom water						
0	170	3,26	37,7	22,0	1,56	bdl

depth [cm]	pH	FeIII [%]
0-1		43,1
1-2	7,54	42,0
3-4	7,62	37,3
5-6	7,81	38,9
7-8	7,78	13,7
9-10	7,95	22,4
11-12	7,78	17,7
13-14	7,84	56,5
15-16	7,76	15,4
17-18	7,98	12,1
19-20	7,70	14,8
21-22	7,78	10,3
23-24	7,76	22,3
25-26	7,78	nd
27-28	7,73	6,8
29-30	7,78	nd

O2 [µM]
164

SL58

depth [cm]	SiO2 [µM]	PO4 [µM]	NO3 [µM]	NH4 [µM]	TA [mM]	H2S [µM]
1-4	375	5,48	2,1	39,8	1,94	bdl
20-23	343	3,26	2,4	67,2	3,05	bdl
39-42	392	3,71	0,5	92,8	2,89	bdl
55-58	478	5,78	bdl	82,4	3,09	bdl
75-78	475	5,78	bdl	110,7	3,15	bdl
95-98	511	7,26	bdl	137,7	3,06	bdl
115-118	509	7,26	bdl	166,1	3,37	bdl

depth [cm]	pH	FeIII [%]
1-4	7,87	43,7
20-23	7,89	13,0
39-42	7,56	7,7
55-58	7,59	8,5
75-78	7,70	27,1
95-98	7,73	18,1
115-118	7,73	10,2

SL60

depth [cm]	SiO2 [µM]	PO4 [µM]	NO3 [µM]	NH4 [µM]	TA [mM]	H2S [µM]
3-6	nd	nd	nd	nd	2,64	nd
17-20	nd	nd	nd	nd	2,89	nd
41-44	nd	nd	nd	nd	3,06	nd

depth [cm]	pH	FeIII [%]
3-6	7,54	47,0
17-20	7,45	48,2
41-44	7,48	55,4

A9 Chemical data of pore water.

TVG48 / core A

depth [cm]	SiO2 [µM]	PO4 [µM]	NO3 [µM]	NH4 [µM]	H2S [mM]	TA [mM]	pH
0-1	264	5,1	20,6	51	bdl	2,5	7,70
1-2	295	5,5	7,8	53	bdl	2,4	7,82
2-3	370	11,9	0,8	81	0,02	3,2	8,20
3-4	321	11,5	1,0	128	0,10	3,8	7,79
4-5	380	30,5	bdl	199	1,22	7,0	8,17
5-6	390	19,9	bdl	63	nd	11,6	8,03
6-7	437	21,9	0,1	232	nd	16,4	7,94
7-8	454	21,2	0,2	287	nd	18,6	8,32
8-9	492	18,2	0,3	1097	6,74	20,2	8,15
9-10	466	13,3	0,6	1521	2,85	18,3	8,17
10-13	470	20,0	0,4	1722	3,09	16,4	8,15
13-16	482	17,7	2,0	1778	3,61	14,1	8,15

TVG48 / core B

depth [cm]	SiO2 [µM]	PO4 [µM]	NO3 [µM]	NH4 [µM]	H2S [mM]	TA [mM]	pH
0-1	296	7,8	14,0	193	0,11	2,7	7,55
1-2	342	11,3	6,2	84	bdl	3,5	7,47
2-3	365	18,0	0,6	140	0,08	3,8	7,79
3-4	374	19,2	bdl	197	0,34	4,5	7,70
4-5	419	23,2	bdl	306	2,03	6,5	7,76
5-6	459	22,5	bdl	548	4,10	11,2	7,88
6-7	433	18,7	0,1	534	2,30	16,3	7,85
7-8	468	22,0	0,7	369	nd	18,7	7,70
8-9	501	18,7	bdl	426	nd	20,5	7,61
9-10	495	23,2	0,3	1457	5,04	18,2	7,76
10-13	473	15,0	2,4	1741	3,28	16,2	7,79
13-16	446	nd	3,9	1837	2,23	14,4	7,55

TVG54

depth [cm]	SiO2 [µM]	PO4 [µM]	NO3 [µM]	NH4 [µM]	H2S [mM]	TA [mM]	pH
0-1	433	2,16	5,3	9,7	bdl	2,29	7,48
1-2	427	1,85	2,3	10,2	bdl	1,56	7,57
2-3	431	1,85	0,5	10,8	bdl	2,35	7,57
3-4	443	2,46	0,4	12,2	bdl	2,57	7,74
4-5	444	2,62	0,9	13,4	bdl	2,64	7,71
5-6	475	3,23	2,8	14,4	bdl	2,61	7,71
6-7	476	3,85	0,3	25,5	bdl	2,57	7,77
7-8	484	4,62	1,2	38,9	bdl	2,57	7,83
8-9	500	5,70	0,5	26,6	bdl	2,64	7,83
9-10	500	6,47	0,6	23,3	bdl	2,76	7,86
10-13	518	6,77	1,2	37,8	bdl	2,76	7,94
13-16	530	8,01	1,0	34,8	bdl	2,59	7,94
16-19	521	8,47	0,2	28,9	0,74	1,85	7,94
19-22	511	8,47	0,6	44,5	2,50	2,28	7,92
22-25	539	8,78	0,2	39,8	4,33	1,68	7,92
25-28	536	9,55	0,3	54,0	4,07	2,59	7,83
28-31	548	11,09	0,7	54,0	5,86	2,59	7,86
31-34	556	11,24	0,0	58,8	8,96	1,45	7,86
34-37	558	12,93	0,7	62,9	9,52	2,73	7,86
37-40	562	14,47	1,3	74,4	8,44	2,34	7,86
40-43	554	18,01	3,4	98,0	nd	3,53	nd

TVG 54 / H2S : data from second subcore, measured with ion selctive electrode

A9 Chemical data of pore water.

TVG 43 / core 1

depth [cm]	SiO2 [µM]	PO4 [µM]	NO3 [µM]	NH4 [µM]	H2S [mM]	TA [mM]	pH
0-1	291	8,5	26,8	38	bdl	2,30	7,23
1-2	302	2,8	9,2	88	bdl	2,53	7,18
2-3	327	5,5	4,4	107	bdl	2,90	7,25
3-4	347	4,8	0,6	134	0,1	3,09	7,42
4-5	374	4,2	bdl	197	0,2	3,58	7,42
5-6	429	6,4	nd	256	0,5	4,40	7,55
6-7	471	9,8	nd	442	0,8	5,32	7,57
7-8	473	9,8	nd	426	1,0	5,58	7,58
8-9	410	10,4	nd	691	1,6	6,65	7,60
9-10	413	10,7	nd	686	1,7	7,20	7,62
10-13	445	11,8	nd	807	2,2	8,57	7,57
13-16	419	10,6	nd	999	2,1	8,18	7,55
16-19	403	9,7	nd	1113	2,1	8,57	7,53
19-22	384	9,7	nd	1197	1,6	8,50	7,64
22-25	386	8,8	nd	1246	2,1	9,23	7,60
25-28	389	10,1	nd	1347	nd	10,70	7,57
28-31	403	9,3	nd	1330	2,1	10,43	7,49
31-34	441	14,6	nd	1181	4,0	12,02	7,70
34-37	463	17,5	nd	1431	4,5	12,19	7,49

TVG 43 / core 2

depth [cm]	SiO2 [µM]	PO4 [µM]	NO3 [µM]	NH4 [µM]	H2S [mM]	TA [mM]	pH
0-1	271	10,0	68,3	37	bdl	2,97	7,23
1-2	297	15,1	20,0	50	bdl	3,28	7,12
2-3	322	14,9	4,4	69	bdl	2,72	7,18
3-4	343	14,9	2,3	94	bdl	2,97	7,25
4-5	386	19,2	0,8	142	bdl	3,10	7,38
5-6	391	19,2	nd	203	bdl	3,34	7,40
6-7	430	20,4	nd	267	0,2	3,72	7,49
7-8	433	21,8	nd	369	0,3	4,09	7,58
8-9	469	18,8	nd	438	0,8	5,02	7,49
9-10	482	20,7	nd	460	0,7	4,93	7,49
10-13	512	16,9	nd	745	0,7	6,74	7,47
13-16	507	20,9	nd	943	1,5	9,02	7,51
16-19	520	20,4	nd	1252	3,3	10,96	7,73
19-22	424	12,8	nd	1373	1,5	11,24	7,64
22-25	456	12,4	nd	1291	1,6	11,49	7,53
25-28	430	10,3	nd	1431	2,5	13,21	7,70
28-31	428	10,1	nd	1597	2,2	12,46	7,38
31-34	422	9,8	nd	1698	2,4	12,71	7,73
34-36	345	9,7	nd	1740	2,2	12,92	7,58

TVG 43 / core 3

depth [cm]	SiO2 [µM]	PO4 [µM]	NO3 [µM]	NH4 [µM]	H2S [mM]	TA [mM]	pH
0-1	379	13,1	nd	592	0,4	5,31	7,62
1-2	410	16,1	nd	568	0,8	5,40	7,66
2-3	418	15,7	nd	725	1,6	7,11	7,51
3-4	404	14,8	nd	943	1,5	7,32	7,51
4-5	343	12,8	nd	1100	0,3	7,91	7,47
5-6	377	12,8	nd	1194	0,8	8,33	7,44
6-7	354	11,2	nd	1262	0,6	8,93	7,60
7-8	380	10,9	nd	1376	nd	nd	7,55
8-9	386	10,9	nd	1298	1,8	10,24	7,51
9-10	nd	nd	nd	nd	nd	nd	7,49
10-13	368	9,1	nd	1347	0,6	9,47	7,64
13-16	386	8,8	nd	1555	nd	nd	7,68
16-19	383	9,3	nd	1568	1,5	11,44	7,36
19-22	422	14,3	nd	1584	nd	nd	7,27
22-25	453	13,0	nd	1695	3,4	13,28	7,55
25-28	454	12,7	nd	1500	nd	nd	7,68
28-31	462	17,8	nd	1379	4,9	14,18	7,14

TVG 43 / surface samples

SampleNo.	SiO2 [µM]	PO4 [µM]	NO3 [µM]	NH4 [µM]	H2S [mM]	TA [mM]	pH
0	274	3,3	nd	109	0,1	3,65	7,73
0	405	4,3	nd	265	0,2	3,29	7,66
0	368	4,6	nd	286	0,3	3,65	7,53

A9 Chemical data of pore water.

TVG 63 A

depth [cm]	SiO2 [µM]	PO4 [µM]	NO3 [µM]	NH4 [µM]	TA [mM]	H2S [mM]
0-1	348	1,80	13,5	20,2	2,25	bdl
2-3	273	2,10	2,7	15,4	2,56	bdl
4-5	215	2,40	0,3	15,4	2,80	bdl
6-7	233	1,95	bdl	13,3	2,63	bdl
8-9	240	1,80	bdl	14,1	2,99	bdl
10-11	248	1,65	bdl	14,0	2,63	bdl
12-13	251	2,10	bdl	12,5	2,72	bdl
14-15	253	1,50	bdl	13,1	2,63	bdl

depth [cm]	pH	FeIII [%]
0-1		41,9
1-2	7,61	51,4
3-4	7,44	8,3
5-6	7,65	9,8
7-8	7,57	7,4
9-10	7,61	3,5
11-12	7,65	0,6
13-14	7,69	4,6
15-16	7,61	3,8

TVG 63 W

depth [cm]	SiO2 [µM]	PO4 [µM]	NO3 [µM]	NH4 [µM]	TA [mM]	H2S [µM]
0-1	345	1,95	1,3	45	3,0	1,62
2-3	320	4,95	4,9	40	nd	3,84
4-5	299	5,40	3,2	58	2,6	2,10
6-7	236	21,31	1,8	73	nd	nd
8-9	237	3,30	1,1	51	2,7	1,70
10-11	238	2,55	3,8	47	2,3	1,14
12-13	nd	2,55	nd	nd	nd	nd
14-15	248	3,00	3,2	34	2,4	0,59
16-17	231	3,00	2,2	34	2,5	0,11
18-19	251	3,75	1,7	49	2,9	8,85
20-21	280	5,40	1,1	80	3,8	45,09
22-23	295	7,50	0,5	124	4,6	67,74
24-25	284	8,70	0,9	146	5,1	43,13
26-27	287	9,60	0,5	159	5,5	43,08
28-29	318	13,36	0,5	199	6,1	115,46
Oberfläche	434	3,3	28,7	5	1,8	0,35
Sonderprobe A	284	9,8	1,0	155	5,3	24,79
Sonderprobe B	538	2,6	2,0	107	3,2	0,98

depth [cm]	pH	FeIII [%]
0-1		9,3
1-2	nd	16,3
3-4	nd	34,0
5-6	nd	25,3
7-8	nd	14,1
9-10	nd	12,3
11-12	nd	22,9
13-14	nd	7,8
15-16	nd	11,7
17-18	nd	18,3
19-20	nd	11,3
21-22	nd	5,4
23-24	nd	7,8
25-26	nd	10,2
27-28	nd	10,1
	7,15	40,8
	8,20	6,0
	7,80	19,6

TVG 63 Y

depth [cm]	SiO2 [µM]	PO4 [µM]	NO3 [µM]	NH4 [µM]	TA [mM]	H2S [mM]
0-1	317	1,20	0,0	25,5	2,66	bdl
2-3	344	1,80	0,8	55,1	nd	bdl
4-5	380	2,40	0,8	43,0	3,04	bdl
6-7	295	2,25	0,9	49,9	3,39	bdl
8-9	283	2,25	0,9	36,0	2,66	bdl
10-11	292	1,35	1,3	32,4	2,44	bdl
12-13	279	1,80	bdl	30,5	2,56	bdl
14-15	247	1,65	bdl	32,0	2,56	bdl
16-17	244	2,25	bdl	28,8	2,50	bdl
18-19	231	1,50	bdl	32,7	2,44	bdl
20-21	233	nd	bdl	26,3	2,37	bdl
22-23	232	1,80	bdl	31,2	2,29	bdl
24-25	233	1,65	bdl	26,1	2,37	bdl
26-27	237	nd	bdl	28,2	2,37	bdl
28-29	200	nd	bdl	31,3	2,44	bdl

depth [cm]	pH	FeIII [%]
0-1		nd
1-2	7,73	6,2
3-4	7,46	12,3
5-6	7,64	2,5
7-8	7,46	2,9
9-10	7,64	6,2
11-12	7,37	6,1
13-14	7,28	7,9
15-16	7,20	5,7
17-18	7,24	4,0
19-20	7,20	8,5
21-22	7,24	9,2
23-24	7,37	8,1
25-26	7,28	11,6
27-28	7,74	8,5
29-30	7,41	13,4
31-32	7,41	5,9

TVG 63 Z

depth [cm]	SiO2 [µM]	PO4 [µM]	NO3 [µM]	NH4 [µM]	TA [mM]	H2S [mM]
0-1	364	2,85	20,1	9,3	2,4	bdl
2-3	373	2,25	16,2	7,9	2,6	bdl
4-5	360	2,70	14,1	5,2	2,4	bdl
6-7	325	2,85	6,6	1,2	2,3	bdl
8-9	281	4,05	0,3	10,9	2,4	bdl
10-11	279	3,75	bdl	9,1	2,5	bdl
12-13	236	3,75	bdl	3,8	2,8	bdl
14-15	230	3,75	bdl	3,1	nd	bdl
16-17	246	3,15	bdl	3,7	2,8	bdl
18-19	245	3,45	bdl	4,1	2,8	bdl
20-21	271	3,15	bdl	1,9	2,8	bdl
22-23	277	3,00	bdl	4,1	2,8	bdl
24-25	293	3,00	bdl	2,2	2,7	bdl
26-27	294	2,55	bdl	0,0	2,7	bdl
28-29	268	3,00	bdl	3,0	2,6	bdl
30-31	266	3,30	bdl	2,2	2,4	bdl

depth [cm]	pH	FeIII [%]
0-1		45,4
1-2	nd	17,5
3-4	nd	16,0
5-6	nd	19,6
7-8	nd	18,6
9-10	nd	14,4
11-12	nd	5,4
13-14	nd	4,6
15-16	7,97	4,6
17-18	7,58	7,6
19-20	7,71	nd
21-22	7,50	9,5
23-24	7,76	6,6
25-26	7,58	26,2
27-28	7,54	5,6
29-30	7,58	3,8
31-32	7,50	nd

A9 Chemical data of pore water.

TVG 64 A

depth [cm]	SiO2 [µM]	PO4 [µM]	NO3 [µM]	NH4 [µM]	TA [mM]	H2S [µM]	depth [cm]	pH	FeIII [%]
0-1	318	5,90	1,7	72,2	5,95	156	0-1		9,7
2-3	292	5,41	0,9	34,7	6,51	234	1-2	7,80	7,4
4-5	312	3,44	0,0	40,2	5,79	298	3-4	7,76	6,1
6-7	312	3,44	0,0	30,0	4,88	211	5-6	7,76	5,9
8-9	308	3,44	0,0	35,4	5,87	364	7-8	7,84	9,1
10-11	305	2,70	0,6	33,7	5,39	226	9-10	8,12	5,2
12-13	302	2,95	0,3	34,2	5,01	216	11-12	7,80	5,8
14-15	277	1,72	0,0	22,4	4,54	336	13-14	7,67	6,4
16-17	286	3,44	0,3	35,4	5,49	249	15-16	7,67	7,3
18-19	273	3,69	0,1	30,9	4,85	312	17-18	7,80	5,0
20-21	281	4,18	0,7	48,1	5,46	590	19-20	7,63	7,1
22-23	291	3,20	0,6	36,5	4,74	258	21-22	7,67	7,1
24-25	291	3,20	1,4	48,5	4,55	367	23-24	7,71	10,3
26-27	328	3,93	0,6	52,4	4,74	529	25-26	7,71	8,6
28-29	326	4,92	0,8	53,3	5,48	429	27-28	7,51	12,4
30-31	330	4,92	0,4	49,6	4,84	291	29-30	7,80	3,8
32-33	327	4,67	0,3	57,8	5,48	307	31-32	7,67	1,7
34-35	343	4,42	0,7	69,3	5,35	377	33-34	7,76	3,3
36-37	343	5,16	0,5	81,0	5,59	436	35-36	7,76	2,9
38-39	347	5,41	0,5	73,3	5,49	346	37-38	7,88	8,5
40-41	346	5,41	0,4	76,1	5,79	211	39-40	7,84	2,1
42-43	344	5,90	0,5	86,1	5,48	451	41-42	7,88	3,3
44-45	353	5,65	0,0	88,5	6,11	326	43-44	7,71	3,3
46-47	370	7,37	0,0	89,6	5,94	437	45-46	7,76	1,6
48-49	363	nd	0,0	95,1	5,94	nd	47-48	7,84	2,0
							49-50	7,67	2,4

TVG 64 B

depth [cm]	SiO2 [µM]	PO4 [µM]	NO3 [µM]	NH4 [µM]	TA [mM]	H2S [mM]	depth [cm]	pH	FeIII [%]
0-1	301	3,53	6,2	7,6	2,56	bdl	0-1		nd
2-3	306	5,01	0,0	8,9	3,02	bdl	1-2	7,43	14,9
4-5	280	5,15	0,0	10,6	3,13	bdl	3-4	7,51	4,0
6-7	280	nd	0,0	16,4	nd	bdl	5-6	7,35	11,1
8-9	278	4,42	0,0	8,7	2,56	bdl	7-8	7,43	nd
10-11	266	3,39	0,0	10,7	2,30	bdl	9-10	7,35	6,3
12-13	234	3,24	0,0	10,5	2,50	bdl	11-12	7,35	20,0
14-15	229	nd	0,0	15,6	nd	bdl	13-14	7,31	12,1
16-17	224	3,83	0,0	10,9	nd	bdl	15-16	7,31	19,1
18-19	205	2,80	0,0	11,8	2,56	bdl	17-18	7,39	5,1
20-21	202	3,09	0,0	8,0	2,61	bdl	19-20	7,43	2,9
22-23	198	2,80	0,2	6,6	2,44	bdl	21-22	7,31	8,8
24-25	184	2,80	2,6	10,9	2,37	bdl	23-24	7,35	60,4
26-27	179	2,21	0,0	8,3	2,44	bdl	25-26	7,35	nd
28-29	187	2,80	0,0	13,6	2,50	bdl	27-28	7,35	29,9
30-31	185	2,36	0,0	14,6	2,61	bdl	29-30	7,35	32,9
32-33	189	2,80	0,0	16,6	2,29	bdl	31-32	7,31	nd
34-35	186	2,80	0,0	10,6	2,65	bdl	33-34	7,39	12,8
36-37	182	2,80	0,0	12,0	2,37	bdl	35-36	7,35	nd

TVG 64 E

depth [cm]	SiO2 [µM]	PO4 [µM]	NO3 [µM]	NH4 [µM]	TA [mM]	H2S [µM]	depth [cm]	pH	FeIII [%]
0-1	na	na	na	na	13,00	bdl	0-1		23,3
2-3	na	na	na	na	9,16	bdl	1-2	7,75	7,6
4-5	na	na	na	na	8,39	bdl	3-4	7,75	4,5
6-7	na	na	na	na	7,77	bdl	5-6	7,83	nd
8-9	na	na	na	na	nd	bdl	7-8	7,71	7,1
10-11	na	na	na	na	7,63	bdl	9-10	7,67	6,0
12-13	na	na	na	na	nd	bdl	11-12	7,63	nd
14-15	na	na	na	na	6,84	bdl	13-14	7,59	12,2
16-17	na	na	na	na	nd	bdl	15-16	7,59	9,1
18-19	na	na	na	na	nd	bdl	17-18	7,55	9,2
20-21	na	na	na	na	7,06	0,5	19-20	7,55	14,8
22-23	na	na	na	na	nd	7,1	21-22	7,51	7,1
24-25	na	na	na	na	10,02	120	23-24	7,63	8,0
26-27	na	na	na	na	nd	70	25-26	7,63	14,9
28-29	na	na	na	na	12,27	158	27-28	7,51	12,7
30-31	na	na	na	na	13,91	388	29-30	7,39	nd
32-33	na	na	na	na	14,91	617	31-32	7,39	nd
34-35	na	na	na	na	14,65	235	33-34	7,43	8,5
35-37	na	na	na	na	15,05	230	35-36	7,47	11,0
							37-38	7,51	8,6

A9 Chemical data of pore water.

TVG 64 F

depth [cm]	SiO2 [µM]	PO4 [µM]	NO3 [µM]	NH4 [µM]	TA [mM]	H2S [mM]
0-1	224	3,68	0,5	12,1	2,87	bdl
2-3	242	3,39	0,0	15,5	2,61	bdl
4-5	249	5,89	0,0	14,6	2,46	bdl
6-7	226	3,24	0,0	13,1	2,63	bdl
8-9	217	2,95	0,0	10,3	2,72	bdl
10-11	226	3,98	0,0	13,3	2,80	bdl
12-13	237	3,83	0,0	13,7	2,72	bdl
14-15	199	3,98	0,0	14,6	2,80	bdl
16-17	246	5,01	0,0	14,0	nd	bdl
18-19	199	4,86	0,5	16,0	2,63	bdl
20-21	188	nd	0,5	19,3	nd	bdl
22-23	185	nd	0,1	15,5	nd	bdl
24-25	184	nd	0,7	18,8	2,56	bdl
26-27	172	nd	0,2	24,4	4,30	bdl
28-29	170	nd	0,2	20,5	nd	bdl
30-31	168	nd	0,4	29,2	nd	bdl
32-33	164	nd	0,4	33,7	3,35	bdl
34-35	nd	nd	nd	nd	4,60	bdl

depth [cm]	pH	FeIII [%]
0-1		28,4
1-2	7,83	8,2
3-4	7,70	7,3
5-6	7,61	5,5
7-8	7,61	5,6
9-10	7,75	4,2
11-12	7,79	3,6
13-14	7,57	4,4
15-16	7,61	6,1
17-18	7,66	2,1
19-20	7,61	7,0
21-22	7,57	6,1
23-24	7,61	4,1
25-26	8,01	5,9
27-28	7,79	6,1
29-30	7,92	5,3
31-32	8,05	3,7
33-34	7,79	6,0

TVG 65 D

depth [cm]	SiO2 [µM]	PO4 [µM]	NO3 [µM]	NH4 [µM]	TA [mM]	H2S [mM]
0-1	242	3,09	22,3	10,3	2,89	bdl
2-3	238	2,80	8,1	8,5	2,76	bdl
4-5	225	2,80	0,4	8,4	3,00	bdl
6-7	223	3,53	0,0	13,4	3,00	bdl
8-9	222	3,39	0,0	12,4	2,89	bdl
10-11	163	1,77	0,0	15,4	3,53	bdl
12-13	197	2,50	0,0	13,3	2,73	bdl
14-15	207	2,95	0,0	19,2	3,37	bdl
16-17	207	3,39	0,0	15,1	3,15	bdl
18-19	219	3,53	0,0	15,9	3,09	bdl
20-21	225	4,12	0,0	20,6	nd	bdl
22-23	213	3,53	0,0	14,3	3,30	bdl
24-25	213	nd	0,0	13,9	3,23	bdl
26-27	109	3,24	0,0	9,7	nd	bdl
28-29	202	3,39	0,0	12,5	2,95	bdl
30-31	203	nd	0,2	13,3	2,89	bdl
32-33	201	nd	0,1	13,5	nd	bdl
34-35	189	3,09	0,3	12,5	2,76	bdl
36-37	190	3,39	0,4	14,6	nd	bdl
38-39	203	3,39	0,4	13,6	2,83	bdl
40-41	210	3,39	0,0	12,0	2,76	bdl
42-43	210	3,53	0,0	14,5	2,76	bdl
44-45	213	3,83	0,2	15,2	2,76	bdl

depth [cm]	pH	FeIII [%]
0-1		35,8
1-2	7,59	16,6
3-4	7,50	21,9
5-6	7,42	10,9
7-8	7,37	13,6
9-10	7,42	11,5
11-12	7,50	15,0
13-14	7,46	9,1
15-16	7,46	1,8
17-18	7,50	3,5
19-20	7,50	2,8
21-22	7,50	0,9
23-24	7,50	1,4
25-26	7,59	4,3
27-28	7,55	1,5
29-30	7,50	nd
31-32	7,55	nd
33-34	7,50	nd
35-36	7,46	nd
37-38	7,55	nd
39-40	7,50	nd
41-42	7,55	nd
43-44	7,63	nd

SO 110/1b
Methane Oxidation Sample Station Locations
Scientist: Michelle Large

SO 110/1b **Alaska**

Date 1996	Stat. No	Instrument	Begin (UTC)	at seafloor max. depth	off seafloor	End (UTC)	Latitude N° Begin; at sf. / End; c	Longitude W° Begin; at sf. / End; off sf.	ter depth HS	Remarks	Samples Taken
23-Jul	23 / 1	ROPOS	*0:28*	3:57	22:29	*1:30*	57:27.316 / ?	147:59.732 / ?	4947 / ?	ROPOS Dive #344	Clam surface triplicate Samples:1,2,3
24-Jul	24 / 1	TV-G	*3:17*	4:53	7:51	*9:43*	27.380 ?) / 57:27	148:00.875 ?) / 148:00.013	743 / (4890 ?)		Poganophoran surface triplicate Samples: 4,5,6 Single Sediment Samples Sample#7= 0-1cm Sample #8= 6-7 cm Sample #9= 2-3 cm
28-Jul	28 / 2	TV-G	*5:06*	6:50	7:00	*10:10*	:27.178 / 57:27.2	147:59.625 / 147:59.668	4954 / 4867		Poganophora surface triplicate: species 1 Samples: 10,11,12 Poganophoran surface triplicate:species 2 Samples: 13,14,15 Clam surface triplicate Samples: 16,17,18
29-Jul	33 / 1	VESP	*16:00*	17:56	23:19	*3:30*	57:27.262	147:59.990	4844		Water Sample triplicate: Niskin #5 Samples: 19,20,21 Single water sample:Niskin #1 Sample:22
2-Aug	40 / 1	TV-GKG	*8:07*	*10:07*	14:34	*16:34*	54:18.17	157:11.82	4808	clams, sediment, precipitates	Clam surface triplicate Samples: 23,24,25 Surface sediment triplicate Samples:26,27,28 Poganophora surface triplicate: species 2 Samples:29,30,31 Poganophora surface triplicate:species 1 Samples: 32,33,34
3-Aug	41 / 1	VESP	18:30	0:04	2:21	4:09	54:18.065	157:11.614	4839 ?	ottles	Water sample triplicate: Niskin #3 Samples: 35,36,37 Water sample triplicate: Niskin #5 Samples: 38, 39 40
3-Aug	43 / 1	TV-G	18:23		0:02		54:18.196	157:11.936	4810		Poganophora surface triplicate: species 1 Samples: 41,42,43 Poganophora surface triplicate: species 1 Samples: 44,45,46 Sediment single samples #47 = 35-36 cm #48 = 16-17 cm #49 = 5-6 cm #50 = 25-26 cm #51 = 9-10 cm #52 = 3-4 cm

GEOMAR REPORTS

1 GEOMAR FORSCHUNGSZENTRUM FÜR MARINE GEOWISSENSCHAFTEN DER CHRISTIAN-ALBRECHTS-UNIVERSITÄT ZU KIEL
BERICHT FÜR DIE JAHRE 1987 UND 1988. 1989. 71 + 6 pp.
In German

2 GEOMAR FORSCHUNGSZENTRUM FÜR MARINE GEOWISSENSCHAFTEN DER CHRISTIAN-ALBRECHTS-UNIVERSITÄT ZU KIEL
JAHRESBERICHT / ANNUAL REPORT 1989. 1990. 96 pp.
In German and English

3 GEOMAR FORSCHUNGSZENTRUM FÜR MARINE GEOWISSENSCHAFTEN DER CHRISTIAN-ALBRECHTS-UNIVERSITÄT ZU KIEL
JAHRESBERICHT / ANNUAL REPORT 1990. 1991. 212 pp.
In German and English

4 ROBERT F. SPIELHAGEN
DIE EISDRIFT IN DER FRAMSTRASSE WÄHREND DER LETZTEN 200.000 JAHRE. 1991. 133 pp.
In German with English summary

5 THOMAS C. W. WOLF
PALÄO-OZEANOGRAPHISCH-KLIMATISCHE ENTWICKLUNG DES NÖRDLICHEN NORDATLANTIKS SEIT DEM SPÄTEN NEOGEN
(ODP LEGS 105 UND 104, DSDP LEG 81). 1991. 92 pp.
In German with English summary

6 SEISMIC STUDIES OF LATERALLY HETEROGENOUS STRUCTURES - INTERPRETATION AND MODELLING OF SEISMIC DATA.
Edited by ERNST R. FLUEH
Commission on Controlled Source Seismology (CCSS), Proceedings of the 8th Workshop Meeting, held at
Kiel - Fellhorst (Germany), August 27-31, 1990. 1991. 359 pp.
In English

7 JENS MATTHIESSEN
DINOFLAGELLATEN-ZYSTEN IM SPÄTQUARTÄR DES EUROPÄISCHEN NORDMEERES: PALÖKOLOGIE UND PALÄO-OZEANOGRAPHIE. 1991. 104 pp.
In German with English summary

8 DIRK NÜRNBERG
HAUPT- UND SPURENELEMENTE IN FORAMINIFERENGEHÄUSEN - HINWEISE AUF KLIMATISCHE UND OZEANOGRAPHISCHE ÄNDERUNGEN
IM NÖRDLICHEN NORDATLANTIK WÄHREND DES SPÄTQUARTÄRS. 1991. 117 pp.
In German with English summary

9 KLAS S. LACKSCHEWITZ
SEDIMENTATIONSPROZESSE AM AKTIVEN MITTELOZEANISCHEN KOLBEINSEY RÜCKEN (NÖRDLICH VON ISLAND). 1991. 133 pp.
In German with English summary

10 UWE PAGELS
SEDIMENTOLOGISCHE UNTERSUCHUNGEN UND BESTIMMUNG DER KARBONATLÖSUNG IN SPÄTQUARTÄREN SEDIMENTEN DES ÖSTLICHEN
ARKTISCHEN OZEANS. 1991. 106 pp.
In German with English summary

11 FS POSEIDON - EXPEDITION 175 (9.10.-1.11.1990)
175/1: OSTGRÖNLÄNDISCHER KONTINENTALRAND (65° N)
175/2: SEDIMENTATION AM KOLBEINSEYRÜCKEN (NÖRDLICH VON ISLAND)
Hrsg. von J. MIENERT und H.-J. WALLRABE-ADAMS. 1992. 56 pp. + app.
In German with some English chapters

12 GEOMAR FORSCHUNGSZENTRUM FÜR MARINE GEOWISSENSCHAFTEN DER CHRISTIAN-ALBRECHTS-UNIVERSITÄT ZU KIEL
JAHRESBERICHT / ANNUAL REPORT 1991. 1992. 152 pp.
In German and English

13 SABINE E. I. KÖHLER
SPÄTQUARTÄRE PALÄO-OZEANOGRAPHISCHE ENTWICKLUNG DES NORDPOLARMEERES UND EUROPÄISCHEN NORDMEERES ANHAND VON
SAUERSTOFF- UND KOHLENSTOFF- ISOTOTPENVERHÄLTNISSEN DER PLANKTISCHEN FORAMINIFERE
Neogloboquadrina pachyderma (sin.). 1992. 104 pp.
In German with English summary

14 FS SONNE - FAHRTBERICHT SO 78 PERUVENT: BALBOA, PANAMA - BALBOA, PANAMA, 28.2.1992-16.4.1992
Hrsg. von ERWIN SUESS. 1992. 120 pp.
In German with some English chapters

15 FOURTH INTERNATIONAL CONFERENCE ON PALEOCEANOGRAPHY (ICP IV): SHORT- AND LONG-TERM GLOBAL CHANGE:
RECORDS AND MODELLING 21-25 SEPTEMBER 1992, KIEL/GERMANY
PROGRAM & ABSTRACTS. 1992. 351 pp.
In English

16 MICHAELA KUBISCH
DIE EISDRIFT IM ARKTISCHEN OZEAN WÄHREND DER LETZTEN 250.000 JAHRE. 1992. 100 pp.
In German with English summary

17 PERSISCHER GOLF: UMWELTGEFÄHRDUNG, SCHADENSERKENNUNG, SCHADENSBEWERTUNG AM BEISPIEL DES MEERESBODENS; ERKENNEN
EINER ÖKOSYSTEMVERÄNDERUNG NACH ÖLEINTRÄGEN. Schlußbericht zu den beiden BMFT-Forschungsvorhaben 03F0055 A+B. 1993. 108 pp.
In German with English summary

18 TEKTONISCHE ENTWÄSSERUNG AN KONVERGENTEN PLATTENRÄNDERN / DEWATERING AT CONTINENTAL MARGINS.
Hrsg. von / ed. by ERWIN SUESS. 1993. 106 + 32 + 68 + 16 + 22 + 38 + 4 + 19 pp.
Some chapters in English, some in German

19 THOMAS DICKMANN
DAS KONZEPT DER POLARISATIONSMETHODE UND SEINE ANWENDUNGEN AUF DAS SEIMISCHE VEKTORWELLENFELD IM WEITWINKELBEREICH. 1993. 121 pp.
In German with English summary

20 GEOMAR FORSCHUNGSZENTRUM FÜR MARINE GEOWISSENSCHAFTEN DER CHRISTIAN-ALBRECHTS-UNIVERSITÄT ZU KIEL
JAHRESBERICHT / ANNUAL REPORT 1992. 1993. 139 pp.
In German and English

21 KAI UWE SCHMIDT
PALYNOMORPHE IM NEOGENEN NORDATLANTIK - HINWEISE ZUR PALÄO-OZEANOGRAPHIE UND PALÄOKLIMATOLOGIE. 1993. 104 + 7 + 41 pp.
In German with English summary

22 UWE JÜRGEN GRÜTZMACHER
DIE VERÄNDERUNGEN DER PALÄOGEOGRAPHISCHEN VERBREITUNG VON *BOLBOFORMA* - EIN BEITRAG ZUR REKONSTRUKTION UND DEFINITION VON WASSERMASSEN IM TERTIÄR.1993. 104 pp.
In German with English summary

23 RV PROFESSOR LOGACHEV - Research Cruise 09 (August 30 - September 17, 1993): SEDIMENT DISTRIBUTION ON THE REYKJANES RIDGE NEAR 59°N
Edited by H.-J. WALLRABE-ADAMS & K.S. LACKSCHEWITZ. 1993. 66 + 30 pp.
In English

24 ANDREAS DETTMER
DIATOMEEN-TAPHOZÖNOSEN ALS ANZEIGER PALÄO-OZEANOGRAPHISCHER ENTWICKLUNGEN IM PLIOZÄNEN UND QUARTÄREN NORDATLANTIK. 1993. 113 + 10 + 25 pp.
In German with English summary

25 GEOMAR FORSCHUNGSZENTRUM FÜR MARINE GEOWISSENSCHAFTEN DER CHRISTIAN-ALBRECHTS-UNIVERSITÄT ZU KIEL
JAHRESBERICHT / ANNUAL REPORT 1993. 1994. 69 pp.
In German and English

26 JÖRG BIALAS
SEISMISCHE MESSUNGEN UND WEITERE GEOPHYSIKALISCHE UNTERSUCHUNGEN AM SÜD-SHETLAND TRENCH UND IN DER BRANSFIELD STRASSE - ANTARKTISCHE HALBINSEL. 1994. 113 pp.
In German with English summary

27 JANET MARGARET SUMNER
THE TRANSPORT AND DEPOSITIONAL MECHANISM OF HIGH GRADE MIXED-MAGMA IGNIMBRITE TL, GRAN CANARIA: THE MORPHOLOGY OF A LAVA-LIKE FLOW. 1994. 224 pp.
In English with German summary

28 GEOMAR LITHOTHEK. Edited by JÜRGEN MIENERT. 1994. 12 pp + app.
In English

29 FS SONNE - FAHRTBERICHT SO 97 KODIAK-VENT: KODIAK - DUTCH HARBOR - TOKYO - SINGAPUR, 27.7. - 19.9.1994
Hrsg. von ERWIN SUESS. 1994.
Some chapters in German, some in English

30 CRUISE REPORTS:
RV LIVONIA CRUISE 92, KIEL-KIEL, 21.8.-17.9.1992: GLORIA STUDIES OF THE EAST GREENLAND CONTINENTAL MARGIN BETWEEN 70° AND 80°N
RV POSEIDON PO200/10, LISBON-BREST-BREMERHAVEN, 7.-23.8.1993: EUROPEAN NORTH ATLANTIC MARGIN: SEDIMENT PATHWAYS, PROCESSES AND FLUXES
RV AKADEMIK ALEKSANDR KARPINSKIY, KIEL-TROMSØ, 5.-25.7.1994: GAS HYDRATES ON THE NORTHERN EUROPEAN CONTINENTAL MARGIN
Edited by JÜRGEN MIENERT. 1994.
In English; report of RV AKADEMIK ALEKSANDR KARPINSKIY cruise in English and Russian

31 MARTIN WEINELT
BECKENENTWICKLUNG DES NÖRDLICHEN WIKING-GRABENS IM KÄNOZOIKUM - VERSENKUNGSGESCHICHTE, SEQUENZSTRATIGRAPHIE, SEDIMENTZUSAMMENSETZUNG. 1994. 85 pp.
In German with English summary

32 GEORG A. HEISS
CORAL REEFS IN THE RED SEA: GROWTH, PRODUCTION AND STABLE ISOTOPES. 1994. 141 pp.
In English with German summary

33 JENS A.HÖLEMANN
AKKUMULATION VON AUTOCHTHONEM UND ALLOCHTHONEM ORGANISCHEM MATERIAL IN DEN KÄNOZOISCHEN SEDIMENTEN DER NORWEGISCHEN SEE (ODP LEG 104). 1994. 78 pp.
In German with English summary

34 CHRISTIAN HASS
SEDIMENTOLOGISCHE UND MIKROPALÄONTOLOGISCHE UNTERSUCHUNGEN ZUR ENTWICKLUNG DES SKAGERRAKS (NE NORDSEE) IM SPÄTHOLOZÄN. 1994.
In German with English summary

35 BRITTA JÜNGER
TIEFENWASSERERNEUERUNG IN DER GRÖNLANDSEE WÄHREND DER LETZTEN 340.000 JAHRE.
DEEP WATER RENEWAL IN THE GREENLAND SEA DURING THE PAST 340,000 YEARS.1994. 6 + 109 pp.
In German with English summary

36 JÖRG KUNERT
UNTERSUCHUNGEN ZU MASSEN- UND FLUIDTRANSPORT ANHAND DER BEARBEITUNG REFLEXIONSSEISMISCHER DATEN AUS DER KODIAK-SUBDUKTIONSZONE, ALASKA. 1995. 129 pp.
In German with English summary

37 CHARLOTTE M. KRAWCZYK
DETACHMENT TECTONICS DURING CONTINENTAL RIFTING OFF THE WEST IBERIA MARGIN: SEISMIC REFLECTION AND DRILLING CONSTRAINTS. 1995. 133 pp.
In English with German summary

38 CHRISTINE CAROLINE NÜRNBERG
BARIUMFLUSS UND SEDIMENTATION IM SÜDLICHEN SÜDATLANTIK - HINWEISE AUF PRODUKTIVITÄTSÄNDERUNGEN IM QUARTÄR. 1995. 6 + 108pp
In German with English summary

39 JÜRGEN FRÜHN
TEKTONIK UND ENTWÄSSERUNG DES AKTIVEN KONTINENTALRANDES SÜDÖSTLICH DER KENAI-HALBINSEL, ALASKA. 1995. 93 pp
In German with English summary

40 GEOMAR FORSCHUNGSZENTRUM FÜR MARINE GEOWISSENSCHAFTEN DER CHRISTIAN-ALBRECHTS-UNIVERSITÄT ZU KIEL
JAHRESBERICHT / ANNUAL REPORT 1994. 1995.
In German and English

41 FS SONNE - FAHRTBERICHT / CRUISE REPORT SO 103 CONDOR 1 B: VALPARAISO-VALPARAISO, 2.-21.7.1995.
Hrsg. von ERNST R. FLUEH. 1995. 140 pp.
Some chapters in German, some in English

42 R/V PROFESSOR BOGOROV CRUISE 37: CRUISE REPORT "POSETIV": Vladivostok - Vladivostok, September 23 - October 22, 1994.
Edited by CHRISTOPH GAEDICKE, BORIS BARANOV and EVGENIY LELIKOV. 1995. 48 + 33 pp.
In English

43 CHRISTOPH GAEDICKE
DEFORMATION VON SEDIMENTEN IM NANKAI-AKKRETIONSKEIL, JAPAN. BILANZIERUNG TEKTONISCHER VORGÄNGE ANHAND VON SEISMISCHEN PROFILEN UND ERGEBNISSEN DER ODP-BOHRUNG 808. II + 89 pp.
In German with English summary

44 MARTIN ANTONOW
SEDIMENTATIONSMUSTER UM DEN VESTERIS SEAMOUNT (ZENTRALE GRÖNLANDSEE) IN DEN LETZTEN 250.000 JAHREN. 1995.
In German with English summary

45 INTERNATIONAL CONGRESS: CORING FOR GLOBAL CHANGE - ICGC '95. KIEL, 28 - 30 June, 1995.
Edited by JÜRGEN MIENERT and GEROLD WEFER. 1996.
In English

46 JENS GRÜTZNER
ZUR PHYSIKALISCHEN ENTWICKLUNG VON DIAGENETISCHEN HORIZONTEN IN DEN SEDIMENTBECKEN DES ATLANTIKS. 1995. 96 pp.
In German with English summary

47 INGO A. PECHER
SEISMIC STUDIES OF BOTTOM SIMULATING REFLECTORS AT THE CONVERGENT MARGINS OFFSHORE PERU AND COSTA RICA. 1996. 159 pp.
In English with German summary

48 XIN SU
DEVELOPMENT OF LATE TERTIARY AND QUATERNARY COCCOLITH ASSEMBLAGES IN THE NORTHEAST ATLANTIC. 1996. 120 pp. + 7 pl.
In English with German summary

49 FS SONNE - FAHRTBERICHT / CRUISE REPORT SO 108 ORWELL: SAN FRANCISCO - ASTORIA, 14.4. - 23.5.1996
Edited by ERNST R. FLUEH and MICHAEL A. FISHER. 1996.

50 GEOMAR FORSCHUNGSZENTRUM FÜR MARINE GEOWISSENSCHAFTEN DER CHRISTIAN-ALBRECHTS-UNIVERSITÄT ZU KIEL
JAHRESBERICHT / ANNUAL REPORT 1995. 1996. 93 pp.
In German and English

51 THOMAS FUNCK
STRUCTURE OF THE VOLCANIC APRON NORTH OF GRAN CANARIA DEDUCED FROM REFLECTION SEISMIC, BATHYMETRIC AND BOREHOLE DATA. 1996. VI, 144 pp.
In English with German summary

52 PETER BRUNS
GEOCHEMISCHE UND SEDIMENTOLOGISCHE UNTERSUCHUNGEN ÜBER DAS SEDIMENTATIONSVERHALTEN IM BEREICH BIOSTRATIGRAPHISCHER DISKONTINUITÄTEN IM NEOGEN DES NORDATLANTIK, ODP LEG 104, SITES 642B UND 643A. 1993. V, 73 pp.
n German with English summary

53 CHRISTIANE C. WAGNER
COLD SEEPS AN KONVERGENTEN PLATTENRÄNDERN VOR OREGON UND PERU: BIOGEOCHEMISCHE BESTANDSAUFNAHME. 1996. 108, XXXVI pp.
In German with English summary

54 FRAUKE KLINGELHÖFER
MODEL CALCULATIONS ON THE SPREADING OF SUBMARINE LAVA FLOWS. 1996. 98 pp.
In English with German summary

55 HANS-JÜRGEN HOFFMANN
OBJEKTORIENTIERTE ANALYSE UND MIGRATION DIFFRAKTIERTER WELLENFELDER UNTER VERWENDUNG DER STRAHLENMETHODE UND DER EDGE-WAVE-THEORIE. 1996. XXI, 153 pp.
In German with English summary

56 DIRK KLÄSCHEN
STRAHLENSEISMISCHE MODELLIERUNG UNTER BERÜCKSICHTIGUNG VON MEHRFACHDIFFRAKTIONEN MIT HILFE DER EDGE-WAVES: THEORIE UND ANWENDUNGSBEISPIELE. 1996. X, 159 pp.
In German with English summary

57 NICOLE BIEBOW
DINOFLAGELLATENZYSTEN ALS INDIKATOREN DER SPÄT- UND POSTGLAZIALEN ENTWICKLUNG DES AUFTRIEBSGESCHEHENS VOR PERU.
1996. IV, 100, 17, 14 (7 pl.) pp.
In German with English summary

58 RV SONNE - CRUISE REPORT SO109: HYDROTRACE. ASTORIA-VICTORIA-ASTORIA-VICTORIA. MAY 23 - JULY 8, 1996.
Ed. by PETER HERZIG, ERWIN SUESS, and PETER LINKE. 1997.
In English

59 RV SONNE - CRUISE REPORT SO110: SO - RO (SONNE - ROPOS). VICTORIA-KODIAK-VICTORIA. JULY 9 - AUGUST 19, 1996.
Ed. by ERWIN SUESS and GERHARD BOHRMANN. 1997.
In English

60 RV AKADEMIK M. A. LAVRENTYEV CRUISE 27. CRUISE REPORT: GREGORY. VLADIVOSTOK-PUSAN-OKHOTSK SEA-PUSAN-VLADIVOSTOK.
SEPTEMBER 7 - OCTOBER 12, 1996. Ed. by DIRK NÜRNBERG, BORIS BARANOV, and BORIS KARP. 1997. 143 pp.
In English